Design Report

Martian Advanced Reconnaissance System

R.N.J. Boelhouwer
E.C. Bunschoten
C.M.J. Debusscher
W. Frijters
R.J. van Goeverden
E.B. Legrand
J. Matton
K. Paliusis
J.K.N. Verheyen

Technische Universiteit Delft

TU Delft

Design Report

Martian Advanced Reconnaissance System

by

Name	**Student number**
Robbert Boelhouwer	4346858
Evert Bunschoten	4455584
Charles Debusscher	4469666
Wout Frijters	4481305
Rob van Goeverden	4291514
Emiel Legrand	4446100
Jorne Matton	4215885
Kipras Paliusis	4456521
Jan Verheyen	4458192

Project duration	April 18, 2018 – July 5, 2018	
Principal tutors	F. Schrijer,	Aerodynamics
	S. van Zuijlen,	Aerodynamics
Coaches	D. Nardi	Structural Integrity & Composites
	I. van Gent	Flight Performance and Propulsion

Cover image credit: NASA / JPL / University of Arizona / Alfred McEwen.

TU Delft

Preface

This is the concluding report of DSE group 21. Over the past two months we did our very best to design something that has never been achieved before: an autonomous *flying* vehicle operating on another planet. This turned out to be extremely challenging, even so that we would call the results in this project a feasibility study rather than a preliminary design project. However, this was very interesting as well in its own sense: we had to be as creative as possible in order to get the design to work and explore every thinkable design option. Additionally, we had to get acquainted with intriguing subjects that reached way beyond the extent of our Bachelor Aerospace Engineering. As such, we can say that we found the DSE a very fruitful (though exhausting) experience in the context of our educational career and future employment.

This being said, we have to thank a few people that played a crucial role during the past few months. First of all, we would like to thank our tutors Sander and Ferry for their patience and constructive feedback, and their sense for detail. Secondly, we are very grateful for the help we got from our coaches Imco and Davide. Their opinion has been extremely important to the group, not to mention the useful input they had on a wide range of subjects. In particular, they connected us with experts when we got stuck in certain design stages in order to get more detailed advice. As such, we cannot stress enough the importance that the tutors and coaches had during our project.

As mentioned, we consulted many experts during the design process for their advice on certain subjects. Therefore we would like to thank Eddy van den Bos for his help with CATIA, Witold Koning for being an invaluable source of information for the Mars Helicopter on the propeller aerodynamics, Dr. Morteza Abouhamzeh for helping to understand ANSYS better and Tom Stokkermans for his help with XROTOR and advice on propeller design.

Thirdly, we have greatly appreciated the feedback from the Project Management and Systems Engineering lecturers and teaching assistants: it has to be said that we would never have properly learned to apply these important design practices without their efforts.

Finally, it should not be forgotten that participating in a project of this scale is only possible due to the vast efforts of the Faculty of Aerospace Engineering and the Delft University of Technology. Therefore, we would like to express our sincerest gratitude towards all the people who spend a lot of time every year to make this project possible.

R.N.J. Boelhouwer
E.C. Bunschoten
C.M.J. Debusscher
W. Frijters
R.J. van Goeverden
E.B. Legrand
J. Matton
K. Paliusis
J.K.N. Verheyen

Delft, June 2018

Executive Summary

After twelve humans have walked on the moon, mankind is now looking forward to making another giant leap by putting humans on Mars. However, before sending a human to Mars, it is crucial that the possible habitat and science zones are identified beforehand. The Martian Advanced Reconnaissance System (MARS) aims to perform this identification and thereby assist in the future colonisation of Mars.

The mission, together with its need and objective have been defined as follows:

- **Mission Need Statement:** *Humanity should investigate habitable zones and regions of scientific interest on Mars in order to prepare for future manned missions.*
- **Mission Statement:** *Project MARS will develop a system that will collect detailed atmospheric and geological information in order to support the identification and mapping of scientific exploration zones on Mars by 2030.*
- **Project Objective Statement:** *Design an autonomous UAV that can be used to map and analyse Martian regions of scientific interest and aid in the exploration of Martian human habitat zones, by 9 students in 10 weeks.*

This mission is unique due to the fact that a UAV is used, instead of rovers or satellites, this allows for some new opportunities. The usage of the UAV had to be decided in order to exploit these opportunities to their fullest extent. One option was to use the UAV as a method of transport, moving the scientific instruments to specific locations to perform measurements. A different approach is to use it as a method of constant observation, performing all measurements from the sky. While the first option provides greater accuracy, it was decided to opt for the second option, as that allows for greater coverage and reliability of the mission. This was therefore used as starting point for the design of the system.

The scientific goals of the mission resulted in the following requirements:

- **Visual mapping:** Visual imaging shall be done with a resolution of 10 cm.
- **Height mapping:** Height mapping shall be done with a 20 cm resolution at a 10 cm height accuracy.
- **Soil composition:** The soil composition shall be determined by hyperspectral imaging with a resolution of 1 m.
- **Shallow ice deposits:** Shallow ice deposits shall be scanned every metre at a depth of 10 m with a height resolution of 10 cm.
- **Dust analysis and Lower atmosphere conditions:** The system shall measure the atmospheric conditions in the lower atmosphere (wind speeds, precipitations, and dust composition and size distribution).

Given the scientific goals of the mission, the UAV has been named VITAS after the measurements it had to perform (Visual imaging, Ice deposit scanning, Trace gas detection, Atmospheric conditions & Soil analysis). However, the detecting trace gases was eventually left out due to very good data already being available. While the core element of the system will be the UAV, a base station will be included in the design. The functions of this base station are e.g. communication towards Earth and power generation, which reduces the tasks that have to be performed by the UAV and consequently can reduce the size and weight of the UAV. The base station is able to perform a part of the scientific measurements, which do not need to be performed at multiple areas, as well. This leads to a division of the scientific payload as follows:

- **UAV:**
  - Visual mapping
  - Height mapping
  - Shallow ground ice deposits
  - Soil composition
- **Base station:**
  - Dust composition and size
  - Wind speeds and precipitation

For this mission, a market analysis has been performed. In this analysis, a look has been taken at the macro- and microenvironment in which the project finds itself.

An STP-analysis (segmentation, targeting and positioning) has been performed on the market in which the system will be placed. From this analysis, the following conclusions have been drawn:

- The main business strategy is to cooperate with existing private and/or government companies.
- The space industry market has many branches, therefore careful targeting is necessary.
- The target markets are ”human habitat on Mars”, ”science” and ”commercial human spaceflight”.
- In order to position the system in the market, it is decided to sell the complete system after development.

It is believed by the MARS team that sustainability is an important aspect of any newly developed project nowadays. Therefore, it is an aspect that has been taken into account heavily during the development of this project. The sustainability of each part of the design will be measured using a life cycle assessment, which consists of four elements: goal definition and scoping, inventory assessment, impact assessment and improvement assessment. Using this life cycle assessment, the possible alternatives for each subsystem are compared to allow for a clear comparison of the sustainability of different options. This allows for the usage of sustainability as a trade-off criterion during design. Aspects which were taken into account during the sustainability analysis are: the reusability and recyclability of a (sub)system and the usage of toxic or otherwise hazardous materials.

The layout of the mission has been defined as being built up of two phases. In the first phase, the UAV will perform a ”hub-spoke” flight pattern over the exploration zone, which allows for easy coverage of the complete exploration zone, but also results in unequal accuracy throughout the exploration zone. The second phase aims to compensate for this, as in this phase, the UAV will travel to specific areas (defined from the data gathered in the first phase), where it will loiter over the area. During this loiter, it will perform continuous measurements, allowing for higher accuracy over areas of interest. When all areas of interest have been mapped to a sufficient extent, the mission will be considered finished.

Using this definition of the mission and its phases, the following schedule for the complete mission has been established:

- **November, 2026:** Take-off from Earth, begin interplanetary journey. Following the Mars launch windows and performing a Hohmann transfer, the expected duration is eight months.
- **June, 2027:** Reach Mars, perform Entry, Descent & Landing (EDL), deploy and prepare to initiate phase 1. It is expected that subsystem calibration, establishing communication and performing system health tests will take up to two weeks.
- **July, 2027:** Begin phase 1 of scientific mission. An average of 0.75 daily flights results in 1028 sols to perform the 770 flights. Therefore, the duration of this phase is 36 months.
- **July, 2030:** Begin phase 2 of scientific mission. As the system is expected to conclude its scientific mission by 2030, the expected maximum duration is the remaining five months.
- **December, 2030:** Planned end of nominal scientific tasks. Land and prepare for reuse.

For the mission, multiple options for launchers have been considered. After performing a trade-off between reliability, payload capabilities, sustainability and cost, it was decided that the Falcon 9 FT and the Atlas V 541 were best fit for this mission. Given its previous usage for Mars missions and high reliability, it was finally decided to make use of the Atlas V launcher.

For the entry vehicle, it was originally decided to use the entry vehicle which was used for the Curiosity rover. However, after some careful considerations, it was decided that some adaptations need to be made to it. Firstly, the shape of the cone will be changed, and the skycrane will be replaced by a thruster system on the base station, based on the one used on the ExoMars 2020 lander. These changes have been made as it was found to be necessary to provide enough storage space for the MARS.

For the landing site, the Jezero crater was chosen because it contains a flat surface, has minerals present, has an elevation below -1000 meters and is less than 30^o latitude from the equator. It is located at 18.855 ° N and 77.519 ° E and has a diameter of 49 km. The landing site is not located at the centre of the crater, as there are some high mountains located on the southern edge of the crater, and it is necessary to prevent landing in the shadow of those mountains.

For the mission, as set up until this stage, a number of possible concepts were generated, for which a total of five elements were analysed in-depth and traded off. For four of these, it became apparent that most investigated options were not feasible, and only one option was realistic for the mission at hand, as displayed in Table 1. The results of this trade-off led to the creation of three total concepts:

- Single integral tailsitter, carrying the entire UAVs scientific payload.
- Four task-specific tailsitters. The scientific instruments are split equally amongst two UAV designs. Two units of both designs are used.
- Four task-specific multicopters. Scientific instruments are split amongst two UAV designs and two of each design are used for the mission.

Table 1: The elements which have been traded off and their winning options.

Element	Remaining option(s)
Power generation	Solar panels
Power storage	Batteries
Propulsion type	Propellers
# and type of base stations	Single, static base station
# and type of UAVs	One or multiple UAVs; tailsitter or multicopter

After careful analysis of each of these concepts and performing a trade-off, it was decided to design a single, integral tailsitter.

VITAS has been designed taking into account the following design principles and constraints:

- The span of the UAV cannot exceed 2.2 m, to fit inside the entry capsule when mounted on the base station.
- Sufficient clearance is required between the propellers and the structure of the UAV.
- In the takeoff phase, controllability around all three axes, sufficiently strong to overcome wind gusts of 10 m/s is required.
- The lifting surface needs to be as large as possible, as the low atmospheric density requires a large surface area to keep the angle of attack limited.
- The UAV needs to have a reliable base when resting vertically on the base station platform.
- The thermal box of the UAV measures $275 \times 170 \times 200$ mm^3 and has to fit inside the UAV fuselage.

From these requirements and constraints, it was decided to use an X-wing canard configuration for VITAS. For maximum stability, the landing legs will be mounted to the wing tips, extending back from the trailing edge. This is also the reason that a canard configuration was chosen, as it would not be possible to include a tail behind the fuselage with this design.

Each of the wings will have a set of contra-rotating propellers mounted on it. The propellers will be mounted to the wing tips, in front of the leading edge, to maximise stability during takeoff and landing. To obtain the required clearance between the propellers and the structure, it was decided to apply the wing taper to the trailing edge of the wing and have a straight leading edge. The canard surface is designed to be fully movable, to allow for maximum controllability during the takeoff and landing phases.

The fuselage is designed as a cylinder with a flattened lower side. The thermal box will be located on that flat side. A part of the bottom plate will be transparent, to allow for a line of sight for e.g. the visual imaging instruments.

The design of the base station was based on the functions it has to perform to properly support VITAS in its mission. The functions are as follows:

- All power generation is performed on the base station, which is then partially distributed to the UAV.
- The base station serves as a landing platform for the UAV.
- The base station assists as a component of the positioning system for VITAS, and will aid the flyer during its landing by allowing for an accurate tracking system.
- The base station is responsible for the processing and storage of all data gathered during the the mission lifetime.
- All communications with Earth will be routed through the base station.
- The general monitoring of the mission progress will be performed by the base station.

It was decided that the base station shall fit solely within the heat shield of the entry capsule, to allow for the rest of the volume to be used by the UAV. The base station itself was designed as an octagonal pyramid, as a perfect cone would cause many complications for manufacturing and attachment. The major structure of the base station will resemble a wireframe structure, to provide the required strength and shape, while keeping the weight low.

The top of the base structure is designed as a flat plate with a hole in the centre. In that hole, a robotic arm will be located. That robotic arm will be equipped with a physical interface to connect to VITAS when it has landed. That connection can be used for charging the UAV and transferring data.

On the lower side of the base station, a landing gear is mounted. The landing gear consists of four landing legs, each of which consists of a primary load-bearing strut and two secondary deployment struts. The primary strut is equipped with a shock-damping system to reduce the loads during the initial touchdown.

Table 2: The total mass and power consumption of the UAV and Base station (values are without contingencies).

System	Mass [kg]	Nominal power usage [W]	Peak power usage [W]
Base station	451.2	94	2670
UAV	13.94	1225	1955

A reliability, availability, maintainability and safety (RAMS) analysis has been performed on the system. The conclusion of that analysis are as follows:

- The total reliability of the mission lies between 54% and 78%.
- The prime maintenance type for the mission is software maintenance. If a problem arises, VITAS will return to the base station and enter a safe mode until a software patch is provided and the ground station on Earth gives the command to continue.
- The total availability of the system is estimated at 88%.
- A total of six hazardous components were identified (batteries, deployables, launcher, structure, propulsion), together with the impact those hazards will have on the complete design.

For the scientific mission, a number of instruments is required. A summary of the instruments is provided in Table 3.

Table 3: An overview of the mass and power usage of the scientific instruments

System	Name	Purpose	Mass [g]	Peak power usage [W]
UAV	Camera + lens	Visual imaging	313	2.5
	Spectrometer + lens	Soil analysis	313	1.6
	Altimeter	Height mapping	590	8
	WISDOM	Ice scanning	400	10
Base station	MEDA	Atmospheric analysis	5500	17

For the structure of the UAV and base station, one of the most important considerations was that the modal frequencies of the systems must be high enough to prevent resonance during the launch. For the VITAS, an additional important consideration was that the mass of the structure must be as low as possible, as mass is a highly critical factor for the UAV. Taking these facts into account and using a simplified model of the UAV structure, a total of five possible materials were determined for the structure of the UAV: two common aluminium alloys, a titanium alloy, a carbon fibre composite, and a beryllium-aluminium alloy. These were then compared on six aspects: The specific modulus, the plate strength performance index, the fatigue limit strength, the toughness performance factor, their manufacturing flexibility and their toxicity. After performing a trade-off between the five materials, the beryllium-aluminium alloy (AM-162) was found to be the material best suited for this design.

Knowing the material for the design, a more in-depth analysis could be performed. The most detailed analysis has been performed on the wings, as they are highly complex structures. A model of the separate parts of the UAV has been made using CATIA V5. Applying the material properties to that model allowed for a detailed analysis of the system in ANSYS 19.0, which served as a method of verification for the performed calculations. The ANSYS analysis led to the conclusion that the design has a sufficiently high modal frequency, and the flight loads can be withstood up to a load factor of four.

For the design of the propellers, it was known that there are three main limiting factors:

- The low density of the atmosphere leads to a low thrust generation.
- The low density also leads to very low Reynolds number, highly viscous flows.
- The low average temperature means the sound speed is lower, which limits the maximum rotational speed of the propeller.

To deal with these factors, it was found necessary to make the propellers as thin plates with about 5% camber. Some further investigation found an opportunity for optimisation by designing two sets of propellers, instead of making all propellers identical. One set of propellers was optimised for cruise performance, while the other set was optimised for takeoff performance. The propellers which are placed diagonally opposite each other match each other in design, to prevent controllability interference.

Using this information, a design for the cruise propellers and takeoff propellers was established and analysed using XROTOR software, due to its wide applications in propeller design. The total thrust required for controllable take-off is 52 N. During take-off both the take-off and the cruise propellers will work together to provide the appropriate amount of thrust, the take-off propellers providing in total 32 N of thrust and the cruise propellers are designed for a maximum thrust during takeoff of 20 N. During cruise 8.4 N of thrust is required, the take-off propellers will then remain in a 'feathered' mode where they will produce no thrust and minimal drag. The cruise propellers will provide all the thrust necessary during cruise.

Concerning stability & control, an investigation was performed into possible airfoils, which was essential for the low-Reynolds flows in which VITAS will have to operate. For this, an XFOIL analysis was performed on ten airfoils. After performing a trade-off between these, it was determined that the SD7003 airfoil was best fit for the mission.

Similarly, an investigation has been performed into possible airfoils for the canard surface. As the canard is designed to be fully movable, a symmetrical airfoil is required for the canard. Therefore, five symmetrical NACA 4-series airfoils were traded off (again using XFOIL analysis). From this trade-off the NACA 0015 was found the best airfoil for this mission.

Using the information on the airfoils of the main wings and the canard, the stability of the system could be investigated. First, the longitudinal static stability of the system was investigated. As VITAS uses batteries, the centre of gravity (c.g.) does not shift during operation. This investigation led to a ratio between the canard surface area and main wing area of 0.15.

Afterwards, stability during vertical take-off and landing (VTOL) was investigated. As the c.g. was determined to be slightly in front of the leading edge of the wing, but behind the propellers, the system is statically stable during the VTOL manoeuvre. An investigation was also performed to determine the influence of gusts on the stability of the system, but it was found that the moment created by gusts can easily be handled by the propellers.

Finally, an investigation was performed into the dynamic stability of the system. It was found that the system is stable in its short period, roll damping and dutch roll modes. The system is found to be neutrally stable in its phugoid mode. Finally, it was determined that VITAS is very slightly unstable in its spiral mode. However, the time it takes for the roll angle to increase to a problematic extent lies in the order of 100's of seconds. Therefore, VITAS has enough time to restore its stability using an active control system.

For the Electrical Power System (EPS), the UAV and base station have been considered separately. For the EPS of VITAS, the primary considerations which had to be made were the total power and energy requirements for the takeoff and cruise phases of the engines. Furthermore, the power requirements of the scientific instruments, the thermal control system and the Command & Data Handling system (CDH) also needed to be taken into account for the sizing of the EPS.

For the EPS of the base station, the communications and CDH subsystems were the main consumers of power. The UAV was also a significant consumer of power, as the base station also has to provide the power to VITAS. The most important parameters of the EPS are summarised in Table 4. A note has to be taken on the amount of lifecycles. For the UAV it is defined at 80% Depth Of Discharge (DOD), while for the base station at 40%. This is due to the fact that the base station has to provide for power even after the VITAS is finished. At this point, the base station will have to deliver less power, ergo designing the base station's amount of life cycles up until the usual 80% DOD would be an over design. The battery is optimised for th

Table 4: Overview of the EPS.

Parameter	**VITAS**	**Base station**
Total power [W]	1230	756
Total energy [Wh]	359	3618
Battery lifecycles [-]	650	1700
Battery mass [kg]	2.619	14.55
Mass of other components [kg]	0.216	31.23

For the communication system, multiple communications channels have been established. The general communication flow is established as follows:

- The base station and VITAS will communicate through an ultra-high frequency (UHF) band wireless link and through a wired link using the physical interface on the robotic arm;
- The scientific data from the instruments will be sent to Earth using the Mars Relay Network (MRN);
- The housekeeping data of the (sub)systems will be sent directly to Earth using the Deep Space Network (DSN);
- Any commands from Earth will be sent directly to the system using the DSN.

Table 5: Mass and power budget of communications, CDH and thermal control subsystems (all values without contingencies).

Subsystem	Mass [kg]	Nominal power usage [W]	Peak power usage [W]
VITAS communications	0.20	2	4.8
VITAS CDH	0.75	12.3	22.5
VITAS thermal control	0.50	11.1	25.1
Base station communications	15.99	33.6	122.8
Base station CDH	11.64	38.5	80.5
Base station thermal control	0.85	0.1	30.1

For the control of the mission, the UAV and base station both require a central Command and Data Handling system. The CDH systems are responsible for the management of all of the subsystems aboard the UAV and base station and the handling of scientific and housekeeping data. In addition, CDH subsystem on VITAS will also function as the flight computer, while the base station CDH system is responsible for the handling of all communication and the compression of scientific data.

Most of the components, such as the EPS, communications, CDH and scientific components are temperature sensitive and are stored inside a thermal box was included in both VITAS and the base station. The base station's thermal box is designed to fit under the landing platform, while the UAV's must fit exactly within the fuselage, such that the bottom of the box is flush with the flat side of the fuselage.

Both of the thermal boxes are designed to use multi-layer insulation to keep the temperature relatively constant. Furthermore, they are equipped with radiators and heat pipes in order to heat the box when the temperature gets too low. In case of the base station, no heating should be necessary, as the systems themselves provide enough heat. However, a radiator is still inserted for redundancy for extreme situations. The thermal box on the UAV will require near-constant heating to remain at a proper temperature.

In order to map the zone properly, an accurate navigation system had to be designed to make sure that proper location data can be added to the gathered scientific data and no areas are unnecessarily covered multiple times or missed. For this, a local navigation pseudolite system was designed. This consists of four small, winged boxes which are deployed from the base station during entry to spread across the exploration zone. These boxes contain GPS transceivers, a battery, solar panels and an atomic clock. Together with the base station, these beacons can provide a GPS-like system across the exploration zone.

An investigation into the future of this mission has been performed. It was concluded that the main paths which will have to be taken are:

- Reaching out to the public, to promote the mission and gain investors;
- Formulating and creating a preliminary design of the mission;
- Evaluating detailed design of the mission and research & development (R&D) for technologies;
- Performing the mission, logistics & operations.

The first one will be performed non-stop until launch. The second one starts right after the feasibility study and lasts until July 2021. The third one will follow immediately after the second one, and will last until October 2026. One month later, in November, the mission will be launched.

The total cost of the mission has been estimated, resulting in an expected total sales price of $6,350,500,000.00, taking into account the expected inflation over the coming years. In order to minimise financial risks, it was decided that the healthiest way to fund this project is through stock finance. This reduces the profits, but results in a lower risk of losing money.

Given the limited time which was available for this design, it is logical that some parts of the design remain incomplete and require further investigation in the future. The major identified subjects which need further investigation in future stages are as follows:

- **Propulsion system:** A full computational fluid dynamics (CFD) analysis of the propellers will be necessary.
- **Structures:** The focus of structural analysis in this project was laid on VITAS, which means that the base station was not investigated as deeply as required.
- **Aerodynamics:** Similar to the propulsion system, a full CFD analysis is important to provide a clearer prediction of the system.
- **Stability & control:** The flight scenarios of VITAS are many and complex, which means the control surfaces have to be sized very specifically. This sizing has not been performed yet.

Contents

Executive Summary ii

1 Introduction 1

2 Mission Objective 2
2.1 The Need for an Aerial Mars System . . . 2
2.2 Mission Concept . . . 2
2.3 Mission Task Requirements . . . 3

3 Market Analysis 4
3.1 Macroenvironment . . . 4
3.2 Microenvironment . . . 4
3.3 Strength, Weakness, Opportunity and Threat Analysis . . . 5
3.3.1 Strengths . . . 5
3.3.2 Weaknesses . . . 5
3.3.3 Opportunities . . . 6
3.3.4 Threats . . . 6
3.4 Segmentation, Targeting and Positioning Analysis . . . 6
3.4.1 Segmentation . . . 6
3.4.2 Target Market . . . 7
3.4.3 Positioning . . . 8
3.5 Identifying Stakeholders . . . 8
3.6 Barriers . . . 8
3.7 Sustainable Development Strategy . . . 9
3.7.1 Method to Measure Sustainability . . . 9
3.7.2 Objectives . . . 9

4 Mission Architecture 11
4.1 Scientific Mission Phases . . . 11
4.2 Mission Schedule . . . 11
4.3 Launcher & Entry Vehicle Selection . . . 12
4.3.1 Launch Vehicle . . . 12
4.3.2 Entry Vehicle . . . 13
4.4 Launch and Arrival Strategy . . . 13
4.5 Landing Site . . . 14

5 Concept Analysis 16
5.1 Driving Requirements . . . 16
5.2 Concept Generation . . . 17
5.3 Analysed Concepts . . . 20
5.4 UAV Concept Trade-off . . . 23
5.5 Sensitivity Analysis and Conclusions . . . 24

6 MARS System Overview 26
6.1 General Overview . . . 26
6.2 UAV Overview . . . 26
6.2.1 Mission Characteristics . . . 27
6.2.2 External and Internal Configuration . . . 29
6.2.3 Subsystems . . . 33
6.2.4 Design Sensitivity . . . 35
6.3 Base Station . . . 35
6.3.1 Characteristics . . . 35
6.3.2 Description . . . 36
6.3.3 Subsystems . . . 37

6.4 Functional Breakdown Diagram . . . 39
6.5 MARS System . . . 42
6.5.1 Logistics. . . . 42
6.5.2 Operations . . . 42
6.5.3 Requirements Compliance Matrix and Feasibility Analysis. . . . 44
6.5.4 Reliability, Availability, Maintainability & Safety Analysis . . . 45
6.5.5 Technical Risk Assessment . . . 48
6.5.6 Resource allocation and breakdown. . . . 50

7 Subsystem Design 52
7.1 Scientific Payload. . . . 52
7.1.1 Visual Imaging . . . 53
7.1.2 Height Mapping . . . 54
7.1.3 Ice Deposits. . . . 55
7.1.4 Soil Analysis . . . 55
7.1.5 Wind, Precipitation and Dust Sensor . . . 56
7.1.6 Trace Gases . . . 56
7.1.7 Scientific Payload Summary . . . 57
7.2 Structures . . . 57
7.2.1 Subsystem Level Requirements . . . 57
7.2.2 Material Trade-off . . . 59
7.2.3 Detailed Structural Analysis . . . 61
7.2.4 Sensitivity Analysis . . . 64
7.3 Propulsion . . . 65
7.3.1 Subsystem Level Requirements . . . 65
7.3.2 Design Considerations . . . 65
7.3.3 Propeller Performance . . . 66
7.3.4 Cruise Propellers . . . 67
7.3.5 Take-off Propellers . . . 69
7.3.6 Weight Estimation . . . 70
7.3.7 Overview . . . 71
7.4 Stability and Control . . . 71
7.4.1 Subsystem Level Requirements . . . 71
7.4.2 Airfoil Selection . . . 72
7.4.3 UAV Stability Characteristics. . . . 75
7.5 Electric Power System . . . 80
7.5.1 EPS of the UAV. . . . 80
7.5.2 Base Station EPS . . . 85
7.5.3 V&V and Sensitivity Analysis . . . 89
7.6 Communication . . . 89
7.6.1 Communication Flow . . . 89
7.6.2 Subsystem Level Requirements . . . 89
7.6.3 Communications Subsystem Design Overview . . . 90
7.6.4 Sizing Method and Results. . . . 92
7.6.5 Calculation Verification . . . 93
7.7 Thermal Control . . . 93
7.7.1 Subsystem Level Requirements . . . 94
7.7.2 Thermal Control Subsystem Design Overview . . . 94
7.7.3 Sizing Method and Results. . . . 96
7.7.4 Verification and Sensitivity Analysis . . . 97
7.8 Navigation . . . 98
7.8.1 Local Navigation Pseudolite System . . . 98
7.8.2 Virtual Landing & Takeoff Strip . . . 101
7.8.3 Navigation Overview . . . 101
7.9 Command & Data Handling . . . 102
7.9.1 Data Volumes and Subsystem Requirements. . . . 102
7.9.2 UAV CDH Overview . . . 104
7.9.3 Base Station CDH Overview . . . 105

8 Future Development **106**
8.1 Project Design & Development Logic . . . 106
8.2 Work Breakdown Structure . . . 107
8.3 Project Gantt chart . . . 109
8.4 Verification and Validation of MARS . . . 111

9 Cost Analysis **112**
9.1 Cost Breakdown . . . 112
9.2 Cost over the years . . . 116
9.3 Funding . . . 116

10 Sustainability **117**
10.1 Implementation in Design . . . 117
10.1.1 Subsystems . . . 117
10.1.2 Environment . . . 117
10.1.3 Existing Systems . . . 117
10.1.4 Reusability . . . 117
10.2 Contribution to Sustainability . . . 118

11 Conclusion **119**

12 Recommendations **120**

Bibliography **122**

A Functional Flow Diagrams **125**

B Martian Environment **131**
B.1 Atmospheric Properties . . . 131
B.2 External Events . . . 131

C Task Division **133**

Nomenclature

Acronyms

AVL	Athena Vortex Lattice
BER	Bit Error Rate
BOL	Begin Of Life
BSH	Battery Supercapacitor Hybrid
CBE	Current Best Estimate
CDH	Command and Data Handling
CFD	Computational Fluid Dynamics
CTE	Coefficient of Thermal Expansion
DOD	Depth Of Discharge
DSN	Deep Space Network
EDL	Entry, Descent and Landing
EIRP	Equivalent Isotropically Radiated Power
ELT	Electra Lite Transceiver
EMS	Electronic Management System
EOL	End Of Life
EPS	Electrical Power System
ESA	European Space Agency
FBD	Functional Breakdown Diagram
FFD	Functional Flow Diagram
FY	Fiscal Year
GPS	Global Positioning System
GS	Ground Station
HGA	High Gain Antenna
HK	House Keeping data
IMU	Inertial Measurement Unit
IR	Infrared
ISO	International Organisation for Standardisation
LE	Leading Edge
LEO	Low-Earth Orbit
LGA	Low Gain Antenna
LNPS	Local Navigation Pseudolite System
MARS	Martian Advanced Reconnaissance System
MEV	Maximum Expected Value
MIPS	Million Instructions per Second
mps	Measurements per Second
MRN	Mars Relay Network
MRO	Mars Reconnaissance Orbiter
MSL	Mars Science Laboratory
MSSS	Malin Space Science Systems
NASA	National Aeronautics and Space Administration
NCA	Lithium Nickel Cobalt Aluminium Oxide
NE	North-Eastern
RAM	Random Access Memory
RAMS	Reliability, Availability, Maintainability, Safety
ROI	Return Of Investment
RTG	Radioisotope Thermal Generator
SBC	Single Board Computers
SDST	Small Deep Space Transponder
SSDR	Solid State Driver Recorder
SSPA	Solid State Power Amplifier
STP	Segmentation Targeting Positioning
SWOT	Strength Weakness Opportunities
TCS	Thermal Control Subsystem
TOW	Take-Off Weight
TRL	Techology Readiness Level
UAV	Unmanned Aerial Vehicle
UHF	Ultra High Frequency
VITAS	Visual imaging, Ice deposit scanning, Trace gas detection, Atmospheric conditions & Soil analysis
WBS	Work Breakdown Structure

Greek Symbols

α	Angle of attack	[°]
α_{surf}	Surface absorptivity	[–]
ϵ	Downwash	[m/s]

ϵ_{box}	Box coating emissivity	[–]
ϵ_{surf}	Surface emissivity	[–]
$\mathrm{H}_{\text{blocked}}$	Sunlight blocked	[°C]
η_{panel}	Solar panel efficiency	[–]
η_{wiring}	Wiring efficiency	[–]
λ	Failure rate	[yr $^{-1}$]
λ_p	Peukert's constant	[–]
λ_{best}	Best case scenario failure rate	[yr $^{-1}$]
λ_{worst}	Worst case scenario failure rate	[yr $^{-1}$]
μ	Dynamic viscosity	[Pa×s]
ρ_{mat}	Material density	[kg/m^3]
ρ_{panel}	Specific solar panel density	[kg/W]
σ	Boltzmann constant	[m^2 kg/(s^2 K)]
σ	Boltzmann constant	[m^2 kg/(s^2 K)]
σ_0	Initial material strength	[Pa]
σ_y	Yield strength	[Pa]
σ_{fat}	Fatigue strength	[Pa]
σ_{tens}	Tensile strength	[Pa]

Roman Symbols

$\bar{c}$	Chord length	[m]
$\overline{x_{ac}}$	Aerodynamic centre location from the leading edge	[m]
$\overline{x_{cg}}$	Centre of gravity location from the leading edge	[m]
$\overline{x_{np}}$	Neutral point location from the leading edge	[m]
a	Degradation factor	[-]
A_{box}	Box surface area	[m^2]
A_{exp}	Exposed area	[m^2]
A_{rad}	Radiator area	[m^2]
A_{surf}	Surface area	[m^2]
A_{sys}	System Availability	[–]
C	Charging capacity	[C]
C_D	Drag coefficient of 3D wing	[–]
C_d	Drag coefficient of 2D airfoil	[–]
C_f	Friction coefficient	[–]
C_L	Lift coefficient of 3D wing	[–]
C_l	Lift coefficient of 2D airfoil	[–]
C_m	Moment coefficient of 2D airfoil	[–]
C_P	Power coefficient	[–]
C_T	Thrust coefficient	[–]
C_{D_0}	Induced drag coefficient	[–]
C_{L_0}	Lift coefficient at zero angle of attack	[–]
C_{l_α}	Airfoil lift coefficient gradient	[–]
$C_{l_{\alpha_h}}$	Tail lift coefficient gradient	[–]
C_{l_α}	Main wing lift coefficient gradient	[–]
$C_{l_{\text{des}}}$	Designed lift coefficient of 2D airfoil	[–]
$C_{L_{\max}}$	Maximum lift coefficient of 3D wing	[–]
$C_{L_{A-h}}$	Lift coefficient of main wing	[–]
$C_{M_{ac}}$	Moment coefficient around aerodynamic chord	[–]
D	Drag	[N]
d_c	Distance from center of gravity to canard	[m]
d_p	Distance from center of gravity to propeller	[m]
d_w	Distance from center of gravity to wing	[m]
D_{tx}	Transmission range	[m]
D_r	Flight range	[m]
DR	Data rate	[bps]
E	E modulus	[Pa]
e	Oswald efficiency factor	[-]
E_b/N_0	Energy per bit to noise power spectral density ratio	[dB]
E_{tot}	Total energy required	[J]
f	Correction factor	[-]
F_{canard}	Force originating from canard	[N]
f_{tx}	Transmitting frequency	[Hz]
F_{wing}	Force originating from wing	[N]
g	Gravitational acceleration	[m/s^2]
g_{Earth}	Gravitational acceleration on Earth	[m/s^2]
g_{Mars}	Gravitational acceleration on Mars	[m/s^2]
G_r	Receiver gain	[dB]
H	Rated discharge time	[s]

h_c	Cruise altitude	[m]
I_{C}	Charging current	[A]
J	Advance ratio	[–]
k	Peukert's constant	[s]
k_i	Correction factor for rotor power	[m/s]
L	Lift	[N]
L/D	Lift to drag ratio	[–]
l_h	Distance from center of gravity to tail	[m]
l_w	Wiring length	[m]
L_{pr}	Precipitation losses	[dB]
L_a	Atmospheric losses	[dB]
L_r	Receiver losses	[dB]
L_s	Free space losses	[dB]
L_t	Transmitter losses	[dB]
m	Mass	[kg]
m_{coating}	Insulation mass	[kg]
$m_{\text{design}_{\text{Mars}}}$	Mass of system on Mars	[kg]
m_{panels}	Solar panel mass	[kg]
$m_{\text{propulsion}}$	Propulsion unit mass	[kg]
m_{prop}	Propulsion subsystem mass	[kg]
m_{rad}	Radiator mass	[kg]
m_{TCS}	Thermal control subsystem mass	[kg]
n	Rotations per second	[Hz]
P	Power	[W]
P_{c}	Cruise power	[W]
P_{hover}	Hover power	[W]
P_{req}	Power required	[W]
P_{TO}	Take-off power	[W]
P_t	Transmitting power	[W]
q	Dynamic pressure	[Pa]
$Q_{\text{diss,box}}$	Power dissipated inside of thermal box	[W]
Q_{diss}	Power dissipated outside of thermal box	[W]
Q_{in}	Heat flowing in	[W]
$Q_{\text{IR,in}}$	IR heat flowing from the outside structure	[W]
$q_{\text{IR,in}}$	Infrared flux of outside structure	[W/m^2]

$Q_{\text{IR,Mars}}$	IR heat incoming from the surface of Mars	[W]
q_{IR}	Infrared flux of Mars	[W/m^2]
Q_{out}	Heat flowing out	[W]
Q_{rad}	Power output of radiator	[W]
Q_{sun}	Heat incoming from the Sun	[W]
q_{sun}	Solar flux	[W/m^2]
R_{sys}	System reliability	[–]
Re	Reynold's number	[–]
Re_{c}	Cruise Reynold's number	[–]
Re_{red}	Reference Reynold's number	[–]
S	Wing surface area	[m^2]
S_b	Propeller blade surface area	[m^2]
S_d	Rotor disk area	[m^2]
S_h	Tail surface area	[m^2]
S_{ref}	Reference wing surface area	[m^2]
S_{wet}	Wet wing surface area	[m^2]
T	Thrust	[N]
t/c	Thickness to chord ratio	[–]
t_c	Charging time	[s]
T_{box}	Thermal box temperature	[K]
t_{op}	Operating time	[yr]
T_{out}	Outside temperature of the UAV/base station	[K]
T_{sys}	System noise temperature	[K]
td	Discharge time	[s]
V_c	Climb velocity	[m/s]
V_i	Induced velocity	[m/s]
V_t	Tip velocity	[m/s]
V_h	Velocity at horizontal tail	[m/s]
V_i	Induced velocity	[m/s]
W/S	Wing loading	[–]
x_{max}	Maximum value in the data set	[–]
x_{min}	Minimum value in the data set	[–]
x_{norm}	Normalised value	[–]
x_{ori}	Original value; to be normalised	[–]

1 Introduction

After twelve humans have walked on the moon, mankind is now looking forward to making another giant leap by putting humans on Mars. Several organisations, both private and governmental, are already planning this journey within the coming two decades. However, before sending a human to Mars, it is crucial that the possible habitat and science zones are identified beforehand. Detailed information is required on the landing site and the exploration zone surrounding it in order to map the human habitat zone and the science regions surrounding it. The Martian Advanced Reconnaissance System (MARS) aims to perform this identification and thereby assist in the future colonisation of Mars.

No aerial vehicle has ever flown on Mars, however there are plans to do so in the near future. On 11 May 2018, NASA published an article on their website showing a design for an autonomous Mars Helicopter to accompany the Mars 2020 rover. According to NASA, the Mars Helicopter aims 'to demonstrate the viability and potential of heavier-than-air vehicles on the Red Planet'.[1] Although this will be the first aerial vehicle on Mars, its capabilities are limited. It has a maximum range of 600 m, at a total mass of 1.8 kg. For an extensive exploration of a large exploration zone, these specifications are not nearly sufficient.

The main goal of this report is to provide a design study on an autonomous Unmanned Aerial Vehicle (UAV) on Mars that will map an exploration zone with a diameter of 49 km. The UAV will map ice deposits, analyse the soil, perform visual imaging and measure atmospheric conditions. Another top-level requirement is to focus on implementing a sustainable design. At last, as no extensive cost analyses have been performed on long range unmanned aircraft on Mars, one will be performed.

After performing extensive research on the Martian environment, different concepts were considered from which one came out to be the best after a trade-off. This concept was then developed further and optimised for the MARS mission. A preliminary study was performed in this report. The first step was to look into statistical data of existing UAVs and current Mars rovers. Next, subsystems were developed for which manufacturer data was conferred. E.g. for the electrical power subsystem, battery manufacturers were consulted to be up to date with current and near-feature technology.

A preliminary aerodynamics study was performed for which panel methods and vortex lattice methods were used. Actual Computational Fluid Dynamics (CFD) analysis was not performed due to the limited time scope of the project. A preliminary structural analysis was executed with the use of ANSYS and the UAV was sized through Athena Vortex Lattice (AVL) and verified through XFLR5, with the configuration being chosen through a trade-off.

The launcher and entry systems were investigated and assessed to determine the optimal choice. The size, mass and vibrational constraints imposed by the chosen system were accounted for. It was also briefly looked into the optimal launch window and transfer trajectory, but an extensive astrodynamics study was beyond the scope of the report.

In Chapter 2 the mission objective is discussed, giving insight in the background of this mission. Next, in Chapter 3 the market analysis is covered, in which the market is segmented, the stakeholders are identified and a sustainable development strategy is set up. The mission architecture is set in Chapter 4, where the mission phases, schedule, launch and entry vehicle and the landing site are discussed. With the outlines of the mission set, different concepts could be considered. The concept analysis, including driving requirement and possible mission concepts, as well as a trade-off for the optimal concept are presented in Chapter 5. Further elaboration on the optimal concept is provided in Chapter 6, where a MARS system overview and its components are presented. The subsystem design for MARS is documented in Chapter 7. The future developments of this project are evaluated in Chapter 8. This includes both organisational and engineering development. In Chapter 9, a cost analysis is performed, both in 2018 current dollars and 2026 dollars. Fiscal year 2026 has been included as that is the launch date. Having knowledge of the inflation in the upcoming years might be useful during later stages of the project. Furthermore, the cost divided over the years of the project is presented as well. Finally, the sustainable development strategy implementation is presented in Chapter 10. The report ends with a conclusion in Chapter 11 and further recommendations in Chapter 12.

[1]URL: `https://www.jpl.nasa.gov/news/news.php?feature=7121` [Cited 20 June 2018]

2
Mission Objective

Before going into the design, a brief introduction to the mission is presented by considering the mission's objectives and long-term goals. In Section 2.1, the motivation to perform the mission is documented, while in Section 2.2 the mission concept is discussed. Lastly, in Section 2.3 the objectives of the scientific mission are listed.

2.1. The Need for an Aerial Mars System

In order to prepare for future manned missions to Mars, it is first required to analyse what the possible human habitat zones are. Therefore the mission firstly includes investigating a possible human habitat zone, followed by further inspection of the scientific regions of interest.

Different machinery was considered for this task. Satellites were an option due to the width of the regions they can analyse, however, more detailed information is sought after. On the opposite side of the spectrum, rovers provide very detailed data, but are significantly limited by the area they can cover and suffer due to obstacles present on the Martian surface. Therefore, it was decided to go for something in between: an autonomous flying drone, which can cover a much wider area than a rover and provide much more detailed data than a satellite.

After knowing the goal of the scientific mission and having a rough idea of its architecture, the following statements were defined:

- **Mission Need Statement:** *Humanity should investigate habitable zones and regions of scientific interest on Mars in order to prepare for future manned missions.*
- **Mission Statement:** *Project MARS will develop a system to collect detailed atmospheric and geological information in order to support the identification and mapping of scientific exploration zones on Mars by 2030.*
- **Project Objective Statement:** *Design an autonomous UAV that can be used to map and analyse Martian regions of scientific interest and aid in the exploration of Martian human habitat zones, by 9 students in 10 weeks.*

2.2. Mission Concept

Due to the unique character of the mission it is crucial to analyse the opportunities presented by this UAV. Never before has there been an UAV over the surface of Mars and thus this mission clearly differentiates itself from previous rover and satellite missions. The UAV being the midpoint between rover and satellite gives it certain advantages with respect to both. Looking into the advantages that an aerial vehicle offers, two distinct mission profiles present themselves.

Firstly, it is possible to see the aerial aspect of the vehicle solely as a way of transport, namely as a way to transport a certain payload from point A to point B. The advantages are that large distances can be covered between experiments/observations and they are all performed on the ground, leading to a greater accuracy. The main disadvantage affect the reliability. The UAV would have to land for every measurement. This would put large constraints on the design of the UAV due to increased weight of the landing mechanism and increased capability of the flight computer. The second way to view the opportunities that an aerial vehicle offers is to see it as a way of continuous observation. In this way, the vehicle does not require to land to perform the observations and thus the coverage and reliability of the mission is highly increased. These advantages come at the cost of accuracy, as no contact with the surface is made to perform the measurements.

Considering the advantages and disadvantages discussed above, seeing the aerial aspect of the mission as a way of observation offers more advantages. Not only will the mission be more reliable and cover more ground, the time required to perform its mission will also be reduced as the observations do not require landing and are continuously performed. Taking all this into consideration the decision was made to use the UAV solely for observation and not for scientific transport as it would constrain the design in terms of weight, range and reliability.

2.3. Mission Task Requirements

The system shall provide visual, topological and soil data on the region of interest and perform an analysis of the lower atmosphere according to the requirements shown in Table 2.1. Most of the tasks, such as visual mapping, height mapping, mapping of shallow ice deposits and soil composition analysis are done on the UAV itself while it is flying over the Martian surface. The tasks that are performed on the base station are tasks that do not need relocation of the instruments, but to take year round measurements from the same spot.

Table 2.1: Overview of the requirements of the tasks

<table>
<tr><th colspan="2">Mission</th><th>Requirement</th></tr>
<tr><td rowspan="4">UAV</td><td>Visual imaging</td><td>Visual imaging shall be done with a resolution of 10 cm.</td></tr>
<tr><td>Height mapping</td><td>Height mapping shall be done with a 15 cm resolution at a 10 cm height accuracy.</td></tr>
<tr><td>Shallow ground ice deposits</td><td>Shallow ice deposits shall be detected at a depth of 10 m with an accuracy of 10 cm every 1 m.</td></tr>
<tr><td>Soil Composition</td><td>The soil composition shall be determined by hyperspectral imaging with a resolution of 1 m.</td></tr>
<tr><td rowspan="2">Base Station</td><td>Dust Composition and size</td><td rowspan="2">The system shall measure the atmospheric conditions in the lower atmosphere (wind speeds, precipitations, and dust composition and size distribution).</td></tr>
<tr><td>Wind speeds and precipitation</td></tr>
</table>

3 Market Analysis

A market analysis was done in order to establish the product's position in the market. First, the current market was analysed through the macroenvironment and the microenvironment which are elaborated upon in Section 3.1 and Section 3.2 respectively. Next, a strengths, weaknesses, opportunities and threats (SWOT) analysis is presented in Section 3.3 based on the macro- and microenvironment. Furthermore, an segmentation, targeting and positioning (STP) analysis has been performed, which can be found in Section 3.4. Aftwards in Section 3.5 the stakeholders are identified and in Section 3.6, the investigation into barriers that have to be overcome are presented. At last, in Section 3.7 the sustainability strategy is presented.

3.1. Macroenvironment

First, the macroenvironment was analysed, which includes social trends, technological features, political environment and the economic situation of the current market.

- **Social Trends:** Green marketing is an uprising trend that involves a strategic effort by firms to supply customers with environmentally friendly merchandise [Grewal and Levy, 2008, p. 101].
  There is demand for green-oriented products, a value that can be added to the project to distinct it from others by making the project reusable.
  Furthermore, space exploration is becoming more popular nowadays with, for example, space tourism and SpaceX performing innovative experiments.
- **Technological:** Technology has been advancing at a very fast pace in the last decades. For each new project in space exploration, more efficient and sustainable materials, engines etc. are used. Research can be done if any new developments are upcoming and can be implemented into the Mars Advanced Reconnaissance System. Examples would be to use more efficient engines or implementing a more cost-efficient camera.
- **Economic situation:** It is important to know the economic situation of involved countries when working on a space project, as it affects the financial situation. Important parameters are the inflation of the involved currencies, but also the exchange rates between them [Grewal and Levy, 2008, p. 105]. For example, if a Norwegian company cooperates with ESA on a certain space mission, it is important to know the exchange rate between the Euro and the Norwegian Krone.
- **Political:** The political environment requires companies to adhere to certain legislation and laws. They should be aware of any legislation concerning fair competition and customer protection, but also industry-specific laws [Grewal and Levy, 2008, p. 106]. The MARS group should take into the ISO-requirements, which is standard in every branch of industry.

3.2. Microenvironment

The microenvironment consists out of the 3Cs: category, company and consumers. In this section the categories belonging to the product are elaborated. It is also looked into how the company can compete with competitors and who the potential consumers are .

- **Category:** The MARS project is classified in the space exploration category, which is booming exponentially. Last year, \$3.9 billion[1] was invested into private companies. This big rise does not only result in more profit but also in more competitors. Currently, it is mainly dominated by some government and private companies such as NASA, ESA and SpaceX.
- **Company:** It is important to know the dominant and uprising competitors in the current market. The competitors consist of direct competitors and indirect competitors. An example of a direct competitor is SpaceX, as the private company is investigating manned space missions to Mars and trying to set up a human habitat. Indirect competitors are space companies who focus on the development of satellites or space tourism as these companies can also take away funds from the project.
  Competitors such as SpaceX can be used as primary examples on how to position a company in the space industry. Furthermore, other competitors should be kept in close vicinity such as Orbital Sciences, Sierra Nevada Corporation, Virgin Galactic, Xcor Aerospace and many other uprising space companies. No joint ventures are

[1] URL: `https://www.cnbc.com/2018/01/18/space-companies-got-3-point-9-billion-in-venture-capital-last-year-report.html` [Cited 3 May 2018]

set up yet as the company is rather new. The competition is fierce and setting up a collaboration might be necessary to be able to compete in the market. One could for example set up a collaboration with SpaceX such that the closest competitor becomes a partner.

- **Consumers:** Some of the competitors can also be used as stakeholders depending on how the MARS group wants to position itself in the market. This will be elaborated upon more in depth in Section 3.4.3.

3.3. Strength, Weakness, Opportunity and Threat Analysis

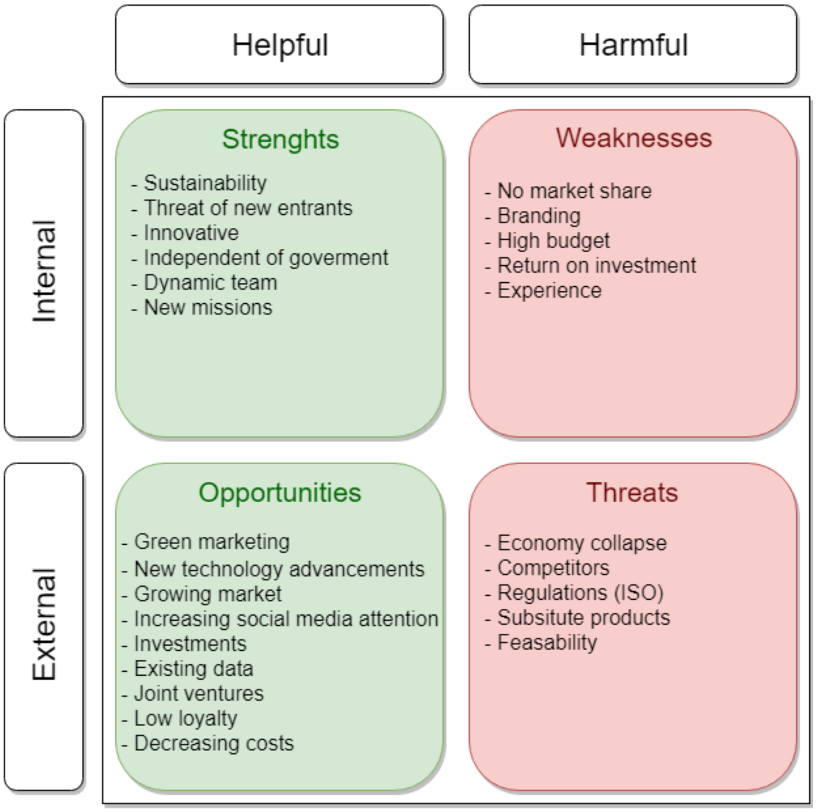

Figure 3.1: SWOT-analysis of the MARS project

The strengths, weaknesses, opportunities and threats (SWOT) for the mission of the MARS have been identified. A breakdown of the SWOT-analysis is given in the following sections.

3.3.1. Strengths

One of the main strengths of the MARS mission is that it aims at sustainability of the mission. For instance, VITAS and the base station shall be recyclable and/or reusable after mission. A more in depth analysis of the sustainability is given in Section 3.7. Furthermore, setting up an interplanetary human habitat is novel. Investors are interested by it and many other new entrants may see its potential. Each year the amount of investments is rising in this branch of the space industry[2], which allows for independency of the government. Novel concepts are also implemented into the project and the team is dynamic. New technology can not only be used as an advantage to attract investors, but it can also be used as a product that can be sold to other companies.

3.3.2. Weaknesses

Currently, as VITAS is the first project for the MARS group, no market share has been acquired yet. This leads to having to make more effort in branding, in order to get the attention of investors and companies. Another weakness arising due this being the first mission is the engineers having no experience in designing a mission of this scale. Being the first one to do so, complicates things even more. Next to that, the mission is expensive. The risk of losing money is a possibility and risk mitigation will have to be performed during the cost analysis to minimise potential losses.

[2] URL: `https://www.cnbc.com/2018/01/18/space-companies-got-3-point-9-billion-in-venture-capital-last-year-report.html` [Cited 8 June 2018]

3.3.3. Opportunities

As identified earlier in Section 3.1, green marketing is an upcoming social trend. Investigation shall be done to define which implementations can add more value than cost. New technology advancements are upcoming, e.g. for power storage, specifications of batteries keep improving and it is expected that the lithium-sulphur batteries will provide for an energy density of 500 Wh/kg[3], which is double that of current battery technology. MARS can also look into joint ventures. Splitting costs of the project to reduce costs and gain more media attention by working together with NASA for example.
With the recent Mars Helicopter, more companies might be interested in developing a UAV that fly on Mars, data and technology can be shared.

3.3.4. Threats

The fact that more companies are interested in the development of an UAV instead of a rover is also a threat. If an opposing project is more beneficial to investors, they can lose interest in VITAS. Furthermore, the mission has to comply with the regulations of space missions, such as those set by the International Organisation for Standardisation (ISO). As it is a novel concept in space, a relatively low reliability is expected for it. With a lot of money being involved, potential shareholders might be anxious to invest.
At last, substitute products might be developed such as a telescope which can finely map the surface of Mars from Earth.

3.4. Segmentation, Targeting and Positioning Analysis

In the STP-analysis, the SWOT-analysis, microenvironment and macroenvironment were put into practice to segment the current market, which allows to target the market that was considered to be the most profitable for the project and how to position the MARS into the market effectively.

3.4.1. Segmentation

The segmentation is split up in two parts, first, the objectives and strategy of the company are set. These have to be consistent with the mission and objectives that have to fulfilled, as well as the SWOT- and environment-analysis. Next, the segments are described.

Objectives and Strategy

In the space industry, a project should attain a return of investment (ROI) of at least 15%. A projected is recognised as too risky if the prospected Internal Rate of Return (IRR) is lower [Wertz and Larson, 1999, p.325]. The business strategy to attain such a ROI is to work together with private and/or government companies. The goal is to have funds for the project and have technical assistance. As the MARS company has no real capital yet, dividends will not be used as investment method; equity funding is the safer option. Analysed Investment methods are discussed in Chapter 9.

Segments

The space market industry had a value of $345.5 billion in 2016[4] and is expected to increase by 4.1% each year. However, the space industry has many branches such as deep space probes or satellites orbiting Earth, which are not a part the category VITAS competes in. Ergo, a more in depth analysis of the space industry was performed. In Figure 3.2[5] the segmentation of the space industry can be observed. In Section 3.4.2, these will be further elaborated upon.

[3]URL: `https://oxisenergy.com/products/` [Cited 12 June 2018]
[4]URL: `https://www.statista.com/statistics/662249/space-industry-volume-worldwide/` [Cited 7 June 2018]
[5]URL: `https://www.industry.gov.au/industry/IndustrySectors/space/Documents/BRYCE-Australia-Global-Space-Industry-Dynamics-Paper.pdf` [Cited 7 June 2018]

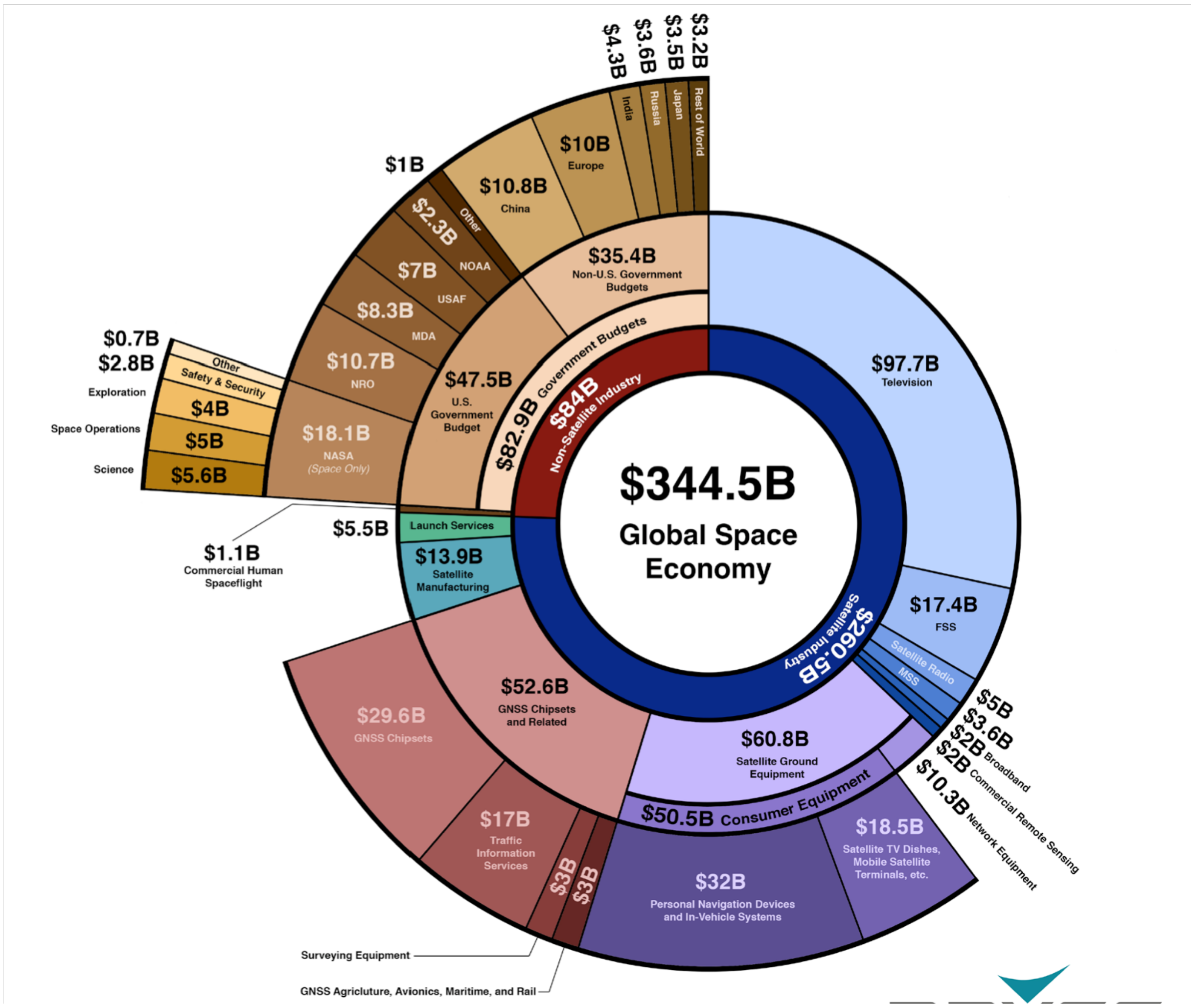

Figure 3.2: The different branches of the space industry [5]

3.4.2. Target Market

The focus was be mainly laid upon companies whom are interested in creating a Martian habitat in the upcoming years. Multiple companies have shown interest and have preliminary plans to put humans on Mars such as Boeing, Blue Origin, SpaceX, Mars One and NASA[5]. Additionally, there are some other branches in the space industry where profit could be gained. The target markets with the according market values are shown in Table 3.1[5] [6] [7]

Table 3.1: Target markets for the MARS project [5] [6] [7]

Branch	Companies/Organisations	Market value [billion $]	Market share [%]
Human habitat on Mars	NASA, Mars One, SpaceX, Boeing	6	1.7
Science	NASA, SpaceX, Boeing	5.6	1.6

It can be seen that the two main target markets, the science branch and human habitation on Mars, do not have a high market value/share yet as well as the other two. This is mainly because spaceflight costs a lot of money and space companies are scared to allocate money into the project as it is assumed the technology has not arrived yet to develop a manned mission to Mars with a high reliability. Furthermore, it should be noted that for the science branch, every company that is interested in using innovative technology, applied in the MARS project, can be a potential customer. NASA, SpaceX and Boeing were put as main customers in this section as it is most likely these companies can benefit the most. However, other companies outside of the space industry should not be excluded. Currently, the 5.6$B is only the science branch of NASA (which is 30.9% of the total capital of NASA). The actual budget for this category is higher.

[6]URL: `http://curious.astro.cornell.edu/ask-a-question/150-people-in-astronomy/space-exploration-and-astronauts/general-questions/921-how-much-money-is-spent-on-space-exploration-intermediate` [Cited 7 June 2018]

[7]URL:`https://science.house.gov/sites/republicans.science.house.gov/files/documents/TheFutureofSpaceCommercializationFinal.pdf` [Cited 7 June 2018]

3.4.3. Positioning

As the mission is expensive and the MARS group's first project, it was concluded that the entire system will be sold. The advantage of selling the system, is that a capital has been raised and a potential second project can be set up immediately. By merely selling the data, a capital will be raised over a longer time span, which might delay future processes, as the MARS group will be in debt.

To get recognition of other space companies and stakeholders, the MARS team will have to carry out public outreach. The MARS can provide for fine mapping, location of ice deposits etc. over a relatively long range as mentioned in Chapter 4. Particularly, the range is an added value compared to the mars rovers. The added value should be examined and quantified. The cost of the mission shall not exceed the value of it, which will be further analysed in Chapter 9. The sustainable aspect of the system should also not be overlooked. It will increase the cost but it does add value as well and may attract the attention of investors. It is believed a manned mission to Mars will cost about $ 6-100 billion depending on the scale of the project[8] [9].

3.5. Identifying Stakeholders

Having performed an STP-analysis, the potential stakeholders can be identified,

- Customers
  - Customers
  - Private & government lead space agencies
  - Future manned mission design teams
  - Future mars explorers
- Service providers
  - Launcher and entry vehicle providers/builders
  - Software development companies
  - Electronics manufacturers
  - Mission control
  - Critical technology development
  - Scientific instrument manufacturers
  - Manufacturing companies
  - Software development companies
  - Communication satellite design/control team
  - Social media companies
  - Research and testing facilities
- Financiers
  - Banks
  - Sponsors
  - Investors
- Goverment parties
  - Mission approval committee(s)
  - United nations
  - Regulatory instances
  - Environmental organisations on earth
  - Office of Planetary Protection
- Communities
  - Academia
  - Scientific community

The stakeholders can be subdivided into five different groups. The customers who are interested in the product, the service providers who will have to be hired to bring the design on the market. Furthermore, the financiers which include sponsors and investors that have to be acquired to collect money to be able to develop the design. Next to that, the MARS team has to take into account regulations of government parties. At last, results could be shared with academia as the gathered data will prove useful for future research and scientific developments.

3.6. Barriers

Hazards such as threats and weaknesses were identified in Section 3.3. The following measures can be taken during the early design stages to reduce these hazards.

- Set up a joint venture to decrease cost risk;
- Reach out to the media about the project to increase attention;
- Try to avoid the use of technology with a low technology rediness level (TRL);
- Attract angel investors to cover for the lack of experience;
- Make the system reusable to distinguish the project from others.

In the end, it is important to make a profit. First, one has to know how much the project costs, which will be presented in Chapter 9.

[8]URL: https://www.mars-one.com/faq/finance-and-feasibility/what-is-mars-ones-mission-budget[Cited 7 June 2018]
[9]URL: https://www.space.com/16918-nasa-mars-human-spaceflight-goals.html[Cited 7 June 2018]

3.7. Sustainable Development Strategy

With more and more environment-related restrictions being put on companies, the implementation of sustainable processes and designs is becoming more and more apparent. Furthermore, the MARS team believes that the aerospace industry carries a moral responsibility in sustainability because often it is seen that aerospace inventions seep through into the daily lives of people.

Therefore, design for lean manufacturing could be further expanded to not only reduce waste in the form of costs to the company but also costs to the environment and ultimately, the tax-payers' money. On the other hand, aerospace applications often require not so environment-friendly measures (think launch vehicles, rare-earth materials in satellites, etc.) and those are employed because an alternative rarely exists.

First, it is important to identify mission relevant sustainability factors. As a second step, aspects of a mission that are bad for the environment and can not be changed and those that can be circumvented by applying a different design philosophy should be identified. A trade-off should be made by weighing off the different factors.

Project MARS has implemented a design philosophy to minimise its environmental impact not only during operation but over the whole life cycle of the system; from manufacturing to performing the mission to recycling the system after the mission has ended.

3.7.1. Method to Measure Sustainability

It is difficult to measure which material or operation is more sustainable due to the type of impact varying heavily over the different methods, as such the goal is to compare the alternatives with each other as efficiently as possible to be able to opt for the correct design choice.
A life cycle assessment was performed where all the alternatives will be measured and compared in four steps [Harvard, 2007].

1. **Goal definition and scoping**: Research is done to what the MARS team means to accomplish and how it is attained. For example, which materials, manufacturing methods can be used etc.
2. **Inventory assessment**: The purpose is to identify opportunities to reduce waste through a cradle-to-cradle analysis. This involves raw materials and energy acquisition, manufacturing, transportation, useful life and EOL (reuse and recycle).
3. **Impact assessment**: In the inventory assessment, the values are measured but it is not known how environmentally impactful they are and how the values compare with each other. This is done in the impact assessment. It is measured how much harm e.g. an emission does through an environmental impact assessment. The weights are measured through fixed point scoring, which ranks the weights from 1 (severe negative impact) to 5 (severe positive impact), allowing for easy summation.
4. **Improvement assessment**: The aim is to develop strategies to improve the product or production process. The MARS team will look at future strategies that can be implemented to improve environmental benefits with their expected implementation costs.

3.7.2. Objectives

Sustainability can be split up in three different disciplines, which is represented in Figure 3.3. In this report, mainly the environmental and economics sections will be elaborated upon. However, the ISO-requirements, which belong in the overlap of the environmental and social section are also taken into account. The objectives for the sustainability aspect of the project are:

- Emissions/pollution should be minimised during manufacturing process
- Use of toxic and hazardous materials should be minimised
- The system should be reusable
- Materials used should be cost-efficient
- The system should comply with the ISO-regulations and exceed them where possible
- Transportation should be minimised during the project
- Emissions should be kept minimal during transportation
- Emissions should be minimised during useful life

The preceding methodology is applied during the design of the project and results are presented in Chapter 10.

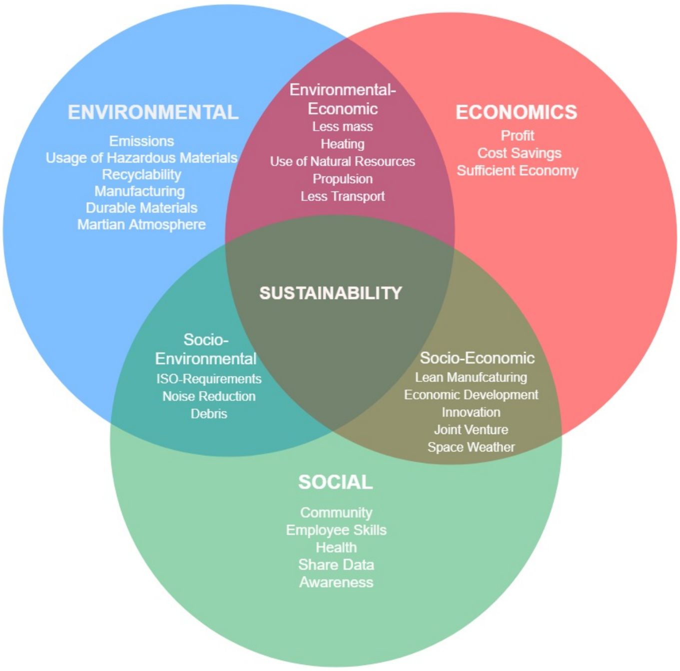

Figure 3.3: Venn-diagram representing the sustainability aspects of the project

4
Mission Architecture

Having introduced the mission and presented a market analysis, it is now worth looking into the mission architecture. In Section 4.1, the different phases of the mission are discussed, followed by Section 4.2, where the planned schedule can be seen. Following, the launch and entry vehicle are selected in Section 4.3. Having selected the relevant vehicles, Section 4.4 documents the strategy of getting to Mars. Lastly, in Section 4.5, the possible landing sites are assessed and the optimal is chosen.

4.1. Scientific Mission Phases

The basic layout of the scientific mission has been defined in two main phases. A schematic overview of each flight of these phases can be seen in Figure 4.1.

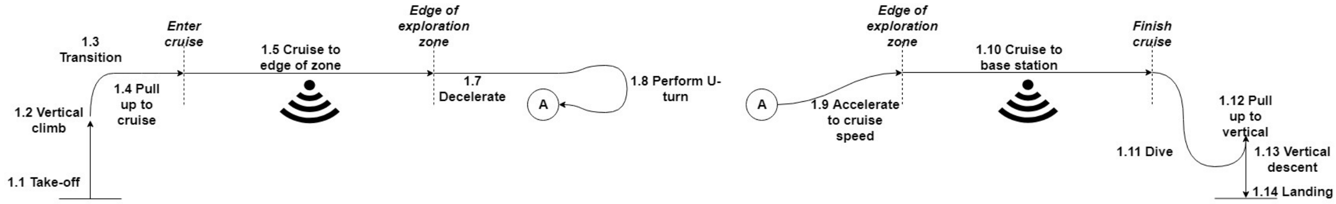

(a) Overview of the hub-spoke phase of the mission

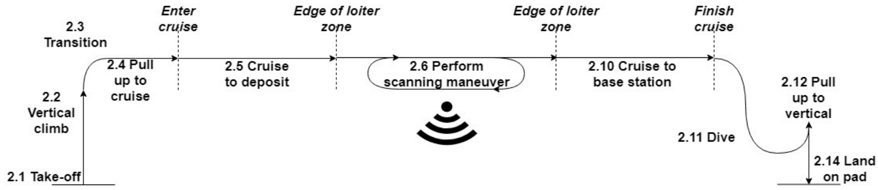

(b) Overview of the loiter phase of the mission

Figure 4.1: A schematic overview of the two planned mission phases

In the first phase, the UAV will repeatedly travel from the base station to the edge of the exploration zone, while scanning and mapping the area it flies over. When it reaches the edge of the exploration zone, it will make a turn, after which it re-enters the exploration zone such that the new scanning area is adjacent to the finished area at the edge of the zone. It then returns its landing platform, where the gathered data is transferred to the base station and the UAV can recharge. This "hub-spoke" flight pattern is repeated until the complete exploration zone has been covered. This method of scanning the complete zone means that areas near the base station will be explored in more detail, as the scanning areas will have significant overlap. Combined with the fact that not all scientific instruments can perform measurements on an equally large area (especially the ice scanner has a very narrow beam), a second mission phase will be necessary for mapping the complete zone to a sufficient level of detail.

The second mission phase consists of a set of targeted flights. Using the information gathered during the first phase, a number of "areas of interest" can be defined. An example is an area where a relatively large amount of ice has been detected nearby, and it is required to know what the exact shape and size of the total ice deposit(s) is/are. The UAV will then fly to the area of interest, where it will loiter over the area for more detailed analysis. It will do this until the complete area has been covered or the battery level becomes dangerously low, after which it will return to the base station to transfer the data and recharge. This phase ends when the entire exploration zone has been mapped to a sufficient level of detail, which will also marks the end of the mission.

4.2. Mission Schedule

The schedule of the mission is as follows:

- **November, 2026:** Take-off from Earth, begin interplanetary journey. Following the Mars launch windows and performing a Hohmann transfer, the expected duration is eight months.
- **June, 2027:** Reach Mars, perform Entry, Descent & Landing (EDL), deploy and prepare to initiate phase 1. It is expected that subsystem calibration, establishing communication and performing system health tests will take up to two weeks.
- **July, 2027:** Begin phase 1 of scientific mission. An average of 0.75 daily flights results in 1028 sols to perform the 770 flights. Therefore, the duration of this phase is 36 months.
- **July, 2030:** Begin phase 2 of scientific mission. As the system is expected to conclude its scientific mission by 2030, the expected maximum duration is the remaining five months.
- **December, 2030:** Planned end of nominal scientific tasks. Land and prepare for reuse.

Only 0.75 flights per day can be performed on average as the solar intensity is too low during winter. The size of the solar panels could not be further increased due to the size constraint of the base station, which is set by the EDL capsule. This is calculated in Section 7.5.

4.3. Launcher & Entry Vehicle Selection

The launcher and entry vehicle choices are discussed in this section. In Section 4.3.1, the selected launch vehicle is discussed. Afterwards, an overview of the entry vehicle for the mission is provided in Section 4.3.2.

4.3.1. Launch Vehicle

The considered launchers and the parameters used for the trade-off procedure are presented in Table 4.1. Only existing, active launchers were considered. Most of the data was gathered from the respective user manuals, while the propellant mass was computed using the launcher stage specifications.

Table 4.1: Considered launchers and their considered parameters. [Arianespace, 2016; SpaceX, 2015; Arianespace, 2012; ULA, 2010; U.S.GAO, 2017]

Specification	Cost [$M]	Launches [-]	Fairing diameter, x height [m]	Payload mass to GTO [kg]	Propellant mass [t]
Falcon 9 FT[1]	62	33	5.2x13.1	8300	550
Falcon Heavy[1]	90	1	5.2x13.1	26700	1450
Atlas V 541[2]	132	78	4.6x16.5	8900	630
Ariane 5 ECA[3]	170	98	5.4x20	11115	930
Soyuz-2 ECA	80	76	3.5x9	3250	260

To trade-off the available launchers, they were assessed in terms of available payload mass, reliability, sustainability and cost. Each aspect was given a score from 1 to 5, multiplied by the respective weight and summed for the total score.

- **Reliability** is the most important aspect. It stems from the killer reliability requirements and is therefore given a weight of 5. Success rates and the total number of launches are considered, with success rates ranked 1 for anything below 90% with steps of 2.5%. The number of launches is evaluated as 1 for 20 or fewer launches with steps of 20. The reliability grade is then taken as the average of the two values.
- **Payload capabilities** was chosen as the second most important aspect. The payload mass to geostationary transfer orbit (GTO) and fairing dimensions are representative of how much payload can be brought to Mars. A grade of 1 was given for a mass in the range of 0 to 5000 kg, while a grade of 5 was given for anything above 20000 kg with steps of 5000 kg in between. The largest fairing volume was given a score of 5 and the smallest a score of 1. An average of the two grades is used for the payload capabilities criteria.
- **Sustainability:** The sustainability of the launcher was evaluated as a less important aspect and given a weight of 2. It does not directly relate to mission success, but sustainability aspects still must be considered. 1 corresponds to a launcher that uses more than 1000 tonnes of propellant and it is then evaluated in steps of 200 tonnes. An additional bonus of +1 is also given to any launcher that reuses any of its stages.
- **Cost:** It is again a less important aspect, as it does not directly constrain the mission success and the typical launch costs are roughly only 2-7 % of the total mission cost of 6.25 $ billion. 5 Is given for launch costs between $60 and 100 million with steps of $40 million lowering the grade by 1.

[1] URL: `http://www.spacex.com/about/capabilities` [Cited 8 May 2018]
[2] URL:`https://www.nasa.gov/press-release/nasa-awards-launch-services-contract-for-next-tracking-data-relay-satellite` [Cited 8 May 2018]
[3] URL:`http://spacenews.com/with-eye-on-spacex-cnes-begins-work-on-reusable-rocket-stage/` [Cited 8 May 2018]

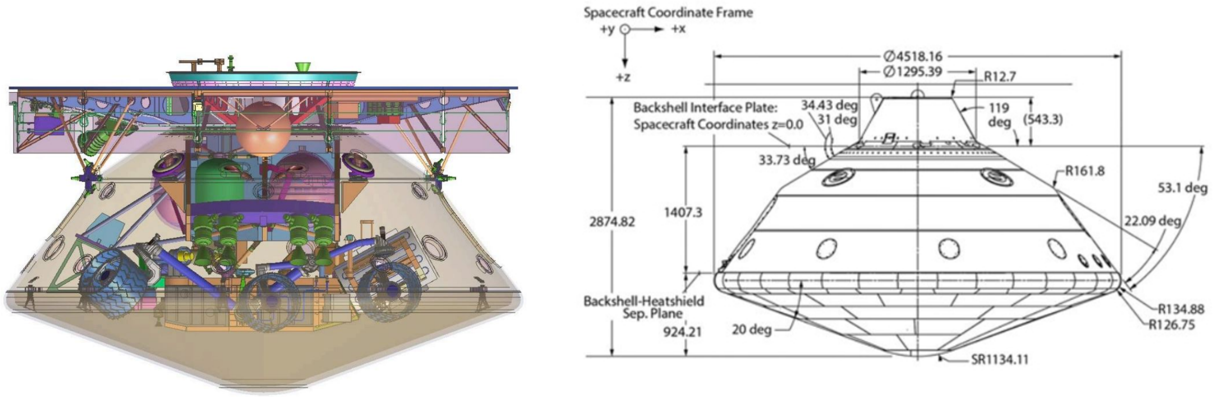

(a) The Curiosity rover within the entry vehicle

(b) Technical drawing with all relevant measurements of the MSL entry vehicle [Lakdawalla, 2018, p. 73]

Figure 4.2: Schematics of the entry vehicle used for MSL

Table 4.2: The trade-off table for the launcher selection

Aspect (Weight)	PL capabilities (3)	Reliability (5)	Sustainability (2)	Cost (2)	Total
Falcon 9 FT	3	3.5	5	5	44.5
Falcon Heavy	4.5	1	2	5	33.5
Ariane 5 ECA	4	4	2	3	40
Atlas V 541	3	4.5	3	4	43.5
Soyuz-2 ECA	1	3	5	5	38

The results can be seen in Table 4.2. The first and second placed launchers- the Falcon 9 FT and the Atlas V are separated by only 1 point, showing that they both perform very well. However, as the Atlas V has been used for several past Martian missions, such as Mars Science Laboratory, MAVEN, Mars Reconnaissance Orbiter, InSight and future missions like Mars 2020, it will be the launcher of choice.

4.3.2. Entry Vehicle

Given the expected large complexity of the system required for this mission, it was assumed that a large entry vehicle would likely be necessary. For that reason, an initial assumption was made to use an entry module which would be highly similar or identical to the Entry, Descent and Landing (EDL) System which was used for the Mars Science Laboratory (MSL) mission to transport the Curiosity rover. This choice was made because the Curiosity rover is the most complex and largest system to land on Mars to this day. Therefore, the MSL EDL System seemed fit to (perhaps with adjustments) transport the MARS. Some schematics of the MSL EDL System are shown in Figure 4.2.

As the design progressed, it was discovered that some changes to the original EDL are required. Firstly, it was decided that the height of the EDL had to be increased in order to ensure enough space for the UAV. This was done by keeping the 53.1° constant over the height of the entry vehicle, thereby removing the corner indicated by R161.8 in Figure 4.2b. This will influence the aerodynamic performance of the entry vehicle, however, this is mainly dominated by the 53.1° angle, which was kept constant. Therefore, this change was considered viable.

Secondly, to further increase the available space, it was decided not to use a skycrane as was used in the MSL mission. Instead, a thruster system was integrated in the base station, as is used in numerous other landers, including the Exomars 2020 lander. The skycrane would add a lot of complexity and uncertainty to the deployment, while it would not provide much benefit in this mission. The main reason in the case of the Curiosity was that the combination of weight and complexity allowed for usage of a thruster system; the rover would become too heavy. For this mission, these constraints do not apply to the same extent as a static base station is considered. Therefore, a thruster system is considered feasible.

4.4. Launch and Arrival Strategy

Having chosen a launch and entry vehicle, the method of getting the system to Mars must also be discussed. The scientific mission is required to conclude by 2030, meaning that it should begin at least a couple of years beforehand. The late 2026 launch window[1] is the prime choice, as that would result in an arrival date in mid-2027, allowing for three and a half years of scientific measurements before the set deadline.

[1]URL: `http://clowder.net/hop/railroad/EMa.htm` [Cited 20 June 2018]

A Hohmann transfer trajectory will be taken to Mars [Wertz and Larson, 1999], a basic representation of which can be seen in Figure 4.3. It was chosen as it is the most fuel-efficient transfer orbit and sustainability is a key consideration for the mission. A total ΔV of 15.5 km/s will have to be delivered by the launcher and a travel time of around 8 months was calculated.

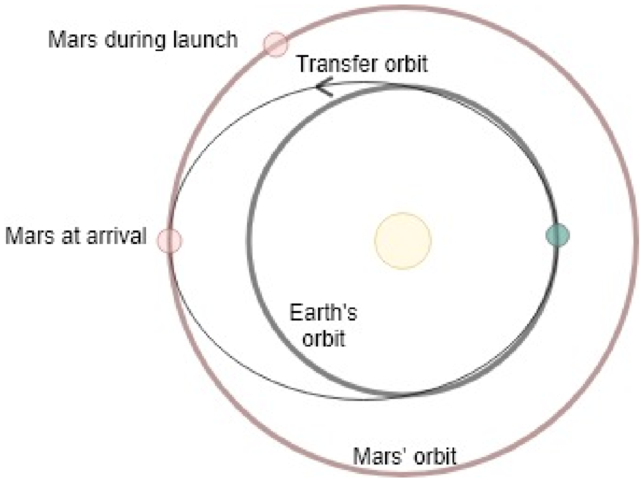

Figure 4.3: Schematic overview of the Hohmann transfer to Mars

During the atmospheric entry, the EDL module will first slow down using its heat shield. Once slowed sufficiently, a parachute will deploy, further slowing the entry module down. Lastly, the thruster system will activate, further slowing the MARS system, until touch down.

4.5. Landing Site

There are a few requirements the landing site should have. Based on these requirements, the most fitting landing site is opted for. The following requirements, set by NASA[2], were chosen:

- LS-1: The landing site shall be maximum 30° latitude from the equator;
- LS-2: The landing site shall have a flat surface around it of at least 15km;
- LS-3: The landing site shall be at an elevation between -1000 and -4000 meters;
- LS-4: There shall be ground water ice deposits near the landing site;
- LS-5: Minerals shall be present near the landing site;
- LS-6: The temperature fluctuation shall be maximum 3°/hour at the landing site;
- LS-7: Sunlight shall not be blocked at the landing site.

Below, some of the requirements are elaborated upon to provide some rationale for them. Near the equator, the average amount of sunlight during the year is the highest and the temperature tends to be higher on average. The landing site should also have a flat surface of about 15km as you do not want a coarse surface. Next to that, in case the vehicle would not be able to land at the pinpointed location, it has some margin to land safely. A landing site at a lower elevation is preferable as the entry phase is very difficult. The atmosphere slows the vehicle down and a lower elevation means more atmosphere to slow you down, thus it is easier to land at a spot at a lower elevation. Furthermore, sunlight should not be blocked by e.g. a mountain.
Possible landing sites were re-identified for the Mars 2020 mission [3]. For the MARS mission, these landing sites are taken into consideration and checked with the requirements of the mission.

Three landing sites are defined, Jezero Crater, NE Sytris Major and Holden, which can be seen in Figure 4.5. It was realised that the Jezero Crater and NE Sytris are only 84 km separated from each other (center to center of the craters) [2], which might be interesting for future missions. VITAS will not be able to cover both zones due to mountains in between, which makes it impossible to land in between the craters.

[2]URL: https://mars.nasa.gov/insight/mission/timeline/prelaunch/landing-site-selection/ [Cited 19 May 2018]
[3]URL: https://www.researchgate.net/figure/Candidate-landing-sites-at-Jezero-and-NE-Syrtis-a-Similar-to-Figure-2a-b-High-sand_fig7_323067490?_sg=bBhGAkJdhIB-wbBmb-wSYzcPQMmbBlavMxiFaKlxEApZSSAYC7gzi1e1GjiPL175f6Ng3RxFdpEr6vkmTclbfw [Cited 19 May 2018]

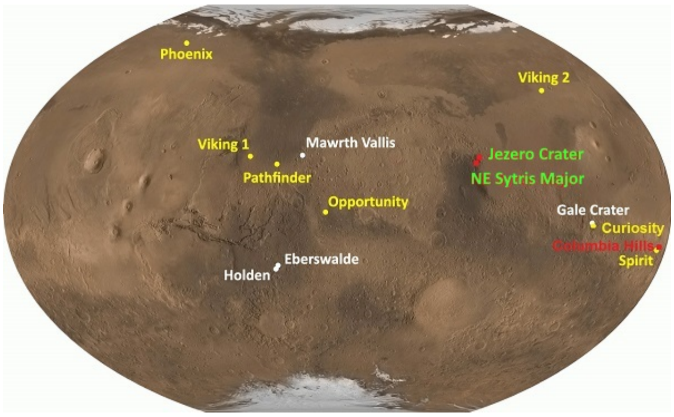

Figure 4.4: Current rovers on Mars and the 3 possible landing sites [2]

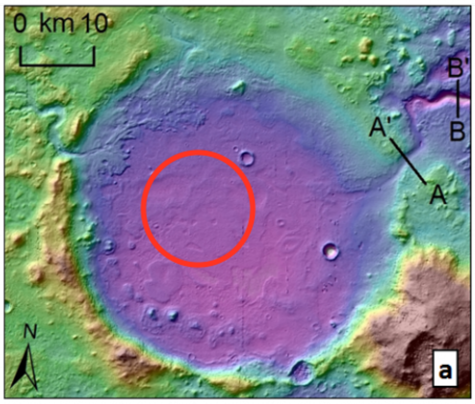

Figure 4.5: Close-up figure of the Jezero crater [5]

However, the Jezero Crater will be the main objective of the MARS mission, as it is believed more minerals are present at the crater [2] and thus a higher chance of a successful mission is present. The Jezero Crater lies at 18.855°N 77.519°E and has a diameter of 49 km [2]. Accurate height maps do not exist yet of the crater, but it is expected that height differences are about 50 m on average with some higher peaks and obstacles which were identified through a height map of Mars. [4] [5]

In Figure 4.5 the red circle represents the estimated landing position, the circle is not exactly in the middle as at the center of the circle and the surface is less rough at the left top corner. Ergo, the range will have to be a bit larger, which will be analysed in Chapter 5. All requirements are met except LS-7. The highest mountains at the south-east edge are about 2 km tall and at the south-west edge are about 1.5 km tall. The amount of sunlight blocked in degrees by mountains equals,

$$\mathrm{H}_{\mathrm{blocked}} = \tan\left(\frac{h_{\text{mountain}}}{d_{\text{mountain}}}\right) \tag{4.1}$$

With $\mathrm{H}_{\mathrm{blocked}}$ the amount sunlight blocked in °C, h the height and d the distance. The worst case scenario was assumed, i.e. the base station lands the furthest possible from the pinpointed location and the closest to the mountains. Filling in the equation with the height of the mountain being 1.5 km and distance to it 15 km, which can be deduced from Figure 4.5, yields 9.9°. With the sun being at an elevation of 9.9°, solar panels do not generate much Watt[6], thus this phenomenon is thus considered negligible.
At last, the largest distance the UAV might have to cover is 69 km (34.5 km radius). Which is from the left top corner to the right bottom corner.

[4]URL: `https://astrogeology.usgs.gov/search/map/Mars/GlobalSurveyor/MOLA/Mars_MGS_MOLA_DEM_mosaic_global_463m` [Cited 19 May 2018]
[5]URL: `https://science.msfc.nasa.gov/content/outlet-forming-flood-jezero-crater-lake-mars` [Cited 19 May 2018]
[6]URL: `https://www.researchgate.net/publication/23887046_Preliminary_design_of_a_long-endurance_Mars_aircraft` [Cited 15 May 2018]

5
Concept Analysis

In this chapter the conceptual analysis of the mission requirements and the design options that were considered are discussed. In Section 5.1 the main system level requirements are listed that flow down from the mission statement. Secondly, the possible design concepts for the mission are discussed and traded off, resulting in three system concepts have been defined in Section 5.2. The three system concepts are evaluated in Section 5.3 and their trade-off is presented Section 5.4. Lastly, a sensitivity analysis and conclusions regarding the winning concept are presented in Section 5.5. The winner concept is then fully documented in Chapter 6 and 7.

5.1. Driving Requirements

From the mission objective, mission architecture, market analysis and sustainable development strategy laid out in Chapters 2, 3 and 4 a couple of top-level system requirements can be derived. These were the primary drivers in the concept exploration and concept trade-off in Chapter 5 and let to the chosen concept which is elaborated upon in Chapter 6. Over the course of the design process some of these requirements were dropped or adjusted when deemed not feasible to implement in a system as described by the stakeholders; this will be mentioned in the respective sections when a requirement change was made.

The system requirements can be split up according to the various stakeholder requirements as well as additional mission requirements that were derived from the chosen landing zone, launcher and sustainability approach.

Stakeholder requirements

- Scientific mission
  - MARS-UAV-SYS-Science-1: The system shall have a range of at least 100 km.
  - MARS-UAV-SYS-Science-2: The system shall perform visual imaging at a resolution of 10 cm.
  - MARS-UAV-SYS-Science-3: The system shall perform height mapping at a 10 cm spatial resolution and a 10 cm height resolution.
  - MARS-UAV-SYS-Science-4: The system shall scan shallow ground ice deposits up to a depth of 10 m and at a resolution of 10 cm.
  - MARS-UAV-SYS-Science-5: The system shall measure soil composition at a resolution of 100 m.
  - MARS-UAV-SYS-Science-6: The system shall measure the composition and size distribution of dust in the lower atmosphere.
  - MARS-UAV-SYS-Science-7: The system shall measure the wind speed and precipitation in the lower atmosphere.
  - MARS-UAV-SYS-Science-8: The system shall measure the following trace gases at a 100 m resolution on 3 heigths: methane, carbon dioxide, atomic oxygen, ozone and argon.
- Safety and reliability
  - MARS-UAV-SYS-Reliability-1: The system shall have a reliability of at least 99.9% for phase 1.
  - MARS-UAV-SYS-Reliability-2: The system shall have a reliability of at least 99.0% for phase 2.
  - MARS-UAV-SYS-Safety-1: The system shall be single point failure free.
- Sustainability
  - MARS-UAV-SYS-Sust-1: The system shall contain no hazardous/toxic materials.
  - MARS-UAV-SYS-Sust-2: The system shall be either reusable or recyclable by the future manned base.
- Miscellaneous
  - MARS-UAV-SYS-Launcher: The chosen launcher shall be an existing/foreseeable model.
  - MARS-UAV-SYS-Operations: The system shall perform the mission autonomously.

Launcher requirements, derived from ULA [2010]

- MARS-UAV-SYS-Launcher-1: MARS shall comply with the Atlas V 541 launcher system.
- MARS-UAV-SYS-Launcher-1-1: MARS shall be able to withstand loads of up 6 g axially and -2 g laterally.
- MARS-UAV-SYS-Launcher-1-2: MARS shall have a natural frequency higher than 15 Hz axially and 10 Hz laterally.

- MARS-UAV-SYS-Launcher-1-3: MARS shall have a mass of no more than 8900 kg.
- MARS-UAV-SYS-Launcher-1-4: MARS shall have a diameter of no more than 4.6 m.
- MARS-UAV-SYS-Launcher-1-5: MARS shall have a height of no more than 16.5 m.

Entry vehicle requirements

- MARS-UAV-SYS-Entry: MARS shall comply with the Mars Science Laboratory Entry Descent and Landing capsule. [Lakdawalla, 2018]
- MARS-UAV-SYS-Entry-1: MARS shall have a diameter of no more than 4.52 m.
- MARS-UAV-SYS-Entry-2: MARS shall have height of no more than 2.33 m.
- MARS-UAV-SYS-Landing: MARS shall comply with the ExoMars-2020 Entry Descent and Landing system.
- MARS-UAV-SYS-Landing-1: MARS shall have a mass of no more than 1137.9 kg[1][2].

Sustainable requirements

- MARS-UAV-SYS-Sust-1-1: MARS shall make no use of RTGs.
- MARS-UAV-SYS-Sust-1-2: MARS shall make no use of hydrazine.

Environmental requirements

- MARS-UAV-SYS-Environment: MARS shall be able to operate in the environment of the Jezero Crater.
- MARS-UAV-SYS-Environment-1: MARS shall be able to operate nominally in a temperature range of 184-242 K.
- MARS-UAV-SYS-Environment-2: MARS shall be able to operate nominally in an air density range of 0.017 - 0.035 kg/m^3.
- MARS-UAV-SYS-Environment-3: MARS shall be able to maintain minimal operations during dust storms.

5.2. Concept Generation

In this section, the possibilities for a system that can meet the top-level requirements are explored. Due to the complexity of the mission, the system is first split up into several elements, so that they could be evaluated separately and then recombined into an entire system concept.
The elements that will be looked into and traded off are as follows:

1. Power generation options;
2. Power storage options;
3. Type of propulsion;
4. Number of base stations;
5. Type of base station;
6. Number and type of UAV.

Power generation. Several options were worth looking into, such as solar, chemical and nuclear energy. Wind energy was also considered, but quickly deemed not feasible due the low density of the Martian atmosphere. The considered options for harvesting solar, chemical and nuclear energy are listed and traded-off in terms of its technology readiness level (TRL), size, degradation and sustainability are presented in Table 5.1. Weights are given to each criteria. Some concepts were deemed unacceptable due to them not meeting a certain requirement are marked in red.

Table 5.1: The trade-off table for power generation

Concept	TRL (5)	Size (4)	Power Density (3)	Degradation (3)	Sustainability (1)	Total score
Fuel Cells	8	1	5	5	3	77
Regenerative fuel cells	3	5	3	5	5	64
Solar panels	9	4	2	4	5	85
RTG	9	4	3	5	1	86
Stirling engine	2	4	4	4	5	55
Fission	1	1	5	2	5	35
Fusion	3	1	5	2	1	41

As can be seen, options like the radio-isotope thermal generators, stirling/fission/fusion engines were dropped due to their low TRL or because they were unsustainable was unacceptable for the set up driving requirements. Solar

[1]URL:https://ewh.ieee.org/conf/icra/2013/workshops/PlanetaryRovers/04-Baglioni,Joudrier/baglioni,joudrier_talk.pdf [Cited 24 June 2018]
[2]URL: http://exploration.esa.int/mars/56933-exomars-2020-surface-platform/ [Cited 24 June 2018]

panels were deemed to be the optimal choice due to their sustainability, reliability, size and longevity, fitting the mission length.

Power storage. Due to the length of the scientific mission - requiring a lot of energy- and the high power requirements, storage options that found a balance between long-term energy storage and high power output were considered. The options considered are listed in Table 5.2:

Table 5.2: The trade-off table for power storage

Concept	TRL (6)	Energy density (4)	Power density (2)	Sustainability (1)	Total score
Batteries	9	4	4	2	80
Regenerative fuel cell	3	5	3	4	48
Supercapacitor (SC)	9	1	5	4	72
Capacitor	9	1	4	3	69
Regenerative fuel cell + SC	2	5	5	5	47
Batteries + SC	9	2	5	3	75

Regenerative fuel cells cannot be considered due to having a too low TRL, while capacitors and supercapacitors cannot provide the energy levels required for the long-term mission. The battery-supercapacitor hybrid is a promising option, but currently their energy density level is of insufficient magnitude. Therefore, only batteries will be considered for the system.
Propulsion type. Several propulsion types were considered for the mission, such as external thrust sources, chemical propulsion, jet engines and propellers. However, all options - except propellers - have issues, deeming them unusable:

- External thrust sources are deemed too unreliable, as they are dependent on weather.
- Chemical propulsion cannot be applied to the mission due to the required longevity. The UAV would run out of fuel far before finishing its mission.
- Jet engines will not work due on Mars due to the lack of oxygen in the atmosphere.

Therefore, the only available propulsion option is the use of propellers.
Number of base stations. None, one and multiple were considered for the quantity of base stations to support the flyer. A base station can provide many benefits, as it could be used for power generation, scientific measurements, data storage, telecommunications and guidance/tracking, all of which are critical for a long-term mission. A single base station was deemed to be the optimal choice, as multiple base stations would have to be deployed kilometers apart to prove beneficial, which, at the current landing accuracy of entry vehicles, is far too unreliable.
Type of base station. Mobile and static types of base stations were looked into. A rover-type ground moving base station imposes too many risks for how little ground it can cover (Curiosity has only travelled 19 km in over 2000 sols[3]). Floating helium-balloon base station was also a consideration, but due to the longevity issues of balloons and large thrust requirements to overcome the Martian winds, that option was deemed unfeasible. Therefore, a single, static base station will be designed.
Number of UAV's. A single and multiple UAV's are considerable options for the mission. A single UAV would simplify the design and mission logistics, whereas multiple would add redundancy and therefore increase the reliability of mission success. Additionally, multiple UAV's could be designed for fewer tasks per flyer, leading to a lighter design. Indeed, both options have considerable benefits and will be considered further.
UAV type. Several UAV types were looked into. Only options capable of vertical take-off and landing were considered due to the rough terrain of the surface of Mars. The identified options and their trade-off criteria/scores can be seen in Table 5.3.

Of the considered options, two were considered to be optimal: the fixed wing tail-sitter and a multicopter. This is due to their excellent vertical take-off/landing capabilities and performing well across the board. However, range is expected to become an issue for the multicopter concept and can prove to be a design killer.

After having evaluated the options for each system element, it was concluded that the mission had to include one or more flyers and a single, static base station. Solar panels will be used for power generation, batteries will be used for power storage and propellers were the optimum choice to generate thrust. To determine the type and number of UAV's to design, a basic evaluation was performed to generate three most promising UAV system concepts. They were split based on number (single/multiple), UAV type (tailsitter/multicopter) and how the payload is integrated. Payload integration was split into three types:

1. Integral, where all instruments are integrated into each design. This is the only option for a single flyer concept.

[3]URL: `https://mars.nasa.gov/msl/mission/whereistherovernow/` [Cited 20 June 2018]

Table 5.3: The trade-off table for UAV-type

Concept	TRL (5)	Size (4)	Flight performance (4)	Mass (4)	Range coverage (2)	Sustainability (1)	Total score
Tail sitter	7	3	4	4	4	4	91
Quad-copter	8	4	5	1	2	3	87
Cyclocopter	1	4	3	1	3	3	46
Biaxial-copter	7	5	4	2	2	2	85
Multi-copter	8	3	5	3	2	2	90
Stopped blade-copter	2	2	4	2	3	4	52
Helium balloon	5	4	1	3	1	1	60

2. Task-specific, where the instruments are split amongst several flyers, leading to a less complex, lighter design.
3. Modular, where the instruments are packed inside modules. The flyers are equipped with a mechanism, capable of picking up and installing a certain module and uninstalling, leaving it for future use, once finished using it.

An overview of the resulting concept options can be seen in Table 5.4.

Table 5.4: Remaining options for the concept generation phase

Amount	UAV	Payload
Single	Tailsitter	Integral
	Multicopter	Integral
Multiple	Tailsitter	Integral
		Task-specific
		Modular
	Multicopter	Integral
		Task-specific
		Modular

Table 5.5: The final options for the concept generation phase

Amount	UAV	Payload
Single	Tailsitter	Integral
	~~Multicopter~~	~~Integral~~
Multiple	Tailsitter	~~Integral~~
		Task-specific
		~~Modular~~
	Multicopter	~~Integral~~
		Task-specific
		~~Modular~~

The shortcomings and benefits of each concept are as follows:

- **Single integral tailsitter UAV** offers the benefits of only requiring a single design, leading to shorter design phase and easier integration with the base station.
- **Single integral multicopter UAV** also offers the benefit of only requiring a single design, but lacks when it comes to power requirements and range capabilities and therefore was not developed further.
- **Multiple integral tailsitter UAVs** might perform the mission in less time and offer redundancy in terms of flyers but it will take up a lot of extra room in the entry vehicle. This concept was therefore not developed further.
- **Multiple task-specific tailsitter UAVs** was a beneficial option due to the ability to optimise the design for each payload, leading to a smaller size per UAV, in addition to the benefits of a single tailsitter design. Having 2 pairs of UAVs, designed to carry half of the payload each offers redundancy, which is key for the mission reliability.
- **Multiple modular tailsitter UAVs** require a very complex modular mechanism design, which would lead to a long development time and increased risk during operations. Additionally, payload instruments vary significantly in mass, leading to a lack of opportunities in optimising the design for a given payload mass. It was therefore not considered further.
- **Multiple integral multicopter UAVs** offered no benefit compared to a single multicopter whilst still having the lower range capabilities. The concept was therefore discarded.
- **Multiple task-specific multicopter UAVs** could be optimised by designing each UAV for its own payload, in addition to having very good vertical take-off and landing capabilities, meaning it could incorporate flying scientific capabilities as well as ground-based sample collecting functions. Again, a configuration of 2 pairs of task specific UAVs was considered for the added benefit of redundant flyers.
- **Multiple modular multicopter UAVs** would also require a very complex modular system design and cannot be optimised for a given payload mass while also having lower range capabilities. This option was therefore discarded as well.

The results of this brief concept analysis are summarised in Table 5.5. As a result, the three listed concepts were further analysed to evaluate their performance. A trade-off was then be performed to select the optimal UAV design concept, which is documented further in this report.

- Single integral tailsitter, carrying the entire UAVs scientific payload;
- Four task-specific tailsitters, the scientific instruments are split equally amongst two UAV designs and two units of both designs are used;

- Four task-specific multicopters, the scientific instruments are split amongst two UAV designs and two of each design are used for the mission.

5.3. Analysed Concepts

In this section, the three winning concepts are analysed in order to come up with some preliminary sizing numbers which were used to support the final trade-off between the concepts, which will be discussed in Section 5.4. For all three designs an overview of of their preliminary performance estimate and mass breakdown is provided in Tables 5.7 to 5.12. Also, the equations used during the sizing procedure are briefly summarised in the form of Table 5.6.

The propeller design was assumed to be identical for all three designs. The reason for this was that the performance of propellers in the Martian environment is generally very poor when compared to Earth. This required a dedicated design procedure, preferably using dedicated software [Colozza et al., 2001; Yonezawa et al., 2016]. Since there was no time in the conceptual design phase to perform this analysis, the propeller performance was based on the design of the Mars Helicopter, which uses a coaxial design with a 1.1 m blade diameter spinning at about 3000 rpm. In order to obtain some preliminary thrust and power figures JBLADE was used. This is a tool based on Mark Drela's XFOIL and the blade element method to determine the characteristics of the propellers.[4] Using this software the maximum thrust of one propeller was estimated to be about 6 N. In all three designs the propellers were paired in a coaxial fashion to save space.
Verification and validation procedures for these results are discussed in Chapter 7.

Table 5.6: Overview of the estimation methods used in the sizing of the tailsitter and multicopter concepts. For the tailsitter, the Oswald efficiency factor e was assumed to be 0.85. Additionally, the wing aspect ratio A and the correction factor k_i were assumed to be 10 and 1.15 respectively. The cruise speed estimation of the multicopter was based on an initial estimate of the advance ratio $J = 0.3$. All these estimates originate from the same source as the corresponding equation.

Estimation	Equation	Source
General		
Power for hover	$P_{\text{hover}} = k_i(V_c + V_i)T + \frac{1}{8}C_{D_0}\rho S_b V_T^2$	Seddon and Newman [2011]
Induced velocity	$V_c + V_i = \frac{1}{2}V_c + \sqrt{\left(\frac{1}{2}V_c\right)^2 + \frac{T}{2\rho S_d}}$	Seddon and Newman [2011]
Tailsitter		
Cruise performance	$P_{\text{c}} = TV_{\text{c}} = DV_{\text{c}} = \frac{mgV_{\text{c}}}{L/D}$	[Hepperle, 2012]
Glide ratio	$L/D = \frac{1}{\frac{qC_{D_0}}{W/S} + W/S\frac{1}{q\pi Ae}}$	Raymer [2012]
Wing loading	$W/S = q\sqrt{\pi AeC_{D_0}}$	Raymer [2012]
Zero-lift drag coefficient	$C_{D_0} = \frac{S_{\text{wet}}}{S_{\text{ref}}}$	Raymer [2012]
Friction coefficient	$C_f = \frac{1.328}{\sqrt{Re_c}}$	John D. Anderson [2017]
Multicopter		
Cruise speed	V_{c} = JnD	Seddon and Newman [2011]

Single Integral Tailsitter

Being a tailsitter, the UAV would able to land and and take-off vertically from the base station. When at sufficient altitude, the transition is made to the horizontal cruise flight configuration, which is much more efficient for ranged flight. This allowed for a much higher range than for example the multicopter designs that do not make use of wings to stay aloft but rather rely on thrust the entire time. As such, the power required for flight was analysed for the landing and take-off configuration (hover) and the cruise configuration separately. Additionally, a mass breakdown of the UAV system is presented in Section 5.3.

The supporting base station provides power to the UAV generated using solar arrays. The results of the preliminary sizing of the base station are shown in Table 5.13. Clearly, the single tailsitter design is in favour in this regard - the added complexity due to the multiple UAV's significantly sized up the base station.
As shown in Table 5.7 the tailsitter meets the most important system requirement: it is able to cover a range of 100 km. Combined with the high cruise speed of 80 m/s, this would mean that the entire exploration zone would be mapped in a much shorter time than the initial estimation of five years.

[4]URL: `https://sites.google.com/site/joaomorgado23/Home` [Cited 22 June 2018]

Table 5.7: Design overview of the single tailsitter

Design inputs			**Performance requirements**			**Aircraft parameters**		
Parameter	*Value*	*Unit*	*Parameter*	*Value*	*Unit*	*Parameter*	*Value*	*Unit*
Payload mass	1.511	kg	Take-off & landing power	1076	W	UAV total mass	11.23	kg
Payload power	40	W	Cruise power	316	W	Battery mass	1.79	kg
Range	150	km	Take-off & landing energy	14.9	Wh	Aspect ratio	10	-
Cruise speed	80	m/s	Cruise energy	164.8	Wh	Surface area	1.35	m^2
Cruise altitude	150	m				Wing span	3.67	m
Climb speed	3	m/s				Wing loading	31.03	N/m^2
T/W ratio	1.14	-				Lift-drag ratio	19.85	-
						# Propellers	8	-

Table 5.8: Mass breakdown of the integral tailsitter design. Mass fractions are based on literature on aircraft and drone sizing. [Roskam, 1985; Raymer, 2012; Bershadsky et al., 2016]

Subsystem	**Estimation method**	**Mass [kg]**
Payload	From mission requirements	1.511
Battery	From range and power requirements	1.79
Engine	0.098 kg per engine (Boelhouwer et al. [2018])	0.784
CDH	From mission requirements	1.03
Structures	23% TOW	2.58
Engine control	2% TOW	0.225
Flight control	1.5% TOW	0.169
Electrical component	2% TOW	0.225
Thermal control	5% TOW	0.561
TOTAL	-	11.2

Four Task-specific Tailsitters

The design of multiple tailsitters was very similar to the design of the single tailsitter. However, rather than carrying all the payload, the scientific payload would be split up over two pairs of tailsitters who would perform one half of the scientific mission, meaning that the payload weight can be lowered per tailsitter and that when one of the four tailsitters fails, the whole mission can still be completed.

The most crucial drawback of the multiple tailsitter concept was the dramatic increase in system complexity. The base station would have to accommodate charging and landing space for four tailsitters, which would increase its size. This would require complicated folding mechanisms in order to fit in the entry capsule. It is clear from Table 5.13 that the multiple tailsitters require much more power and base station mass than the single tailsitter. Additionally, The larger solar arrays again negatively influence the complexity of the system because they require and additional folding mechanism.

Table 5.9: Design overview task specific tailsitters

Design inputs			**Performance requirement**			**Tailsitter parameters**		
Tailsitter 1			**Tailsitter 1**			**Tailsitter 1**		
Parameter	*Value*	*Unit*	*Parameter*	*Value*	*Unit*	*Parameter*	*Value*	*Unit*
Payload mass	0.767	kg	Take-off & landing power	778	W	UAV Mass	8.29	kg
Payload power	10.4	W	Cruise power	217	W	Battery Mass	1.25	kg
			Take-off & landing energy	10.8	Wh	Surface area	0.97	m^2
			Cruise energy	113	Wh	Wing span	3.12	m
Tailsitter 2			**Tailsitter 2**			**Tailsitter 2**		
Parameter	*Value*	*Unit*	*Parameter*	*Value*	*Unit*	*Parameter*	*Value*	*Unit*
Payload mass	0.744	kg	Take-off & landing power	773	W	UAV Mass	8.23	kg
Payload power	27.0	W	Cruise power	216	W	Battery Mass	1.24	kg
			Take-off & landing energy	10.7	Wh	Surface area	0.97	m^2
			Cruise energy	112.5	Wh	Wing span	3.11	m
General			**General**			**General**		
Parameter	*Value*	*Unit*	*Parameter*	*Value*	*Unit*	*Parameter*	*Value*	*Unit*
Range	150	km	-	-	-	# Propellers	6	-
Cruise speed	80	m/s				Aspect ratio	10	-
Cruise altitude	150	m				Wing loading	31.03	N/m^2
Climb speed	3	m/s				Lift-Drag ratio	19.85	-
T/W ratio	1.16	-						

Table 5.10: Mass breakdown of the task-specific tailsitters design. The four tailsitters consist out of two identical designs for redundancy. Hence, only two designs are shown in this table. Mass fractions are extracted from literature. [Bershadsky et al., 2016]

Subsystem	**Estimation method**	**Tailsitter 1 [kg]**	**Tailsitter 2 [kg]**
Payload	From mission requirements	0.767	0.744
Battery	From range and power requirements	1.25	1.24
Engine	0.098 kg per engine (Boelhouwer et al. [2018])	0.706	0.706
CDH	From mission requirements	1.03	1.03
Structures	23% TOW	1.91	1.89
Engine control	2% TOW	0.166	0.165
Flight control	1.5% TOW	0.124	0.123
Electrical components	2% TOW	0.0166	0.0167
Thermal control	5% TOW	0.414	0.411
TOTAL	-	**8.29**	**8.23**

Multiple Task-specific Multicopters

While the first two designs were very much alike, the multicopter design was radically different. The multicopters are inherently less efficient in flight than the tailsitter designs, but have the distinct advantage of improved manoeuvrability and hovering capabilities. This is an important advantage over the other designs, where controllability during landing and takeoff will be of crucial importance. A failed landing or takeoff would not only cause fatal damage the UAV, but might also endanger the base station as well. Therefore, this is the most important advantage of the multicopter design.

Table 5.11 provides an overview of the performance characteristics. As expected, the multicopter performed far worse: its range is only 12.5 km, which does not meet the mission requirements at all. Its range was shortened due to the required cruise power, which was about six times higher than for the tailsitter designs (which were also flying a lot faster). The larger cruise power originated from the fact that hovering requires a lot more power than during fixed wing flight for the same weight - this is only marginally compensated by the ‘wing’ effect on the rotor disk, which was estimated to reduce the power required during flight with 30% compared to hover. The climb speed of 4 m/s was not chosen randomly. Since increasing the climb speed had both a positive (less time required to climb reduces energy needed) and negative (more power required during climb), it was possible to optimise the climb speed, minimising the required battery mass.

In Table 5.13 it is shown that the multicopters also required by far the largest base station due to the high power requirements and the landing space.

Table 5.11: Quantitative design description of the task-specific multicopter design option. Payload mass and power are given for both configurations.

Design inputs			**Performance requirements**			**Aircraft parameters**		
Parameter	*Value*	*Unit*	*Parameter*	*Value*	*Unit*	*Parameter*	*Value*	*Unit*
Payload mass	0.767/0.744	kg	Take-off & landing power	2208	W	UAV mass	12.47	kg
Payload power	10.4/27.0	W	Cruise power	1436	W	# Propellers	10	-
Range	12.5	km	Take-off & landing energy	23.0	W h	Disk loading	1.31	kg/m^2
Cruise speed	13.2	m/s	Cruise energy	377.78	W h	Advance ratio	0.3	-
Cruise altitude	150	m				Battery mass	3.18	kg
Climb speed	4	m/s						
T/W ratio	1.3	-						

Table 5.12: Mass fractions used to estimate the total multicopter mass. Please note the high impact of the propellers due to their very large size compared to the multicopter. [Wertz and Larson, 1999; Bershadsky et al., 2016]

Subsystem	**Estimation method**	**Mass [kg]**
Payload	From mission requirements	0.77
Engines	0.098 kg per engine (Boelhouwer et al. [2018])	0.98
Batteries	Range and power requirements	3.17
Propellers	0.167 kg per propeller	2.17
Command and data handling	From mission requirements	1.03
Structures	19% of total mass	2.37
Electrical components (cabling)	5% of total mass	0.62
Thermal control	5% of total mass	0.62
Total	-	**12.47**

Table 5.13: Comparison of the base station sizing for the three different concepts. The single tailsitter is clearly in favour here due to its simpler design. Total system mass refers tot the mass of the UAV(s) and the base station combined.

Parameter	**Single tailsitter**	**Multiple tailsitters**	**Multiple multicopters**
Total system mass [kg]	507	771	1355
Solar array area [m^2]	23.9	35.8	70.1
Battery mass [kg]	10.3	15.4	30.2

5.4. UAV Concept Trade-off

The three UAV fleet concepts were subjected to a trade-off to determine the optimal option. They were assessed in terms of several weighted criteria, which are as follows:

1. **Robustness/Reliability (5)**. This criterion stems from the mission reliability requirement. It was given the highest weight, as it was directly related to how likely the mission would be successful. Reliability and robustness were determined by the impact a malfunction, TRL and the design's ability to survive launch/vibration loads.
2. **Scientific yield (4)**. This criterion stems directly from the scientific data gathering mission requirements. It was given the second highest weight because it was directly connected to how successful the mission would be. The grade was determined by how fast the design can map a area less than 5 km diameter, more than 5 km diameter, whether it could explore areas over 20 km away from the base station and how easily it could access hard to reach zones.
3. **Complexity (3)**. This criterion was chosen because it affects many aspects of the design, such as the reliability, number of interfaces to consider, development time and cost. In the end, the most straight-forward design was desired, but for very complex missions, no simple solutions would be feasible and therefore, a lower weight

of 3 was given. This aspect was graded by looking into the required complexity of the base station, system logistics and whether a UAV deployment mechanism would be required.

4. **Sustainability (2)**. The final aspect was chosen based on the sustainability user requirements. Although important to consider, it wouldn't directly affect the success of the mission and was therefore given the lowest weight. It was evaluated based how much material would needed for construction, how efficiently material would be used, the risks of contaminating Earth/Mars and the reusability of the flyer.

Table 5.14: The trade-off for the UAV concept

Aspect (weight)	Reliability (5)	Scientific yield (4)	Complexity (3)	Sustainability (3)	Total
Single tail-sitter	10	16	12	10	48/280
4 task-sp. tail-sitters	15	20	3	6	44/280
4 task-sp. multicopters	15	8	6	4	33/280

The resulting trade-off table can be seen in Table 5.14. In terms of reliability, the multiple UAV concepts were favoured due to being able to continue the mission in case a single flyer were to malfunction. The tail-sitter concepts topped the multicopter in terms of scientific yield, as they were not as limited by range and operate at much higher cruise speeds. In terms of complexity, the single flyer concept overcame the other two, as the base station only had to support a single UAV and it was most likely to fit inside the entry vehicle without the need for a deployment mechanism. Lastly, in terms of sustainability, the single tailsitter far exceeded the other two concepts again, as it was least likely to contaminate the surface of Mars with crashed flyers, it required the lightest base station and the dry/payload mass fraction of the UAV was the lowest.
It can be seen that the integral tail-sitter concept was the winner overall, but the four task-specific tail-sitters were a close second. Therefore, a sensitivity analysis was performed before concluding the optimal design concept for the MARS mission.

5.5. Sensitivity Analysis and Conclusions

To perform the sensitivity analysis on the trade-off method, the weights of the main aspects were varied to see whether the outcomes differed significantly if the criteria were slightly changed. In addition, it was also analysed how the outcome changes if certain criteria were to be removed. This was performed in the following way:

1. First, an analysis was performed on what would happen if the reliability criterium was removed, which would better reflect on the expected scientific performance and complexity of a design.
2. The complexity aspect was removed to analyse what would change if the design was not limited by simplicity preference.
3. The weights of scientific yield and reliability will both be set to 5 to analyse whether only assessing the mission in terms of how likely it is to be successful leads to severely different results.
4. Lastly, the complexity was given a weight of 5, while keeping the weight of reliability unchanged and removing the scientific and sustainability aspects. This showed the winner which was most likely to be operational, regardless of whether it could perform the scientific mission.

The results of the sensitivity analysis are summarised in Table 5.15. Note, that Case 0 refers to the results using the normal weights for each criteria.

Table 5.15: The sensitivity analysis for the concept trade-off

Case	0	1	2	3	4
Single tail-sitter	48	38	20	52	30
4 task-specific tail-sitters	44	29	21	49	20
4 task-specific multicopters	33	18	19	35	25

Removing the reliability aspect resulted in a clear winner with the integral tail-sitter with a larger gap in points than the normal weights. This shows that the single design would indeed be less favourable in terms of reliability due to its lack of redundant flyers.
In case 2, when the complexity aspect was removed lead to a new winner, being the four task-specific tail-sitters, but the concepts overall scored very similarly. This showed that the multi-UAV designs would indeed be favourable

in terms of reliability and scientific yield, but are significantly brought down by the challenges imposed of having to operate more than one flyer throughout the mission.
Focusing specifically on the scientific yield and the reliability on the mission again lead to the two tail-sitter concepts being close contenders. The integral tail-sitter performed better, which showed that the design would be the optimal one in case complexity and sustainability aspects were not to be considered. However, in the future the task-specific tail-sitters could become the better option.
Lastly, in case 4, the integral tail-sitter outperformed the multi-fleet concepts. This showed that the redundancy benefit of having additional flyers was lower than the added complexity to the mission. Indeed, having several flyers would complicate the base station design significantly, which meant that a mission without a base station could favour having several flyers instead of one.

To conclude, even though the four task-specific tail-sitter and multicopter designs performed very well in terms of reliability and scientific yield, they significantly complicated the base station design and were much less favourable in terms of sustainability. These designs might be a better choice though, in case no base station was to be used for the mission. The major shortcomings of the rotorcraft originate from their low mass efficiency and high power requirements, which lead to poor performance in terms of scientific yield and sustainability. The single integral tail-sitter design was the victorious concept due to its strong performance in terms of scientific yield and what it lacked in reliability, made up for by being the least complex design and being very favourable in terms of sustainability. This was the design that was further developed for the MARS mission.

6
MARS System Overview

Based on the choice for the mission concept as discussed in Chapter 5, the design process continued with the detailed design phase. In this chapter, the overall results of this phase are presented. Section 6.1 provides a general overview of the mission. Consequently, Section 6.2 discusses the final design and the name of the UAV, after which the base station design is addressed in Section 6.3. Fourthly, Section 6.4 gives an overview of the results of the functional analysis of the system. Finally, the intricacies of the system as a whole (i.e. the base station and the UAV) are analysed in Section 6.5.

6.1. General Overview

In this section the Functional Flow Diagram (FFD) is presented. The FFD provides a detailed analysis of all functions that the system has to perform, as well as the relations between them. The FFD starts with a general top level and goes into more detail further on. The top level FFD can be seen in Figure 6.1. This includes all phases ranging from pre-launch operations to the end of life.

Figure 6.1: Top level of the FFD.

The lower levels of the FFD are split over the different mission phases:

- *Phase 0:* includes everything from manufacturing until the launch of the mission;
- *Phase 1:* spans from the launch of the mission until the entry in the Martian atmosphere;
- *Phase 2:* includes the entry, descent and landing part as well as deploying the system once on the surface of Mars;
- *Phase 3:* covers the scientific measurement part of the mission;
- *Phase 4:* deals with the end of mission phase;
- *Phase 5:* is the final phase of the mission and handles the end of life.

For a more detailed breakdown of the mission, the reader is referred to Appendix A.

6.2. UAV Overview

VITAS is an electrically propelled flying X-wing design visualised in Figure 6.2. Its tailsitter design combines the versatility of a helicopter with the performance and flight range of a plane. In order to prepare for the arrival of human exploration mission on Mars, VITAS will perform both detailed visual mapping and height mapping of the Jezero Crater. Furthermore, it will be capable of detecting ice deposits up to 10 meters deep in the Martian soil and gathering wind speed data. In Section 6.2.1 an overview of the mission characteristics is given. In Section 6.2.2, VITAS is further elaborated upon in term of its internal and external configuration. Then, in Section 6.2.3 an overview is given on the various subsystems that are embedded into the UAV. Finally, in Section 6.2.4 a sensitivity analysis is performed w.r.t to the performance of the UAV.

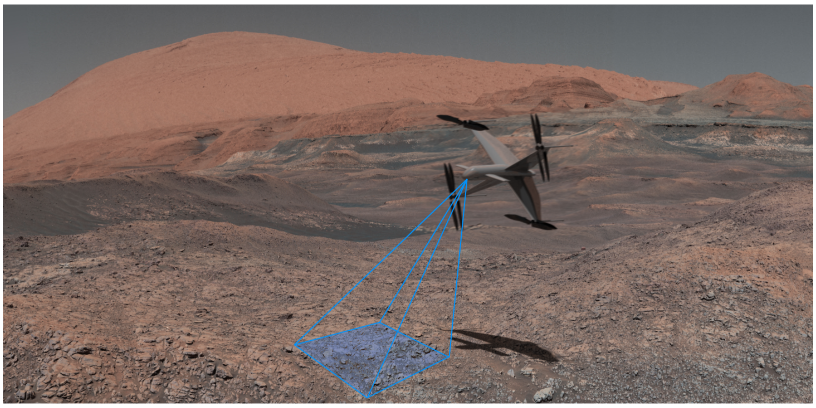

Figure 6.2: VITAS flying on Mars, image credit: NASA's Curiosity Rover

6.2.1. Mission Characteristics

The Jezero crater being chosen as landing site (Section 4.5) induces certain requirements on the design. It has a diameter of about 49 km and thus an area of approximately 1963 km^2. This puts serious requirements on the UAV, needing a flight range of at least 50 km to be able to reach the edge of the crater and return. As this UAV design is tailored to the mission it was decided to drop the range requirement (MARS-UAV-SYS-Science-1) to 55 km such that it fits better in the designed mission. (As an industry standard, at least 10% extra cruise range is advised for when detours need be taken and to account for insecurities during flight.)

To achieve this kind of range, VITAS has to be very light and take as many batteries as possible. Radical design optimisation for weight reduction resulted in a total system mass of 14 kg. To achieve this weight, materials like beryllium had to be utilised. VITAS utilises a tail sitter design to be able to perform landing and take-off, as the surface of Mars is covered with rocks which would render conventional ways of landing unusable. A fixed wing UAV has the advantage over a copter design of requiring less power and energy to fly longer ranges and the added benefit of being able to cover large areas in a short time. For flight, VITAS utilises a combination of two coaxial cruise propeller and two coaxial take-off propellers. During take-off, all propellers work together and produce a total amount of 51.94 N of thrust at air density ρ = 0.017 (which is the most critical for take-off) to achieve a thrust to weight ratio of 1.05. In cruise, the take-off propellers remain feathered while the cruise propellers produce a total of 8.42 N of thrust at air density ρ = 0.017 (meaning range will go down when density goes up) to maintain a cruise speed of 82.5 m/s. The propellers operate between 2100 and 2800 rpm and have a diameter of 1.21 m. This design resulted in a total flight range of 60.6 km.

After landing in the Jezero crater, MARS will first perform some system checks and establish a communication link with the Deep Space Network. Then the necessary scientific instruments can be calibrated and the system made ready to perform its mission. The first few flights will consist of verifying the system's flight performance as well as the functioning of the system as a whole. The MARS system operates fully autonomously, but can receive mission updates from Earth depending on the mission evolution or regions in the Jezero crater that need further investigating.

The first part of performing a scanning run, is performing the VTOL manoeuvre and transition to cruise flight. Because of the relatively big (1.21 m) diameter of the propeller blades, the blades will first spin up to full speed with a low pitch angle. When the required RPM for take-off is reached, the blades will change their pitch and VITAS will take-off. This whole procedure will take as little time as possible while still operating safely.

VITAS will then transition to cruise and reach a cruise altitude of 150 m. When flight performance is nominal, VITAS will start mapping the Jezero crater, collecting data about the soil, ice deposits and taking both visual imagery as well as generating a detailed height map of the surface and store it on the 28 GB of onboard memory. It is necessary to have accurate position data to map the collected data to the correct position on the Martian surface. A combination of an Inertial Measurement Unit as well as a localised GPS system will track the UAV to within a 10 cm accuracy (take a look at Section 7.8 for more detailed information). Additionally the UAV will transmit position, performance and housekeeping data to the base station. The base station in turn transmits mission updates to the UAV such as weather warnings or commands from mission control. When the edge of the crater is reached a pull up manoeuvre is performed to lower the speed and the UAV takes a relatively short turn to head back to the base station. The logical steps involved performing the mission is depicted in Figure 6.4.

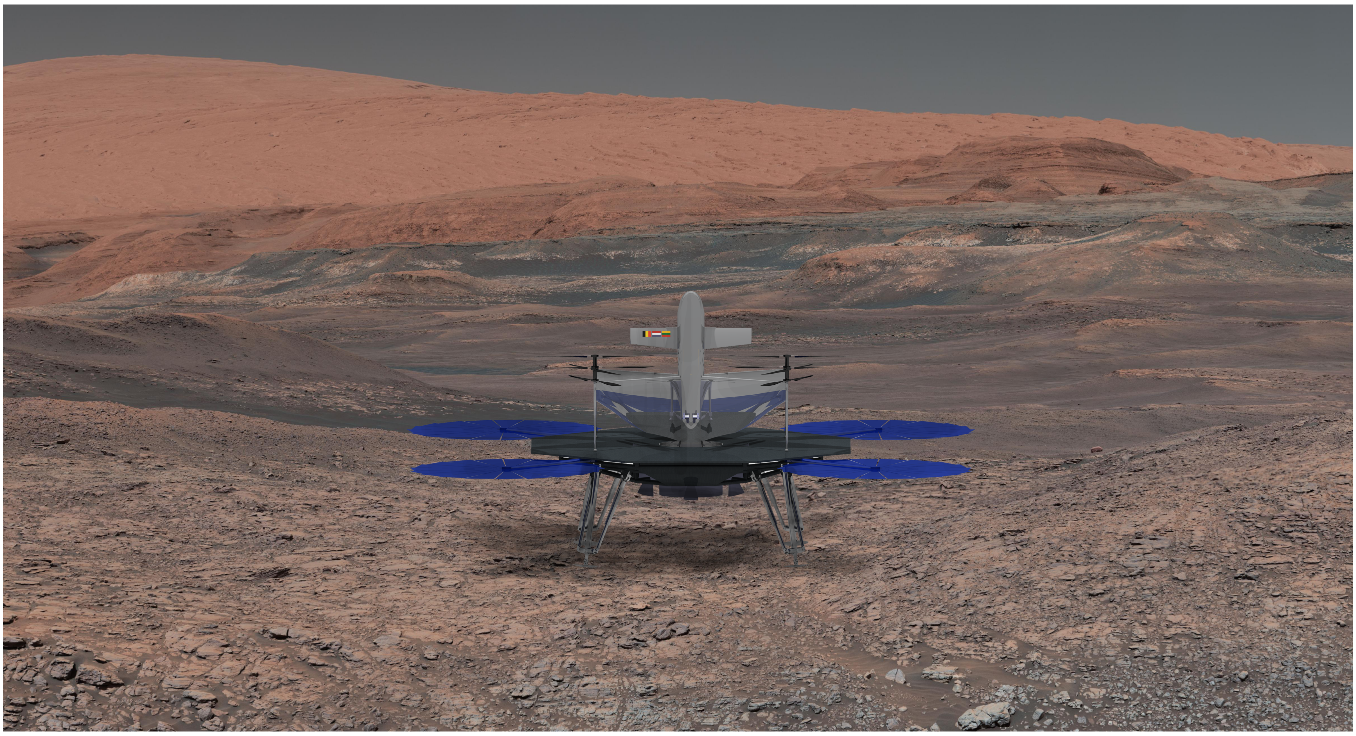

Figure 6.3: VITAS while resting on the base station.

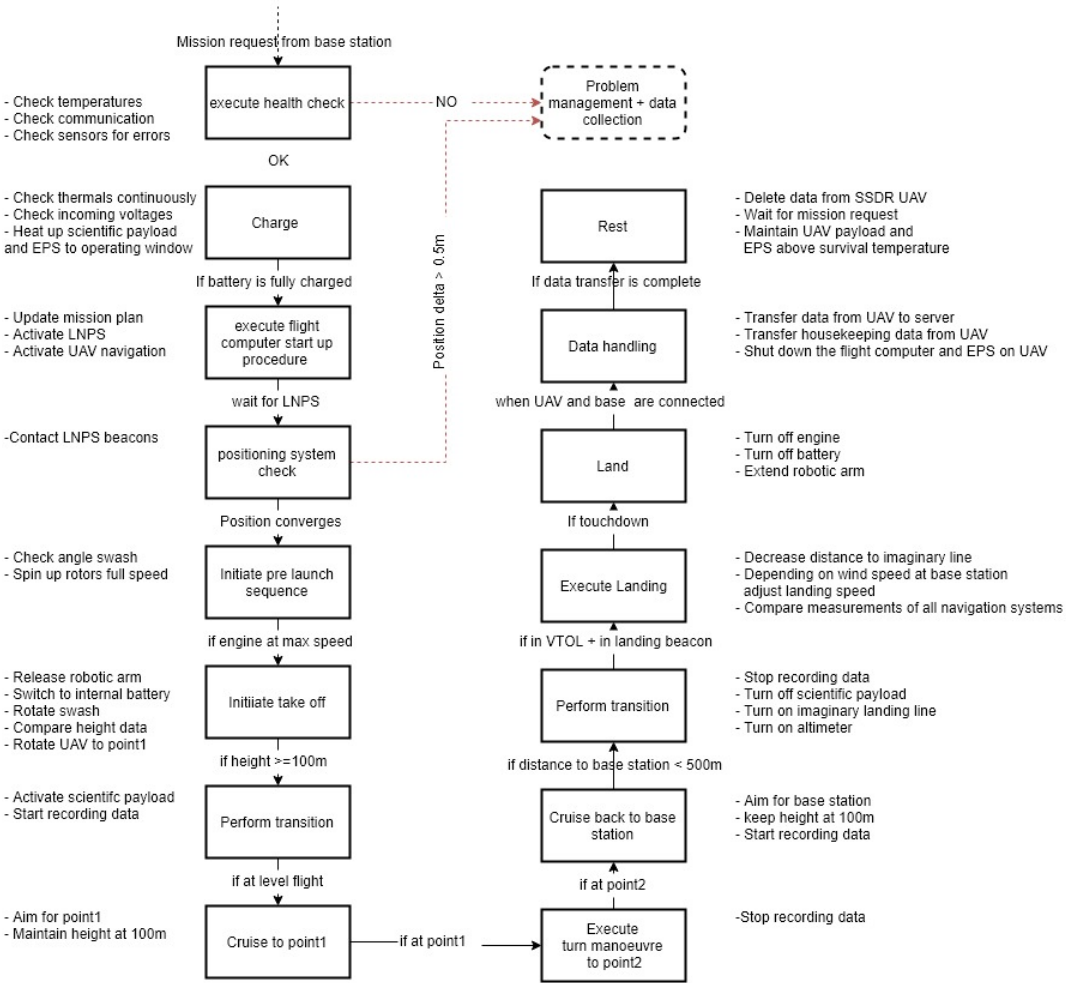

Figure 6.4: Software diagram in mission.

After about 10 min of flight time VITAS lands back on the base station. After performing the landing manoeuvre, utilising a system similar to what automated landing systems use on airfields (see Section 7.8), VITAS lands on the base station. On the base station, VITAS will upload the uncompressed data, along with housekeeping data to the base station, which relays all data to Earth. VITAS has its charging and data port located on the bottom of the fuselage. A robotic arm located on the base station will make the connection with the UAV. It takes 4.9 hr to charge VITAS to full energy. It is expected that about 0.75 flights per day can be performed (Section 4.2). Figure 6.3 show an impression of the UAV resting on the base station.

6.2.2. External and Internal Configuration

External Configuration

In Chapter 5 the choice for a tailsitter configuration was treated. This section will further refine this design based on the constraints and design principles that the UAV needs to comply with.

- The span of the UAV is limited to 2.2 m in order to fit in the entry capsule while being mounted on the base station, as mentioned in Section 6.3. It was also decided that any folding of the wings would result in an unacceptable level of system complexity for autonomous operation.
- The large size of the propellers was a driving factor in the design as well. Eight propellers have to be mounted on the UAV in a symmetric fashion (in coaxial pairs), each with a diameter of 1.21 m. Obviously, sufficient clearance has to be guaranteed between the propellers and the structure of the aircraft itself.
- During takeoff the UAV needs a sufficient degree of controllability around all three axes; therefore mounting all propellers inline would require cyclic control of the propeller blades as well. Even then, pitch control (i.e. control around the axes along which the propellers are aligned) would be very limited. Additionally, it would not be possible to align all propellers as it would require a wingspan of more than 3.3 m, which is not possible without wing folding. For this reason it was deemed necessary to separate the propellers pairs along both axes, i.e. either in an 'x' fashion or in a '+' fashion, like some conventional tailsitters use. The different configurations are illustrated in Figure 6.5. A box design was discarded because it would require more material and therefore be heavier. The aerodynamic advantages of a box design would not be obvious: the production of lift would definitely be better than an x-wing design due to the larger spacing between the upper and lower wings. However, since in this low-Reynolds number regime viscous drag prevails, wetted area needs to be minimised as much as possible. This is where the X-wing would have an advantage over the box design. [1]
- The thin air of Mars requires a large surface area in order to keep the angle of attack during cruise limited. Therefore, the lifting surface needs to be as large as possible. For an x-wing configuration this also means that the dihedral of the wings should be minimised as much as possible, as a higher angle reduces the lift effectively produced by the wings.
- The UAV needs to have a solid base when resting vertically on the base station platform. It was chosen to mount the supports on the wing tips in order to provide sufficient stability.
- The thermal box of the payload has a volume of $275 \times 170 \times 200$ mm^3 and has to be fitted inside the fuselage of the UAV.

Taking into account all these considerations, an X-wing design was chosen for the UAV rather than the '+' configuration. The driving reason was the propeller clearance and the amount of lifting surface: to use a '+' configuration, large vertical struts had to be mounted on the fuselage that would not contribute to the production of lift. Of course, the X-wing design increases the wing area drastically, although the production of lift is not as large as for a normal wing, both due to the large dihedral angle and the interference between the two lifting surfaces. [Raymer, 2012] The propellers are mounted in front of the wings in order to improve longitudinal stability (as mentioned this is a critical aspect of a canard aircraft) and increase the airflow over the wings even at lower velocities. The aircraft will rest on supports mounted on the wing tips, which also means that it is impossible to include a tail behind the main wing. This is the reason why a canard was chosen for pitch control. The canard is fully movable for the sake of controllability during the transition phase: although the main wing will be fully stalled for any angles of attack higher than 10°, the angle of attack of the canard can be adjusted at will [Monteiro et al., 1995]. This allows for longitudinal control regardless the angle of attack of the rest of the aircraft.

[1]URL: `http://www.atmosuav.com/` [Cited 24 June 2018]

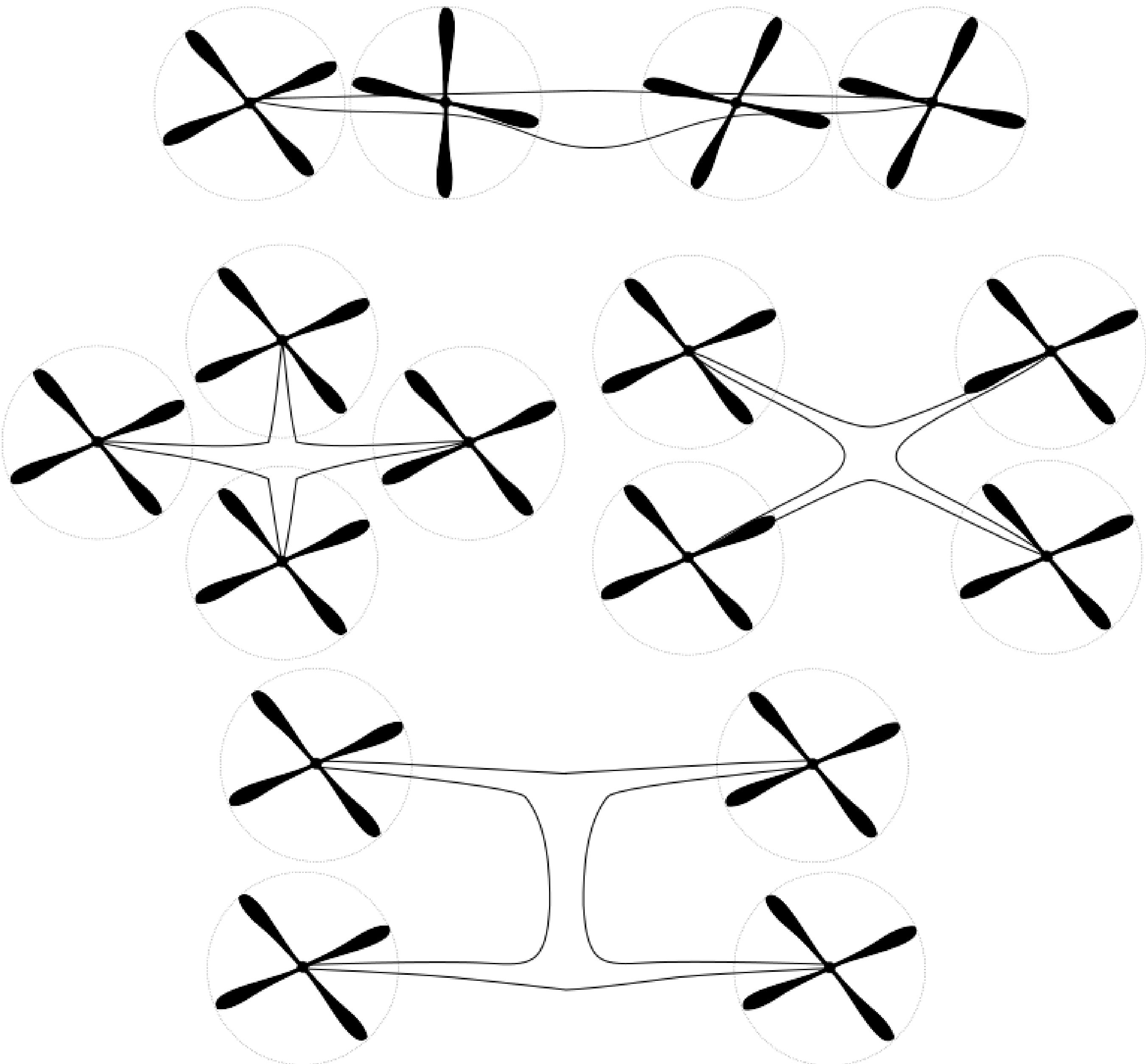

Figure 6.5: Different UAV configurations. On top, the inline configuration is shown. The central left and right diagrams represent the ‘+’ configuration and ‘x’ configuration respectively. The configuration on the bottom is the ‘box’ design.

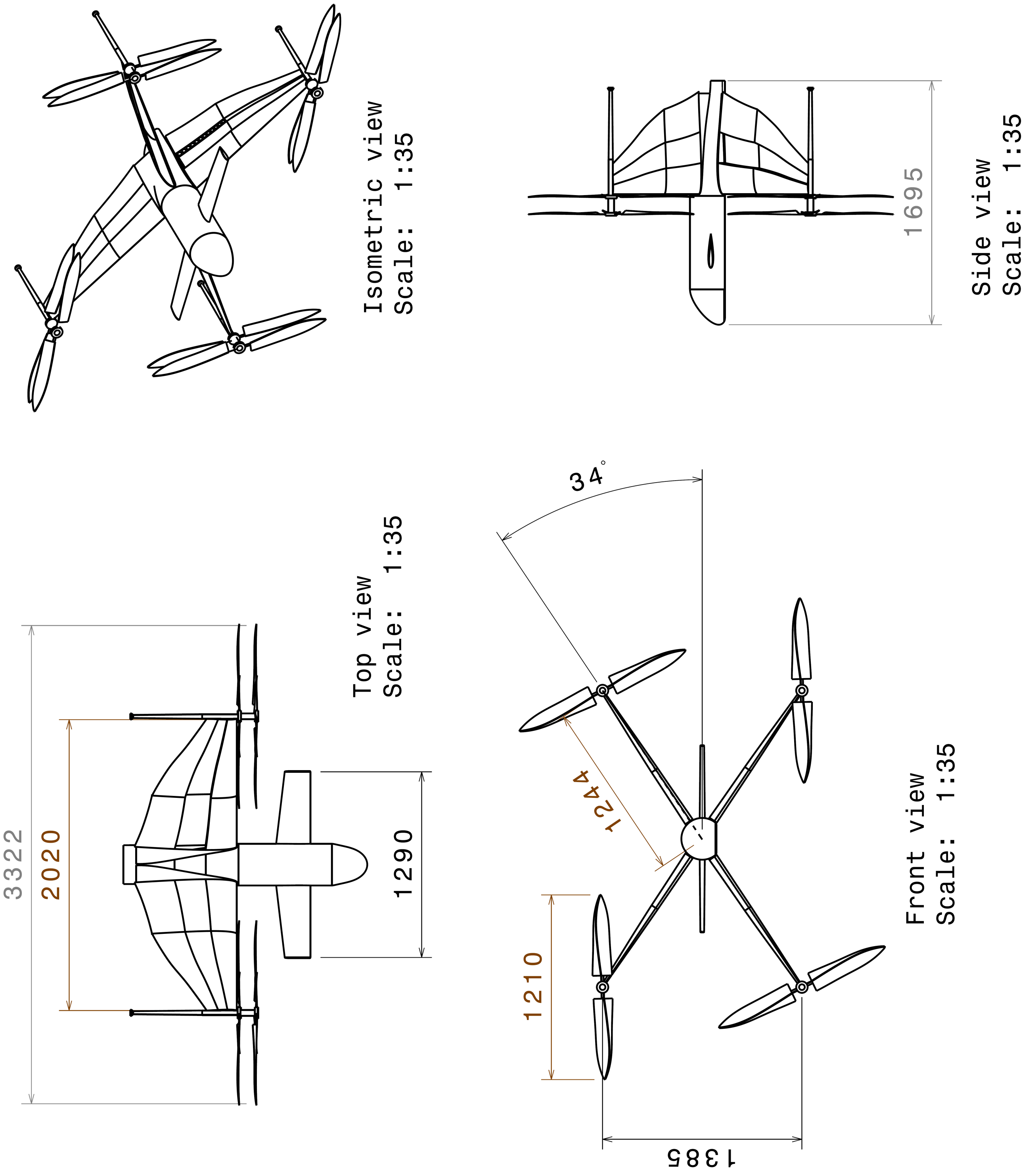

Figure 6.6: Front, top, side and isometric view of VITAS. Dimensions are in millimetres.

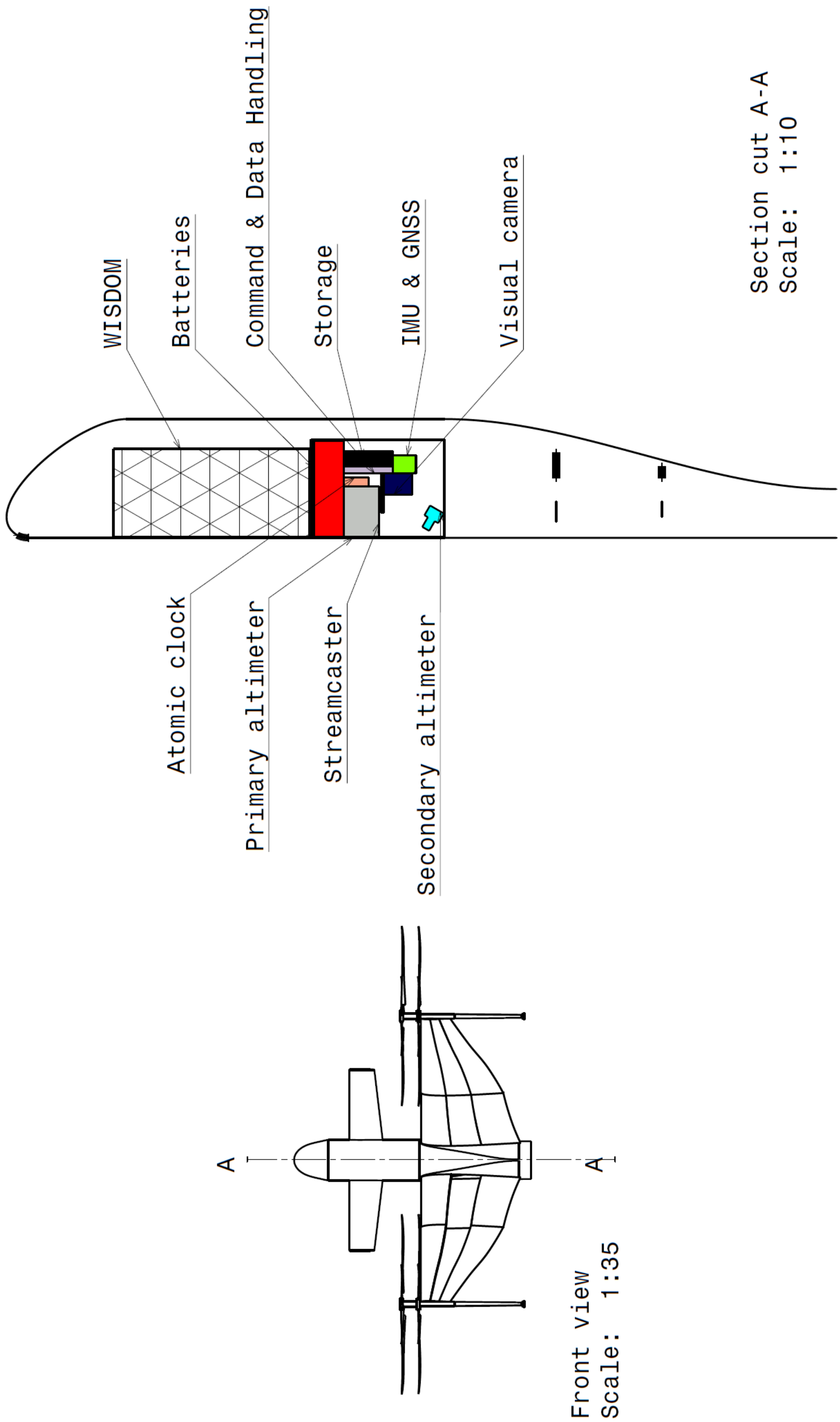

Figure 6.7: Internal layout of VITAS

Internal Configuration
Figure 6.7 shows the internal configuration of VITAS. The subsystems can be divided into their respective functional groups, these can be seen reflected in Table 6.1.

6.2.3. Subsystems

Scientific Payload
VITAS houses a suite of scientific instruments:

- Visual imaging
  - ECAM-C50 will take pictures at a spatial resolution of 10 cm..
- Ice deposits radar
  - WISDOM will scan ice deposits of up to a depth of 10 meters every meter at a height resolution of 10 cm.
- Altimeter
  - Puck Light will make a detailed height map of the Jezero crater at a 20 cm spatial resolution and a 10 cm height resolution.
- Hyperspectral imaging
  - MQ022HG-IM-LS150-VISNIR will take hyperspectral images such that the composition of the soil can be analysed

Propulsion
The VITAS drone utilises eight coaxial propellers with 1.21 m diameter blades in an X-wing configuration. VITAS utilises a combination of four coaxial cruise propeller and four coaxial take-off propellers. During take-off all propellers work together and produce a total amount of 51.94 N of thrust to achieve a thrust to weight ratio of 1.05. In cruise, the take-off propellers remain feathered while the cruise propellers produce a total of 8.42 N of thrust to maintain a cruise speed of 82.5 m/s. The propellers operate between 2100 and 2800 rpm and have a diameter of 1.21 m. This design resulted in a total flight range of 60.6 km.

Electronic Power Subsystem
The UAV will have to be powered to perform its flight. The VITAS has one lithium-ion battery that has a mass of 2.619 kg. During the take-off, more power will have to be generated than during the cruise. Due to this, the discharge current will be 14 A during take-off and 8.5 A during cruise. As the UAV has to perform 770 flight cycles, the batteries needs a minimum life time of this amount as well. Usually the Depth of Discharge (DOD) is defined at 80%, the battery reaches this point already at 650 cycles, however as the batteries are slightly over designed for the range, at 780 cycles the range is 51.31 km, which is sufficient for the mission profile. Furthermore, the subcomponents of the UAV such as the voltage regulator weigh in total 0.216 kg, which yields a mass of 2.859 kg for the EPS.

Structures
In order to cope with the rough environment on Mars, the structure of the UAV had to be sturdy, capable of surviving large temperature shifts, radiation and had to provide integrity for a long lifetime, while maintaining a minimal weight. This lead to the material of choice to make the UAV out of to be a beryllium-aluminium alloy(AM-162) which is more than capable of dealing with the Martian environment and has superior material properties compared to other metals. Despite its toxicity, the health risks were deemed to be avoidable with proper assembly features. The UAV wings are sheet metal structures, reinforced with spars in order to provide structural integrity during launch and entry. The fuselage provides space and protection for the scientific payload and batteries and provides attachment for the canard surface. The landing legs are designed to cope with a rough landing on the pad, making sure the UAV won't tip while stationary.

Stability and Control
During flight the UAV will encounter random disturbances caused by gusts and will have to remain stable and controllable. The main wing surface is 1.84 m^2 with the SD7003 airfoil and the canard surface is equal to 0.28 m^2 with the symmetrical airfoil NACA 0015. In order to guarantee the longitudinal stability the UAV has been equipped with a canard surface. The canard has been set to be able to rotate at high angles of attack in order to increase the stability during VTOL. The longitudinal and lateral dynamic modes of the UAV are stable, but the damping coefficients are relatively low compared to conventional UAV's on Earth, thus active control is necessary at all times.

Thermal Control
To provide for thermal control, all of the UAV's temperature sensitive components, such as the scientific instruments or EPS components were placed inside an insulated thermal box. Radiators and heat pipes were placed inside the box to keep it at the required temperature range and help distribute the heat. The shape was made such that it would fit inside the fuselage and not compromise the center of gravity location.

Navigation
The UAV is equipped with an extra altimeter which is angled forward to 'see' in front of it. It has two antennas and a transceiver that is shared with the communication subsystem to communicate with the LNPS.

Communication
The UAV is equipped with a transceiver, shared with the navigation subsystem and a UHF patch antenna for wireless data transfer to and from the base station. A physical connection will be used by connecting the base station's robotic arm for data transfer, while the wireless UHF patch antenna will be used as a payload data transfer backup and for receiving commands from the base station during flight.
Command and Data Handling
The UAV will function autonomously on Mars and record the data gathered with the scientific payload. This subsystem requires radiation hardened components due to the Martian and space environment it will thrive in. Therefore the UAV needs a radiation hardened single board computer (SBC) for the autonomous computations and 2 radiation hardened solid state drive recorders in order to have enough bandwidth for the scientific data. The SBC would also combine the information from the navigation and scientific data so the data has an exact location.
Overview
In Tables 6.1 and 6.2 and Figure 6.8 an overview is given in terms of a breakdown of the system's mass and power budget.

Table 6.1: Mass breakdown VITAS

Functional group	**Parameter**	**Value**	**Unit**	*Contingency [%]*
Structural group	Wing	2.60	kg	15.00%
	Fuselage	1.02	kg	15.00%
	Canard	0.26	kg	15.00%
Scientific group	Scientific payload	1.62	kg	5.00%
Electronic Power group	EPS	2.46	kg	15.00%
Propulsion group	Propulsion	2.37	kg	15.00%
Support group	CDH	0.75	kg	5.00%
	Navigation	0.49	kg	10.00%
	Thermal	0.54	kg	10.00%
	Communications	0.18	kg	10.00%
	Flight control	0.12	kg	15.00%
	Total mass (without contingency)	**12.38**	**kg**	**0.00%**
	Total mass (with contingency)	**14**	**kg**	**12.26%**

Table 6.2: Power and energy breakdown for VITAS

Parameter	**Value**	**Unit**
Power		
Cruise power	1230	W
Take-off power	1955	W
Auxiliary power	92	W
Scientific Payload	*22*	*W*
CDH	*17*	*W*
Thermal	*25*	*W*
Communications	*2*	*W*
Navigation	*10*	*W*
Energy		
Cruise energy	291	Wh
Take-off energy	18	Wh
Total energy	327	Wh

Figure 6.8: Power breakdown for VITAS

6.2.4. Design Sensitivity

In this section a sensitivity analysis is performed on the design in the form of visualising the effect on the flight range when a mass change in a functional group would occur. A drop in weight could be the result of various causes: due to technological advancements, optimisation, etc. A gain in weight could be the result of the well known snowball effect, or due to the choosing of a different payload. The weight of the batteries was changed accordingly to keep the mass of the UAV at 14 kg resulting in a quasi linear relationship between the weight change of a subsystem and the flight range.

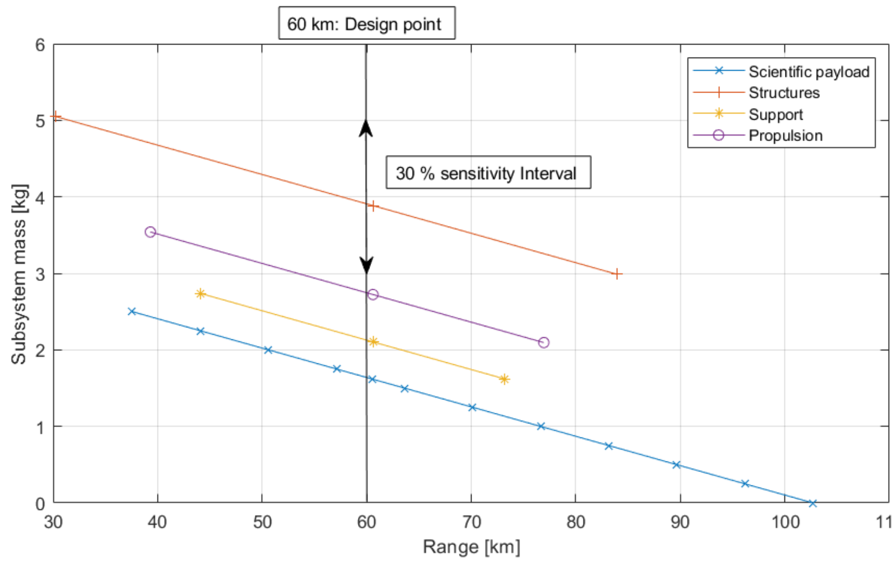

Figure 6.9: Sensitivity interval of the functional groups (except EPS) as seen divided in Table 6.1. Scientific payload ranges from 0-2.5 kg. For the other subsystems (Structures, Support and Propulsion) an interval of 30% was chosen to show the sensitivity to a change in those subsystems

6.3. Base Station

This section briefly describes the design of the base station. In Section 6.3.1, an overview is provided of the base station's general characteristics and functions. Afterwards, in Section 6.3.2, a general description of the base station's appearance and major components can be found. Finally, a brief overview of each of the base station's subsystems is provided in Section 6.3.3.

6.3.1. Characteristics

The base station is designed mainly as a supporting platform for VITAS, both in a literal and figurative sense. In this design, this entails that many of the essential functions for mission performance, such as power generation and communication towards Earth have been integrated in the base station. This relieves the requirements of the UAV, allowing for a more optimised design. The base station's functions are therefore established to be mostly supportive functions. These include providing a method of charging the UAV, and relaying the gathered scientific data to Earth. All of the functions are briefly discussed below.

Power Generation & Distribution
This function is one of the most important for relieving the requirements of VITAS, and consequently allowing for a large reduction in size and weight. If the power generation had to be performed on the UAV, this would have required either an extremely large area of solar panels (and a large amount of batteries for the nights) or an RTG with a large amount of fuel to provide power for multiple years. Both of these options would have led to a design which would likely not be able to lift itself and/or would not be able to be transported to Mars.
Therefore, the power generation takes place on the base station using four circular solar panels of approximately the same size as NASA's InSight mission. As the power generation is centralised on the base station, some power transfer interface is required from the base station towards the UAV. Therefore the charging of the VITAS batteries is also a major function of the base station.

Landing Platform
Another extremely important function of the base station is that it serves as a landing platform for the UAV. This entails multiple aspects. Firstly, it has to be able support the weight of VITAS when it is landed. Secondly, it has to provide enough space that the UAV is able to arrive from every angle. This allows VITAS more freedom in its approach and means that no extra manoeuvres are required during the already complex landing. Finally, it has to be able to change the inclination of its landing surface. This is included to make sure that the landing platform can always be positioned horizontally, even if the base station lands on an inclined surface.

Guidance
The guidance function consists of two parts. First of all, the base station will act as a reference component of the VITAS navigation system. Secondly, the base station will also contain a secondary set of smaller navigation beacons which can be used during the landing sequence to determine its position relative to the landing platform.

Storing & Processing Data
The data which is generated on VITAS during each of the flights will be stored on the base station. There it will also be processed further, after which the data can be relayed towards Earth. As the base station performs these functions, the required data storage capacity and processing power of the UAV can be reduced greatly.

Communications Relaying
The communications towards and from Earth will all be regulated inside the base station. This includes the transmissions of (partial) scientific data, the transmissions of system housekeeping data and the reception of possible mission updates. This allows for a smaller communications system on the UAV.

Mission Operation
The base station will also provide general monitoring of the mission operations. This entails that its systems will monitor the gathered data, and use that to establish what areas still require (more) analysis. This information can then be used to determine optimal flight paths for VITAS's upcoming flights, after which the relevant flight data can be transferred towards VITAS's flight computer. The monitoring data can also be used to determine the overall mission progress, which can then be communicated towards Earth.
In case a mission update has been received from Earth (e.g. a request for more in-depth investigation into a specific area), the base station will also be able to process that update and integrate it into the flight data for VITAS.

6.3.2. Description
For the detailed design of the base station, it was decided to use the total available space within the chosen entry vehicle as a starting point, as that would immediately provide an upper boundary to the dimensions of the base station structure. As described previously in Section 4.3, the entry vehicle is based on the entry vehicle which was used for the Curiosity rover. The available entry vehicle space was divided into space designated to the UAV and space designated to the base station. As the main functionality of the base station was to provide a landing platform for the UAV, the upper part of the base station had to be as large as possible. It was therefore decided to make the division at the disk with the highest possible radius. The space below was dedicated to the base station and the space above it to the UAV. This resulted in a maximum volume for the base station in the shape of a cone with a base radius of 2000 mm and a height of 700 mm. These values were estimated from the schematic previously shown in Figure 4.2b, to which a margin was applied to take the required connection frames into account.

(a) Bottom view of the ESA ExoMars 2020 lander [2]

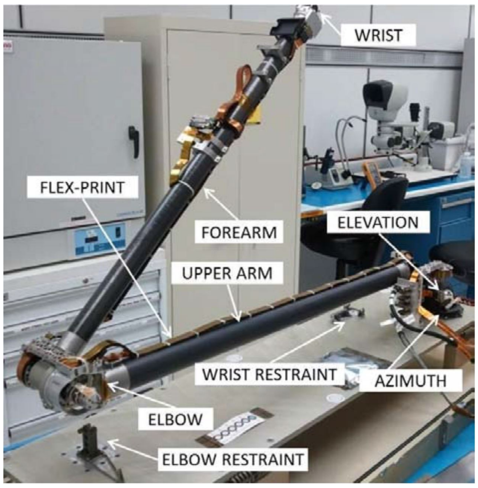

(b) The Instrument Deployment Arm as used on the InSight lander [Fleishner, 2013]

Figure 6.10: Current Mars landers used as reference for the base station design

Continuing from this cone-shaped volume, it was quickly decided that the base station itself would not be shaped as a cone, as a curved outside would only complicate the manufacturing and the attachment of e.g. a landing gear. For that reason, it was decided to use an octagonal pyramid as a basis for the base station structure. The octagonal shape was chosen as it would allow a relatively large amount of spaces for attachments, while not reducing the total volume of the base station too much. This decision was quickly followed by the fact that having a fully closed outer surface of the base station would not provide significant benefits, while there would be a significant increase in the mass of the system. For that reason, it was decided to make the basic structure of the base station consist of a wireframe of beams, similar to the way the ExoMars lander is designed, which can be seen in Figure 6.10a. [2]

The top of the base station is made as a flat plate with a hole at the centre. This plate is attached to the lower frame at each of the corners of the octagonal base. This plate functions as a landing platform for VITAS. Inside the central hole in the platform, a robotic arm is located, which can connect to VITAS when it has landed. That connection will be used for the charging of VITAS batteries. Around the hole, a total of four short-range antennas are sunken into the top plate. These antennas can be used by VITAS for highly accurate navigation, allowing for very fine adjustments to its location during landing. The design of this arm is based on the design of the Instrument Deployment Arm which is used on the NASA InSight lander, which can be seen in Figure 6.10b.

On the lower side of the base station, the landing gear is mounted. For the design of the landing gear, there are two main design options, being a cantilever configuration or an inverted tripod configuration, as described by Witte [2015]. The difference between the two configurations can be seen in Figure 6.11. Neither of the configurations is inherently better than the other option, but for this design it was decided to use the cantilever configuration, as that provides larger ground clearance for the system. In this case, the secondary struts of the landing gear will be responsible for the deployment of the gear, whereas the primary strut will be responsible for carrying the main gear loads. Inside the primary strut, a shock damper will be located, which can reduce the loads on the system during touchdown. The primary strut of each landing gear will also be equipped with a linear actuator, which allows for a small extension of each of the landing gears. In this manner, the system will be able to provide a horizontal landing surface for VITAS.

6.3.3. Subsystems

For the proper functioning of the base station and to provide the ability to support VITAS completely, some dedicated subsystems are required. These subsystems will be described here briefly, whereas the detailed design of these systems will be provided in Chapter 7.

Thermal Control

The thermal control system on the base station consists of one thermal box shaped to fit within one of the octagonal facets of the base station. This thermal box contains the temperature-sensitive systems of the base station, including the majority of the EPS and communications system components, as well as the required insulation and technology

[2] URL:`http://www.russianspaceweb.com/exomars2018-2017.html` [Cited 20 June 2018]

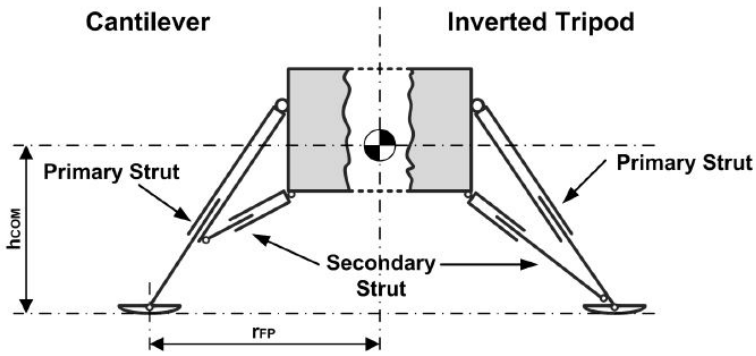

Figure 6.11: A schematic overview of the cantilever (left) and inverted tripod (right) landing gear configurations

Figure 6.12: A deployment test of InSight's solar panels

to maintain the inside of the box within the allowed temperature range.

Electrical Power System

The EPS on the base station consists of a power generation system and a power storage system. For the power generation, four solar panels are used, which are extended from the base station. For the solar panels, the same concept is used as on NASA's InSight mission: folded triangles deploy as a circular solar panel, see Figure 6.12. Due to the solar panels having to fit inside the base station, the radius of the circle is limited to 1.2 m. The power storage for the base station consists of a series of lithium nickel cobalt aluminium oxide (NCA) batteries, which are stored within the thermal box.

As the EPS also provides the power to the UAV, the EPS also uses the robotic arm which is mounted on the base station. The robotic arm is equipped with a connection to charge batteries of VITAS.

Command & Data Handling

The CDH subsystem of the base station is the main data handling system for the mission. It processes all the data which passes through the base station. For this mission, this means that all the scientific data which is gathered by VITAS and transferred into the base station is then compressed and stored by the CDH subsystem, after which a selection of data is prepared for transmission to Earth. Any communication from Earth (e.g. a mission update or request for specific data) is also processed by the base station CDH, after which the relevant subsystems or the VITAS flight computer can be updated with the relevant data. Finally, the CDH receives and processes the housekeeping data of the relevant subsystems, which is regularly communicated to Earth.

Navigation

The base station has a major contribution to the navigation system. First of all, one of the navigation system's beacons is positioned inside the base station. Secondly, the base station provides the attachment for the external navigation beacons during the travel towards Mars, and provides the system to deploy those beacons during the

EDL phase of the mission. Finally, the base station contains minor beacons which can be used by VITAS to position itself properly above the base station during the landing phase.

Communication
The communication subsystem of the base station consists of many different components, as it is responsible for multiple channels of communication. First of all, it manages the communication with VITAS. Secondly, it is used for communication with Earth through the Mars Relay Network. Finally, it communicates directly with Earth's Deep Space Network. The combination of these communication channels requires a large number of different antennas, amplifiers and transceivers.

An overview of the total mass and power budget for the base station is provided in Table 6.3. At last, an overview of the base station design is shown in Figure 6.13.

Table 6.3: The total mass and power consumption of each of the base station subsystems

Subsystem	Mass [kg]	Mass percentage	Nominal power [W]	Peak power [W]
Structure	314.93	70.0	-	-
Thermal	0.85	0.19	0.1	30.1
EPS	96.73	21.50	-	-
CDH	11.64	2.59	38.52	80.53
Navigation	4.37	0.97	8.6	18.3
Communication	15.99	3.55	33.6	122.8
Science payload	5.5	1.22	1.7	17
Total	**450.0**	**100**	**82.5**	**268.7**

6.4. Functional Breakdown Diagram

The functional breakdown diagram (FBD) gives an overview of the functional tasks the system will have to be able to accomplish in order to successfully complete the mission. The FBD has been split into three branches on its top level:

- *Perform mission within external constraints:* the system will have to comply with certain constraints imposed by dependencies on external systems;
- *Perform mission to the best capabilities:* these functions arise from the mission objectives;
- *Reuse system after initial mission:* these requirements originate from the sustainability and re-usability requirements.

The external constraints branch has been further divided into travelling constraints and Martian entry constraints. They imposed mainly sizing and material requirements on the design. For example, the system has to fit inside the entry vehicle in order to be delivered to Mars. While travelling to Mars, the material should not deteriorate, therefore an appropriate material had to be selected. The majority of the functions of the system will stem from the scientific mission it will perform. For this branch, the main subdivision has been made between the two main tasks of the final system: operating autonomously across Mars and gathering and processing data. This roughly mirrors the final division between the propulsion, control and electrical power subsystems and the scientific instrumentation and communication subsystems. The FBD can be seen in Figure 6.14.

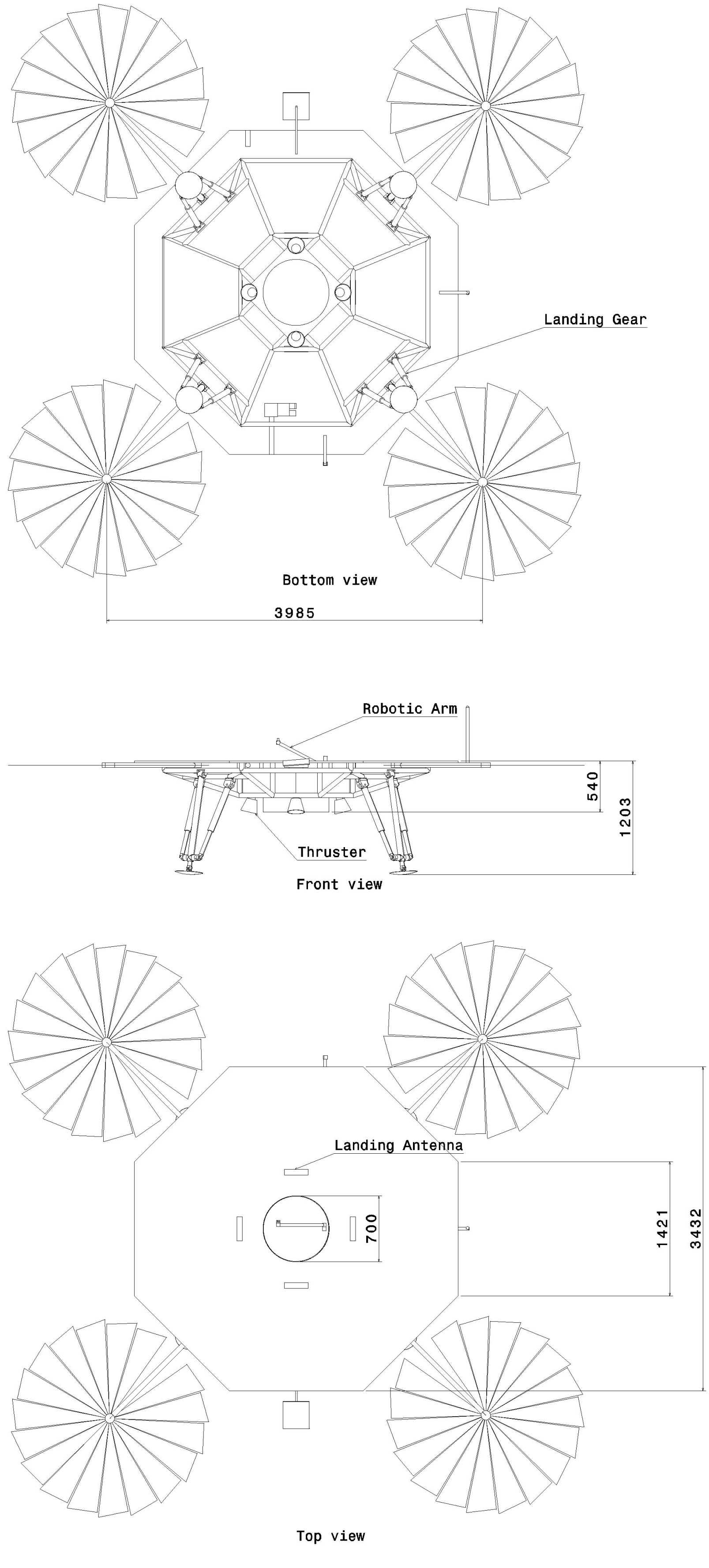

Figure 6.13: Bottom, front and top view of the deployed base station. Dimensions are in millimetres.

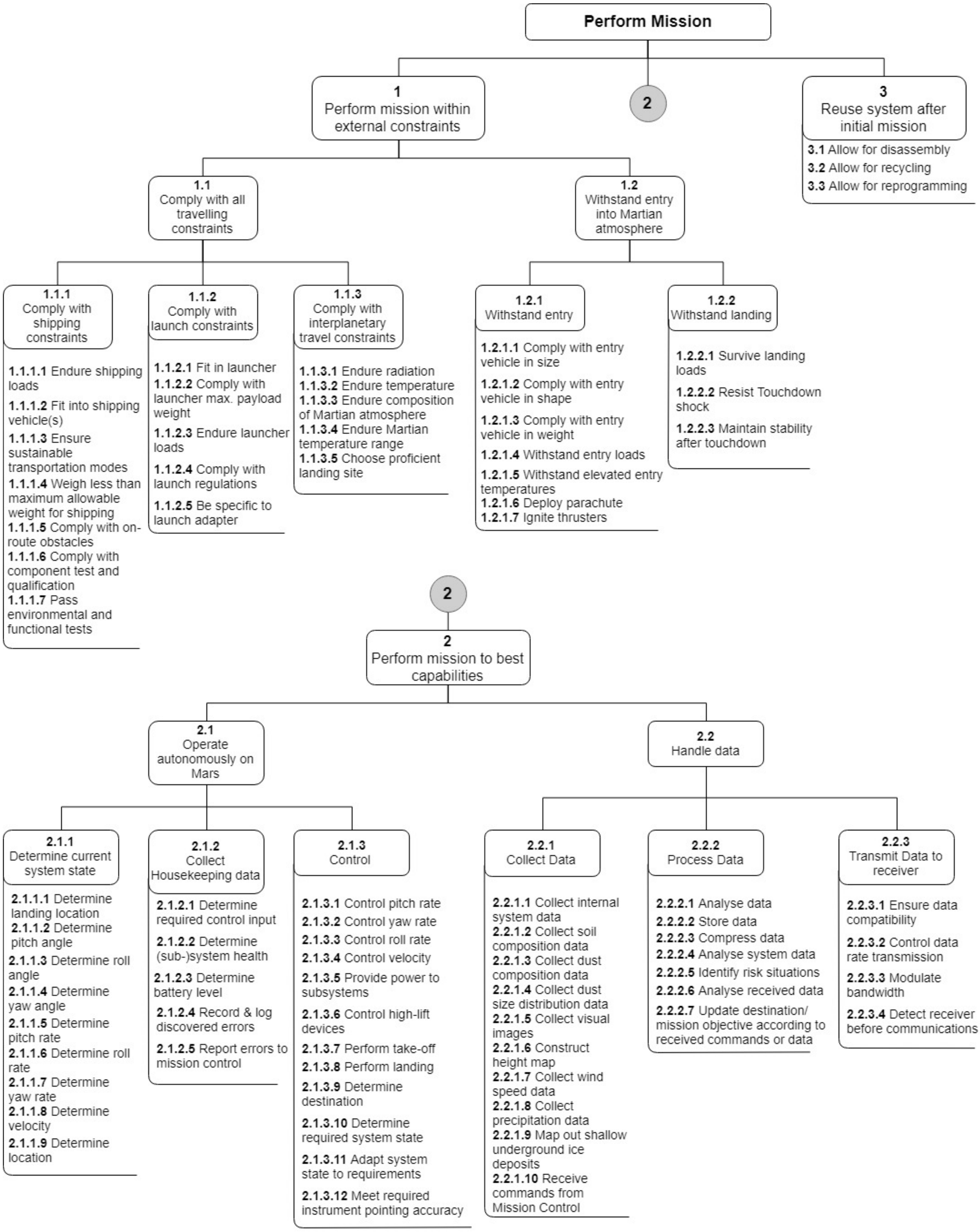

Figure 6.14: The FBD for the MARS mission

6.5. MARS System

In this section, an overview of the MARS system is provided.

6.5.1. Logistics

As mentioned in Section 6.3, the base station mainly functions as support for VITAS. The interaction between VITAS and base station will be further described in this section. VITAS requires some guidance during for landing correctly on the base station. To do so, four antennas are place on top of the base station that will help to navigate VITAS in its final landing phase. In Chapter 7 this system will be further elaborated upon.

A physical connection between the base station and VITAS is established by the use of a robotic arm. The design of this robotic arm is based on the instrument deployment Arm, which is used on NASA's InSight lander. The robotic arm has three joints, just like a human arm: a shoulder joint, an elbow joint and a wrist joint. It uses a camera and targets on the tail of the UAV to aim the connector. The connector serves two purposes: it charges the UAV while also transmitting the data from the UAV to the base station.
The design shall have to be manufactured, tested, assembled and integrated. In Figure 6.15 the process is depicted. In Chapter 8 it is presented at which time the process is executed and which other processes run in parallel.

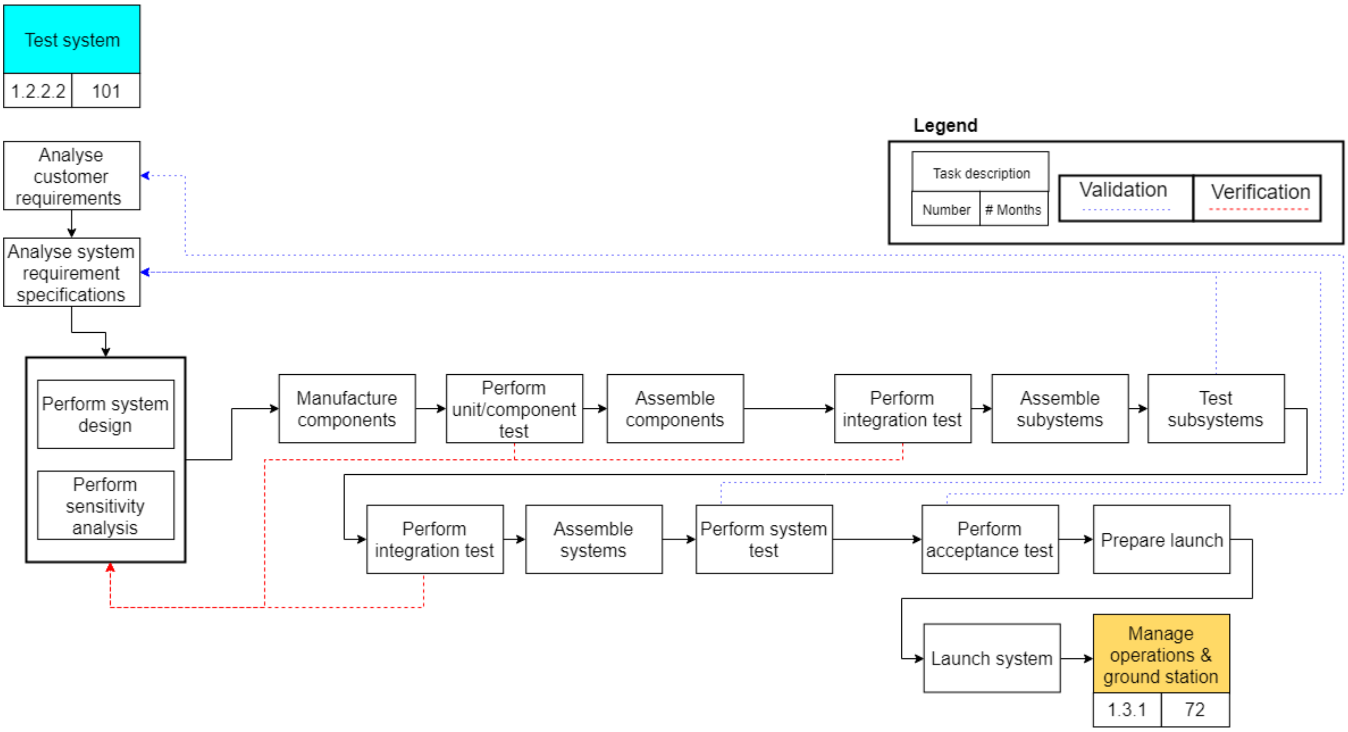

Figure 6.15: Testing process of the system.

Furthermore, more steps have to be taken for the logistics aspect of the mission and are briefly mentioned below:

- **Manufacturing:** The manufacturing aspect is beyond the scope of the report. However, it is an integral part of the mission and has to be analysed in depth in future stages of the project.
- **Transportation:** Raw material will have to be acquired and the system has to be transported. A detailed plan will have to be set up to minimise the distance covered as it minimises cost and emission.
- **Storage:** All components and material will have to be stored. If a joint venture can be set up, storage facilities might be shared. Otherwise and external storage facility has to be allocated

6.5.2. Operations

The operations can be split up into two phases, pre-launch and post-launch. First the pre-launch operations will be discussed and afterwards post-launch.

Pre-launch Operations

- **Management:** During the design stage of the system, the project has to be supervised by a management team. Poor communication can lead to significant costs and delay of the project.
- **Launch:** Preparing the launch requires a lot detail. Safety protocols have to be set up, employees have to be hired, it has to be regulated et cetera. In Figure A.2, a more detailed version is presented.

- **Public relations:** To keep everyone up to date and to create awareness of the brand, public relations will have to be carried out during the design phase. A marketing team will have to be acquired and a plan has to be set up. Investors will have to be attracted, awareness will have to be created and a budget will have to be acquired.

Post-launch Operations

VITAS is going to cover the exploration area in the way that is shown on Figure 6.16. Starting from the base station it will fly a straight line to the outskirts of the exploration zone. There it makes a U-turn and heads back to the base station by covering the ground path next to the first one. This will sum up to a flight of approximately 50 km and the next flight can be performed after VITAS has been charged at the base station. The next flight direction can be taken perpendicular to the previous flight in order to cover a broader range of area in the earlier stages of the mission. Using this flight pattern, VITAS covers a narrow 'pizza slice' of the exploration zone, with a maximum width which is twice the scanning width, namely 200 m. Approximately 770 flights are necessary to cover the entire exploration zone.

With a flight velocity of 82.5 m/s, each flight will take approximately eleven minutes including take-off and landing. Afterwards, the UAV will charge itself on the base station and transfer its data to the base station. It will then prepare for the next flight. The charging time of the batteries takes approximately five hours, this will allow for an average of 1.5 flights per day. During summer, there is more daylight and thus more than one flight can be conducted per day. During winter, when daytime is shorter the amount of flights is limited to one per day.

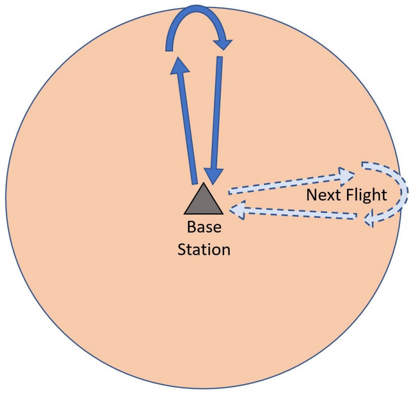

Figure 6.16: Schematic overview of the flight path of the UAV.

The UAV will have to be monitored from the ground. The top level steps that are taken are depicted in Figure 6.17.

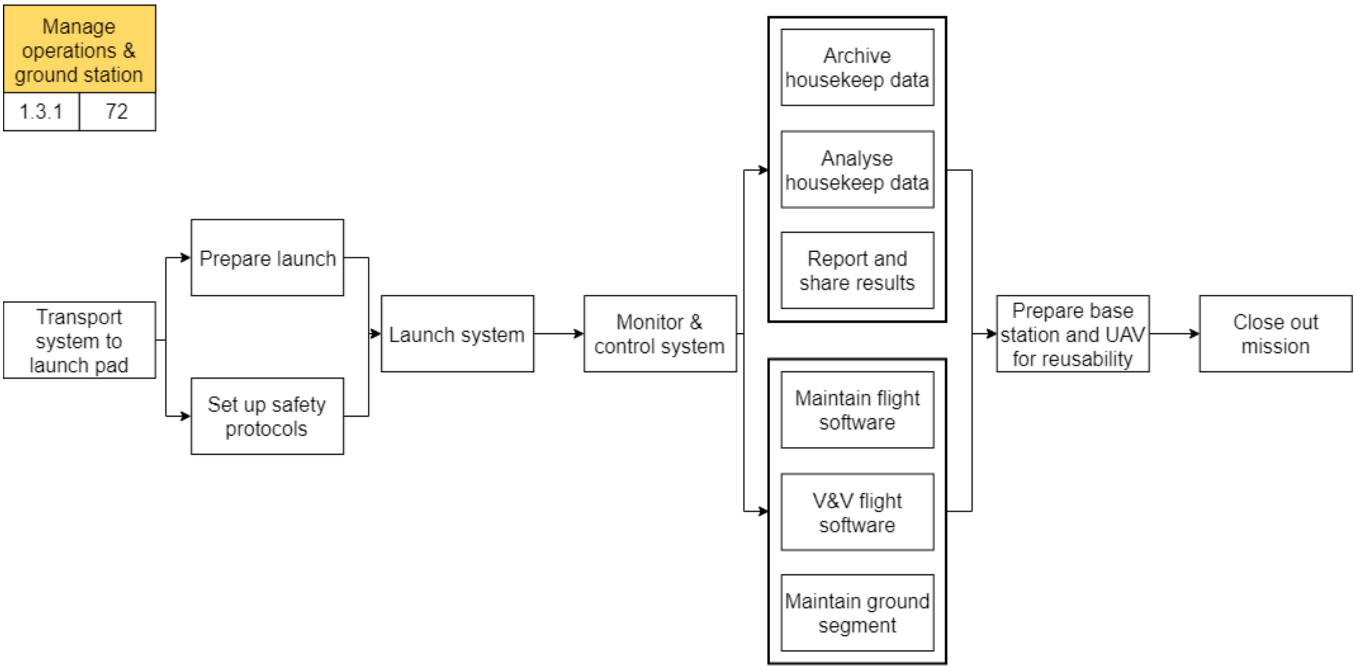

Figure 6.17: Top-level flow diagram of the ground segment

Other operations have to be performed during the mission, however working these out in detail is beyond the scope of the report. Several aspects are briefly mentioned below.

- **Management:** The entire operations centre will have to be supervised by a management team. Poor communication can lead to significant costs and delay of the project.
- **Public relations:** To keep everyone up to date and to create awareness of the brand, public relations will have to be carried out during the mission. A marketing team will have to be acquired and a plan has to be set up.
- **Closing out the mission:** The mission will not abruptly end. The system has to be prepared for reusability and documents will have to be archived. A detailed flow of this process can be found in Figure A.6 and Figure A.7

Furthermore, in Figure A.3, Figure A.4 and Figure A.5 steps that are taken during the mission are depicted.

6.5.3. Requirements Compliance Matrix and Feasibility Analysis

Figures 6.18 and 6.19 give an overview of how the original top level requirements have been met. Requirements that have not been met are greyed out and indicated with an ×-symbol. Requirements FM-2 and FM-3 have not been met as the accuracy has been lowered. The former is a result of a trade-off performed in Section 7.1.2, where some of the resolution was sacrificed for a more lightweight altimeter. The latter is a result of the lack of available lightweight instruments to measure the shallow ice deposits, as elaborated upon in Section 7.1.3.

All the *CM* requirements have been dropped as the UAV will not perform coarse mapping. The UAV has a sufficiently powerful data handling system and power system such that no instruments accuracy has to be dropped in order for the UAV to function. Therefore all mapping is done with the fine mapping criteria.

Requirements PM-4 and PM-6 could not be met as the range of the UAV could not cover an area with a diameter of a 100 km as described in Section 7.5.1. The exploration zone has been reduced to 50km diameter, which as a result make it impossible to investigate an extra ten areas with a 10 km diameter within this area. However, some smaller areas will be subject to extra investigation as described in section 4.1.

The safety and reliability requirements could not be met as they were not realistically achievable for such a complex space mission. A description of the reliability is given in Section 6.5.4. Requirement SR-3 could not be met as most systems that make up the mission are unique and essential. Failing of the launcher or UAV would end the whole mission. The only way around this scenario is to have a second similar mission, which is realistically not doable.

ST-1 is not met as, although the material is toxic, it is the material that scored the best on the trade-off in Section 7.2.2.

The last top-level requirement that could not be met is the engineering budgets requirements EB-4. As described in Section 7.2, numerical estimations were made for the launcher and landing loads, but not for the entry loads. This came out of the fact that the chosen entry vehicle as it had already been used for the Curiosity-mission.

Name	Top-level system requirement	✔/✘	Revised Requirement	
FM	**Fine mapping**			
FM-1	Visial imaging at 10cm resolution	✔		7.1.1
FM-2	Height map at 10cm resolution and 10cm height resolution	✘	Height map at 20cm resolution and 10cm height resolution	7.1.2
FM-3	Shallow ground ice deposits at 10m depth with 10cm resolution	✘	Shallow ground ice deposits at 10m depth with 1m resolution	7.1.3
FM-4	Soil composition at 100m resolution	✔	Soil composition at 1m resolution	7.1.4
FM-5	Dust composition and size distribution in the lower atmosphere	✔		7.1.5
FM-6	Atmosphere conditions in the lower atmosphere (wind speeds, precipitation)	✔		7.1.6
CM	**Coarse mapping**			
CM-1	Visual imaging at 1m resolution	/	Does not apply	/
CM-2	Height map at 1m resolution, 10cm height resolution	/		/
CM-3	Soil composition at 1km resolution	/		/
CM-4	Trace gas emissions at 1km at 3 heights	/		/

Figure 6.18: Compliance matrix

PM	**Performance**			
PM-1	Autonomous operation	✔		7.8
PM-2	Phase 1 within 2 years of landing	✔		4.2
PM-3	Fine mapping of human habitat zone (2km diameter)	✔	Fine mapping of exploration zone (50km diameter)	7.5
PM-4	Coarse mapping of exploration zone (100km diameter)	✘		
PM-5	phase 2 within 3 years after phase 1	✔	phase 2 within 1 years after phase 1	4.2
PM-6	Fine mapping of at least 10 science regions of interest (10km diameter each assumed)	✘	Additional fly-overs for regions of interest (variable number and diameter, depending on findings)	4.1
SR	**Safety and reliability**			
SR-1	Reliability should be > 99.9% for phase 1	✘	Reliability between 70.6% - 86.9% for phase 1	6.5.3
SR-2	Reliability should be > 99.0% for phase 2	✘	Reliability between 53.3% - 77.7% for phase 2	6.5.3
SR-3	Design should be single point failure free	✘	Unattainble	
ST	**Sustainability**			6.5.4
ST-1	No hazardous/toxic materials	✘	Use of AM120	
ST-2	After the reconnaissance mission, the system should be either reusable or recyclable by futur manned base	✔	UAV can be reused by installing new batteries	
EB	**Engineering Budgets**			
EB-1	Choice for launcher to be based on existing/foreseeable launchers (but no launcher design required)	✔		4.3
EB-2	Total system volume/size/mass should comply with launcher payload restrictions/interfaces	✔		4.3
EB-3	Mass and power budgets for the entry/landing (sub)system may be derived from existing systems	✔		4.3
EB-4	Launching and entry/landing loads should be taken into account	✘	Entry loads have not been taken into account as the entry vehicle is based upon an existing design	7.2
CT	**Cost**			
CT-1	A realistic cost estimation should be provided that covers: design, manufacturing, delivery and operation costs	✔		9

Figure 6.19: Compliance matrix

6.5.4. Reliability, Availability, Maintainability & Safety Analysis

In this section the Reliability, Availability, Maintainability and Safety (RAMS) characteristics of the MARS mission are determined. Although the acronym suggests otherwise, it makes more sense to first treat reliability and maintainability before treating availability, as the latter one is related to the first two. At last, a safety analysis is performed.

Reliability Analysis

According to Hamann and van Tooren [2006], reliability can be defined as 'the probability that a system will perform in a satisfactory manner for a given period of time when used under specified operating conditions'. In order to increase the reliability of the mission, several measures were taken into account during the design of the system.

- *Parts selection:* it was opted to choose for components which preferably had been proven on their reliability under the operational conditions on Mars. Components that have not been proven yet, will be tested for their reliability in the Martian environment in the future stages of the project.
- *Redundancy in design:* if possible, parallel redundancy was added to the system as this will increase its reliability. However, this increase in reliability was always traded off against the increase in cost and mass of the system. Especially for VITAS redundancy would come at a great expense due to the snowball effect.
- *Defining failure modes:* it is also useful to identify all system components that can fail without obstructing the mission operation. This also includes defining at what point in time the redundancy of components is allowed to reduce.

The reliability of a single component has an exponential distribution over the operating time t, i.e.,

$$R_{\text{sys}} = e^{-\lambda t_{\text{op}}} \tag{6.1}$$

where λ is the failure rate of the component [Wertz and Larson, 1999]. The system reliability is calculated by multiplying the reliability of its components. According to Zandbergen [2018], the overall spacecraft failure rate lies between 0.056 and 0.139. Using these values and Table 24-3 from Wertz and Larson [1999], the failure rates per spacecraft component were calculated, which are displayed in Table 6.4.

Table 6.4: The percentage of failures related to each spacecraft component and their corresponding failure rates for the first year and the second till the fifth year.

Subsystem	**1 year**	λ_{worst}	λ_{best}	**5 years**	λ_{worst}	λ_{best}
Attitude control	12%	0.0111	0.0045	11%	0.0153	0.0062
Thruster/Fuel	20%	0.0278	0.0112	16%	0.0222	0.00896
Control processor	0%	0.00	0.00	4%	0.0056	0.0022
Mechanisms/Structure/Thermal	10%	0.0139	0.0056	11%	0.0153	0.0062
Payload instrument	2%	0.0028	0.0011	3%	0.0042	0.0017
Battery/Cell	2%	0.0028	0.0011	10%	0.0139	0.0056
Electrical distribution	8%	0.0111	0.0045	10%	0.0139	0.0056
Solar array	17%	0.0236	0.0095	12%	0.0167	0.0067
Telemetry tracking and command	23%	0.0320	0.0129	18%	0.0250	0.0101
Unknown	6%	0.0083	0.0034	5%	0.0070	0.0028

During the cruise phase to Mars, almost all subsystems are inactive and it is assumed that only the attitude control and unknown failures can occur. This leads to a failure rate of 0.0194 for the worst case and 0.0079 for the best case during the first seven months. After the system has landed on Mars, all subsystems are active and therefore the failure rate will be between 0.056 and 0.139. Plotting the reliability curves for these failure rates leads to Figure 6.20. With a total mission duration of 5 years, the reliability of the mission will be between 53.5% and 77.7%.

Maintainability Analysis

In every space mission, maintenance is a crucial part in order to be successful, especially for missions with a long duration like MARS. Maintenance can be split into two types: hardware and software maintenance. Hardware maintenance is crucial during the production and assembly phase of the mission. This also includes an analysis of the storage and possible repairs of components during this phase.

After launch the prime maintenance that will take place is software maintenance. If bugs and/or errors appear, the system will enter a safe mode in which the UAV is landed at the base station and waits for further commands from the ground station (GS) on Earth. The system will then wait for software updates sent from the GS. The full procedure for software maintenance is shown in Figure 6.21.

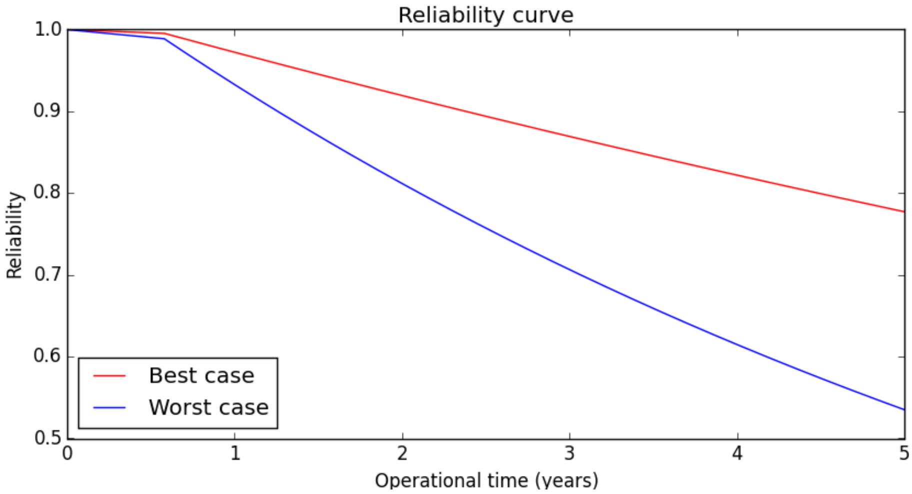

Figure 6.20: The reliability curve for the MARS mission.

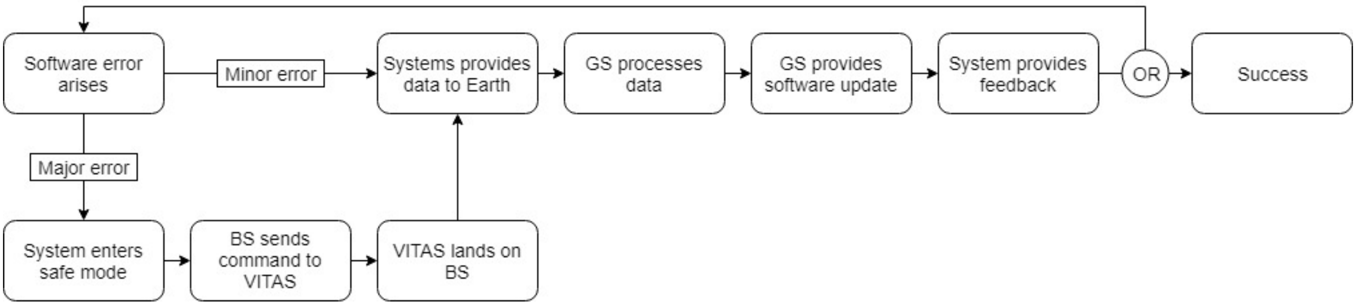

Figure 6.21: The system procedure in case a software error occurs.

Availability Analysis

The availability of the system A_{sys} is the portion of the time that the system is operational, i.e.,

$$A_{\text{sys}} = \frac{t_{\text{up}}}{t_{\text{total}}} \tag{6.2}$$

in which t_{total} is the sum of the downtime and the uptime, t_{up} [Wertz and Larson, 1999]. The largest share in the downtime is the cruise phase in which the system travels to Mars, this phase will take approximately seven months. As said in the maintainability analysis, there is also some downtime in case the system is waiting for software updates. However, it is impossible to predict if this will happen and even if so, the duration will probably be negligible compared to the cruise phase duration. Therefore, it was decided not to take this into account for the availability calculations. As the total mission duration (from launch until end of mission) is approximately five years, the availability of the system is estimated to be 88.3%.

Safety Analysis

When designing for safety, the MARS system itself, other systems, humans, the terrestrial environment and the Martian environment have to be protected from hazards. This should be taken into account from the begin of the design up and until the end of life. Using Table 14-16 from Wertz and Larson [1999], the safety hazards for different components and their corresponding impacts on the design were determined. The result is shown in Table 6.5.

Table 6.5: Safety impacts on the MARS mission design

Component	Hazard	Design impact
Batteries	Fire, explosion, toxic materials	Battery design rules, charging restrictions, cell monitoring
Deployables	Impact with personnel, interference with launch vehicle operations	Extra electrical switches
Launcher	Explosion, crashing	Implement safety measures for toxic materials
Structure	Toxic materials	Develop safe production strategy, develop after mission strategy
Propulsion	Fire, explosion, toxic fluid/gas	Pressure vessel design guidelines, extra valves, extra electrical switches
EPS	Short circuit	Wire insulation

6.5.5. Technical Risk Assessment

For each engineering project, a risk management plan is crucial in order to be successful. Possible future risks were identified and assessed for their likelihood and consequence level. Mitigation techniques were then established and applied to the identified risks.

Risk identification

The technical risks of MARS have been organised according to the mission phases as defined in Chapter 4. All identified risks are shown in Table 6.7, including their likelihood and consequence level and the corresponding risk value. Using the risk values, the risk map shown in Table 6.6 was created.

Table 6.6: Initial risk map, with risk numbers corresponding to Table 6.7.

Catastrophic	1.3; 1.4; 1.5; 2.2	2.5; 2.6; 3.2; 3.4	3.11		
Critical	2.4	0.3; 1.1	0.1; 0.5; 3.12		
Marginal	3.6; 3.9; 5.2	1.2; 2.1; 2.3; 3.1; 3.3; 3.7; 3.13; 5.1	0.2		3.5
Minor	4.1		0.4; 3.8; 3.10		
Negligible					
Conseq./Likel.	Rare	Unlikely	Possible	Likely	Certain

Mitigation techniques

In order to mitigate the identified mission risks, different mitigation techniques were identified and applied.

The likelihood of certain risks has been lowered by opting for (sub)system design with a high TRL. Another way of mitigating the likelihood is by performing extensive research on the relevant subsystems, as e.g. some of the instruments for scientific research had originally not been designed for usage on Mars. By performing research on whether or not these systems can perform in the Martian environment, a clearer image of the performance of such products has been established which was used to reduce the likelihood of such risks.

In order to reduce the consequence level of a given risk, the chosen methods depend on the type of risk involved. For risks which are more organisational in nature (e.g. the risks in phase 0), it is useful to have a backup plan in place in case the risk seems to emerge. For scheduling risks, this also includes making sure that there is always a margin to overshoot the schedule, to make sure that small delays are not directly problematic.

When considering purely technical risks, the most effective way to reduce the consequence of a given risk is by adding one or more levels of redundancy for the involved (sub)system(s). This technique is not applied to a very large extent in this project, as the total mass of the UAV-system is of key importance for this mission and had to be kept as low as possible, therefore other methods were applied to mitigate the total risks involved. For some very light-weight subsystems, or subsystems within the base station, this method was considered.

In the process of deciding upon design options, some risk mitigation techniques were taken into account as well. For example, the risk of a crash of the UAV during take-off or landing was considered too high. To reduce the

Table 6.7: All identified risks

Phase	Risk ID	Risk	Likelihood	Consequence	Risk value
0	0.1	Manufacturing delay	6	7	42
	0.2	Shipping delay	5	6	30
	0.3	Redesign of (sub)system required	4	8	32
	0.4	Mission cost exceed mission budget	6	3	18
	0.5	Required technology not ready in time	5	8	40
1	1.1	Launch delay	4	8	32
	1.2	(Sub)system damaged	3	6	18
	1.3	Collision with an object in LEO	1	10	10
	1.4	Solar storm	1	10	10
	1.5	Launcher failure	1	10	10
2	2.1	Landing in incorrect location	4	6	24
	2.2	Crash landing	2	10	20
	2.3	One or more subsystems do not initiate	3	5	15
	2.4	Solar panel deployment failure	2	8	16
	2.5	Failure during guided entry	3	10	30
	2.6	UAV detachment from base station failure	4	9	36
3	3.1	Mission not finished in time	4	6	24
	3.2	Engine/propeller failure	4	9	36
	3.3	Scientific instrument damaged	3	5	15
	3.4	Data transmit to Earth fails	3	9	27
	3.5	Getting caught in a dust storm	9	6	54
	3.6	Unforeseen Martian environmental circumstance	2	6	12
	3.7	Software error	3	5	15
	3.8	Scientific data not saved properly	5	3	15
	3.9	Sci. and location data mismatched	2	5	10
	3.10	Deviation from trajectory	5	4	20
	3.11	UAV crash during take-off/landing	6	10	60
	3.12	Navigation failure	5	8	40
	3.13	Required accuracy not met	3	5	15
4	4.1	End of mission command not processed well	2	3	6
5	5.1	System components not recyclable/reusable	4	5	20
	5.2	Manned mission unable to recover component	2	5	10

Table 6.8: The mitigation applied to each risk

Risk ID	Parameter lowered	Mitigation technique
0.1 till 0.3	Consequence	Adding time margins in schedule
0.4	Likelihood	Adding contingencies in mission budget
0.5	Likelihood	Performing extensive research on all subsystems
1.1	Consequence	Choosing adequate launch window
1.2	Consequence	Adding redundancy
2.5	Likelihood	Choosing proven concept
2.6	Likelihood	Adding redundancy
3.2	Likelihood	Thoroughly investigating the propulsion design
3.4	Likelihood	Adding redundancy
3.5	Consequence	Adding time margins in mission schedule
3.11	Likelihood	Reducing the amount of takeoffs and landings
3.12	Likelihood	Adding redundancy
3.13	Consequence	Contingencies in amount of mission cycles

likelihood of this risk, it was decided to minimise the amount of take-offs and landings. This resulted in a change of the soil sample requirement, as this would require a huge amount of take-offs and landings.

Updated risk map

The mitigation techniques as described have been applied to the crucial risks for the project, as can be seen in Table 6.8. The result of applying these mitigation techniques yields Table 6.9.

Table 6.9: The updated risk map after applying mitigation techniques

Catastrophic	1.3; 1.4; 1.5; 2.3; 2.5; 2.6; 3.2; 3.4	3.11			
Critical		0.5; 3.12			
Marginal	3.6; 3.9; 5.2	2.1; 2.2; 2.4; 3.1; 3.3; 3.7; 5.1			
Minor	4.1	0.3; 0.4; 1.1; 1.2; 3.13	0.1; 0.2; 3.8; 3.10		3.5
Negligible					
Conseq./Likel.	Rare	Unlikely	Possible	Likely	Certain

The main risks to be investigated further are risk 0.5, 3.5 and 3.11. These currently form the highest risk for the mission and therefore, the focus should lie on mitigating these risks.

6.5.6. Resource allocation and breakdown

The resource allocation for the detailed design of each subsystem can be seen in Section 6.5.6. The allocated mass and power can be seen in on the left column ”Allocated resources”, the middle column titled ”Estimated resources” is the allocated resources plus their contingencies. In the column ”Current resources” the values resulting from the detailed subsystem design and the new contingencies are present. On the right column titled ”Estimated final resources”, the allocated resources plus their contingencies at the current design stage can be seen. This is representative of the values that are expected once the design is complete.

In Figure 6.22 the estimated UAV mass is compared to the required and target values over the design period. After May 21, action was taken in order to keep a viable design, a redesign of the propeller blades, as described in Section 7.3, was done to raise the required weight up to 14 kg. On June 26, the actual weight fell under the target weight and no further actions was necessary.

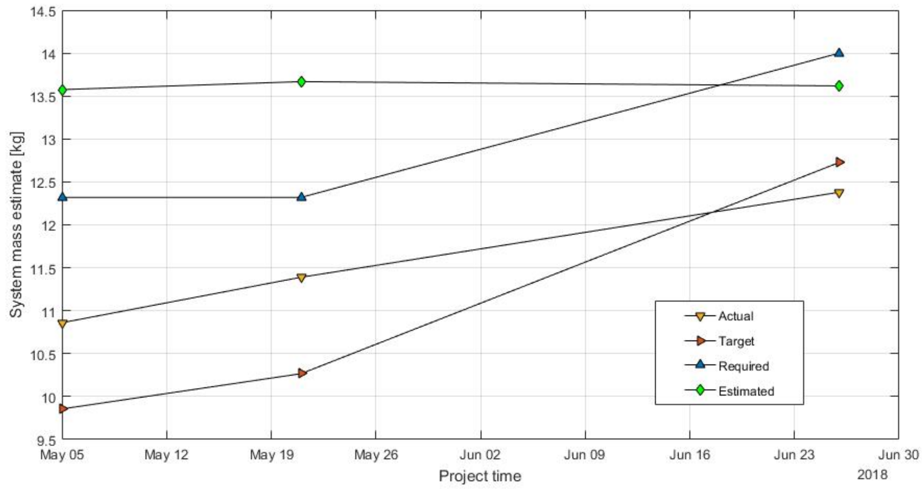

Figure 6.22: The change of the mass with and without contingency over time

Table 6.10: The resource allocation and budget breakdown with the contingency expressed in percentage.

Subsystem	**Allocated resources**		**Cont. [%]**	**Estimated resources**		**Current resources**		**Cont. [%]**	**Estimated final resources**	
	Mass [kg]	Power [W]		Mass [kg]	Power [W]	Mass [kg]	Power [W]		Mass [kg]	Power [W]
Scientific	1.5	35	15	1.725	40.25	1.62	22.1	5	1.7	24.31
CDH	1	20	15	1.15	23	0.75	12.25	5	0.79	12.86
Navigation	0.61	10	15	0.7	11.5	0.49	10.08	10	0.54	11.09
TCS	0.61	25	15	0.7	28.75	0.5	11.1	10	0.55	12.21
Communication	0.61	10	15	0.61	11.5	0.18	1.6	10	0.20	1.76
Propulsion	2.12	1000	15	2.44	1150	2.37	1870	15	2.72	2150.5
Structures	2.43	-	15	2.8	-	3.89	-	15	4.47	-
EPS	3.1	-	15	3.55	-	2.47	-	15	2.84	-
Flight control	0.18	20	15	0.21	23	0.12	20	15	0.14	23
Total UAV:	**12.65**		**15**	**14**	**-**	**12.38**	**-**	**13**	**14**	**-**

7 Subsystem Design

MARS consists of the VITAS drone and a base station, both of which contain various subsystems responsible for specific tasks. The design approach and results for each subsystems will be discussed in this chapter. The choice and design of the scientific instruments on the UAV and the base station will be discussed in Section 7.1. In Section 7.2, the design process and results of the support structure of the UAV are presented. Next, the propulsion unit design will be elaborated on in Section 7.3. The design of the Electric Power Subsystem(EPS) used on the UAV and base station is discussed in Section 7.5, followed by the communication subsystem design in Section 7.6. For more information about the thermal control subsystem design, Section 7.7 should be looked into. The navigation subsystem is discussed in Section 7.8 and the chapter is concluded by the design process of the Command and Data Handling(CDH) subsystem in Section 7.9.
Figure 7.1 and Figure 7.2 show the layout of the hardware and how they interact with each other.

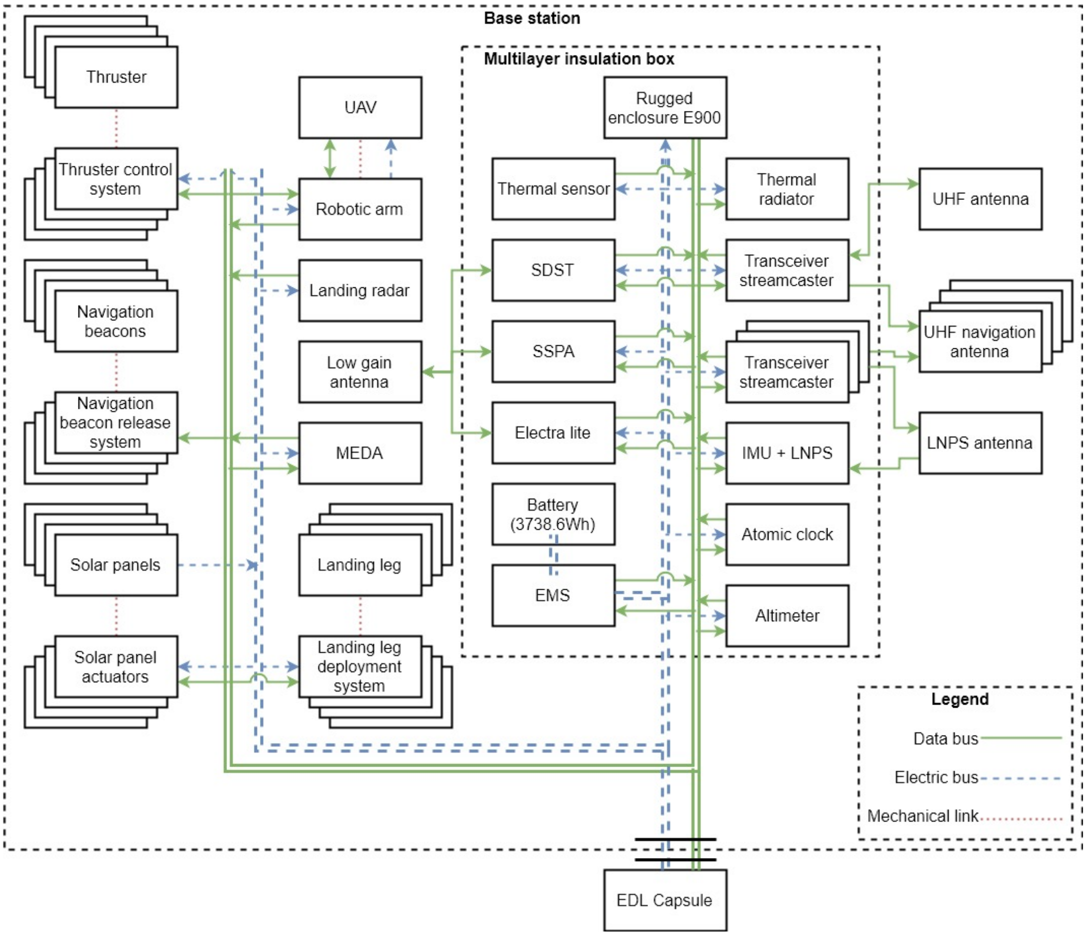

Figure 7.1: Hardware diagram of the base station.

7.1. Scientific Payload

As aforementioned in Chapter 2, the future of space exploration is bound to move towards manned missions to Mars by 2035. In order to enable and facilitate this goal, more detailed information of the exploration zone, the Jezero Crater (selected in Section 4.5), is needed. The scientific payload of MARS will provide for additional information of the exploration zone, and therefore can contribute to the advancement of the space exploration missions. The selected scientific payload presented within this section is chosen based on the scientific requirements from Section 5.1. Each requirement is introduced, and subsequently elaborated upon.

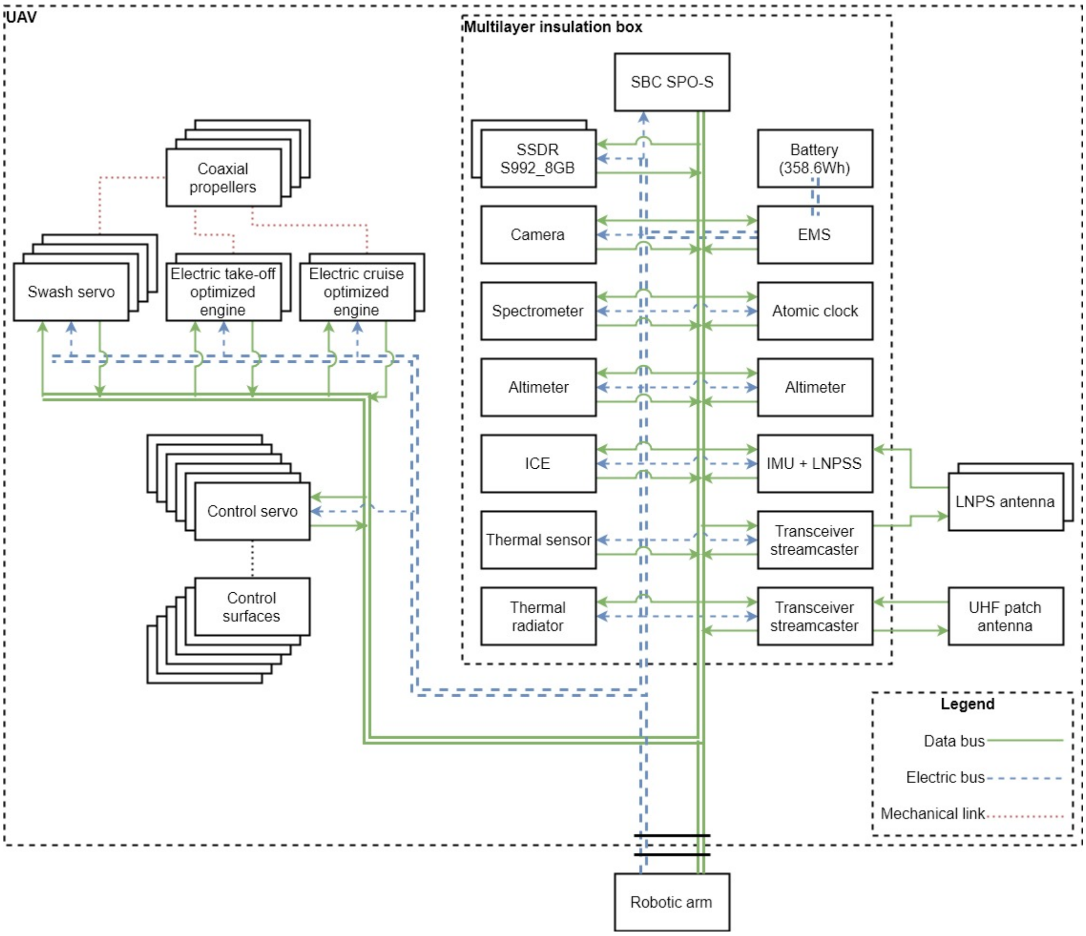

Figure 7.2: Hardware diagram of VITAS.

- MARS-UAV-SYS-Science-2: The system shall perform visual imaging at a resolution of 10 cm.
- MARS-UAV-SYS-Science-3: The system shall perform height mapping at a 10 cm spatial resolution and a 10 cm height resolution.
- MARS-UAV-SYS-Science-4: The system shall scan shallow ground ice deposits up to a depth of 10 m and at a resolution of 10 cm.
- MARS-UAV-SYS-Science-5: The system shall measure soil composition at a resolution of 100 m.
- MARS-UAV-SYS-Science-6: The system shall measure the composition and size distribution of dust in the lower atmosphere.
- MARS-UAV-SYS-Science-7: The system shall measure the wind speed and precipitation in the lower atmosphere.
- MARS-UAV-SYS-Science-8: The system shall measure the following trace gases at a 100 m resolution at 3 heights: methane, carbon dioxide, atomic oxygen, ozone and argon.

7.1.1. Visual Imaging

Visual imaging of the landing site is of paramount importance, as it shows the terrain, the layout, and the environment of the exploration zone. This instrument will act as the eyes of this mission, as well as any future mission, both manned and unmanned.

There are existing pictures of the Martian terrain and environment previously taken by Mars missions. Although the Martian rovers have already taken high resolution images but not from a lot of different areas as the rovers cover little ground during their lifetime. So far, the furthest driving Martian rover travelled 40 km[1]. As presented in Section 6.2, VITAS would fly 40 km in approximately 500 seconds, and would thus exceed any current rover in area covered.

Furthermore, there are also Martian satellites with visual imaging capabilities, the most capable being the MRO with a resolution of 0.3 m at a height of 300 km [2]. If the visual imaging device reaches the required resolution of 0.1 m, it would improve the resolution nine times.

For the selection of the visual camera and consequent lens system, previous space missions where analysed. Malin

[1]URL: https://www.jpl.nasa.gov/news/news.php?release=2014-245 [Cited 24 June 2018]

[2]URL: https://marsoweb.nas.nasa.gov/HiRISE/instrument.html#components [Cited 24 June 2018]

Space Science Systems (MSSS) provided cameras for nearly all missions to Mars. The MSSS inventory of cameras includes one that is compatible with the MARS-UAV-SYS-Science-2 requirement, and is directly available for purchase.
The C50[3] camera, combined with an ECAM-NFOV [4], can produce a horizontal field of view of 53^o necessary for a swath width of 100 m while flying at an altitude of 100 m. In order to obtain a horizontal resolution of 0.1 m the camera needs 1000 pixels on its horizontal axis. The speed of VITAS in cruise is 82.5 m/s, thus a vertical resolution of 825 pixels per second is required. The amount of pixels on the horizontal axis multiplied with the vertical resolution per second equals the total pixels per second required from the camera. This combined with 8 bit per colour per pixel and capturing blue (400-500 nm), green (500-575 nm) and red (575-750 nm) results in a data throughput of 19.8 megabit per second (Mbps). In Table 7.1 it is shown that the camera selected, C50, is more than capable and only needs to record a frame every 0.87 seconds. It was therefore concluded that requirement MARS-UAV-SYS-Science-2 was met.

Table 7.1: Visual camera fact sheet and its capabilities in different frame size settings.

Model	C50
Mass [kg]	0.26
Idle power [W]	1.75
Nominal power [W]	2.5
Bits per pixel	24

Frame size	Frames per second
2650x1944	3
2560x1600	3.5
2048x1536	2.5
2048x1080	4
1280x720	8
640x480	20

7.1.2. Height Mapping

Height mapping of the landing site and the exploration zone would provide a total overview of the surrounding area when combined with the visual imaging. Space missions that perform height mapping use very heavy and powerful equipment, but equipping this for VITAS is suboptimal. Thus, in order to find a remedy to this end, the example of height mapping drones on Earth is considered, as they utilise altimeters to perform height mapping. Subsequently, an in-depth analysis was performed, which resulted in the accumulation of the height mapping instruments shown in Table 7.2. To determine if the instrument is capable of performing the scientific mission, the measurements per second (mps) of each instrument was compared to what is required. The required mps is calculated based on:

$$MPS = \frac{d_{\mathrm{w}}V}{RES}, \tag{7.1}$$

where d_{w} is the swath track width, V is the UAV's speed and RES is the resolution. Using a width of 100 m, V of 100 m/s and a RES of 0.1 x 0.1 m, resulting in 825000 mps. Even though VLP-32C comes close, none one of the altimeters presented in Table 7.2 are capable of producing this result. The weight of VLP-32C exceeds the foreseen weight, and therefore the choice was made to use VLP-16 Lite for the mission and consequently sacrifice on resolution. The final resolution was set to 0.2 m and requirement MARS-UAV-SYS-Science-3 was not met. With the new resolution the mps becomes 206 250, this combined with 3.35 bits per measurement, which includes location data, results in a data rate of 5.17 Mbps. From this it was concluded that requirement MARS-UAV-SYS-Science-3 was not met, thus the proposed alteration of the requirement is as follows:

- MARS-UAV-SYS-Science-3: The system shall perform height mapping at a 20 cm spatial resolution and a 10 cm height resolution.

Table 7.2: Altimeter accumulation of different altimeters. [5] [6] [7] [8]

Name	Mass [g]	Power [W]	MPS	Range [m]	Accuracy [cm]
LeddarOne	14	1.3	140	40	5
VLP-32C	925	10	600 000	200	3
VLP-16	590	8	300 000	200	3
YS Surveyor	1500	15	300 000	100	3

[3]URL: `http://www.msss.com/brochures/c50.pdf` [Cited 24 June 2018]
[4]URL: `http://www.msss.com/brochures/xfov.pdf` [Cited 24 June 2018]

Table 7.3: Ice deposits detection instrument

Name	Mass [g]	Power [W]
WISDOM	400	10

7.1.3. Ice Deposits

For a Martian human mission to be self-sufficient, water in the form of ice deposits is necessary. Satellites and rovers can use different methods to detect shallow ice. Satellites commonly use neutron detectors, which look for neutrons reflected by the Mars surface. Neutrons that have been slowed down by a particular amount after having been reflected, point to the presence of water. Rovers can also make use of radars, as they are close to the actual surface. The radar sends radio waves towards the ground, and the signal is picked up again and analysed for water traces. These traces are found due to a reduction of strength in the returned signal, as ice absorbs only a part of the frequencies being sent. A driving criteria when selecting instruments for VITAS is that it has to be as lightweight as possible. The first option is the WISDOM which consists of two antenna's and is used on ExoMars. The second option is the RIMFAX that will be equipped on Mars 2020. It was concluded to use the WISDOM due to its lighter weight (400 g versus a weight of 3500 g for the RIMFAX), it will be equipped on the UAV. The UAV will roam the Martian surface while the antenna's transmit radio waves down in an effort to detect ice deposits at a depth of up to 10 m [Ciarletti and Clifford, 2017]. This has never been tested on a flying platform, however, due to the limited scope of this project, the feasibility was brought to the attention by ESA and awaits subsequent advice. First estimations would prove that the Martian atmosphere has little impact on the measurement, due to its low permittivity of the ahmosphere [9]. The requirement MARS-UAV-SYS-Science-4 demands for this measurement to have a spatial resolution of 10 cm, as this instrument scans for ice in an infinitely thin line which VITAS drags along. The requirement MARS-UAV-SYS-Science-4 is proposed to be altered as follows:

- MARS-UAV-SYS-Science-4: The system shall scan shallow ground ice deposits up to a depth of 10 m, at a height resolution of 10 cm and will do this every 1 m.

For every measurement point the WISDOM gathers 80 000 bits, if the WISDOM measures every meter in flight with a speed of 82.5 m/s the resulting data rate is 6.6 Mbps.

7.1.4. Soil Analysis

For a Martian human mission to be successful, the locating and extracting of minerals and resources is important. There are three main ways to analyse soil. First, the drilling of soil samples and heating these in order to extract the gases necessary for measuring the soil composition. This method is used on the Curiosity rover, with the gas extracting system having a mass of 40 kg and a 5 kg drill. Secondly, the option to point a powerful laser onto one spot and fire the laser until gases are expelled. Taking microscopic pictures of the released gases reveals the composition of that one spot. Finally, performing soil properties mapping using a remote sensor, namely a hyperspectral camera. Hyperspectral cameras can be seen as three dimensional cameras, where two dimensions are spatial and the third one is spectral. The main difference between a hyperspectral camera and a normal camera is that, the hyperspectral camera is sensitive to protons outside of the visible spectrum as well. Instead of only having 3 overlapping light sensors (red- green- blue), each pixel is sensitive to frequencies outside the standard visible spectrum as well. As a result, each pixel has its own spectral emission that can be examined using spectroscopy.

The type of soil laying can be determined by comparing the reference light spectrum and the reflected light spectrum obtained by an individual pixel. By looking for absorption or emission signatures in the obtained spectrum, the soil can be identified and as a result mapped out. In order to increase the accuracy of the measurements, it is practical to have a reference soil sample. This allows to associate dips in the obtained spectrum with a particular mineral that was present in the soil sample. In order to get a reference for the soil sample on Mars, the results from the SAM instrument on board of Curiosity is used.

This technique is commonly used on satellites [Cudahy et al., 2000], and has been proven to work on airborne vehicles on Earth as well [Kruse et al., 2003]. The hyperspectral cameras used for this purpose are commonly VisNIR cameras, which are sensitive to the near-infrared and visible spectrum. The accumulation of investigated hyperspectral cameras are presented in Table 7.4.

[5] URL: https://leddartech.com/app/uploads/dlm_uploads/2018/04/Spec-Sheets-LeddarOne-ENG-12avril2018-web.pdf [Cited 24 June 2018]
[6] URL: http://velodynelidar.com/vlp-32c.html [Cited 24 June 2018]
[7] URL: http://velodynelidar.com/vlp-16-lite.html [Cited 24 June 2018]
[8] URL: http://www.microgeo.it/public/userfiles/LaserScanner/yellowscan-surveyor.pdf [Cited 24 June 2018]
[9] URL: https://www.liebertpub.com/doi/10.1089/ast.2016.1532 [Cited 24 June 2018]

Table 7.4: A summary of hyperspectral cameras. [10] [11] [12]

Camera	Mass [g]	Power [W]	Frequency [Hz]	Pixel/line [-]	Wavelenghts [nm]
OXI NIR-100s	220	2	30	2048	600-950
XIMEA LS150-VISNIR	32	1.8	85	2048	470-950
Headwall's NANO	540	13	300	640	400-1000

The XIMEA LS150-VISNIR was chosen because it was lighter than headwall's NANO and could gather more data than the OXI NIR-100s. The XIMEA LS150-VISNIR is the same type of sensor (CMOS) as the one used in the visual C50 camera, with the only difference being that one is a bare sensor and the other one is a space grade camera, respectively. Ifthe XIMEA LS150-VISNIR was used on a space mission it would need the same space grade package as the C50. So the mass and size of XIMEA LS150-VISNIR is assumed to be the same as C50. By packing them together in one space grade shell, the packaging mass of both sensors is reduced by 1/6. An overview of the final mass and size of the two cameras is given in Table 7.5.

Table 7.5: The updated visual and hyperspectral camera.

Model	Mass [g]	Size [mm]
Old XIMEA LS150-VISNIR	32	26x26x31
Old C50	256	78x58x44
New XIMEA LS150-VISNIR	213.3	78x58x44
New C50	213.3	78x58x44
New Total:	**426.6**	**156x58x44**

The XIMEA LS150-VISNIR is capable of measuring 150 different wavebands of colour, each colour is allocated 8 bits. To keep the data rate within reason, the choice was made to have a 1 m resolution. This resolution resulted in a data rate of 9.9 Mbps. Requirement MARS-UAV-SYS-Science-5 was met as the original requirement stated to have a resolution of 100 m.

7.1.5. Wind, Precipitation and Dust Sensor

The wind speed, atmospheric and dust sensor will be placed at the base station, as the instrument does not require a certain altitude. The Mars 2020 will use a collection of instruments, called MEDA[13], that provide wind speed and direction, temperature, humidity, dust particle size and amount measurements. A sol of measurement of the whole system results in a data return of 88 Mbit.

7.1.6. Trace Gases

Trace gases (gases that take up less than 1% of the volume of the atmosphere), despite their low concentration often dictate climate conditions on a global scale. CO_2 and methane are good examples of this for Earth, being responsible for the gross of global warming. On Mars, methane can be an indicator for organic life.[14] Past Martian lander missions, like the Phoenix lander, Curiosity, but also future mission like Mars2020 and ExoMars2020 have and are going to search for those trace gases as an indicator of Mars supporting or having been able to support life. The trace gas deemed most interesting to investigate was methane. With the recent addition of the ExoMars Trace Gas Orbiter, which is measuring a variety of trace gases at an extremely high sensitivity (methane up to sub ppb levels [Vandaele et al., 2011]), this part of the science mission was deemed redundant. Mainly because the instruments that could be installed on VITAS to achieve the same level of accuracy would weigh too much for the system to fly. Implementing a trace gas measurement system on the base station is a possibility, but would not provide better results than the aforementioned satellite. In addition the mission scope of MARS is different, MARS will investigate the Martian surface for human arrival. Therefore, the focus was shifted towards that aspect and the stakeholder requirement MARS-UAV-SYS-Science-8 was dropped.

[10] URL:https://gamaya.com/smallest-hyperspectral-camera/ [Cited 24 June 2018]
[11] URL:https://www.ximea.com/en/products/hyperspectral-cameras-based-on-usb3-xispec/mq022hg-im-ls150-visnir [Cited 24 June 2018]
[12] URL:http://www.analytik.co.uk/wp-content/uploads/2016/03/nano-hyperspec-datasheet.pdf?x29422 [Cited 24 June 2018]
[13] URL: https://mars.nasa.gov/mars2020/mission/instruments/meda/ [Cited 25 June 2018]
[14] URL: https://www.jpl.nasa.gov/news/news.php?feature=7154 [Cited 20 June 2018]

7.1.7. Scientific Payload Summary

In this subsection an overview is presented of the selected scientific payload. Their mass, power and data rate can all be found in Table 7.6. The scientific data is bundled into a single data package in Section 7.9, taking into account the location data of each pixel in the altimeter data. The location data comes from Section 7.8.

Table 7.6: An overview of the selected scientific payload

UAV						
Name	**Mass [g]**	**Power [W]**	**Size [mm]**	**mps/pps**	**Bits per measurement**	**Mbps**
Visual camera	213.3	2.5	78x58x44	825 000	24	19.8
Spectrometer	213.3	1.6	78x58x44	4125	1200	9.9
Altimeter	590	8	103.3Dx71.7	206250	3.35	0.65
WISDOM	400	10	200x410x180	82.5	80 000	6.6
2x Lenses	200	0	56Dx86	0	0	0
Total	**1616.6**	**22.1**				**41.5**
Base Station						
Name	**Mass [g]**	**Power [W]**	**Size [mm]**	**mps/pps**	**Bits per measurement**	**Mb/sol**
MEDA	5500	17	-	-	-	88

7.2. Structures

The supporting structure for the UAV and the base station are key system elements, since they provide not only housing and space for other subsystems, but also makes up a significant part of the total system mass and cost. The structural element therefore has interfaces with nearly any other subsystem in the system. Before the actual design could start, it was important to first list all structural elements on board of the UAV, as well as the base station. From the preliminary design phase, it became clear that the UAV would have a fixed wing configuration with a payload bay, some control surfaces and propellers for propulsion.

7.2.1. Subsystem Level Requirements

Each structural element on the UAV and base station shall be able to cope with the various loading conditions it experiences throughout the mission and during launch. Since all elements are to be transported to Mars on board the Atlas V rocket, all structural elements must survive the vibrations experienced during launch. For the wings, the lifetime of the mission has to be taken into account, so that they should be able to survive the normal flight loads acting on the wings for all flight cycles. Also, a worst case scenario was constructed, in which the wings are designed to survive the flight loads with a load factor of 4, which is representative of the conventional load factors used for aircraft. Since this was considered to be a once-in-a-lifetime event, the internal stress wasn't allowed above the material yield strength. The landing legs were exposed to a similar worse-case scenario, but now simulating a rough landing, which is discussed more in detail in Section 7.2.3.
The requirements for all structural elements are listed below.

- **UAV:**
- MARS-UAV-STRUC-1: The wings, fuselage, landing leg and canard surface shall have a modal axial frequency of at least 60 Hz in stored configuration.
- MARS-UAV-STRUC–2: The wings, fuselage, landing leg and canard surface of the UAV shall have a lowest modal lateral frequency of at least 15 Hz in stored configuration.
- MARS-UAV-STRUC-3: The maximum internal stress during launch and entry shall remain below the material yield strength.
- MARS-UAV-STRUC-4: The maximum internal stress during normal flight shall remain below the material fatigue limit strength.
- MARS-UAV-STRUC-5: The maximum internal stress during flight with a load factor of 4 shall remain below half the material yield strength.
- MARS-UAV-STRUC-6: The maximum internal stress during normal landing shall remain below the material fatigue limit strength.
- MARS-UAV-STRUC-7: The maximum internal stress during landing on one leg shall remain below the material yield strength.
- MARS-UAV-STRUC-8: The wing, fuselage, landing leg and canard surface structures shall be an assembly of removable parts.
- MARS-UAV-STRUC-9: The fuselage shall provide sufficient storage space for the on-board subsystems.

- MARS-UAV-STRUC-10: The fuselage shall have a straight and transparent window located at the visual instruments.
- MARS-UAV-STRUC-11: The landing legs shall provide a 10 cm clearance between the UAV fuselage and the landing platform while stationary.
- **Base station:**
- MARS-BASE-STRUC-1: The base station shall have a modal axial frequency of at least 60 Hz in stored configuration.
- MARS-BASE-STRUC-BS-2: The base station shall have a modal lateral frequency of at least 15 Hz in stored configuration.
- MARS-BASE-STRUC-BS-3: The base station structure shall provide sufficient storage space for the locally stored subsystems.
- MARS-BASE-STRUC-BS-4: The internal stress during launch and entry shall remain below the material yield strength.
- MARS-BASE-STRUC-BS-5: The internal stress during thruster firing shall remain below the material yield strength.

The process of designing the structural elements can be seen in the work flow diagram illustrated in Figure 7.3. Since the structure of both the UAV and the base station mostly depend on the stored subsystem dimensions and the aerodynamic shape of the UAV, these parameters served as the inputs for the structural design.

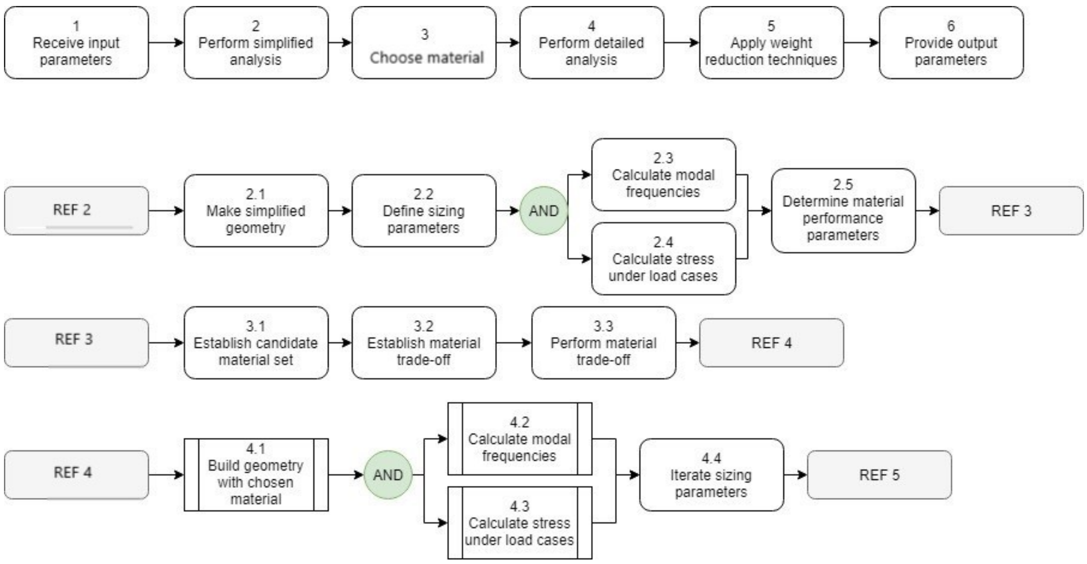

Figure 7.3: Work flow diagram used for the design of the internal structure of the VITAS drone

By performing an analysis of the structural elements in a simplified form, it was possible to determine what material parameters would result in the best structural performance while maintaining a low weight. In Figure 7.4, a sketch of the UAV in stored configuration can be seen. The rigid walls represent support struts which increase the structural stiffness of the most slender bodies on the UAV. In Figure 7.5, the individual, simplified structural elements can be seen, alongside their respective cross-sections. The fuselage and wing are composed out of two sections. This was done in order to allow for different thicknesses in different locations of the element, which could result in a more optimised structure compared to using a uniform thickness. For the fuselage, section 1 is the payload bay section and section 2 the wing-fuselage connection. For the cross section of each section, the respective average circular radius was used for analysis. For the wing, a similar approach was used. The wing was separated in two sections at 40 % of the wing span, where the wing surface area was almost exactly split in two. On each section, the average chord length was used as a uniform cross section. The mass suspended in the fuselage is the mass of the on-board payload, as well as the fuselage mass itself. For the wing, landing leg and canard, the only mass oscillating is that of the body itself, being concentrated in the centre of mass. The coordinate system used in both figures was used during the structural analysis only.

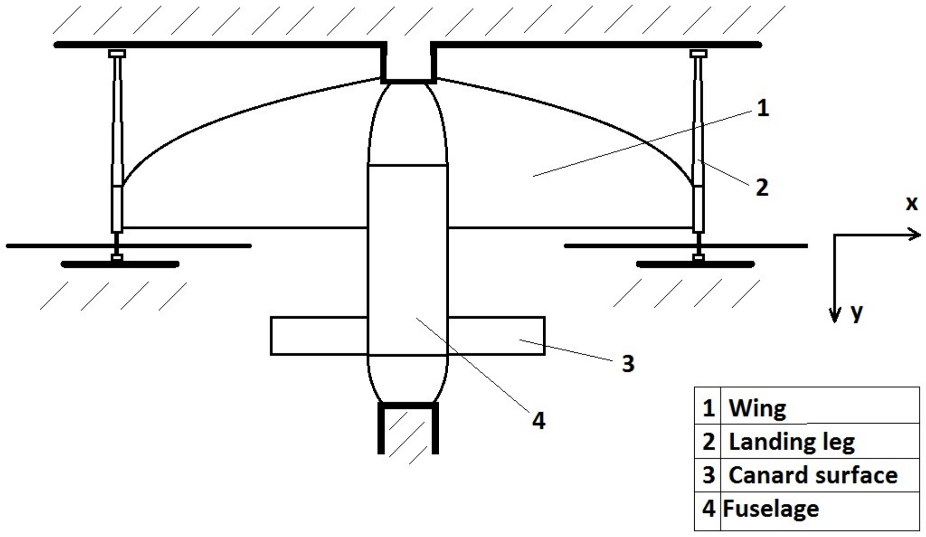

Figure 7.4: UAV stored in entry capsule constraint by support struts and base station

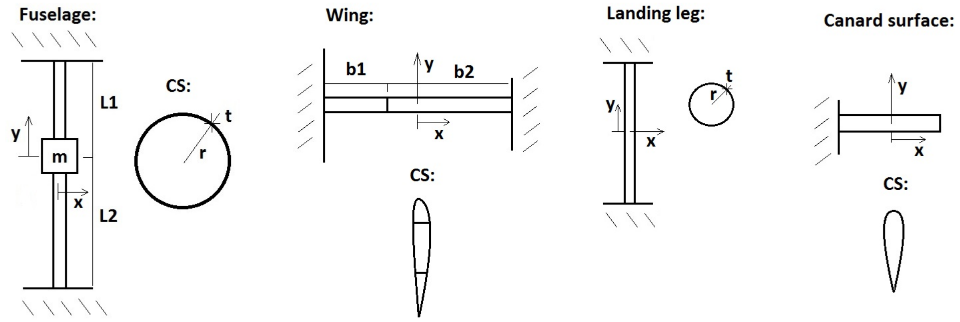

Figure 7.5: Stored structural element simplification used for the determination of performance factors

By analysing the natural frequencies of the simplified structural components shown in Figure 7.5 using an analytical approach, it became clear that in order to keep the structural mass limited, the factor $\frac{E}{\rho_{\text{mat}}}$ should be optimised, in which E is the material Young's Modulus and ρ_{mat} the material density. During this analysis, the eigenfrequency of the individual parts was calculated, using a thin-walled approach for the cross section as a function of material properties. This makes up one of the performance factors which will be used in the material trade-off. Another performance factor, which has to do with thin plate performance is $\frac{\sqrt{\sigma_y}}{\rho_{\text{mat}}}$, in which σ_y is the material yield strength. Since VITAS is mostly built out of thin sheets, this performance indicator was deemed critical.

7.2.2. Material Trade-off

After determining the material performance factors from the analytical analysis, it was possible to perform a material trade-off. The first step was establishing a list of viable materials to be used on VITAS. This list was composed by investigating the materials used in current and previous Mars missions, as well as looking at structural elements used in aviation. From this investigation, the following alloys were used in the trade-off:

- **AL 2024-T6:** Aluminium alloy which is used in general aviation for fuselage panels and wing sections. Due to its high strength-to-weight ratio and good fatigue properties, it was considered a viable candidate for application.
- **AL 6061 T6:** A more sturdy, but more dense aluminium alloy than the 2024 alloy. This alloy exhibits good weldability, which allows for easier assembly. Its used in more high-stress components such as guns and helicopter rotors.
- **TI-6AL-4V:** In military aviation, titanium is often applied due to its superior strength and toughness compared to aluminium. Titanium is also often applied in space applications, such as the frame used in the Curiosity rover.
- **IM/997 carbon fibre composite:** Carbon fibre has anisotropic properties, which enables a part to be for a specific load case while maintaining a low weight. This is the main reason why the material is applied in high-performance sports equipment, race cars and aircraft. The material will also prove itself in the upcoming Mars

2020 mission, with the Scout copter blades being made of carbon fibre. The composite used in this trade-off is a relatively new composite, which has better fracture toughness properties than other carbon fibre composites.

- **AM-162:** This material is a more exotic alloy. It's composition is 62% beryllium and 38% aluminium. Beryllium, being the second lightest metal on the periodic table, is significantly less dense than any other metal used in aerospace structures. In combination with the aluminium, the material becomes less brittle, making it a strong candidate for high-performance structures where a low weight is desired. Additionally, the material has excellent thermal and fatigue properties. The material is currently mostly used in military applications and is planned to be used as the main support structure for the upcoming James Webb telescope.

After finding the candidate materials, the parameters relevant for the trade-off could be established.

- **Specific modulus $\frac{E}{\rho_{\text{mat}}}$:** This factor resulted from the simplified load analysis, which influences the modal frequencies of the material. A higher specific modulus for the same part geometry results in a higher modal frequency, as well as less internal stress during harmonic response.
- **Plate strength performance index $\frac{\sqrt{\sigma_y}}{\rho_{\text{mat}}}$:** This is an optimisation factor for designing thin plates for high strength. A plate made of a material with a higher factor can resist the same loads as a material with a lower factor, but with a lower weight, which is desirable for VITAS.
- **Fatigue limit strength σ_{fat}:** Since VITAS is to be used for many flights and is to be reused after the mission, the structure has to endure many load cycles. Below the fatigue limit strength, the material does not degrade due to cyclic loading, giving it long lasting performance.
- **Toughness performance factor $\frac{\sigma_y^2}{2E}$** During its mission, VITAS will endure many shocks and possible impact of flying debris. In order for the structure to survive these harsh conditions, the used materials should not shatter during peak loads.
- **Manufacturing flexibility:** Since the surfaces of VITAS are curved and thin, the used material must allow to be shaped this way.
- **Toxicity:** Since the mission hardware has to be designed to be disassembled and reused by human colonists on Mars, the material must allow for safe handling and not pose a significant health risk. Toxic materials have the added disadvantage of requiring special manufacturing conditions on Earth, which can drive up costs significantly.

In Table 7.7, the candidate materials, as well as their score on the trade-off criteria can be seen. For manufacturing and toxicity, "5" refers to the best performance and "1"- the worst (so A means easiest to manufacture and the least toxic). The data for generating this table was collected from the work of Kumar et al. [2001] and Aerospace Specification Metals Inc[15].

Table 7.7: UAV material trade-off table.

Material	$\frac{E}{\rho_{\text{mat}}} \cdot 10^6$	$\frac{\sqrt{\sigma_y}}{\rho_{\text{mat}}}$	σ_{fat} [MPa]	textbf$\frac{\sigma_y^2}{2E} \cdot 10^6$	Manufacturing (1-5)	Toxicity (1-5)
AL 2024T6	26.04	6.68	124	0.82	5	3.5
AL 6061T6	25.52	6.15	96.5	0.55	4	3.5
Ti-6Al-4V	25.69	6.69	510	3.40	1	5
IM/997(UD)	90.66	33.13	1310	2.37	3	2
IM/997(T)	7.81	6.14	54	0.33	3	2
AM-162	93.90	7.99	165	0.2	2	1

As can be seen in Table 7.7, both aluminium alloys perform consistently over all trade-off criteria, but also do not excel in any field. The titanium alloy is the superior metal in terms of fatigue and toughness, but due to its reactivity at high temperatures is difficult to manufacture. The carbon fibre composite has high performance over all citeria. If these were the only factors, the composite would be the best choise. However, the Martian environment has some negative effects on composite materials. Due to its anisotropic properties, carbon fibre composite has a varying thermal expansion coefficient, dependent on the fibre orientation. Due to the high temperature flux on Mars (-100 at night to 0 at noon), stress between laminates, as well as additional friction between fibres and polymer matrix occurs. This was investigated in a study by Park et al. [2011], which was also conducted at low atmospheric pressure, which also complies with Martian conditions. By extrapolating the results of this study to the equivalent number of cycles that VITAS would have to endure during its mission, the ultimate strain would degrade by almost 14%. Not only does the temperature cycle affect the material, but the increased UV radiation on Mars has significant effects on

[15] `http://www.aerospacemetals.com/` [Cited 19 June 2018]

the polymer matrix. In tests conducted by Kumar et al. [2001], IM/997 was exposed to 500 hours of UV radiation, which resulted in a 4.2% polymer matrix strength degradation. Assuming the degradation of the polymer to follow a behaviour like

$$\sigma_{\text{tens}} = \sigma_0 e^{-a \cdot t}, \tag{7.2}$$

with σ_{tens} being the tensile strength of the polymer after t hours, σ_0 the initial strength and a the degradation factor, which was calculated to be $8.58 \cdot 10^{-5}$ according to the article. By simulating an exposure of 5 years on Mars, the resulting degradation was about 15%. This UV degradation could be negated by applying a polycarbonate layer. This would also increase the fracture toughness of the material. However, applying a 1 mm coating to the outer skin would result in a 40% weight increase, which counteracted the low density of the composite itself. Due to the combined degradation effects of the Martian environment, the carbon fibre composite was discarded as the best option.

The next best option in the trade-off table was considered to be the AM-162 alloy. As can be seen in Table 7.7, the alloy has the best specific modulus and sheet metal performance of all candidates. In terms of manufacturing, the machines required are not that different than that used for aluminium manufacturing. However, drilling and cutting has to be done at lower speeds, resulting in longer manufacturing times. Also, due to the toxicity of its chips, some special precautions have to be implemented such as thorough ventilation and protective clothing. No cure for beryllium poisoning exists yet and the effects can be lethal without counteracting the symptoms. However, since only one UAV has to be built, the probability of contamination would be low. In order to make deconstruction during future human missions safe, chips and fine particles could be prevented by implementing assembly features such as plastic screw guides and rubber fittings. Due to the possibility of mostly negating the negative effects of the AM-162 alloy, it was decided to be the material of choice for VITAS. The most relevant material properties are given in Table 7.8.

Table 7.8: AM-162 material properties

Property	**Value**	**Unit**
Density	2103	kg/m^3
E-modulus	200	GPa
Yield stress	282.7	MPa
Ultimate stress	337.8	MPa
Fatigue limit stress	165.5	Mpa
Poisson's ratio	0.17	-
CTE	7.7	K^{-1}

7.2.3. Detailed Structural Analysis

After choosing the material and knowing the dimensions of the wing and other components, a detailed analysis of the structural components could be performed. As can be seen in Figure 7.3, the process started with building the geometry. For this, CATIA V5 was chosen to be the design tool. This choice was mainly based on familiarity of the software by all team members, which would ease the integration of subsystems designed by different team members. The wing was divided into several panels, sheets and spars as can be seen in Figure 7.6.

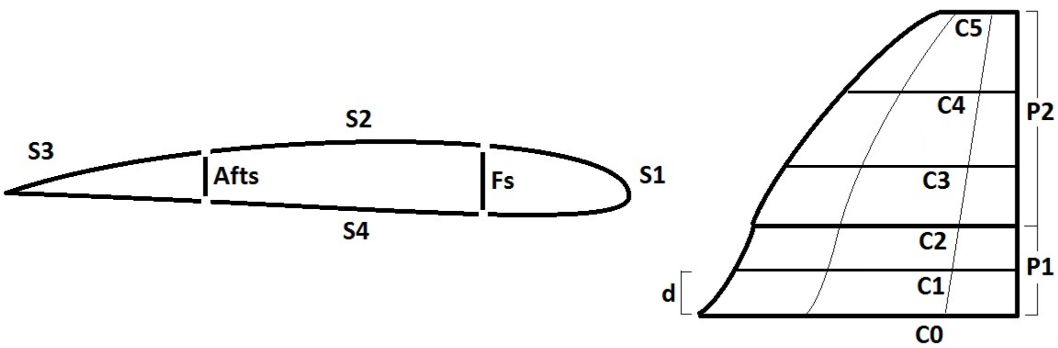

Figure 7.6: Part layout used in the wings.

Table 7.9: Wing chord lengths and spacing.

Section	C0	C1	C2	C3	C4	C5	d
Length [mm]	720	648	598	490	346	216	214

The reason why the wing was divided into this many panels was for optimisation. Some parts of the wing might experience lower loads than others, resulting in a reduced required thickness for that part. The chord dimensions and spacing can be seen in Table 7.9.

Because of the low weight and large wing surface area, the aerodynamic loads were expected to be low. Nevertheless, two spars were placed as reinforcement over the entire wing span. In VITAS, the spars have a different function than in conventional aircraft. The spars in VITAS have the main function of increasing the modal frequency of the wing, by constraining local sheet edges from moving during vibration. Since the spars have to carry little of the structural loads, their structural weight was allowed to be reduced by placing holes in them. In the final wing design, the spars have been placed at 30% and 60% of the chord. The reason for these particular values will be discussed in Section 7.2.4. The internal stress was calculated using ANSYS 19.0. This program allowed for complex geometries to be analysed under many different load types using finite element analysis. ANSYS can directly use geometries from CATIA, which provided a useful interface. The meshed wing used for the analysis can be seen in Figure 7.7. The contacts between the wing components were automatically set by ANSYS.

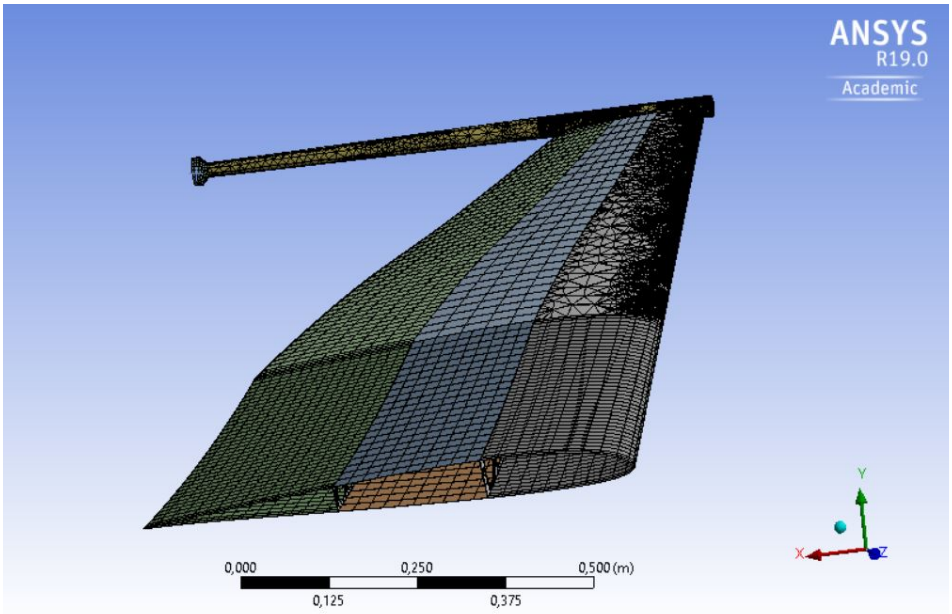

Figure 7.7: Meshed wing used for the ANSYS analysis.

ANSYS had a dedicated tool capable of calculating the modal frequencies of a structure with given boundary conditions('Modal Analysis'). In case of the wing, the root, engine nacelle and landing leg foot were fixed by struts during launch using the 'Fixed Support' option in ANSYS, as can be seen in Figure 7.4. If the lowest modal frequency exceeded 60 Hz, the structure was subjected to the maximum acceleration during launch due to the combined effect of vibration and net acceleration from the launcher, which were 7.5 g and 2.5 g respectively ([ULA, 2010]). This was done in a 'Static Structural' analysis, using the same boundary conditions as during the modal analysis and simulating the accelerations as 73.58 m/s^2 in y-direction and 24.52m/s^2 in x-direction (Figure 7.4 coordinate system). After noting down the wing surfaces with the lowest and highest stress and deformation, the wing was subjected to flight loads under normal conditions. The load case can be seen in Figure 7.8, with the values derived from resulting lift and drag at an angle of attack equal to 8^o. This angle was chosen as it resulted in the largest aerodynamic force vector. The mass suspended at the wing tip represents the propulsion module, weighing 680 grams. The lift and drag acting on the wing were taken as forces evenly distributed over the wing surface. Although during flight a more elliptical distribution is achieved, it was assumed that the resulting internal stress would not be much different, since the lift distribution has almost the same shape as the wing due to the reduced effect of tip vortices.

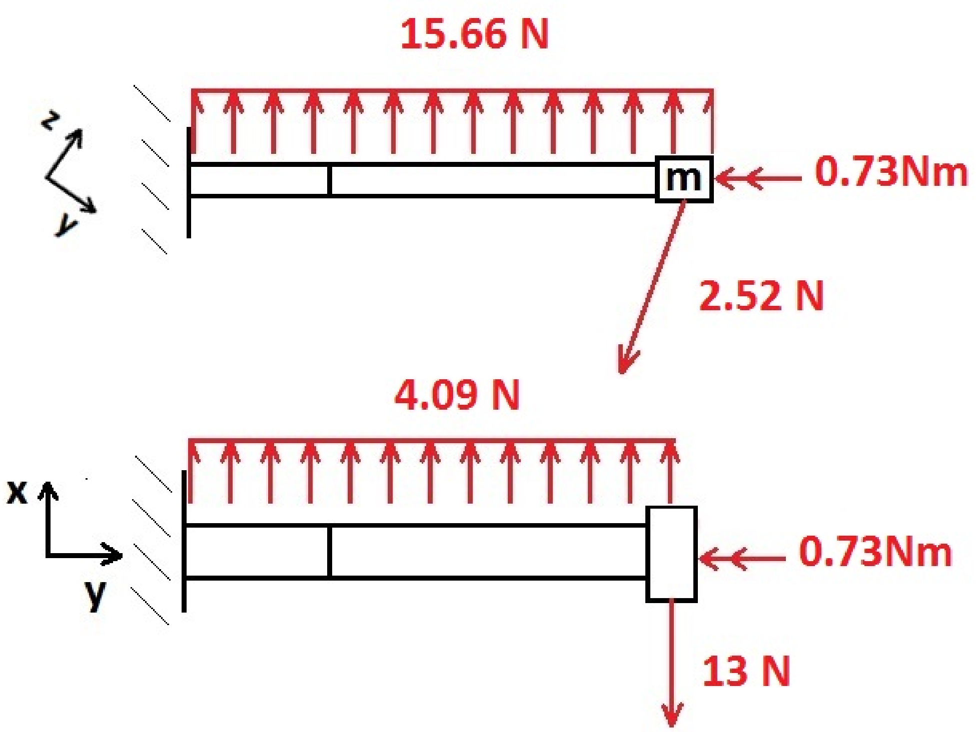

Figure 7.8: Assumed nominal flight loads(load factor n= 1) acting on the wing.

If the maximum stress in the wing would not exceed the fatigue limit stress of the AM-162 alloy, changes had to be made. After this, a load factor of 4 was applied to the aerodynamic loads, simulating a strong gust. The distributed loads were set in ANSYS as 'Force' inputs distributed over the wing surface in the same directions as in Figure 7.8. The aerodynamic moment was simulated with a -0.605 Nm component in y-direction and a -0.408 Nm component in z-direction, with the coordinate system shown in Figure 7.8. In order to simulate the wing weight, the entire structure was subjected to a -3.71 $\mathrm{m/s^2}$ acceleration in z-direction. The entire cross section at the root(spars and skin) was constraint using the 'Fixed Support' option. After analysing all load cases, parameters such as thicknesses and spar locations would be changed according to the critical load locations, with the intention of reducing the weight, while complying with the requirements. The results of the analysis can be found in Table 7.11. The resulting panel thicknesses are described in the following table.

Table 7.10: final wing panel thicknesses

Component	Thickness [mm]	Component	Thickness [mm]
S1P1	0.2	S1P2	0.2
S2P1	0.3	S2P2	0.2
S3P1	0.2	S3P2	0.2
S4P1	0.3	S4P2	0.2
Front spar P1	0.5	Front spar P2	0.5
Aft spar P1	0.5	Aft spar P2	0.5

With the panel thicknesses given in Table 7.10, the resulting wing weight was 649 g. However, this is not the wing weight, as it should also include the added weight of joints and screws. For that reason, a contingency of 15% was added, resulting in a wing weight of 746 g.

For the fuselage, a similar approach was used. However, in this case, the fuselage would be subjected to a 9.15 N load in z-direction in the nose due to the lift of the canard surface at 8^o angle of attack and the on-board payload of 7.4 kg. The reason for this 8^o angle of attack was the fact that the aerodynamic force vector of the NACA0015 airfoil was the largest at this angle. Therefore, the highest canard loads were expected to occur at this angle. The payload weight was simulated using the 'Distributed Mass' option and applying it to the inside of the fuselage, while subjecting the entire structure to a -3.71 $\mathrm{m/s^2}$ acceleration in z-direction. The wing roots at the tail were constraint using the

'Fixed Support' option. The results of this stress analysis can be seen in Table 7.11. The overall thickness of the fuselage was set to 0.3 mm. The internal stress was significantly lower than the AM-162 fatigue limit strength, so in theory the sheet thickness could have been further reduced. However, due to concern regarding the aerodynamic pressure on the skin, as well as the need for suspension of the scientific payload, the sheet thickness was kept limited to 0.3 mm. This brought the structural mass of the fuselage to 888 grams, which including added assembly weight would weigh 1.02 kg.

The canard surface was assumed to be less of a critically loaded part than the other structural components, due to its small size, hence high modal frequency. Also, the flight loads were not very large (9.15 Newton for the entire canard surface). Even with a skin thickness of 0.2 mm and a load factor of 2, the maximum internal stress was only 2.6 MPa. Since 0.2 mm was the thinnest sheet thickness regarded safe, it was left this way.

The landing leg was for analysis put under an angle of 75^o on the landing pad under four times the Martian gravitational acceleration to simulate a rough landing. By increasing the landing leg thickness to 0.55 mm, the resulting stress went below the material yield strength.

For the base station structure, not much investigation was performed due to time constraints. However, the structure as presented in Chapter 6 is very similar to the structure used for the ExoMars mission. Since the base station is not as constraint by mass as the UAV, the support structure would not have to be optimised as much with respect to the already existing design.

Table 7.11: Maximum internal stresses, loads, frequencies and masses of the structural components

Wing		
Parameter	**Value**	**Unit**
Launch stress	32.8	MPa
Flight load (n=1)	15.9	MPa
Flight load (n=4)	49.6	MPa
Lowest modal frequency	71.6	Hz
Mass	746	g

Fuselage		
Parameter	**Value**	**Unit**
Launch stress	48.1	MPa
Flight load	11.9	MPa
Lowest modal frequency	134	Hz
Mass	1022	g

Landing Leg		
Parameter	**Value**	**Unit**
Rough landing load	105.7	MPa
Mass	101	g

Canard		
Parameter	**Value**	**Unit**
Flight load (n=2)	2.6	MPa
Mass	261	g

7.2.4. Sensitivity Analysis

For the structure of the VITAS drone, the modal frequencies and the structural mass were important parameters, which are influenced by various other parameters. In this subsection, the influence of parameter change will be discussed.

The modal frequency of a structure depends on the density and stiffness of the used materials, but also on the uncut lengths of parts. As mentioned earlier, the spars in the wing were mainly placed as anchor points for the wing skin panels. This reduces the effective width of the panel, thereby increasing its natural frequency. By moving the two spars closer together, the effective width of the top and bottom sheet (S2 and S4) decreases, but increases the width of the leading and trailing edge parts (S1 and S3). By varying the distance between the spars, it was possible to visualise the effect of spar distance on the lowest modal frequency of the structure.

Space between spars [% of chord]	Modal frequency [Hz]
50	68
40	71
30	77
20	62
15	48

Table 7.12: effect of inter spar space on modal frequency

In Table 7.12, the modal frequency for several values of spar spacing can be seen. The highest value for modal frequency occurred with a spar spacing of 30% of the chord, which is the reason for the chosen spacing.

7.3. Propulsion

The propulsion subsystem contains two major parts: the propellers and the electric engines. Performance data for both is readily available and accurate results can be obtained, at least on Earth. For Mars, both these aspects of the propulsion system require extensive analysis to determine reliable performance values.
As Section 7.3.2 will further elaborate upon, propeller design for the Martian environment is complicated, mainly because of the extremely low Reynolds numbers that rule the laws of aerodynamics. Doing a full propeller analysis, where the most optimal propellers would be designed and fully analysed in Computational Fluid Dynamics (CFD) was deemed out of the scope of this design study. The same goes for the electrical engines, because of the large propeller blades and the high rpms that are needed to generate a sufficient amount of thrust, a torque of about 1 Nm is needed, while keeping the weight as low and the efficiency as high as possible. These kind of engines are not readily available and would, again, require extensive analysis.
In order to simplify things and still get reliable results, it was chosen to base the design of the propellers and engines for the most part on previous Mars missions and mission proposals. The only reliable source of information on both, and which was comparable in terms of performance to the MARS mission, could be retrieved from the soon to be launched NASA Mars 2020 mission. As an addition to the rover, an accompanying helicopter dubbed the ”Mars Helicopter” will function as a technology demonstrator[16].
Both the propellers and the engines were sized according to performance data retrieved form this mission. It was chosen to implement eight coaxial propellers, due to both size constraints and an increase in power efficiency of about 5% when utilising coaxial propellers as mentioned by Coleman [1997]. Furthermore, it was assumed that the efficiency of the motor system would remain practically constant at around 78%, as Koning et al. [2018a] indicated the efficiency remained quasi constant throughout the tests.

7.3.1. Subsystem Level Requirements

A set of driving requirements was set up from the knowledge of past missions and the design point of the UAV. Take-off thrust is based on needing at least a 1.05 thrust to weight ratio for controllable take-off. [Raymer, 2012] Cruise thrust is derived from the cruise drag at an airspeed of 82.5 m/s and air density of 0.02 kg/m^3. The diameter of the propeller blades were limited due to space constraints and the fact that the Mars helicopter will utilise propellers of the exact same dimensions, providing a way to verify performance data.

- MARS-UAV-SYS-Propulsion-1: The propulsion system shall provide at least 55 N of thrust during take-off
- MARS-UAV-SYS-Propulsion-2: The propulsion system shall provide at least 8.42 N of thrust during cruise
- MARS-UAV-SYS-Propulsion-3: The propellers shall have diameter of at most 1.21 m

7.3.2. Design Considerations

The development of an adequate propulsion system for Martian aircraft has been a subject to intensive research very recently. Especially the research of Koning et al. [2018a] and Yonezawa et al. [2016] has been of significant value for this design. As it turns out, the design of propellers for the thin atmosphere on Mars is far from trivial. For more details about the Martian atmosphere, the reader is referred to Appendix B. The main design challenges are threefold: [Yonezawa et al., 2016]

1. Since the density of the Martian atmosphere is only about 0.02 kg/m^3, the thrust generated is very low regardless of the design when compared to the same propeller on Earth. This density would correspond to an altitude on Earth of 31 km, which is 2 km higher than the current altitude record for aircraft on Earth.[17]

[16]URL: `https://mars.nasa.gov/news/8335/mars-helicopter-to-fly-on-nasas-next-red-planet-rover-mission/` [Cited 15 June 2018]
[17]URL: `https://www.nasa.gov/centers/dryden/news/ResearchUpdate/Helios/index.html` [Cited 22 June 2018]

2. The density also has another important effect: it dramatically increases the viscosity of the flow. The effect of viscosity in airflows is characterised by the Reynolds number, 67 times lower for the same characteristic length and velocity on Mars than on Earth. For the scale of the propellers considered, the Reynolds number varies between 8000 and 15000. This very low-Reynolds number regime is subject to major viscous effects, such as the formation laminar separation bubbles (illustrated in Figure 7.9). The viscous effects not only make the operation of propellers less efficient, but also complicate the prediction of flow patterns using conventional computational methods. [Koning et al., 2018a; Drela, 2001]
3. Since the average temperature is lower on Mars (in the order of 242 K) and the composition of the atmosphere (mainly CO_2, which has a lower ratio of specific heats), the speed of sound on Mars is only 244 m/s. In order to avoid drag divergence, the propeller tips cannot travel much faster than Mach 0.7. Therefore, the propellers cannot operate at the same rotational speeds as they do on Earth, limiting the attainable thrust even more.

In order to cope with these effects, some design principles apply. First and foremost, propeller drag losses can be subdivided into two contributions: profile losses and induced losses. Using more propeller blades reduces the induced losses but causes a growth in profile losses. As demonstrated by the research of Yonezawa et al. [2016], the profile losses prevail in the low-Reynolds number regime of the Martian atmosphere due to viscosity effects. Hence, the propeller should have two blades.

Secondly, a proper choice for the airfoil has the largest influence on the viscous drag. Generally, low-Reynolds number flows call for thin airfoils with considerable camber. However, the lower the Reynolds number, the more flat or cambered plates come into favour. The reason for this is that flat/cambered plates force transition right after the leading edge (provided that the LE is sharp enough). This causes the entire upper surface to be be supercritical. Although this increases the skin friction significantly, separation is delayed due to the higher momentum of the boundary layer. This results in a considerable reduction of the profile drag. Please note that ‘supercritical’ refers to flow boundary layer being turbulent and should not be confused with supercritical airoils. The avoidance of laminar separation bubbles on the upper surface not only improves the performance of the airfoil, but also makes the behaviour of the boundary layer more predictable. [Koning et al., 2018a] The extensive research conducted by Koning et al. [2018a] shows a maximum thrust that is 7% higher and a 5% increase of the Figure of Merit for a cambered plate airfoil compared to the conventional design used for the Mars Scout Helicopter.

Finally, it was chosen to use swashplates on the propellers for thrust control. Although most modern multicopter UAV'ss make use of varying rotational speeds of their propellers for control, this design option was not deemed feasible. The reason for this is that the large diameter of the propellers results in a very large mass moment of inertia. In order to spin up or slow down the propellers quickly (which is a crucial requirement for fast control during takeoff and landing), the torque that the engines need to deliver would be unacceptably high. A major drawback of a swashplate mechanism is that it adds a lot of complexity to the system. However, since the propellers are mounted in an X-configuration, there is no need for cyclic control on the propellers. This greatly reduces the complexity of the system when compared to a conventional swashplate capable of both cyclic and collective control.

7.3.3. Propeller Performance

As discussed in the previous section, the usage of cambered plates for propeller blades is advised on Mars. Research performed by Koning et al. [2018a] concluded that flat plates with about a 5% camber are optimal for this design consideration. Koning et al. [2018a] also provides performance data for a coaxial, 1.21 m diameter, 5% cambered flat plate design. This could then easily be used to evaluate take-off performance of the coaxial propellers. Cruise performance still needs to be evaluated. After extensive analysis it could however be concluded that these propellers, which are designed for hover and slow forward movement could not provide the amount of thrust required during cruise.

A short feasibility study was performed and it was decided to, instead of using eight identical coaxial propellers optimised for take-off, implement a design that would utilise four coaxial propellers optimised for cruise during cruise, and utilise both the four coaxial propellers optimised for take-off and the four coaxial propellers for cruise during take-off. This can be seen visualised in Figure 7.10.

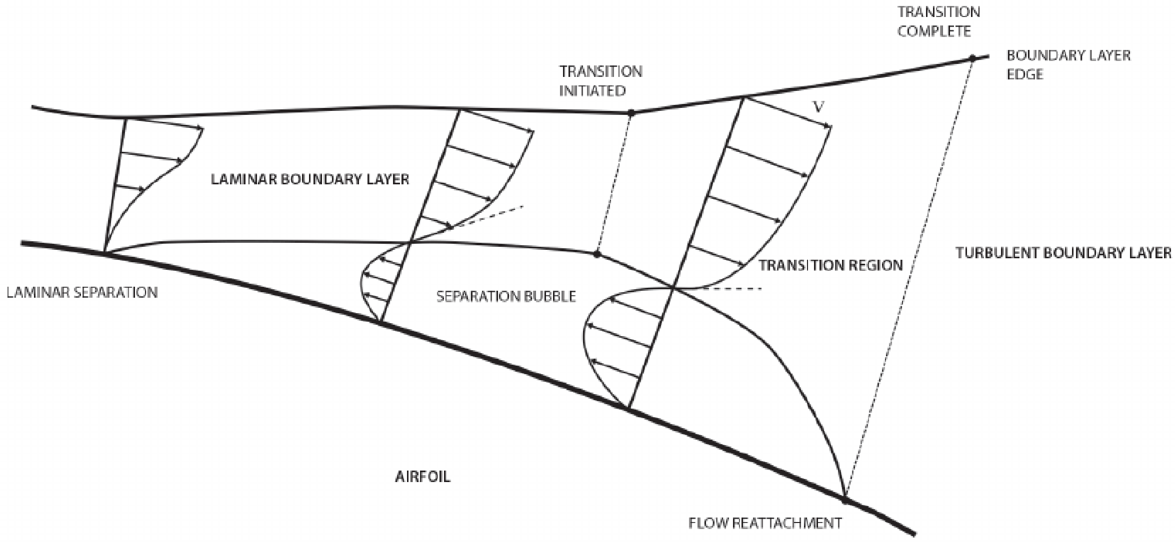

Figure 7.9: Schematic of a laminar separation bubble (LSB). The low surface momentum of the laminar boundary layer is not able to cope with the adverse pressure gradient in the retarded flow zone very well. This results, as shown in the picture, in a localised region of reversed flow: the separation bubble. When the transition to a turbulent boundary layer occurs, the boundary layer grows quickly in size. After some distance the turbulent boundary layer reattaches with the surface. Due to the turbulence present in the boundary layer, the energy from the freestream is transferred better to surface, increasing the momentum of the flow. [John D. Anderson, 2017]

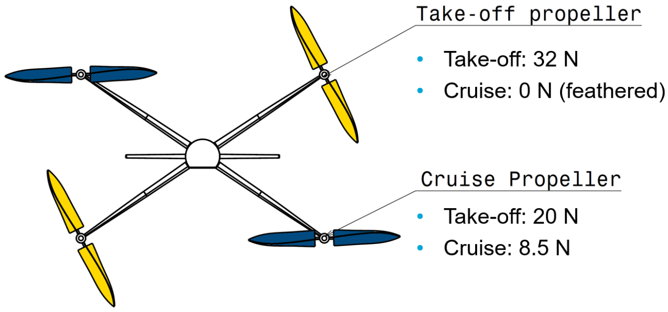

Figure 7.10: Propeller configuration. In yellow, the take-off propellers are depicted. In blue, the cruise propellers can be seen. Due to the symmetry of the thrust, this does not introduce problems for stability and controllability.

7.3.4. Cruise Propellers

Take-off performance could be derived from the data presented by Koning et al. [2018b]. The previously described design choice required a design and a performance evaluation of cruise propellers for Martian condition. XROTOR, and specifically the variation with the CROTOR extension added: CROTOR v755-ES1[18] was used to both: design the cruise propellers and quantifying their performance.

The first thing to do is to input the correct data for the airfoil that is being used into the <AERO.> workbench. XROTOR gives users the possibility to switch between graded momentum/potential flow, discrete/non-discrete vortex model and a self-deforming/rigid wake. For the calculations, the potential flow formulation, due to the higher accuracy, the non-discrete vortex model (discrete only advised for non-radial lifting lines) and a self-deforming wake was chosen. One of the major caveats of using potential flow formulation is that it cannot account for viscous effects directly and has to apply a correctional factor depending on the Reynolds number:

$$C_D = \left[C_{D_0} + \frac{dC_D}{dC_L^2} \cdot (C_{L_0} - C_L)^2\right] \cdot \left(\frac{Re}{Re_{\text{ref}}}\right)^f \tag{7.3}$$

With f being a correction factor, depending on the flow regime:

[18]URL:http://www.esotec.org/sw/crotor.html [Cited 20 June 2018]

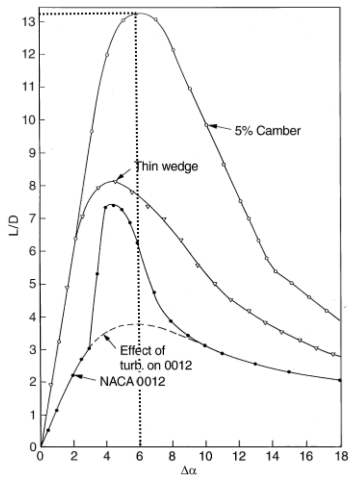

Figure 7.12: Lift over drag ratio of various wing planforms with aspect ration A = 6 depicting their performance over a range of angles of attack from zero lift at a Reynolds number of 20700, retrieved from Laitone [1997]

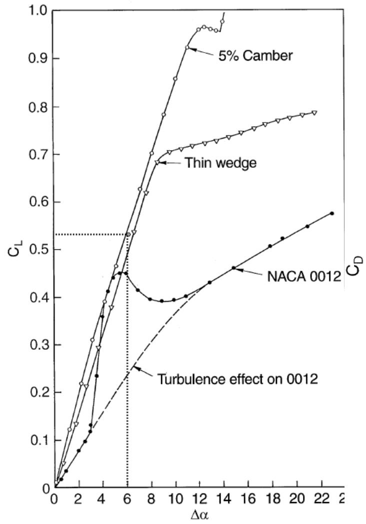

Figure 7.13: Lift coefficient C_L of various airfoils with aspect ratio A = 6 depicting their performance over a range of angles of attack from zero lift at a Reynolds number of 20700, retrieved from Laitone [1997]

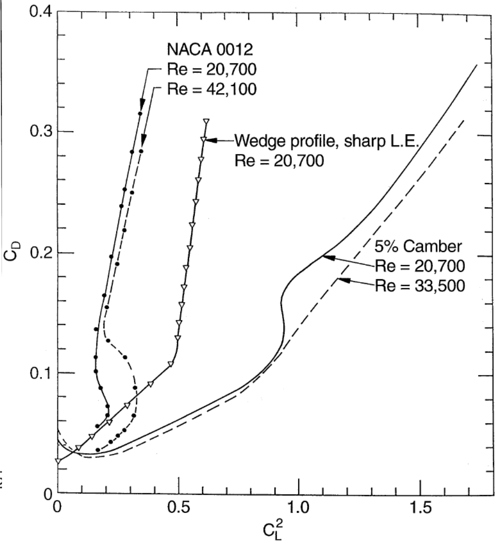

Figure 7.14: Variation of the drag coefficient C_D with the lift coefficient squared C_L^2 for rectangular wings with aspect ratio A = 6, retrieved from Laitone [1997]

- f = -0.1 to -0.2 for high-Re turbulent flow (Re > 2,000,000)
- f = -0.5 to -1.5 for low-Re regime (200,000 > Re > 800,000)
- f = -0.3 to -0.5 for mostly laminar flow (Re < 100,000)

As the propellers will be operating at Reynolds number values of in the order of $O(10^3)$ to $O(10^4)$. A correction factor of -0.4 was chosen. In the menu entry <AERO.>, as seen in Figure 7.11, performance data on the chosen airfoil can be entered.

```
.AERO   c>  disp

 Section 1   r/R = 0.000
 =====================================================================
 Zero-lift alpha (deg):  -3.20        Minimum Cd           : 0.0320
 d(Cl)/d(alpha)       :  4.730        Cl at minimum Cd     : 0.340
 d(Cl)/d(alpha)@stall :  0.575        d(Cd)/d(Cl**2)       : 0.0990
 Maximum Cl           :  0.96         Reference Re number  :   20700.
 Minimum Cl           : -0.50         Re scaling exponent  : -0.4000
 Cl increment to stall:  0.100        Cm                   : -0.100
                                      Mcrit                :  0.800
 =====================================================================

Defined aerodynamic sections:
  N     r/R    CLmax    CLmin    CDmin    Mcrit    REexp        REref
  1  0.0000  0.9600 -0.5000  0.03200  0.8000 -0.4000   0.2070E+05
```

Figure 7.11: Overview of the input data in the <AERO.> workbench. Data on 5% cambered plates was derived from Figures 7.12, 7.13 and 7.14.

3D data on 5% cambered plates was retrieved from Laitone [1997], and is presented in Figures 7.12, 7.13 and 7.14. In Laitone [1997], Laitone performed a number of wind tunnel test of various aifoils at Reynolds numbers as low as 20000. Although certain sections along the rotor experience Reynolds numbers as low as 1000, Laitone [1997] reflected that the cambered plate performance did not vary greatly with respect to the Reynolds number. Therefore, a solid database for reliable performance values could be established.
After the airfoil data was set up, the <DESI.> workbench could be used. Flight performance evaluation was performed under the following conditions:

- ρ = 0.020 kg/m^3

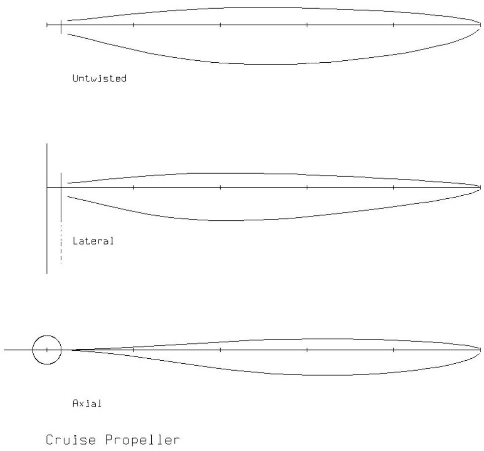

Figure 7.15: Layout of the generated design by XROTOR.

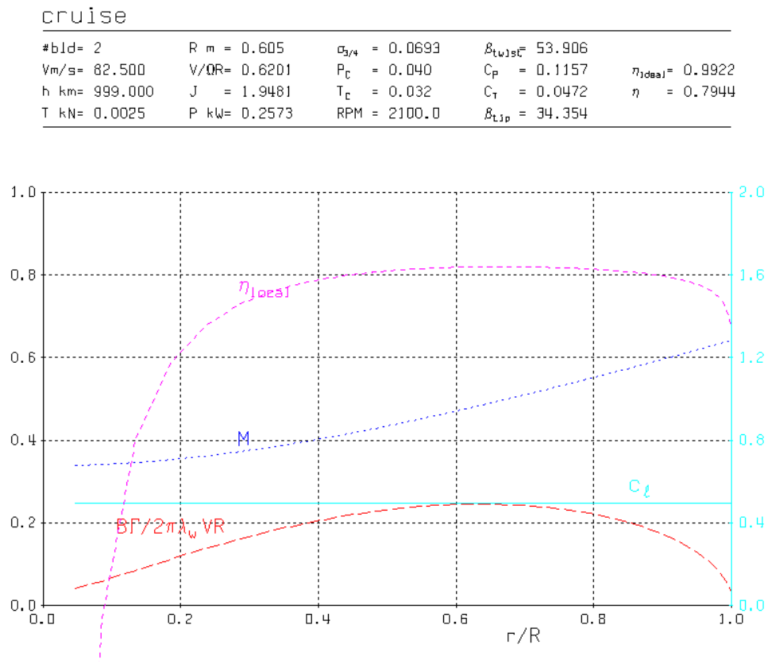

Figure 7.16: Propeller performance as generated by XROTOR. The design was optimised for the rpm required, the optimal value was found to be 2100 rpm, this lays within the capabilities of the motor used by Balaram et al. [2018]

- μ = 1.13 · 10^5 kg/(m s)
- V = 82.5 m/s

After running the program for a thrust requirement of 2.48 N per cruise propeller as derived in Equation 7.4,

$$T_{\text{prop}} = \frac{0.5\rho V^2 S C_D}{4 \cdot 1.05} \tag{7.4}$$

where T_{prop} is the power required per cruise propellers, ρ = 0.02 kg/m^3 is the air density, V = 82.5 m/s the cruise speed, C_D = 0.078 is the drag coefficient at maximum lift to drag ratio as derived by the control & stability department Section 7.4. Furthermore, the thrust requirement is lowered by 5% as it is assumed that the coaxial design is able to deliver at least 5% extra thrust as reflected in literature [Coleman, 1997] and [Koning et al., 2018b].
Figure 7.15 and 7.16 present the design of the cruise propellers.

7.3.5. Take-off Propellers

With the sizing of the cruise propellers finished, the sizing of the take-off propellers is straightforward. The layout of the take-off propellers can be seen in Figure 7.17. The biggest difference between the two propellers is that the twist distribution is different, this is due to the change of the tangential wind speed due to the cruise speed of 82.5 m/s.

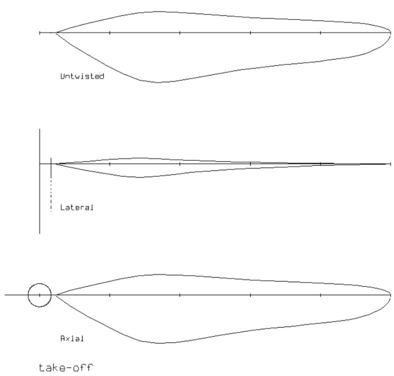

Figure 7.17: Layout of the mars helicopter rotor, replicated from Koning et al. [2018a]. Notice specifically the difference in twist distribution wrt the cruise propeller (Figure 7.15)

Figure 7.18 provides data on the performance of a 5% cambered plate for the NASA Mars Helicopter Design as analysed by Koning et al. [2018b]. Both the thrust C_T and the power C_P coefficient are equal to

$$C_T = \frac{T}{\rho S_b V_T^2}, \tag{7.5}$$

$$C_P = \frac{P}{\rho S_b V_T^3}, \tag{7.6}$$

where T = 16 N per coaxial propeller was found to be the optimal point w.r.t. to power usage (the cruise propellers still need to provide 10 N of thrust per coaxial propeller to achieve a thrust to weight ration of 1.05), S_b = 1.15 m^2 the propeller blade area and V_T = 177.4 m/s the tip speed of the propeller. The thrust and power relation under the design circumstances can be seen in Figure 7.19.

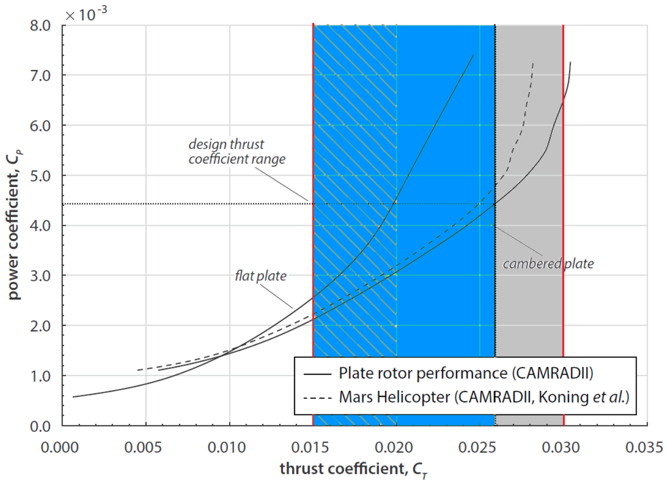

Figure 7.18: Relation between thrust coefficient C_T and power coefficient C_P for air density ρ = 0.017 kg , retrieved from Koning et al. [2018b]. The hatched area depicts the C_T range that the Mars Helicopter Rotor was designed for, the blue area depicts the fly-able thrust region for VITAS. The zone between the red lines is the possible thrust coefficient requirements that can occur depending on the atmospheric temperature.

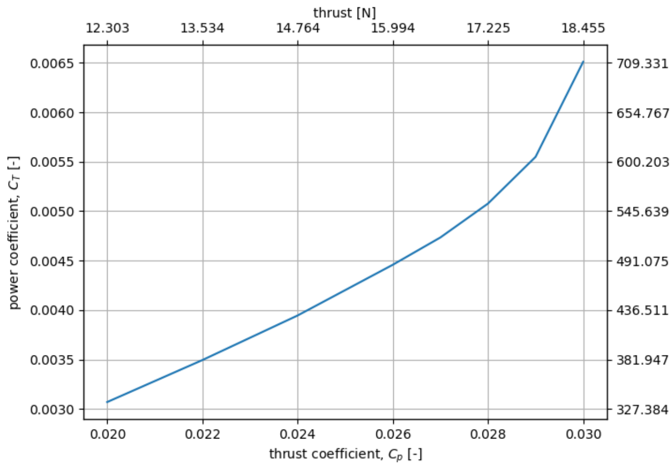

Figure 7.19: Relation between thrust coefficient C_T and power coefficient C_P for air density ρ = 0.017 kg and their respective thrust and power, reconstructed from Koning et al. [2018b].

As can be seen in Figure 7.18, VITAS will not be able to operate nominally under certain circumstances. A measure that will have to be taken is waiting for the right conditions to fly; during the night (when it is colder and the air density goes up) flight is nearly always possible. During the day and especially during the summer (also see Section 7.7), fluctuations in the atmosphere's temperature can limit the amount of available flight time. It is therefore necessary to closely monitor these fluctuations such that the right time window can be chosen to perform the measurements.

7.3.6. Weight Estimation

Based on Figure 7.20, and data presented in Grip et al. [2018] it could be concluded that the total mass of the two contra-rotating propellers and engines, including the necessary periferals and equipment, would be 0.68 kg (Equation 7.7, g is the gravitational acceleration).

$$m_{\text{prop}} = m_{\text{design}_{\text{Mars}}} \cdot \frac{g_{\text{Mars}}}{g_{\text{Earth}}} \tag{7.7}$$

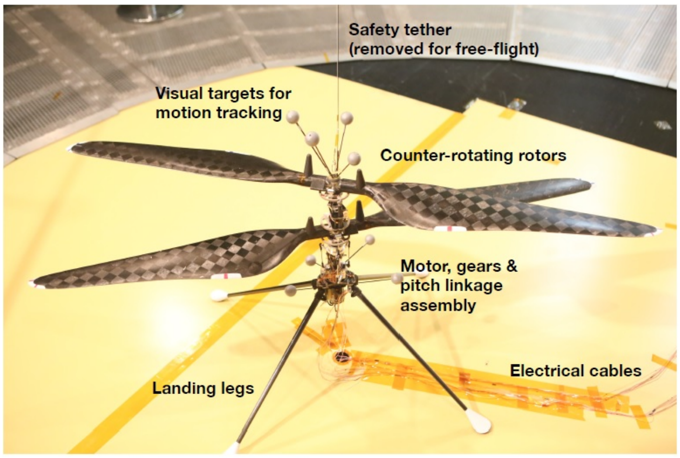

Figure 7.20: Test setup of the NASA Mars helicopter design, retrieved from Grip et al. [2018]. To simulate the Martian conditions properly, all unnecessary equipment like batteries, avionics, etc. was discarded such that an equivalent weight was achieved resulting in a test mass of 0.68 kg. This mass was used to estimate the unit mass of the propulsion system.

7.3.7. Overview

An overview of the total propulsive system performance is provided in Table 7.13.

Table 7.13: Overview of the total propulsive system performance at air density ρ = 0.017 kg/m^3. Total system mass = 2.723 kg

	Take-off			Cruise		
	Thrust [N]	Power [W]	rpm	Thrust [N]	Power [W]	rpm
Cruise Propellers	19.94	552	2700	8.42	888	2100
Take-off Propellers	32	973	2800	0	0	0
Total (incl. 78% motor eff.)	**51.94**	**1955**		**8.42**	**1138**	

7.4. Stability and Control

This section discusses the stability and control characteristics of the UAV and how it was designed. Firstly, the subsystem level requirements are summarised in Section 7.4.1. Section 7.4.2 treats the selection of the airfoils for both the main wing and the canard surface. Finally, the stability characteristics of the UAV are analysed in greater detail Section 7.4.3. Please note that ‘transition’ in this chapter refers to the phase where the UAV changes its attitude from vertical flight to horizontal flight, and not to boundary layer transition (unless explicitly specified).

7.4.1. Subsystem Level Requirements

During the mission the UAV will have to perform a vertical take-off, cruise over the Martian surface, take measurements and land vertically on the landing station to upload the data and reload the batteries. It is crucial that the UAV remains stable and controllable during all these phases, as any error would mean the end of the mission. The basic configuration has been described in Section 6.2.2.

This section will describe the design process and analyse how well it performs in the Martian environment. During all phases the UAV will encounter gusts with velocities of 2 to 10 m/s depending on the season[19]. These gusts need to be taken into account as uncontrollable factors that will influence the control and stability of every phase. During dust storms the wind velocities can go up to 30 m/s for which the UAV is not designed to fly in and will remain at the base station.

The following list gives an overview of the requirements for control and stability:

- MARS-UAV-CS-1: The UAV’s centre of gravity will be located between the wing and the canard.
- MARS-UAV-CS-2: The UAV shall be able to transition from vertical take-off mode to cruising mode and back to vertical landing mode.
- MARS-UAV-CS-3: The eigenvalues of the dynamical modes of the UAV shall have a negative real component.
- MARS-UAV-CS-4: The UAV shall remain shall be controllable during VTOL.
- MARS-UAV-CS-5: The UAV shall be able to resist perturbations with a magnitude of up to 10 m/s in all direction.

[19]URL: `https://nssdc.gsfc.nasa.gov/planetary/factsheet/marsfact.html` [Cited 22 June 2018]

7.4.2. Airfoil Selection

This section discusses the selection of a suitable airfoil for the main wing and the canard surface. For both cases, a Reynolds number between 3×10^4 and 6×10^4 is assumed. The different airfoils are analysed using Mark Drela's XFOIL [Drela, 1989]. The use of XFOIL has been validated extensively for low-Reynolds number airfoil design (in particular for the model RC-airplanes) [Selig et al., 2011].

Main wing

The choice of a proper airfoil for the main wing is of vital importance to optimise the cruise performance of the UAV. In this flow regime, viscous effects are very predominant, such as the formation of laminar separation bubbles starting from a certain angle of attack. This results in the characteristic 'kink' in the airfoil lift curve.

For the main wing a selection of airfoils was analysed using XFOILS on an angle of attack range from −2° to 10°, with a Reynolds number range from 2×10^4 to 8×10^4. The airfoil selection was based on a brief literature study on low-Reynolds number airfoil selection [Monteiro et al., 1995; Selig et al., 2011; Selig and Guglielmo, 1997]. In total ten airfoils were included in a trade-off, after which the SD7003 airfoil was finally chosen. The trade-off was based on five criteria which are listed in Table 7.16 together with their weights. Table 7.14 shows the results from the XFOIL analysis for all airfoils. Finally, Section 7.4.2 provides the normalised airfoil data. The data was normalised as follows,

$$x_{\text{norm}} = \frac{x_{\text{ori}} - x_{\text{min}}}{x_{\text{max}} - x_{\text{min}}}$$

where 'norm' refers to the normalised value and 'ori' to the original value. The final simulation results are shown in Figure 7.21.

Table 7.14: Results from the airfoil analysis using XFOIL.[20]

Airfoil name	C_l/C_d @ $C_{l_{\text{des}}}$	t/c	C_m	$C_{L_{\text{max}}}$	$\alpha_{C_{L_{\text{max}}}}$
AG16	19.66	7.12	-0.0589	1.002	7.6
E193	10	10.23	-0.0749	1.035	8.4
E211	11.36	10.96	-0.0698	1.776	9.4
E387	11.55	9.07	-0.0876	1.194	8
E71	17.93	5.71	-0.112	1.332	7.4
NM29	22.23	6.6	-0.058	1	7.6
SD2030	12.77	8.56	-0.0398	1.604	8.6
SD6060	11.43	10.37	-0.0391	1.036	9.4
SD7003	19.24	8.51	-0.0518	0.975	7.8
SD7080	14.20	9.16	-0.0614	1.142	9

Table 7.15: Normalised scores of all the airfoils based on the simulation results as shown in Table 7.14.

Airfoil name	C_l/C_d @ $C_{l_{\text{des}}}$	t/c	C_m	$C_{L_{\text{max}}}$	$\alpha_{C_{L_{\text{max}}}}$	**Score**
AG16	7.9	2.7	7.3	0.3	1.0	5.1
E193	0.0	8.6	5.1	0.7	5.0	3.7
E211	1.1	10.0	5.8	10.0	10.0	5.8
E387	1.3	6.4	3.3	2.7	3.0	3.4
E71	6.5	0.0	0.0	4.5	0.0	3.0
NM29	10.0	1.7	7.4	0.3	1.0	5.7
SD2030	2.3	5.4	9.9	7.9	6.0	5.1
SD6060	1.2	8.9	10.0	0.8	10.0	5.2
SD7003	**7.6**	**5.3**	**8.3**	**0.0**	**2.0**	**6.0**
SD7080	3.4	6.6	7.0	2.1	8.0	5.0

[20]URL: `http://airfoiltools.com/search/index` [Cited 22 June 2018]

Table 7.16: Overview of the trade-off criteria used in for the selection of the main wing airfoil.

Criterium	Weight [%]	Rationale
C_l/C_d @ $C_{l_{des}}$	40	Determines the performance of the UAV during cruise. Since range is the predominant performance factor, this criterium has been given the highest weight.
t/c	30	A thicker wing is lighter due to its more favourable section properties. Because of the higher mass moment of inertia the bending stresses of the wing will be lower. The weight of the structure is critical for the feasibility of the design; therefore this factor has been given a weight of 30%.
C_m	15	The higher the C_m, the larger the margin between stability and controllability will be. Since a canard configuration is chosen for the UAV, the stability of the aircraft is not as straightforward as a conventional configuration: an airfoil with a strong pitching moment will make it impossible to stabilise the design.
$C_{l_{max}}$	10	A higher $C_{l_{max}}$ allows for a lower stall speed, and is beneficial for the transition phase between the VTOL and cruise configuration. However, it is very hard to reliably assess the wing performance close to the stall point, and a dedicated control mechanism will have to be present for the transition phase anyway. Therefore, the weight for this criterium is rather low.
α @ $C_{l_{max}}$	5	This parameter indicates how long the wing stall can be 'delayed'. Stall at higher angles of attack means that less power is required during the transition phase. For the same reasons as mentioned for the previous criterium, the weight of this criterium is kept rather low.

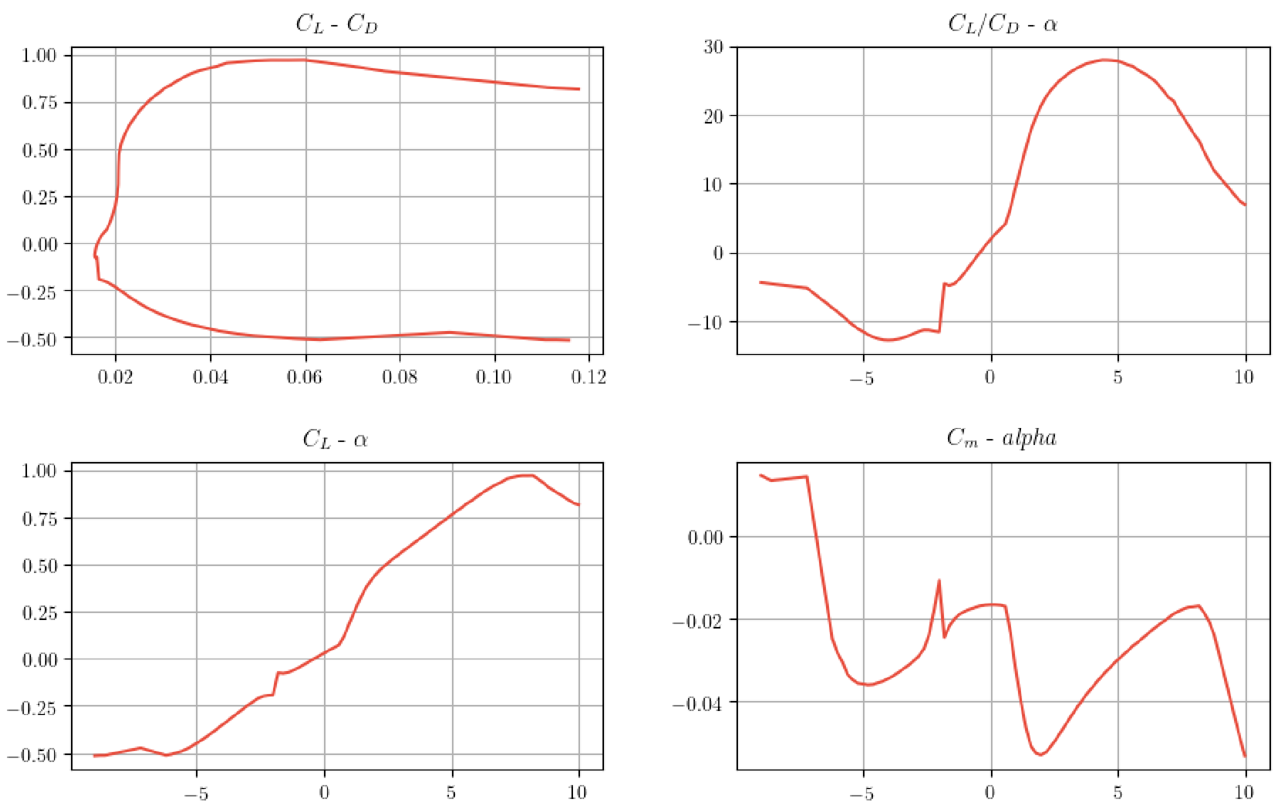

Figure 7.21: Overview of the simulation results as predicted by XFOIL for the SD7003 airfoil at a Reynolds number of 5×10^4.

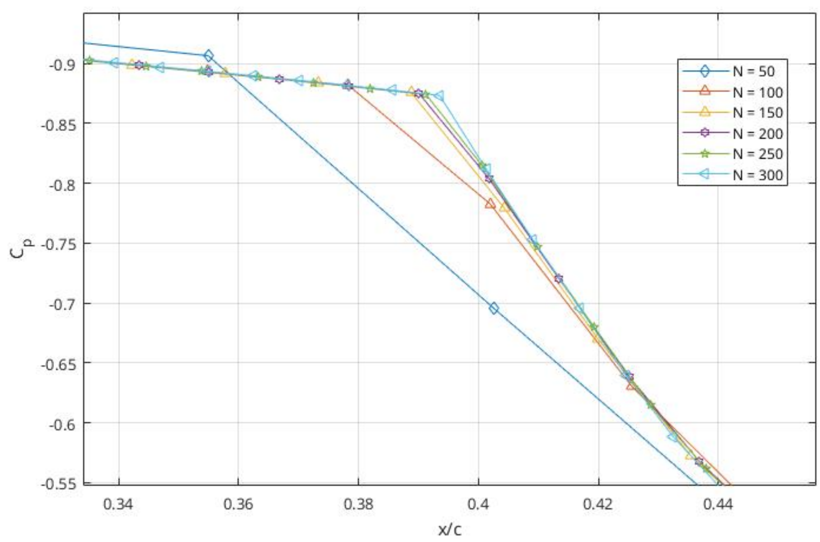

Figure 7.22: Close up of the C_p diagram of the SD7003 airfoil (α =5°, Re =6 × 10^4). The laminar separation bubble is the only part on the chord length where a grid refinement has any significant influence on the accuracy of the simulation. From a panel number (N) of 150 and higher the differences are minimal.

To assess the robustness of the choice of the SD7003 airfoil, a sensitivity analysis was performed on the weights of the trade-off. The result of the sensitivity analysis was actually rather unfavourable, as the choice for the airfoil seemed to strongly depend on the weight of the C_l/C_d criterium, at which the SD7003 excels. However, due to the low score of the SD7003 on the $C_{L_{\max}}$ and $\alpha_{C_{L_{\max}}}$ criterium, the NM29 and E211 both came into favour when the weight of the C_l/C_d criterium was lowered b 5%. Therefore, it is recommended that the performance advantage of the SD7003 airfoil when compared to the NM29 is analysed more closely with more advanced tools or a wind tunnel test in future design stages. For now however, it was decided that the SD7003 shows the best performance overall. The the verification of the XFOIL simulation was performed using two methods:

- A sensitivity analysis on the Reynolds number and the freestream velocity.
- A grid convergence study, with the 'grid' being the number of panels used to approximate the airfoil surface.

The sensitivity analysis did not result in any surprising conclusions: as expected, the airfoil performance gradually deteriorates with decreasing Reynolds number due to early separation and high viscous drag. At very low Reynolds numbers (2×10^4), it is clear that XFOIL is no longer capable of representing the severe separation in the model used; the method only converges for a very limited range of angles of attack. Relatively minor changes ($\pm$ 5 m/s) in freestream velocity did not have any significant influence on the simulation outcome. The grid convergence study showed that sufficient grid refinement is necessary in order to accurately represent the presence of the LSB. This phenomenon is already mentioned in the user manual of XFOIL. Apart from LSB, even a very coarse grid of 50 panels showed no significant errors when compared to a 300 panel grid. Figure 7.22 presents the grid convergence around the LSB. [21]

From a 150 panels or more no considerable changes were present in the results when the grid was refined. For validation purposes, the final results for the SD7003 were compared to the extensive wind tunnel data acquired by Selig et al. [2011]. The predicted results turned out to be reasonably close to the validation data: the lift production of the airfoil is very accurately simulated, while there is some overestimation of the drag produced by the airfoil. This is probably due to inaccuracies in the modelling of the boundary layer and the resulting viscous drag. The results from the validation process for the SD7003 airfoil are shown in Figure 7.23.

[21]URL: `http://web.mit.edu/drela/Public/web/xfoil/xfoil_doc.txt` [Cited 22 June 2018]

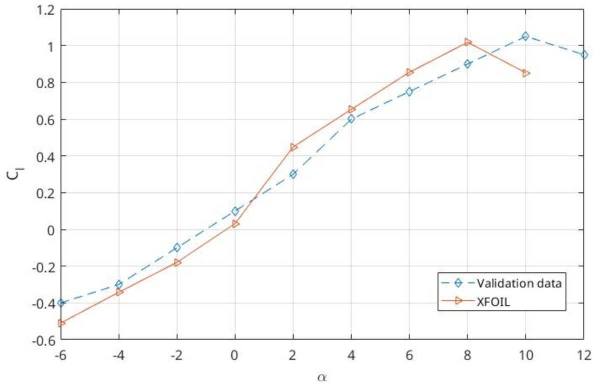

(a) C_l - α

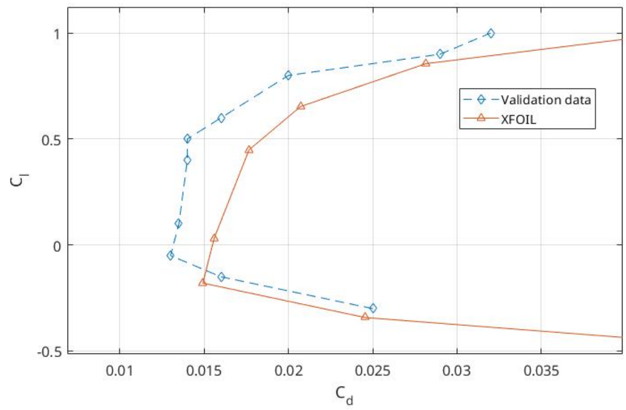

(b) C_l - C_d

Figure 7.23: Validation results for the XFOIL simulations of the SD7003 airfoil at a Reynolds number of 6×10^4. 300 panels were used to approximate the airfoils.

Canard Surface

A similar approach is taken for the canard airfoil selection. Since the canard surface must be able to generate both positive and negative lift, its airfoil will have to be close to symmetric. During the preliminary design phase symmetry was assumed for the airfoil. When at a later stage the cruise angle of attack is known some camber may be added to the canard to optimise for cruise flight while still maintaining the 'inverted' lift capability. The latter step is kept as a recommendation for more detailed design phases.

An XFOIL analysis was done to compare five NACA 4-series airfoils with thickness to chord ratio of 5, 10, 15, 20 and 25. From these, NACA0015 showed the best performance both in lift curve slope and $C_{l_{\max}}$. This was the airfoil chosen for the canard surface.

7.4.3. UAV Stability Characteristics

A careful analysis of the stability characteristics is necessary to check whether the UAV can perform all the flight phases. The UAV should not transition from a stable situation to an unstable on its own and should be able to return to a stable situation when encountering a disturbance. As a result, the longitudinal stability, the VTOL transition and the dynamic stability of the UAV are investigated in the following parts.

Longitudinal Static Stability

Sizing a functional design using the configuration that has been derived in Section 6.2.2 is done in a iterative process using the program Athena Vortex Lattice (AVL) developed by Mark Drela and Harold Youngren. It allows to perform an aerodynamic and flight-dynamic analysis of an arbitrary configuration using vortex lattice model for lifting surfaces. AVL requires three data files that describe the geometry, mass distribution and phase of flight to complete the analysis. By generating these files through a Python program quick iterations can be performed in order to obtain a function design. The driving parameter of the iteration process was to obtain a design with the optimal $\frac{C_l}{C_d}$ so that the range is maximised. In order to size the canard surface for longitudinal control, the stability and control characteristics of the UAV had to be analysed. Additionally, an analysis of the mass distribution was performed to obtain the center of mass. Using the so-called scissor-plot, depicted in Figure 7.24, the required tail surface could be obtained graphically from a given center of mass. [Olivero, 2018]

The limit for stability is based on the fact that the center of mass of the aircraft should always be located in front of the so-called neutral point (where neutral stability occurs). The location of the neutral point can be computed using

$$\bar{x}_{np} = \bar{x}_{ac} + \frac{C_{L_{\alpha_h}}}{C_{L_\alpha}}\left(1 - \frac{d\epsilon}{d\alpha}\right)\frac{S_h l_h}{S\bar{c}}\left(\frac{V_h}{V}\right)^2$$

, where $\bar{x}$ refers to the fact that the longitudinal locations are normalised with the mean aerodynamic chord (MAC).

In addition, the limit for controllability is based on the necessity that the aircraft has a trim point, i.e. when all moments cancel out. This requires in essence that the control surface is able to counteract the moments generated by the main wing around the center of mass. The equation for the controllability equation is

$$\bar{x}_{cg} = \bar{x}_{ac} - \frac{C_{m_{ac}}}{C_{L_{A-h}}} + \frac{C_{L_h}}{C_{L_{A-h}}}\frac{S_h l_H}{S\bar{c}}$$

,

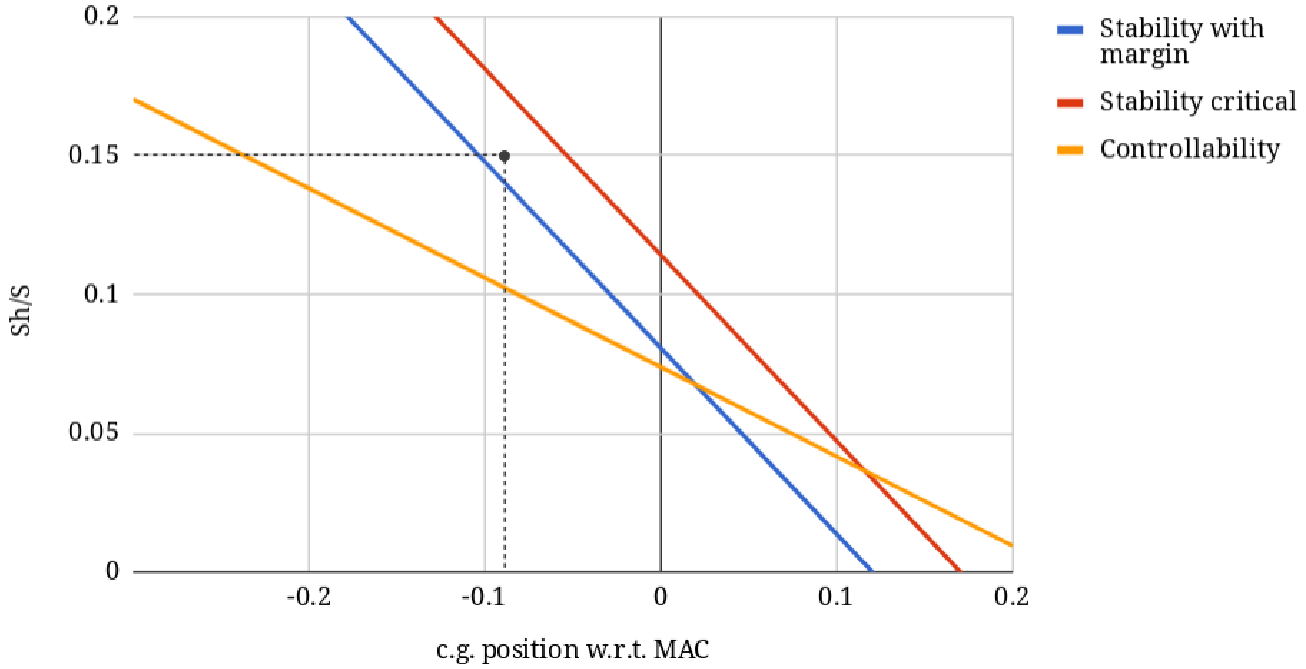

Figure 7.24: Scissor plot of the UAV design. The scissor plot shows the allowable margins for the c.g. margins in function of a certain canard size. The c.g. position of the UAV is at located 9% of MAC before the leading edge of the main wing. Hence, S_h/S was chosen to be 0.15.

where the location of the aerodynamic center, x_{ac} was estimated using the empirical methods discussed by Torenbeek [1996]. The lift slope properties of the main wing and canard surface were based on the data obtained from XFOIL, corrected using the 3D correction:

$$C_{L_\alpha} = \frac{C_{l_\alpha}}{1 + \frac{C_{l_\alpha}}{\pi A e}}$$

.
Finally, the center of mass was determined to be at $\bar{x}_{cg}$ = -0.096, i.e. just in front of the leading edge of the main wing. Using Figure 7.24, the canard surface was chosen to be 0.276 m^2.

The obtained dimensions were used to model the UAV in XFLR5 in order the verify AVL's results for the main wing sizing and the location of the center of mass. The obtained results in XLFR5 showed a negligibly small off-set due to the lack of flexibility the program offers to create the model. The program is made to analyse traditional configurations and thus the X-wing resulted in some overlap in the lifting surfaces. In order to avoid the overlap the bottom X-wings were moved slightly outwards. As a result, the model generated in AVL and the model generated in XFLR5 are not a perfect fit and some variance in the results is apparent.

VTOL

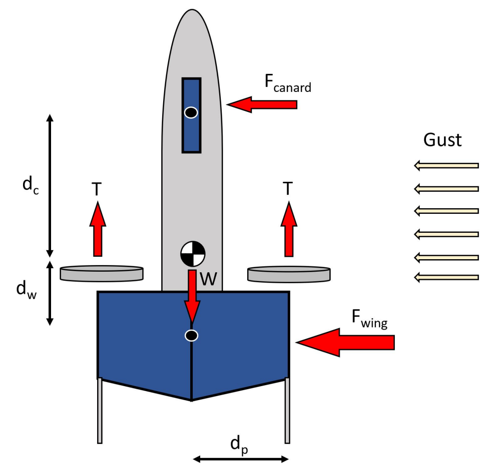

Figure 7.25: Simplified free body diagram of UAV during gust

In order to perform VTOL, the UAV has to produce enough thrust to perform a controlled vertical ascend or descend. To ensure controllability, the UAV has to remain stable during the whole manoeuvre and resist the unpredictable gusts of wind or it will tip over. Due to its X-wing configuration, the UAV has the advantage of having a disposition of the propellers similar to a quadcopter. In order to increase the inherent stability of the UAV, it is crucial to put the centre of gravity lower than the propellers. This will cause the propellers to perform a *pulling* action rather than a *pushing* action, which results in a statically stable UAV.

Only being statically stable may not be enough to resist the gusts, thus attitude control needs to be incorporated. This is done by controlling the thrust produced by each individual co-axial propeller. The individual thrust can be controlled by introducing a swashplate or varying rpm of each propeller. The latter is not a feasible option as the rate of change in rpm would be to low due to the large moment of inertia of the propellers.

Assuming the worst case scenario where a gust of 10 m/s strikes the UAV perpendicular to the wing surface while hovering as seen in Figure 7.25 some back-of-the-envelope calculations can be made. A preliminary estimation of the moment caused by the gust can be generated around the centre of gravity. Assuming a drag coefficient of 1.28 for a flat plate in a 3-D flow[22], a projected surface area of 1 m^2 for the main wing and 0.15 m^2 for the canard, and using the distances d_c of0.5 m and d_w of 0.3 m between the geometric centres and the centre of gravity, the moment can be determined to be equal to 0.02 N/m. This moment needs to be counteracted by creating an opposite reaction moment with the four pairs of co-axial propellers. Deducting from the geometry that the moment arm of each propeller d_p is0.6 m, each propeller needs to adjust its thrust by 0.008 N. As these values are on the lower side and can be provided by the propellers, the UAV can be controlled and stabilised during VTOL using the propeller thrust.

[22] https://www.grc.nasa.gov/www/K-12/airplane/shaped.html [Cited 22 June 2018]

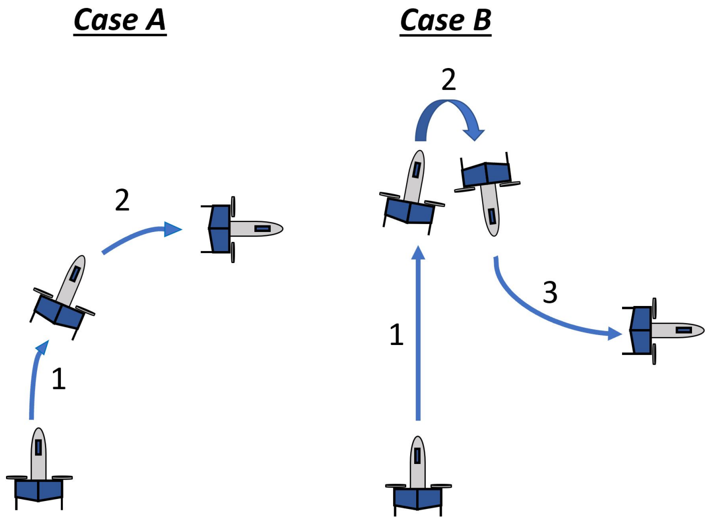

Figure 7.26: Transition modes during take-off. Case A: The propellers provide enough thrust to execute a controlled rotation while ascending. This is the most time efficient method. Case B: The propeller do not provide enough thrust to perform the rotation while ascending, thus the UAV has to reach a certain altitude to gain enough velocity to perform a controlled rotation.

The transition from vertical take-off to cruise and from cruise to vertical landing is a very delicate and critical phase as the UAV's has to change its attitude by 90° as fast as possible without losing too much (or any) height. Determining the optimal transition flight path and guaranteeing the controllability of the UAV during the transition is a complex task [Stone and Clarke, 2018].

Multiple approaches are possible to perform a controlled transition, as shown in Figure 7.26. In this figure take-off is used as an example, but the same reasoning can be applied for the transition from cruise to landing. In case A the UAV's propellers deliver enough thrust to effectuate a 90^o pitch change while accelerating upwards. This transition method is the most efficient time wise, but requires more power for the propellers to deliver enough thrust. However, as soon as their is a horizontal velocity component, part of the UAV will generate lift and will thus decrease the thrust required by the propellers. In Section 7.5.1 it was derived that the thrust-to-weight-ratio is 1.05. If the UAV maintains the same attitude at full thrust, there is 5% of the thrust that can be used to obtain an horizontal acceleration component. The maximum angle at which the UAV can still hover is equal to 18° from the vertical and would deliver a 1.22 m/s in the horizontal direction. As a result, the UAV would potentially be able to generate some lift while rotating, lowering the thrust required. Nevertheless the power is a limiting factor in the design. Thus a less-power consuming method is desired. In case B, the UAV performs a vertical ascend during phase 1, performs a U-turn in the vertical plane in phase 2 and dives down in phase 3. Phase 1 is required to gain enough height for the UAV to dive down in phase 3 so that it can gain enough velocity to perform a controlled pitch change. It is crucial for the UAV to have gained enough height as the the U-turn will be barely controllable due to the low velocity. There is an optimal point between case A and case B where the combination of power and time required is set to a minimum. Further analysis needs to be conducted in order to find the optimal flight path.

The control surfaces play a crucial role during the transition. Firstly, the canard surface can change its incidence angle by 90° in order to be able to control the UAV at lower velocities during the pitch changes. Secondly, each X-wing is equipped with a ruddervator placed behind the trailing spar, which offers a control surface of about 40% of the chord. The ruddervator by themselves do not offer much control at low velocities, but as they are placed behind the propellers, so a constant accelerated airflow is created over them, generating control forces.

Dynamic Stability
In order to check for the dynamic stability the following dynamic modes given in Table 7.17 need to be considered. The eigenvalues have been determined by XFLR5 with the current model.

Each mode is represented by a complex number and its conjugate. The real part of the value represents the the damping (negative) or amplifying (positive) of the mode. The imaginary part gives a value of for the frequency of the mode. The longitudinal dynamics responses can be plotted in a root locus diagrams and their corresponding times response. As the eigenvalues are not plotted in function of a design variable only the fixed eigenvalues are plotted in an eigenvalue diagram.

Table 7.17: This table gives an overview of the dynamic modes and their eigenvalues.

Dynamic Mode		Value
Longitudinal	Short period	-0.20 ± 1.08i
	Phugoid	0.01
Lateral	Roll damping	-0.52
	Dutch roll	-0.04 ± 0.71i
	Spiral mode	-0.01

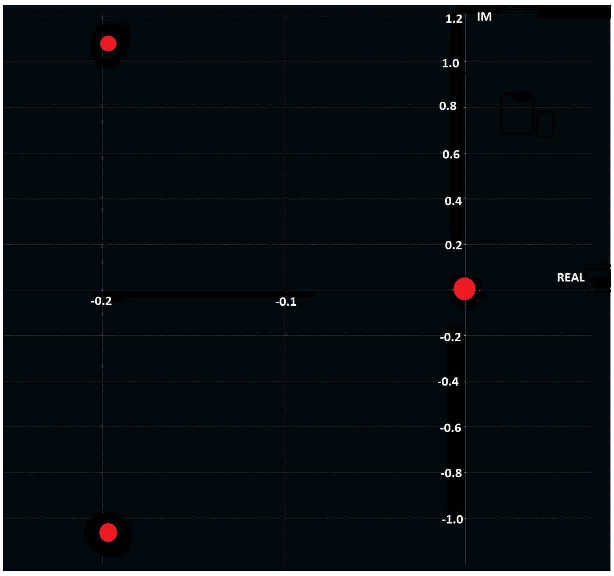

(a) From left to right: Short period and Phugoid

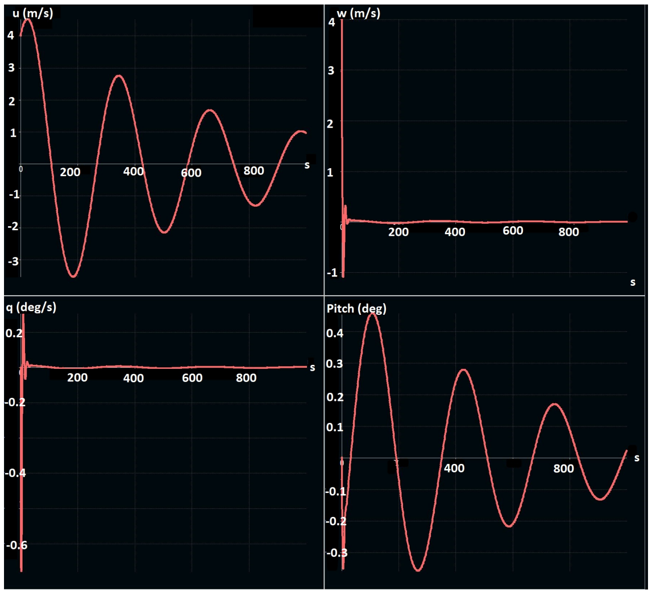

(b) Time response for given eigenvalues of UAV to a disturbance of 4 m/s in x-direction and 4 m/s in z-direction. From left to right: Velocity u in x-direction, velocity w in z-direction, pitch rate q and pitch angle θ all plotted on time given in seconds.

Figure 7.27: Eigenvalue diagram (a) and time response (b) of the longitudinal dynamic modes generated using XFLR5

All values on eigenvalue diagram are located on the negative real side of the diagram. As a result, all the longitudinal dynamic modes are damped and thus stable. In Figure 7.27a, the phugoid is located very close to the origin and only has a real value, meaning that is not amplified or damped and has no frequency. As a result, this mode will not be noticeable as its magnitude is negligible. The short period mode has a relatively high frequency and is damped. However, the damping value is about -0.2, meaning that before the UAV comes back to its original stable position it will oscillate a long time. This can be seen in Figure 7.27b where the time response to a gust with a velocity of 4 m/s in both x- and y-direction is plotted. It can be seen that the rolling moment and velocity in y-direction are quickly damped. However, the UAV's pitch and velocity in x-direction are is still oscillating after more than 800 seconds. Although the magnitudes of these values are small, this indicates that constant active control will be necessary during flight in order to counter gusts.

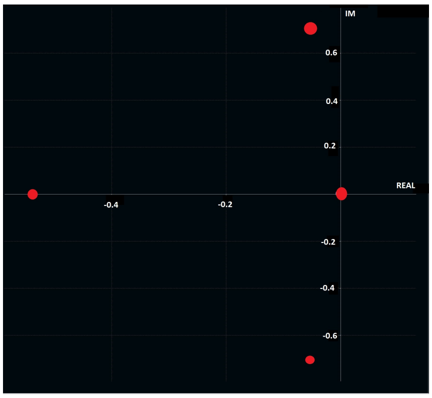

(a) From left to right: Roll damping, dutch roll and spiral damping.

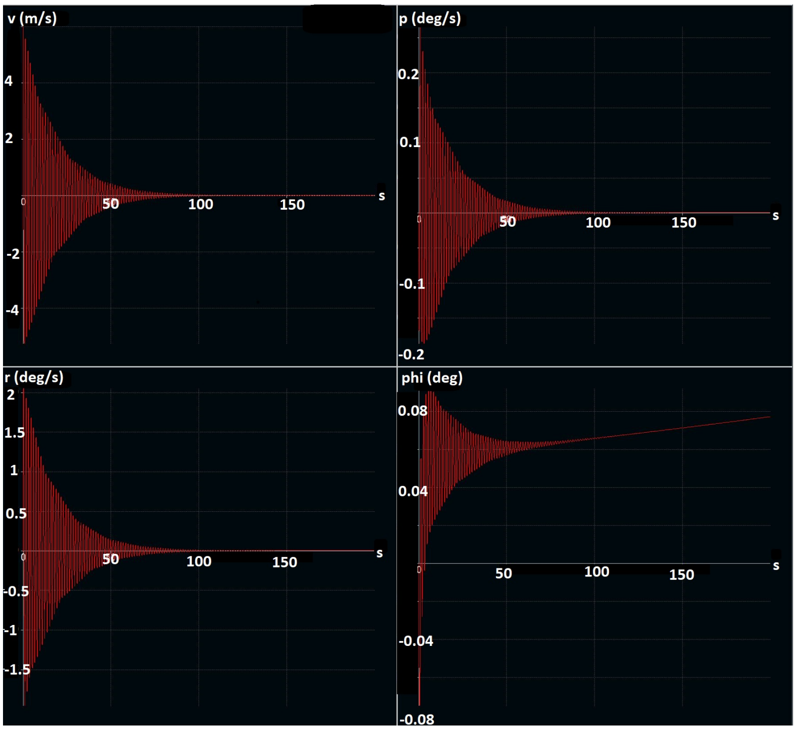

(b) Time response for given eigenvalues of UAV to a disturbance of 4 m/s in y-direction. From left to right: Velocity *v* in y-direction, roll rate *p*, yaw rate *r* and roll angle ϕ all plotted on time given in seconds.

Figure 7.28: Eigenvalue diagram (a) and time response (b) of the lateral dynamic modes generated using XFLR5

The eigenvalue diagram in Figure 7.28a shows the three lateral modes. The roll damping mode is a real negative value on the utter left. The pair of imaginary eigenvalues represent the dutch roll and slightly to the right of the origin the spiral mode is shown. As the spiral mode's eigenvalue is real and positive, it means that if the UAV enters the spiral mode it will not return to its original value. This would be a major issue if the value was very positive, but as shown in Table 7.17, its magnitude is very close to zero. Therefore the spiral divergence will occur slowly and will give the UAV enough time to actively change its attitude in order to escape the spiral. This phenomena is shown again in Figure 7.28b in the bottom right graph where the time reponse of the UAV to a disturbance of a gust of 6 m/s is plotted. The roll angle, named phi in the plot, slowly increases with time without ever returning to its original position. The time scales of these graphs are in the order of a 100 seconds, which is more than enough time for the UAV to correct its attitude change caused by the gust.

7.5. Electric Power System

The EPS is vital for the design for both the base station and UAV as enough power and energy has to be generated to operate the base station and lift-off the UAV. In Chapter 5, it was determined batteries were the best option for energy storage. In Section 7.5.1 the batteries for the UAV are sized and in Section 7.5.2 the batteries for the base station are sized.

Batteries with a higher power density and energy density tend to have a lower life cycle[23]. For the take-off and descent, the power required is the main constraint and for the cruise the energy required is the main constraint. This yields two different batteries: one with a high energy density and one with a high power density.
Furthermore, the influence of the Martian atmosphere should be analysed in detail. For example, the temperature is lower than on Earth, which influences the available capacity of the battery.

7.5.1. EPS of the UAV

Before the batteries can be sized, efficiencies have to be taken into acocunt. Power gets dissipated due to the inefficiencies from transferring energy through subcomponents, the deficiencies are presented in Table 7.19. [24], [25]

[23]URL: `http://www.amicell.co.il` [Cited 22 May 2018]
[24]URL: `http://batteryuniversity.com/learn/article/elevating_self_discharge` [Cited 22 May 2018]
[25]URL: `http://batteryuniversity.com/learn/article/discharge_characteristics_li` [Cited 22 May 2018]

26

Table 7.18: Efficiency of power conversion components. [24][25][26]

Subcomponents	**Efficiency**
Voltage regulator	95%
Wiring	98.5%
Motor	90.5%
CPU	99%
Distribution system	99%
Total	**82.2%**

A note has to be taken on the self-discharge. The battery of the UAV should be recharged right before take-off to minimise the capacity loss due to self-discharge. For all the subcomponents, except for the wiring, no contingency is used as the exact values are known. For the wiring efficiency the estimation is shown in Equation 7.8[26]

$$\eta_{\text{wiring}} = 1 - 0.0015 \cdot l_w, \tag{7.8}$$

where l_w is the wiring length. The length has been assumed to be 10 m, which is based on statistics[26].
Furthermore, the effect of the operating temperature on the battery is presented in Figure 7.29.

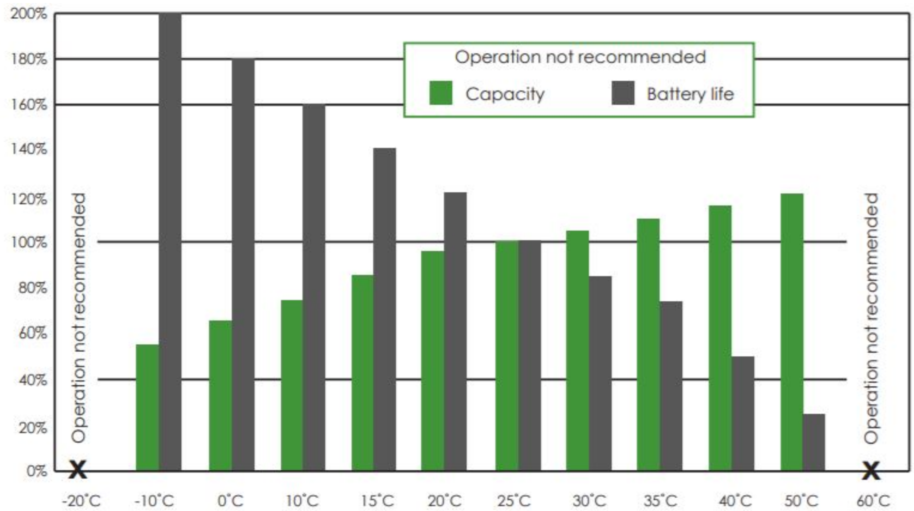

Figure 7.29: Influence of operating temperature on battery life and capacity.[27]

A balance has to be found between the life cycles required, power required for thermal control and reduction on capacity. The maximum continuous discharge current decreases as well. Next to that, as it is hard to maintain a consistent temperature through thermal control, a contingency has to be taken. The operating temperatures of the scientific instruments have to be taken into account as well, which will be elaborated upon in Section 7.7.2.
It was concluded that the average operating temperature is around 15°C and thus the amount of life cycles increase by 130% compared to the nominal value and the capacity decreases by 82%.
The final factor that influences the capacity is the discharge current. Every battery has its rated discharge current, and if the actual discharge current exceeds or deceeds this value, the capacity can be positively or negatively affected. As flying on Mars requires a lot of power, the rated discharge current has to be exceeded. The decrease in capacity is

$$t_d = H \cdot \left(\frac{C}{IH}\right)^k, \tag{7.9}$$

with t_d the actual discharge time, H the rated discharge time, C the rated capacity, I the rated discharge current and k Peukert's constant. Once the battery specifications are obtained, the actual discharge time can be determined.

[26]URL: `http://colonialwire.com/wp-content/uploads/2013/09/WIRE-WEIGHTS1.pdf` [Cited 22 May 2018]
[27]URL: `https://www.heliant.it/images/FV/ev_temperature_effects.pdf` [Cited 17 June 2018]

The flight duration per cycle is 0.226 hours, which is determined in Chapter 4, by dividing the distance covered by the cruise velocity. Then the time duration of the take-off and descent is included, which leads to the minimum value required for the discharge time. The actual capacity can then be determined when the specifications of the battery is obtained.
The battery should have a of 789 cycle life (Chapter 4), if the UAV wants to cover the entirety of the Jezero crater. Life cycles are defined at 80% depth of discharge (DOD), as the batteries will be designed for end of life (EOL), the batteries will be able to provide 20% more than the required capacity at begin of life (BOL). Life cycles are defined at 80% DOD, as the total available capacity per life cycle decreases more heavily once the battery has reached that stage.
As analysed in Section 7.3, the power and energy requirements for the UAV are including the power conversion and 15% contingency. The requirements are shown in Table 7.19.

Table 7.19: Power & energy requirements

Phase	Power [W]	Energy [Wh]
Take-off	2379	18.1
Cruise	1497	290.7

Furthermore, the chosen motor has constraints on the volts and amperes it can handle. The battery should be sized such that those values are not exceeded. The maximum volts the motor can handle is 36 V, and the maximum current is 15.26 A as mentioned in Chapter 5.

A rechargeable lithium-ion battery provided by Panasonic[28], which had the most fitting specifications for the system. The currently used batteries are not custom made and one might expect that the battery will improve when the design is developed. However, during the feasibility design, these possible improvements are not taken into account. This yields the specifications for the UAV-battery as provided in Table 7.20, with all contingencies, power conversions and Peukert's law included.

Table 7.20: Specifications of the UAV battery

Specification	Value	Unit	Specification	Value	Unit
Voltage per cell	3.2	V	Mass	2.62	kg
Current per cell	8.5 / 14	A	Rated discharge time	0.7	h
Amount of cells in series	9.	-	Energy density	136	Wh/kg
Amount cells in parallel	6	-	Power density	560	W/kg
Total Voltage	28.8	V	Volumetric energy density	620	Wh/l
Total current	51.0	A	Life cycle	650	-
Capacity	12.45	Ah	Charging time	4.88	h
Total power	1502 / 2419	W	Discharge time	0.24	h
Total Energy	358.6	Wh	Operating temperature	-20 to 60	C
Mass per cell	0.043	kg	Size	0.95	L

As more power is required during take-off, the discharge current will be 14A. During cruise it can be lowered to 8.5A to increase the range of VITAS. Furthermore, the voltage drops over the span of each cycle. The average volt per cycle is 3.2 V[31] and that was used to simplify calculations.
Peukert's law is included in the table and is calculated as follows. In Equation 7.9, k represents Peukert's constant for which 1.05 a typical value is for rechargeable batteries [29]. The other values can be taken out Table 7.20. The rated capacity C equals 2.5 Ah, which is obtained by dividing the total capacity dived by the amount of cells in parallel. The rated discharge current H is 0.7h and the actual discharge current is 8.5A or 14A depending on the phase. Filling in the values for the take-off and cruise situation, an actual discharge time of 0.241 h is obtained.

[28]URL: https://eu.industrial.panasonic.com/products/batteries-energy-products/secondary-batteries-rechargeable-batteries/lithium-ion-batteries/series/cylindrical-type/ACI4002/model/UR-18650ZTA [Cited 17 June 2018]

[29]URL: https://www.researchgate.net/figure/Peukert-constant-of-various-lithium-ion-battery-brands_fig12_231169804 [Cited 8 May 2018]

Nominal specifications of the battery during its mission and entire life are represented in the following figures[30].

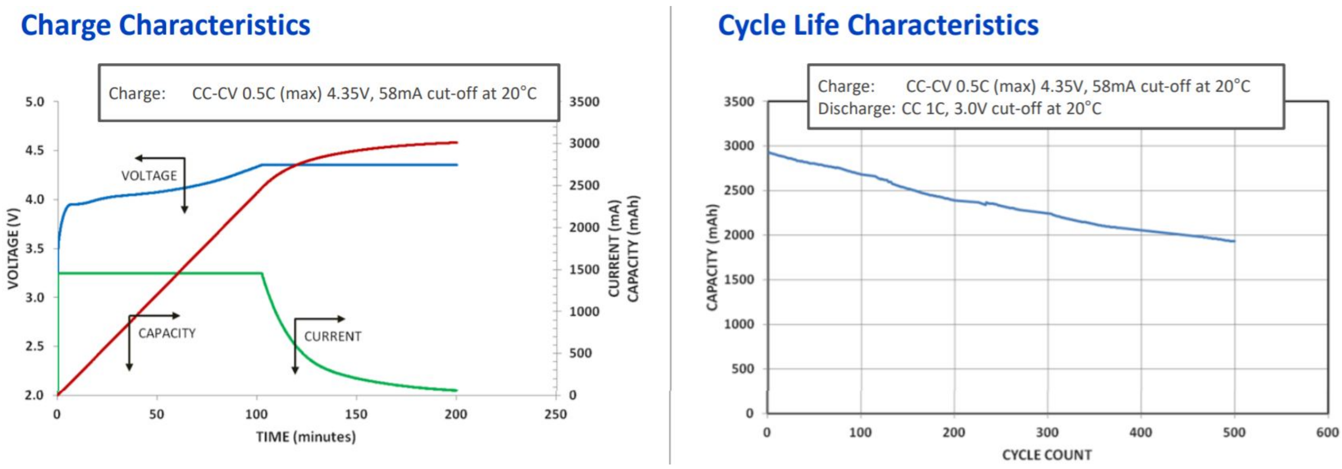

Figure 7.30: Charge and cycle life characteristics for the UAV battery [30]

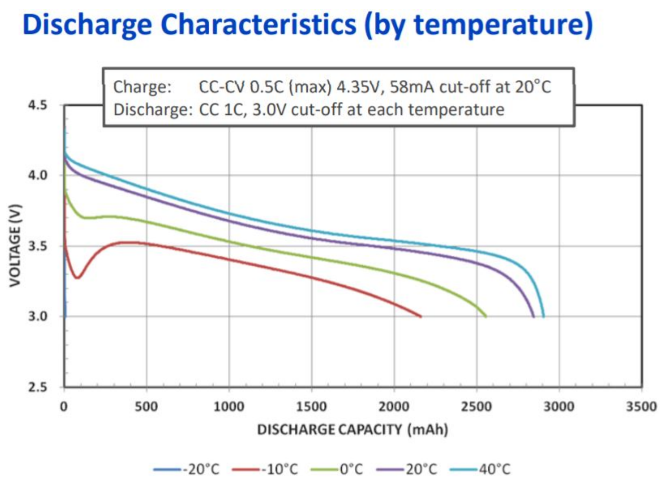

Figure 7.31: Discharge characteristics for the UAV battery [30]

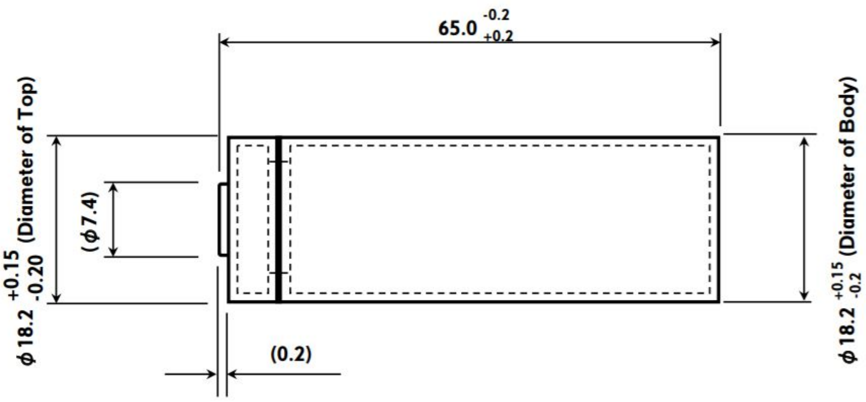

Figure 7.32: Size of each cell of the battery UAV [31]

The total amount of life cycles is increased by 130%, which is defined at a DOD of 80%, yielding a life cycle of 650. Next to that, the capacity had to be decreased to 83% of its nominal value. The charging time is slightly higher due

[30] URL: `https://industrial.panasonic.com/cdbs/www-data/pdf2/ACI4000/ACI4000C17.pdf` [Cited 17 June 2018]
[31] URL: `https://www.powerstream.com/p/us18650vtc4.pdf` [Cited 17 June 2018]

to charging at a lower temperature and a lower charging current. The charging efficiency is 0.92 [30], yielding

$$t_c = \frac{C}{I_C \cdot \eta_{\text{charging}}} \tag{7.10}$$

with $\frac{C}{t_c}$ chosen to be 0.2C, which is a recommended value to ensure 100% capacity after charging while not harming the amount of life cycles, the charging time equals 4.879 h.
With the batteries designed for the UAV, yields the equation of the range D_R in meters with capacity loss due to operating temperature and power conversion included,

$$D_R = \frac{\lambda_p \cdot V_c \left(E_{tot} - \frac{P_{TO} \cdot h_c}{3600 \cdot V_c}\right)}{3600 \cdot P_c}, \tag{7.11}$$

where D_R is the resulting range, λ_p is the Peukert's ratio, equal to 0.93, V_c, h_c, P_c are the velocity, altitude and power during cruise, P_{TO} is the take-off power and E_{tot} is the total energy required. This results in a range of 60.55 km at 80% DOD, with data accumulated from Table 7.20 .

As one could note, the amount of life cycles the UAV can perform is 650 as mentioned in Table 7.20. However, as the range is 60.55km, it is slightly over-designed. Over the next 130 life cycles, the capacity drops to 85%, which means at the end of the mission the range will be 51.467 km. Ergo, it will be difficult to reach the outer edges. If ice deposits happen to be present at the edges, these will have to be surveyed first during the fine mapping as then the range is bigger.

EPS UAV Subcomponents

The masses and sizes of the components can be retrieved found in Table 7.21. [32] [33] [34] [35] [36] [37] [38]

Table 7.21: UAV components EPS excluding batteries[33] [35] [37] [38] [36] [34]

Component	Unit size [mm^3]	Unit mass [g]	Amount	Total volume [mm^3]	Total mass [g]
Latching current limiters	2700	6.5	10	27000	65
Shunt regulator	15	1	30	450	30
Transistor switch	27	1.13	15	405	16.95
Battery indicator	5	1	2	10	2
Connector	15	1.5	10	150	15
Voltage regulator	102486	15	1	102486	15
Discharge regulator	24	5	2	48	10
Boost regulator	8	2	10	80	20
Wiring	20.81	18.4567	2	41.62	36.91
Battery management	199350	5	1	199350	5
Total				**330020.6**	**215.86**

Gathering the data in the tables yields the UAV's electrical diagram in Figure 7.33, with the amperes and voltages taken from Chapter 7.

[32] URL: `http://www.esa.int/esapub/bulletin/bullet100/JACKSON.pdf` [Cited 18 May 2018]
[33] URL: `http://courses.engr.uky.edu/ideawiki/lib/exe/fetch.php?media=classes:07c:eps499:ee499_project.pdf` [Cited 18 May 2018]
[34] URL: `https://ntrs.nasa.gov/archive/nasa/casi.ntrs.nasa.gov/19820013380.pdf` [Cited 18 May 2018]
[35] URL: `http://www.unmannedsystemstechnology.com/2012/08/analytic-systems-develops-power-products-for-unmanned-aerial-systems/` [Cited 18 May 2018]
[36] URL: `http://abbott-tech.com/products/dc-to-ac-inverters/kn-pn-ln-tn-linear-inverters/` [Cited 18 May 2018]
[37] URL: `https://ieeexplore.ieee.org/stamp/stamp.jsp?arnumber=5433399` [Cited 18 May 2018]
[38] URL: `http://www.analog.com/media/en/technical-documentation/data-sheets/lt1110.pdf` [Cited 18 May 2018]

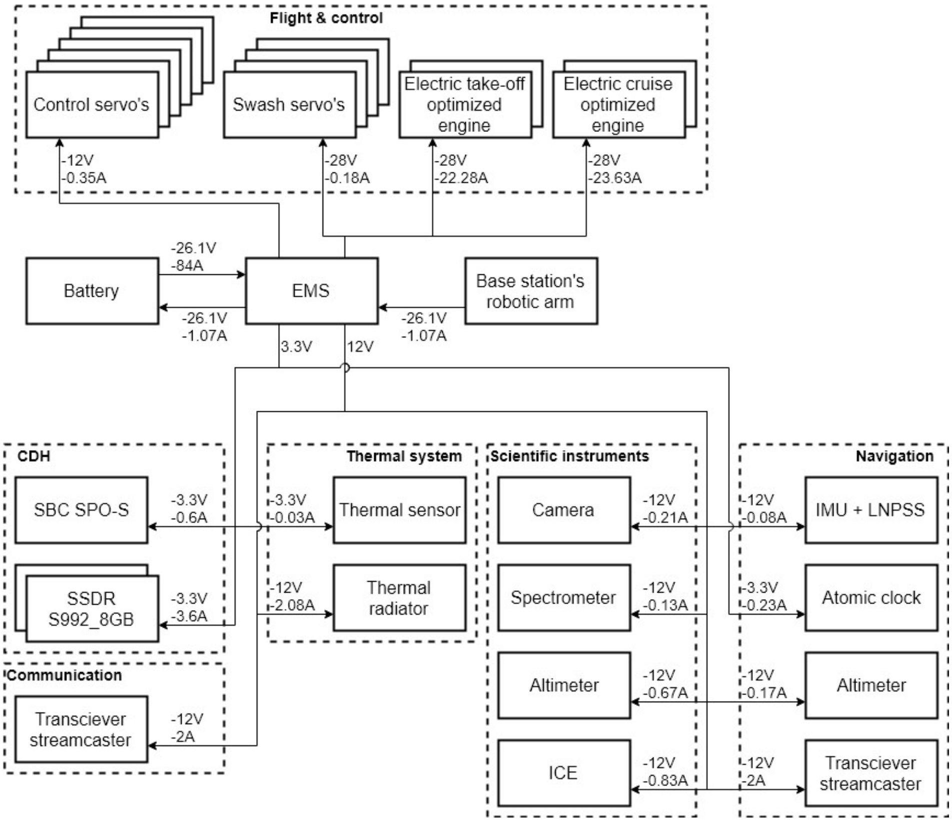

Figure 7.33: Electrical diagram UAV

7.5.2. Base Station EPS

The sizing of the base station battery is done similarly as in Section 7.5.1. The EPS of the base station consists mainly out of the battery and the solar panels. Similar to the UAV EPS sizing, a contingency of 15% has been taken on the estimated values of the energy and power required.

First, the power conversion's efficiency are estimated in Table 7.22.

Table 7.22: Power conversion efficiency of the base station.

Subcomponent/factor	Efficiency
Charger UAV	92%
Voltage regulator - Switching system	97%
Wiring	92%
Self-discharge	99%
Faradaic efficiency	99%
Distribution system	99%
Total	**81%**

The power requirements are estimated in Section 6.3.1. As the mass is less critical in the base station, the temperature can be maintained due to good thermal control and the overall efficiency increases. However, as the EPS of the base station is bigger compared to the UAV, the effect of the improved thermal management gets nearly nullified [30]. This yields the following table, which is combined with a power conversion of 81%, a contingency of 20% (usual contingency for preliminary design stage [Wertz and Larson, 1999]) and a thermal efficiency of 82% as discussed in Section 7.5.1. The total required BOL power requirement can be found in Table 7.23.

Table 7.23: Power requirements base station.

Subsystem	Nominal Power usage [W]	Peak power usage [W]
Total	186.24	371.87
Thermal control	0.1	30.1
Communications	33.6	122.8
CDH	38.52	80.53
Navigation	8.6	18.3
UAV	17.66	103.14
Scientific instruments	1.7	17

The base station will have to provide power for all components until the UAV is done flying. Afterwards, the base station will have to provide power for the thermal control, scientific instruments present on the base station and transmitting data, which equals 73.4 W. Thus, the base station is designed for two different mission stages. The first stage consists out of 789 cycles, as the UAV has to perform 789 flights. The second stage requires 837 cycles as the mission takes in total 4.6 years to transmit the data. Ergo, the amount of life cycles the base station offers is rated at EOL, which is 40% DOD and not 80% DOD. Nevertheless, the base station will still be able to maintain at least a 80% DOD after 789 cycles. Having the battery operating at the rated discharge current would be optimal to maintain the capacity according to Peukert's law. Furthermore, the base station has a worse efficiency namely due to more wiring.

Solar Panel Sizing
With the power requirements set, the solar panels can be sized. The solar panel specifications are presented in Table 7.24.

Table 7.24: Solar panels specifications

Specification	Value	Units
Average solar intensity	90	W/m^2
Efficiency	29.5	%
Density	2.1	kg/m^2
Power loss due to dust	66.66	%

Due to fine dust being present on the surface on Mars, less power can be produced, about 66,66% gets lost according to Petrescu and Petrescu [2011], which yields

$$m_{\text{panels}} = \frac{P_r \cdot \rho_{\text{panels}}}{q_{\text{sun}} \cdot \eta_{\text{panels}}}. \tag{7.12}$$

Filling in data from Table 7.24, a panel mass m_{panels} of 36.07 kg can be obtained, which leads to a volume of 17.69 m^2 for the four solar panels. This is estimated with the average solar intensity over the entire year. Which means more energy will be accumulated during summer and less during winter. As the maximum area for the solar panels is 18.09 m^2 as mentioned in Chapter 4, the solar panels cannot be sized up and not enough energy can be generated for the UAV to lift-off. Ergo, roughly estimated, the UAV mission will take 25% longer due to a low solar intensity during the winter. Which is a safe estimation, as in the end the UAV will be take-off during winter days at least each five days if the lowest solar intensity is taken [39].

Battery Sizing Base Station
Leading to the following specifications of the base station battery, which is a NCA battery provided by Panasonic.

[39]URL: `https://ntrs.nasa.gov/archive/nasa/casi.ntrs.nasa.gov/19890018252.pdf` [Cited 28 June 2018]

Table 7.25: Battery specifications.

Specification	Value	Specification	Value
Voltage per cell [V]	3.6	Mass [kg]	14.55
Current per cell [A]	0.7	Rated discharge time [h]	0.05
Amount of cells in series	30	Energy density [Wh/kg]	251
Amount cells in parallel	10	Power density [W/kg]	361
Total Voltage [V]	108	Volumetric energy density [Wh/l]	676
Total current [A]	7	Life cycles [-]	1700
Capacity [Ah]	33.5	Operating temperature [°C]	-20 to 40
Total power [W]	756	Charging time [h]	4
Total Energy [Wh]	36	Discharging time [h]	4.69
Mass per cell [kg]	0.049	Size [dm^3]	5.23

The specifications and sizing can be observed in the figures below. the amount of life cycles is up until the point the capacity of the battery reaches 1.005 Ah (40% DOD, which can be deduced from Figure 7.34). The amount of lifecycles is also increased by 130% due to the operating temperature (same as for the UAV).

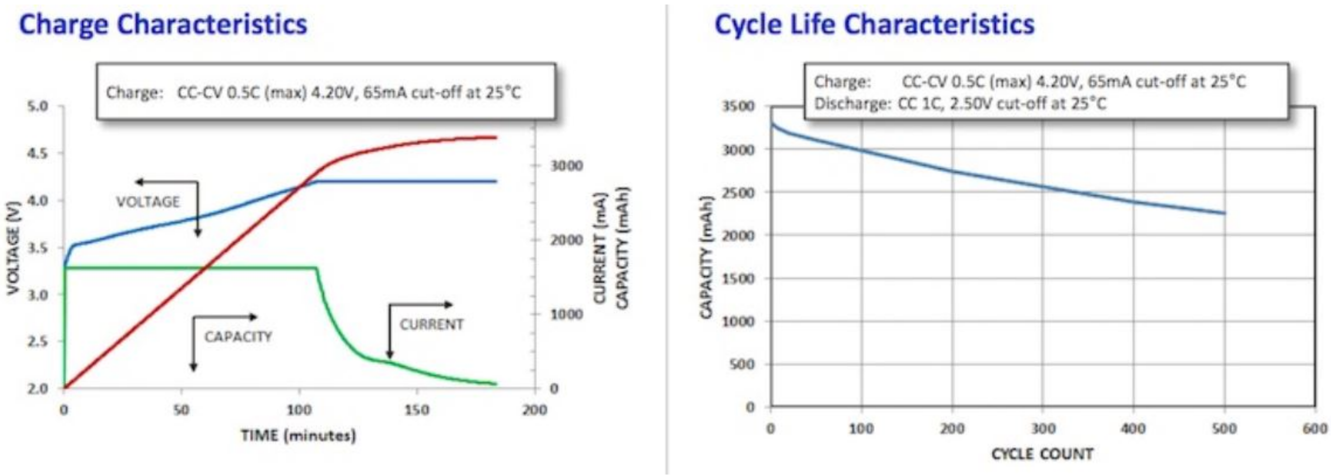

Figure 7.34: Charge and cycle life characteristics for the base station battery [30]

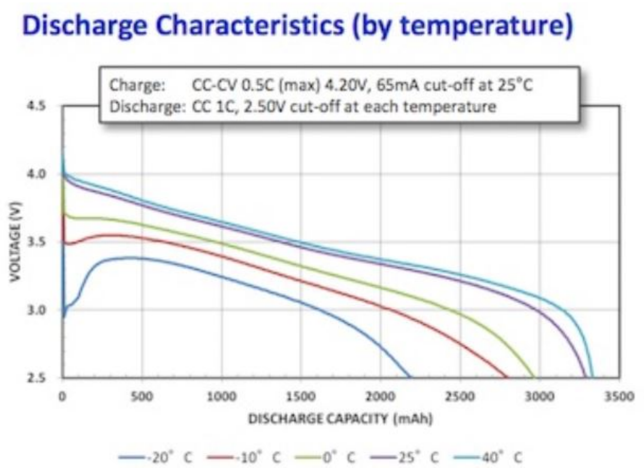

Figure 7.35: Discharge characteristics for the base station battery [30]

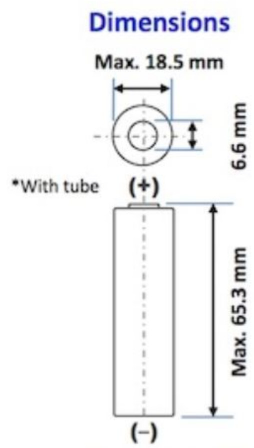

Figure 7.36: Size of one battery cell of the base station battery [30]

Similarly to the UAV, the subcomponents of the EPS for the base station were investigated[33 35 37 38 36 34].

Table 7.26: Base station EPS components [33] [35] [37] [38] [36] [34]

	Unit volume [mm^3]	Unit mass [kg]	Amount	Volume [mm^3]	Mass [kg]
Latching current limiters	2700	0.0065	10	27000	0.065
Shunt regulator	15	0.01	2	30	0.02
Transistor switch	27	0.0013	15	405	0.017
Inverter	880000	6.84	1	880000	6.84
LC3-charger	89856	6.6	2	179712	13.2
Voltage regulator	102486	1.5	2	204972	0.3
Charge regulator	367488	0.35	2	734976	0.7
Discharge regulator	694800	0.575	1	694800	0.57
Wiring	208	9.37	1	208	9.37
Battery management	226800	0.1	1	226800	0.1
Base station total				**2949066**	**31.23**

This yields the electrical diagram for the base station as presented in Figure 7.37, the data of required ampere and volt has been acquired from Chapter 7.

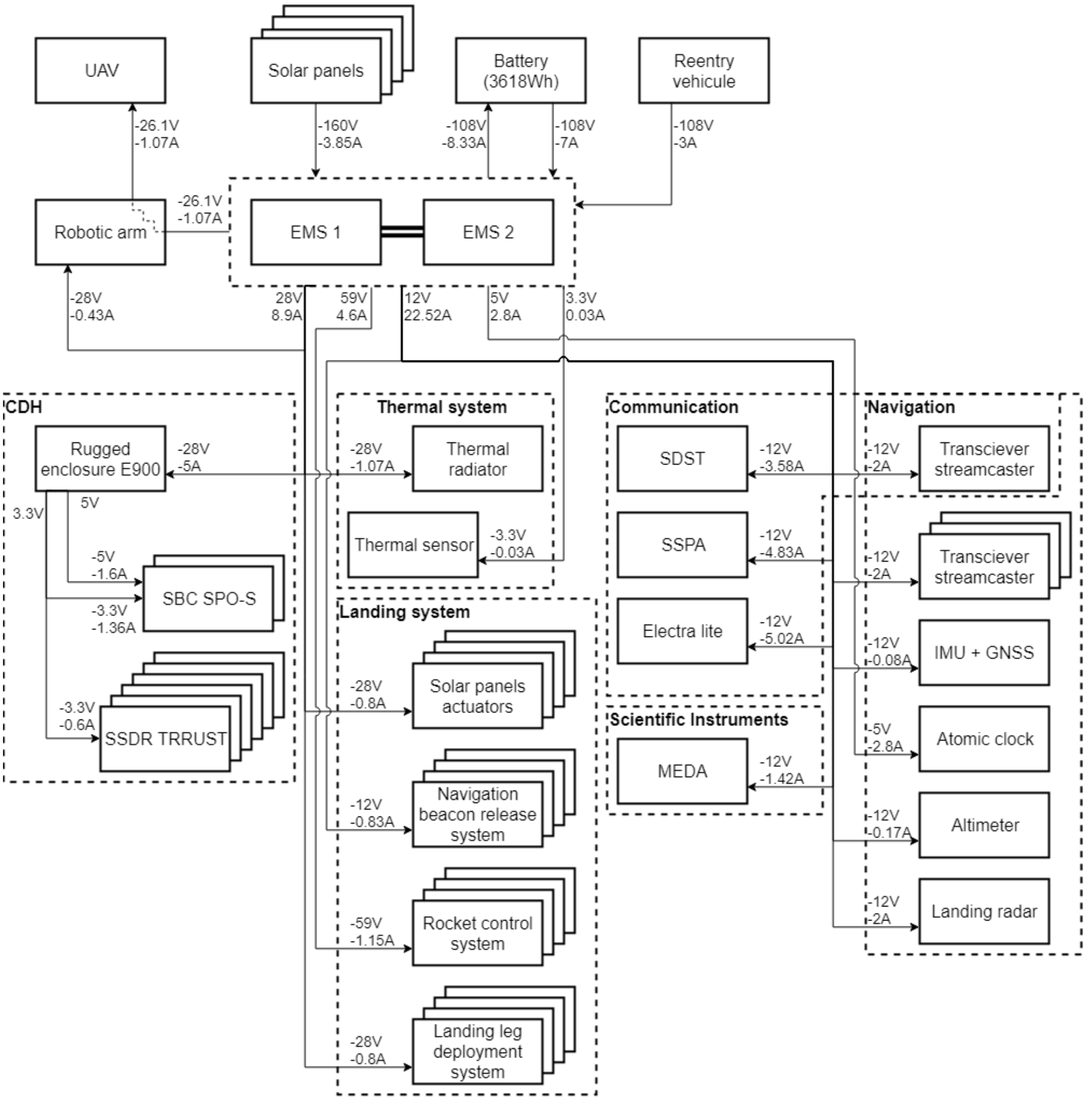

Figure 7.37: electrical diagram base station

7.5.3. V&V and Sensitivity Analysis

Several unit tests were performed to verify the results for the battery sizing. For instance the obtained Wh/kg should be the same as the given Wh/kg by the manufacturer. The mass and energy were determined through adding up the amounts of cells and multiplying the total capacity of the battery times the total amount of volt the 54-cell battery could provide for. The total mass was estimated to be 2.619 kg for the UAV and total energy to be 358.56 Wh, which yields a energy density of 136.9 Wh/kg. The provided energy density by the manufacturer was 175 Wh/kg, this is a 25% difference but this was expected as there is a total capacity loss due to the operating temperature and due to Peukert's law. The same can be done for the power density and the volumetric energy density. The same unit tests were also performed for the base station. Next to that, during later design stages, a battery model could be set up to verify the results through the program.

Validation has not been performed yet. The batteries could be tested in a lab to check the total capacity, the life cycles etc.

A sensitivity analysis of the batteries is given in Chapter 6 where the range is plotted against the mass of the batteries.

7.6. Communication

In this section, the communication subsystem design method and the results are presented. Firstly, in Section 7.6.1, an overview of the communication flow is shown. Following, in Section 7.6.2, the subsystem level requirements are quantified. In Section 7.6.3, the communications subsystem design is presented, while Section 7.6.4 and Section 7.6.5 document the sizing method used, results and verification of the calculations.

7.6.1. Communication Flow

To help define the requirements for the communication system, it must first be looked into the communication flow of the system. A simplified overview of the defined data links can be seen in Figure 7.38. Firstly, as will be discussed in Section 7.9.1, the base station must be able to transfer and store high amounts (28 Gb) of scientific data from the UAV after each flight, requiring a very reliable and high speed connection. The compressed data must also be sent back to Earth. Sending all the mission's scientific data (10 Tb) back to Earth directly would take too much time(>10 years), so the Mars Relay Network (MRN) will be used for that purpose, which greatly enhances the data rates for Martian surface missions [Edwards et al., 2012]. This imposes requirements on the type of transceivers are used on the system, as the Martian orbiters use a UHF link for the lander missions.

Looking into the MRN downlink capabilities, it is currently able to relay over 1200 Mb/sol for the Mars Curiosity Rover and is expected to have data rate capabilities of over 1500 Mb/sol for the Mars 2020 mission [Edwards et al., 2014]. This shows that higher daily data rates can be expected for future missions and therefore, it is predicted that the MARS mission will have an average data rate of 2000 Mb/sol. To make sure that this is achievable a 2048 kbps data rate link will be established with the MRO, for which an received signal strength of -99.1 dBm is needed.

A direct link with Earth is also needed to receive commands and send housekeeping (HK) data. This will be done through the Deep Space Network (DSN), which is an international network of antennas, used to support interplanetary missions and aid in exploration of the solar system[40].

7.6.2. Subsystem Level Requirements

To have a reliable data link, it was important to consider the quality of received data. To do so, the bit error rate (BER) value had to be minimised. In this case, a typical maximum BER of 10^{-5} is considered acceptable [Wertz and Larson, 1999]. This imposes a requirement on the bit energy per noise-density of the signal, which for a quadrature phase shift keying modulation technique leads to an E_b/N_0 requirement of 9 dB [41] .

Thus, the following subsystem requirements could already be established:

- MARS-BASE-COM-1: Each communication link of the base station shall have a bit energy per noise density of 9 dB.
- MARS-BASE-COM-2: The base station shall have a wired and wireless data link with the UAV.
- MARS-BASE-COM-3: The base station shall transmit a signal which is received by the MRO with a strength of -99.1 dBm.
- MARS-BASE-COM-4: The base station shall be able to receive and transmit data using UHF and X-band frequencies.
- MARS-UAV-COM-1: The UAV shall transmit its payload data to the base station at a data rate of 10 Mbps.

[40]URL: `https://mars.nasa.gov/msl/mission/communicationwithearth/` [Cited 20 June 2018]
[41]URL: `http://complextoreal.com/wp-content/uploads/2013/01/linkbud.pdf` [Cited 20 June 2018]

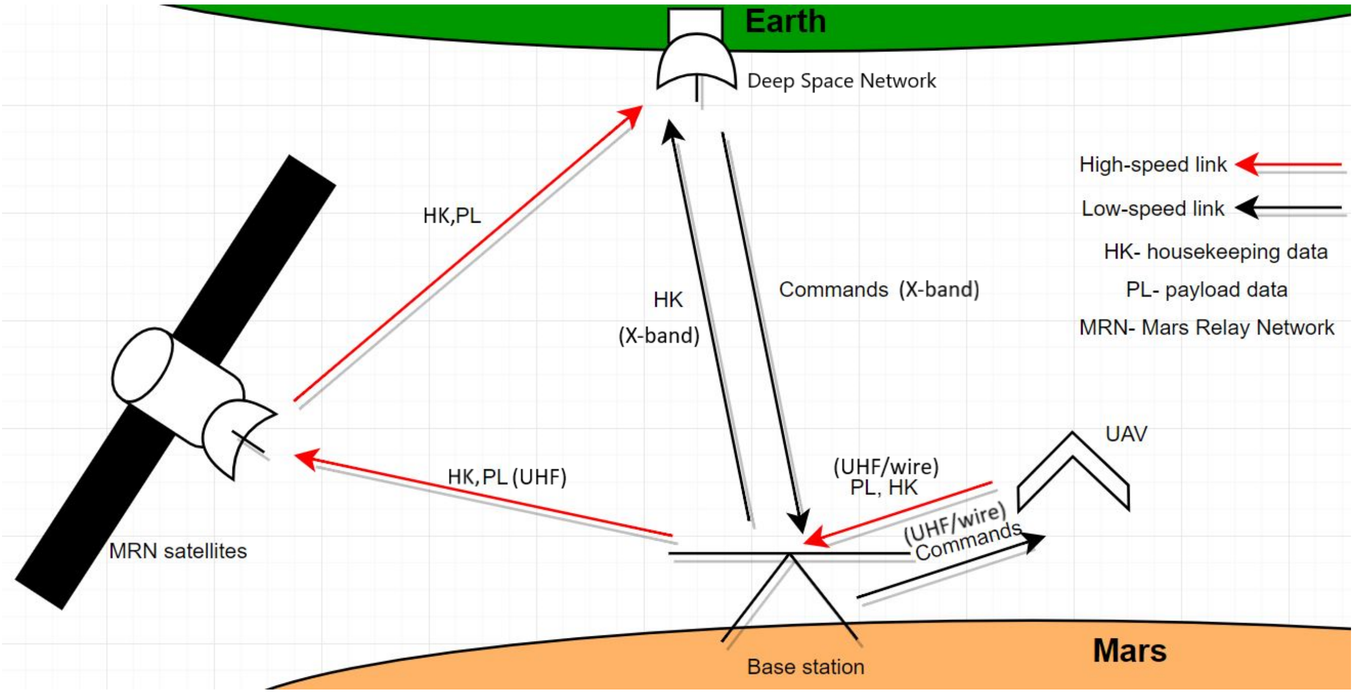

Figure 7.38: Communication flow between the UAV, base station and Earth

7.6.3. Communications Subsystem Design Overview

An overview of the communication block diagram can be seen in Figure 7.40. The data links present in the diagram are a physical/wireless UHF two way base station-UAV connection, a wireless UHF one way base station-MRN link and a two way direct base station- Earth link.

The antennae present on the base station in a fully deployed configuration can be seen in Figure 7.39.

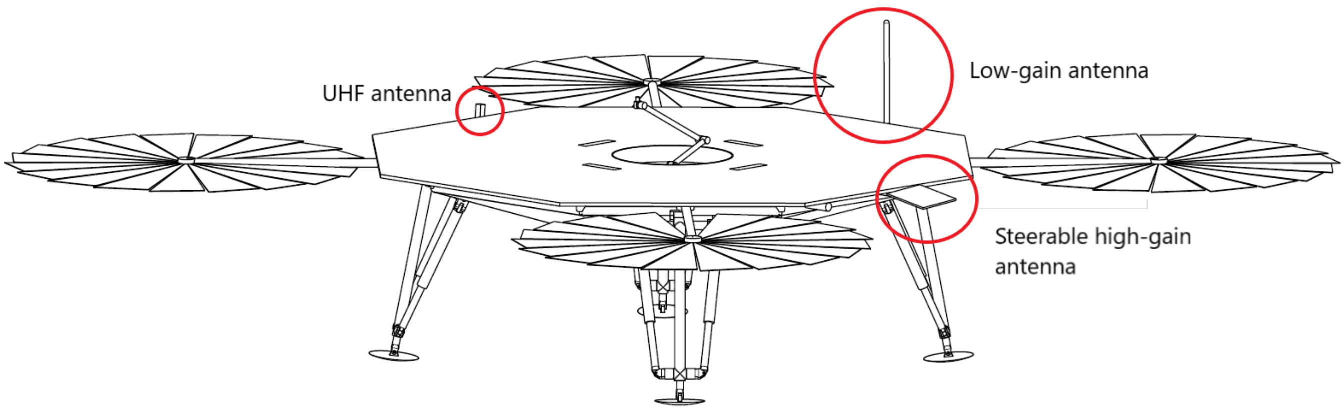

Figure 7.39: LGA, HGA and the UHF antenna on the base station

Base station- Earth, direct.
The base station is equipped with an X-band transceiver unit consisting of a small deep space transponder (SDST) and solid state power amplifier (SSPA), capable of generating 15 W of transmission power[42]. The transceiver unit is connected with a steerable high-gain patch antenna (HGA) and an omnidirectional low gain antenna (LGA) [Taylor et al., 2006]. When contacting Earth, LGA is first used to establish a connection and give pointing directions to the HGA, which then orientates itself using its gimbal and establishes a stronger link with the DSN, sufficient for data transfer.

The MARS system will have an average contact time of 1 hour with the DSN per sol[43] allowing to transmit and receive small packets of data. This leads to capabilities of transmitting up to 150 kb of HK data and receiving commands of up to up to 3 Mb daily.

Base station- MRN.

[42]URL: https://descanso.jpl.nasa.gov/DPSummary/MER_article_cmp20051028.pdf [Cited 20 June 2018]
[43]URL: https://mars.nasa.gov/msl/mission/communicationwithearth/busysignals/ [Cited 20 June 2018]

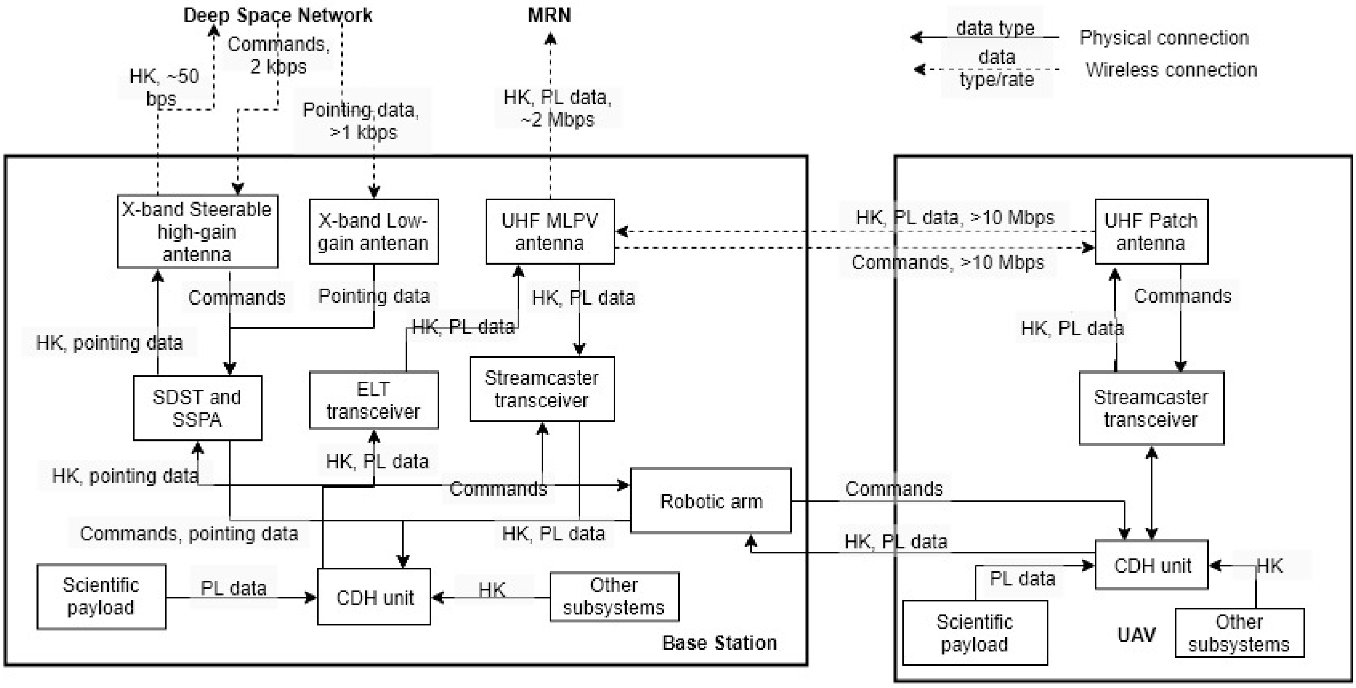

Figure 7.40: Communication subsystem block diagram of UAV and base station

The base is equipped with an Electra Lite UHF transceiver [Edwards et al., 2012] and an omnidirectional MLPV UHF antenna[44]. With 10.5 W of transmitting power, the ELT transceiver leads to the maximum data rate established with the Mars Relay Network satellites and an average of data rate of 2000 Mb/sol is expected. To transmit the entire 8 Tb of lossless compressed scientific data would still require over 10 years and it was therefore established that instead, first, the entire 1.2 Tb packet of lossy data will be transmitted over a period of 1.5 years, while the losslessly compressed data will be transmitted only when specifically commanded from Earth. In case 25% of the loss-free data is requested, the transmissions will be complete by 2030.

Base station- UAV.

The base station and the UAV have two connections: a physical one, going through the robotic arm and a back-up wireless UHF connection. The base station uses the same MLPV UHF antenna and one of the streamcaster transceivers[45] from the navigation subsystem due to its support of >100 Mbps data rates and dual frequency band capabilities. The wireless connection will be able to downlink the UAV's 50 Gb of daily, uncompressed flight data to the base station in about 1.5 hours.

The mass and power budget breakdown of both UAV and base station's communication subsystem can be seen in Table 7.27. The nominal power in most cases refers to the power the transceivers use in receiving mode, while the peak power resembles the transmission mode power.

[44]URL: `https://www.welotec.com/catalog/en/antennas/uhf-antennas/mlpv430-antenna.html` [Cited 20 June 2018]

[45]URL: `https://cdn.silvustechnologies.com/wp-content/uploads/2018/02/StreamCaster_4200_Datasheet.pdf` [Cited 20 June 2018]

Table 7.27: Mass and power budget breakdown of the communication subsystem

Base station			
Component	**Mass [kg]**	**Nominal power [W]**	**Peak power [W]**
Low-gain antenna	0.43	0	0
High-gain antenna and gimbal	8	0	0
UHF MLPV antenna	0.14	0	0
Small deep space transponder	2.7	0	0
Solid state power amplifier	1.3	11	58
Transceiver streamcaster	0.42	1.6	4.8
Transceiver Electra Lite	3	21	60
Total	**16.0**	**33.6**	**122.8**
UAV			
Component	**Mass [kg]**	**Nominal power [W]**	**Peak power [W]**
Transceiver streamcaster (bare configuration)	0.119	1.6	4.8
UHF patch antenna	0.085	0	0
Total	**0.204**	**1.6**	**4.8**

7.6.4. Sizing Method and Results

To size the communications subsystem and choose fitting components, two slightly different methods were used. The base station's links with the DSN and UAV were both sized to have a maximum data rate at the maximum distance with an uncoded E_b/N_0 of at least 9 dB , which is expressed in Equation 7.13 [Wertz and Larson, 1999] as:

$$\frac{E_b}{N_0} = 10log_{10}P_t - L_t + G_t - L_s - L_a - L_{pr} + G_r - L_r + 228.6 - 10log_{10}DR - 10log_{10}T_{\text{sys}}, \tag{7.13}$$

where P_t, L_t and G_t are the transmitter's power, gain and loss which summed up result in the Equivalent Isotropically Radiater Power (EIRP). This is fully controlled by the transmitting antenna and transceiver parameters. L_s, L_a, L_{pr} are the space, atmospheric and precipitation losses, combined into the path losses L_{path}. G_r, L_r are the receivers gain and loss. The sum of the listed parameters result in the received power, which was the key value for the base station-MRN link. The final two parameters DR, T_{sys} are the data rate and the complete system noise temperature, which lead to the bit energy per noise-density.

EIRP is fully determined by the transmitting component's parameters. The biggest component of the path losses- the space loss L_s is calculated with Equation 7.14:

$$L_s = 10log_{10}\left(\frac{4\pi D_{tx}}{3 \cdot 10^8 f_{tx}}\right)^2, \tag{7.14}$$

where D_{tx} is the transmission range and f_{tx} is the transmission frequency.

The resulting link budget calculations can be seen in Table 7.28. For each link, a transmitter loss of 6 dB, a combined atmospheric and precipitation loss of 3 dB [Wertz and Larson, 1999] and a total system temperature of 500 K was assumed [Edwards et al., 2003].

For the uplink and downlink of the base- DSN connection a distance of 2.68 AU was taken to determine the worst case data rate. The base station's transmitter and receiver gain were both taken for the HGA [Olea et al., 2010]. The DSN's transmitter power, gain and receiver gain and losses were taken for the 70 m diameter parabolic antenna[46]. As can be seen from the resulting E_b/N_0 (>9 dB), a data rate of 10 bps and a downlink data rate of 2000 bps are both established in the worst case distance scenario. If an average distance of 1.32 AU is used, the resulting uplink data rate increases to 60 bps. In case Mars and Earth are only 0.6 AU away, data rate further increases to 500 bps.

[46]URL: `https://sandilands.info/sgordon/communications-with-mars-curiosity` [Cited 20 June 2018]

Table 7.28: Link budget calculations of the key connections

Parameter/link	**Base-DSN**	**DSN-Base**	**UAV-Base**	**Base-MRO**	**Unit**
Transmitting freq.	8200	7145	405	400	MHz
Transmitting power	15	38000	1	10.5	W
Transmitter gain	22	73.23	0	0	dB
Transmitter loss	6	6	6	6	dB
EIRP	**32**	**119**	**-6**	**4.2**	**dB·W**
Range	$401 \cdot 10^9$	$401 \cdot 10^9$	5	315000	m
Space loss	282.8	281.6	38.6	134.4	dB
Combined path loss	**286**	**284.6**	**41.6**	**137.4**	**dB**
Receiver gain	74.5	16	0	5	dBi
Receiver losses	2	2.5	6	0.42	dB
Data rate	10	2000	10000000	2048000	bps
System temperature	500	500	500	500	K
E_b/N_0	10.75	14.94	69	9.94	dB

The UAV- base station uplink was evaluated, due to its high data rate requirement, to guarantee a timely transfer time of the PL data. The UAV's transmitting parameters were taken from the streamcaster transceiver's and its patch antenna[47] technical datasheets. Due to the much smaller transmission range, the space loss is much smaller and a very high data rate can be established, mainly limited by the transceiver's supported rate of 100 Mbps. Even at the edge of the exploration zone, the UAV would be able to transmit at a rate of 300 kbps, showing that wireless payload data transfer is not going to be a challenge between the UAV and base station.

Finally, the base station- MRO uplink was looked into, as establishing a maximum supported data rate of the MRO was set as a requirement for effective contact with the other MRN satellites. The transmitting parameters were taken that of the installed Electra Lite Transceiver and UHF antenna, while the receiver and range parameters were taken from [Edwards et al., 2003]. Summing the EIRP, path losses, receiver gain and losses results in a received signal strength of -128.6 dB or -98.62 dBm, which leads to the required data rate of 2048 kbps.

7.6.5. Calculation Verification

Several unit tests were performed to verify the results of the link budget spreadsheet used. Firstly, it was tested whether the space loss factor scales with the 2nd power of the range. Increasing the range between the UAV and base station from 5 to 500 (factor of 100) resulted in the space loss growing from 38.6 to 78.6 dB- a difference of 40 dB. Converting 40 dB back results in a scaling factor of 10^4, which is indeed the square of 100, meaning that this unit test is passed.

Additionally, a system test was performed. Inputs were used as presented in the link budget calculation in [Edwards et al., 2003] table 4's X-band column. The resulting EIRP was equal to 48.7 dB, as compared to the presented 78.1 dBm, which, when converted to dB, is 0.6 lower. The computed space loss was equal in both cases, equal to 186.5 dB, while the computed link margin was 6.1 versus the presented 7.7 dB. The EIRP difference could be due to some input that was not mentioned in [Edwards et al., 2003], while the difference in link margins is likely due to the assumption of constant atmospheric loss of 6 dB. However, the differences are less than 2 dB in both cases, which is considered marginal and are likely due to some difference in inputs. Therefore, the test is considered to be passed.

7.7. Thermal Control

In this section, the thermal control subsystem design will be documented. The subsystem requirements are firstly established in Section 7.7, followed by the design overview in Section 7.7.2. Lastly, the sizing method and the results are presented in Section 7.7.3, while a brief verification as well as a sensitivity analysis of the model used is documented in Section 7.7.4.

[47] URL: `https://cdn6.endurosat.com/modules-datasheets/UHF_Antenna_User_Manual_Rev1.3.pdf` [Cited 20 June 2018]

7.7.1. Subsystem Level Requirements

In order to operate in the extreme temperature variations present on the surface of Mars, a thermal control subsystem had to be looked into. It is tasked with maintaining the scientific payload, as well as all other subsystem components within their operational temperature ranges throughout the duration of the mission. To determine the subsystem requirements, it was first looked into the most sensitive components. The most sensitive components per subsystem are listed in Table 7.29, with the driving ranges marked in bold.

Table 7.29: Main temperature sensitive components of the base station and UAV

Base station	
Subsystem/component	**Operational temp. range [^{o}C]**
EPS	**[-20, 40]**
NCA batteries	[-20, 40]
Remaining EPS components	[-20, 40]
Communications	[-40, 65]
Transponder	[-40, 65]
Solid state power amplifier	[-40, 65]
Transceiver Streamcaster	[-40, 65]
Transceiver Electra Lite	[-45, 72]
C&DH	[-40, 65]
SSDR TRRUST VPX RT	[-40, 85]
Case E900 Compact	[-55, 70]
Flash memory Alitech SP0-S	[-40, 65]
Navigation	**[-10, 65]**
Inertial measurement unit	[-50, 85]
Atomic clock SA.3Xm	[-10, 75]
Transceiver Streamcaster	[-40, 65]

UAV	
Subsystem/component	**Operational temp. range [^{o}C]**
EPS	[-20, 40]
NCA batteries	[-20, 40]
LPO batteries	[-20, 40]
Remaining EPS components	[-20, 40]
Scientific instruments	**[0, 50]**
Camera ECAM-C50	[-30, 60]
Camera ECAM-NFOW	[-55, 60]
Altimeter Puck Light	[-10, 60]
Spectrometer MQ022HG	[0, 50]
Communications	[-40, 65]
Transceiver Streamcaster	[-40, 65]
C&DH	[-40, 65]
Flash memory Alitech SP0-S	[-40, 65]
SSD Alitech S992	[-40, 65]
Navigation	**[-10, 35]**
Inertial measurement unit	[-50, 85]
Atomic clock LN CSAC	[-10, 35]
Altimeter LeddarOne	[-40, 85]

It can be seen that most sensitive subsystems are the EPS and navigation for the base station, while the scientific instruments and navigation drive the temperature range for the UAV. The base station operational temperature ranges must therefore be maintained within -10 and 40 ^{o}C, while the UAV must remain within 0 and 35 ^{o}C.

Looking into the Martian surface temperatures[48], they strongly between day and night- around 100 K. Therefore, it was decided not to keep the entire system at the required temperatures and instead insulate the sensitive components and heat them inside *thermal boxes*.

Considering the higher level stakeholder requirements, size constraints and the list of operational temperatures, the following TCS subsystem-level requirements were established:

- MARS-BASE-TCS-1: The thermal box of the base station shall remain within -10 and 40 ^{o}C throughout the mission duration.
- MARS-BASE-TCS-2: The base station thermal box shall fit under the landing platform.
- MARS-BASE-TCS-3: The base station TCS shall not contain radio-isotope heater units (RHU).
- MARS-UAV-TCS-1: The UAV thermal box shall remain within 0 and 35 ^{o}C throughout the mission duration.
- MARS-UAV-TCS-2: The UAV thermal box shall not exceed a mass of 0.7 kg.
- MARS-UAV-TCS-3: The UAV thermal box shall fit within the fuselage constraints.
- MARS-UAV-TCS-4: The UAV TCS shall not contain RHU's.

7.7.2. Thermal Control Subsystem Design Overview

The design of both thermal boxes and the component placement can be seen in Figure 7.41. The rough dimensions of the cuboid UAV box are 275 x 170 x 200 mm, optimized to fit within the fuselage, while the base station's optimal

[48]URL: `https://mars.nasa.gov/mer/spotlight/20070612.html` [Cited 18 June 2018]

box shape was found to be a trapezoidal, 355 x 445 x 345/180. The boxes for the most part are covered using 7 layers of insulation. Each layer consists of a 0.025 mm backed and coated kapton inner cover, 0.01 mm aluminized kapton interior layer and a 0.16 mm dacron netting separation, leading to a total thickness of 1.4 mm [Gilmore, 2002].

Both heat boxes contain radiators, which will be capable of outputting 30 W of heat, operating at a temperature of 30 ^{o}C. They will be turned on whenever the temperature sensors inside the box indicate that the box is within 5 degrees from its lowest temperature limit. The UAV's radiator will have to operate at full capacity throughout nights, outputting 25 W of heat, while during day time operations, an output of 10 W will be required. The base station's radiators do not have to output any heat due to the high amounts of heat dissipated by the transceivers and CDH components, but are still placed inside the box in case some components, such as the Electra Lite transceiver, malfunction and stop dissipating heat.

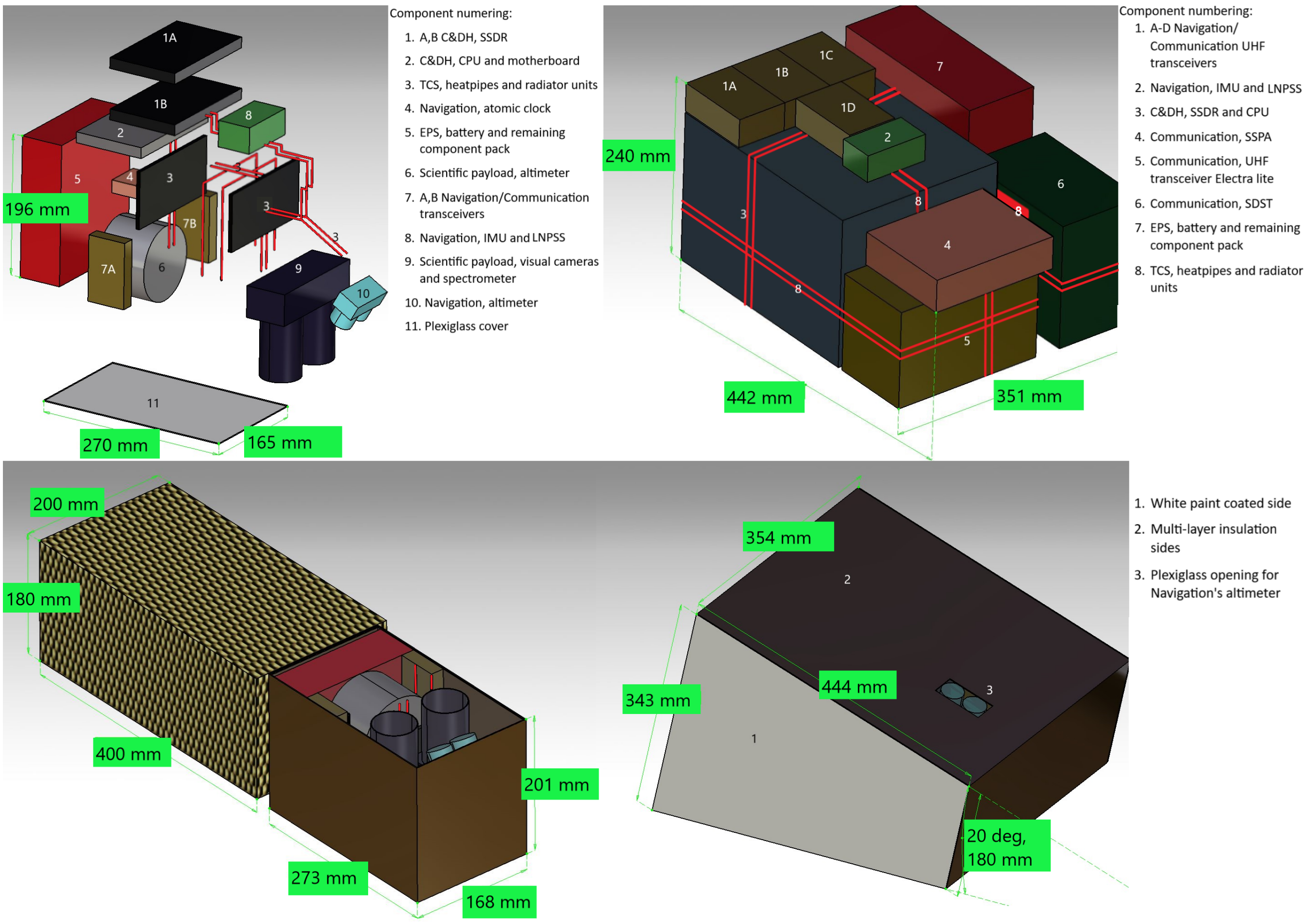

Figure 7.41: UAV thermal box (left), exploded component view (top) and closed, upside down box (bottom) next to the ICE instrument. The base station thermal box (right), component placement view (top) and closed up view (bottom).

Ammonia filled heat pipes are connected to the radiators and wrapped around the components in both boxes. They are meant to help maintain a uniform temperature inside the boxes by distributing the heat dissipated by the components and radiators.

The subsystem components that were chosen to place inside the thermal boxes were all listed in Table 7.29. The bottom part of the UAV's thermal box, visible in the bottom left of Figure 7.41 is covered with plexiglass, so that the scientific and navigation instruments would not have their views obstructed.

A bare aluminium coating was chosen for the outside surface of the base station and UAV to limit their emissivity Wertz and Larson [1999]. The bottom and half of a side of the base station's thermal box is coated using Z93 white paint to increase the heat transfer outside of the box during peak operations. The inside of both UAV and base station are coated using 3M black velvet paint to increase the heat radiated by the outside structure into the box.

The mass and power budgets of both systems are presented in Table 7.30. Again, it can be seen that the base station will not require any active thermal control throughout the mission and radiators will only be used in case some components fail to operate and do not dissipate enough heat.

Table 7.30: Power and mass budget breakdowns of TCS

	UAV			Base station		
Component	m [kg]	P_{day} [W]	P_{night} [W]	m [kg]	P_{day} [W]	P_{night} [W]
Radiator	0.21	10	25	0.27	0	0
Heat pipes	0.15	0	0	0.30	0	0
Temp. sensors	0.03	0.1>	0.1>	0.03	0.1>	0.1>
Multi-layer insulation	0.11	0	0	0.25	0	0
Total	**0.50**	**10**	**25**	**0.85**	**0.1>**	**0.1>**

It can be seen that both boxes were sized to meet the volumetric constraint requirements, do not include any RHU's and meet the mass requirements. It will also be shown than the temperature requirements are met in the upcoming subsection.

7.7.3. Sizing Method and Results

In this subsection, the sizing method, including the assumptions made, equations used will be discussed. The Python file used for the sizing can be accessed via this github link. The assumptions that were made are as follows:

- For the temperature computations, a steady-state energy balance was used.
- Heat loss due to convection was assumed to be equal to the radiated heat when computing base station and UAV outside temperatures and the UAV thermal box temperature. This was based on the work of Braun et al. [2006], which mentions that the ARES Mars airplane transferred about half of its heat to the outside by convection and half by radiation.
- Only heat transfer by radiation was considered for the base station thermal box, as it is fully shielded from the outside atmosphere.
- Only the heat input from the radiator, outside structure and the components housed inside the box were used for the energy balance of the thermal boxes. This is because the outer structure of the UAV and base station fully cover the boxes from the incoming solar flux and IR planetary radiation.

To compute the equilibrium temperatures of the base station and the UAV, the heat balance was calculated according to Equation 7.15 [Wertz and Larson, 1999]:

$$Q_{\text{in}} = Q_{\text{out}} \rightarrow Q_{\text{IR,Mars}} + Q_{\text{sun}} + Q_{\text{diss}} = 2Q_{\text{rad}}, \tag{7.15}$$

where $Q_{\text{IR,Mars}}$, Q_{sun} and Q_{diss} are incoming heat from the Mars surface, solar flux and heat dissipated by the components outside the thermal box, while Q_{rad} is the resulting heat radiated by the UAV/base station. In the UAV's case, Q_{rad} is multiplied by 2 to account for heat losses due to convection. The equilibrium temperature is thus calculated using Equation 7.16:

$$Q_{\text{rad}} = \epsilon_{\text{surf}} T_{\text{out}}^4 \sigma A_{\text{surf}} \rightarrow T_{\text{out}} = \sqrt[4]{\frac{Q_{\text{sun}} + Q_{\text{IR,Mars}} + Q_{\text{diss}}}{2\epsilon_{\text{surf}} \sigma A_{\text{surf}}}}, \tag{7.16}$$

where $\epsilon_{\text{surf}}, A_{\text{surf}}, T_{\text{eq}}, \sigma$ are the emissivity of the coating, surface area, equilibrium temperature and the Boltzmann constant. To compute the temperature of the thermal box $T_{\text{eq,box}}$, Equation 7.17 was used:

$$T_{\text{eq,box}} = \sqrt[4]{\frac{Q_{\text{rad}} + Q_{\text{IR,in}} + Q_{\text{diss,box}}}{\epsilon_{\text{box}} \sigma A_{\text{box}}}}, \tag{7.17}$$

where $Q_{\text{rad}}, Q_{\text{IR,in}}, Q_{\text{diss,box}}$ are the heat inputs from the radiator, outside structure of the UAV/base station and the electric components stored inside the thermal boxes.

A simplified flowchart of the thermal box sizing method can be seen in Figure 7.42. The environmental conditions and the surface parameters lead to the equilibrium temperatures of the base station and the UAV. The temperature is then related to the radiated flux incoming to the thermal box, which together with the chosen radiator and the electronic component heat input leads to the temperature of the thermal box. If the temperature of the thermal box is outside the required range, the surface properties of the thermal box (amount of insulation, emissivity, absorbtivity, exposed box area) or the heat input are adjusted until the equilibrium temperature is acceptable.

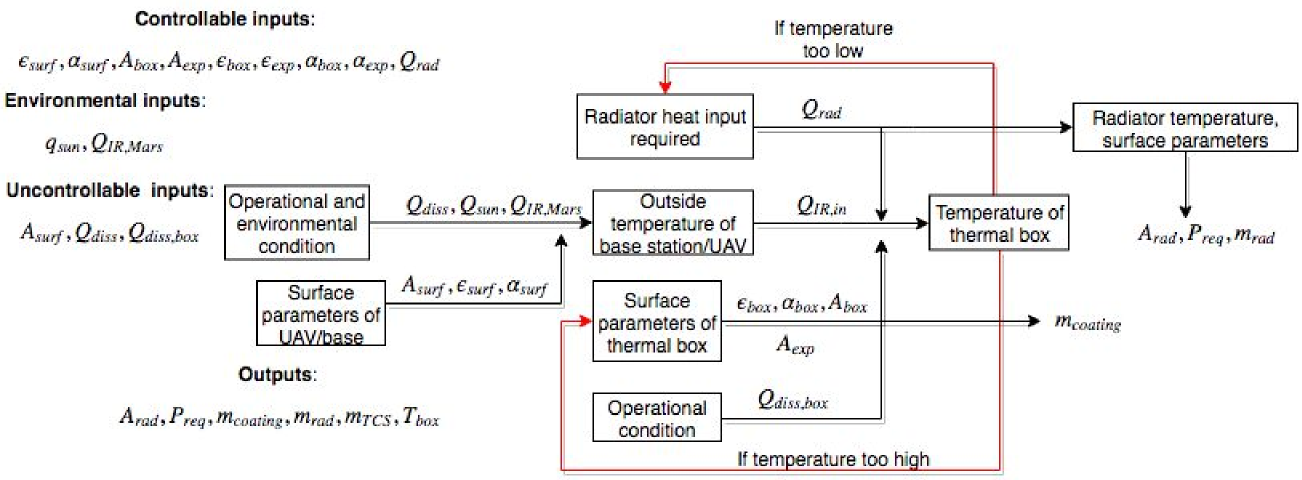

Figure 7.42: Simplified flowchart of TCS sizing method

To determine the most extreme conditions for the thermal box to withstand, several operational conditions (Q_{diss}, $Q_{\text{diss,box}}$) and environmental inputs ($Q_{IR,Mars}$, q_{sun}) were considered. Regarding operational conditions, the coldest cases were determined to occur during standby of both UAV and base station during winter nights, while the hottest cases occur during summer days, when the UAV is operational and the base station is in payload data transmission mode.

Table 7.31: Equilibrium temperatures of the designed thermal boxes in the most extreme conditions

Condition	Q_{diss} [W]	q_{sun} [W/m^2]	q_{IR} [W/m^2]	T_{out} [K]	$Q_{\text{diss,box}}$ [W]	Q_{rad} [W]	$q_{\text{IR,in}}$ [W/m^2]	T_{box} [K]
Base station, transmission, summer day	150	530	162	298	100	0	27	311
Base station, standby, winter night	25	0	120	200	62	0	5.5	274
UAV, cruise, summer day	15	530	162	294	20	11	25	278
UAV, standby, winter night	5	0	120	195	7	25	5	278

7.7.4. Verification and Sensitivity Analysis

To verify the sizing method, a unit check was performed to check whether the equilibrium temperature computations are functioning as intended. To do so, the average equilibrium temperature of Mars was computed, using an incoming solar flux of 605 W/m^2, surface emissivity of 0.9, absorbtivity of 0.75[49], incoming IR radiator of 0 and a surface area of 144.8·10^9 km^2 resulted in an average temperature of -57 ^{o}C, which is slightly lower than the average temperature of -55 ^{o}C[50], which is due to the equation neglecting convection due to atmospheric gasses. The computed temperature is still very representative of the actual values and it was concluded that this unit test is passed.

In addition, a sensitivity analysis was performed, to test how a percentage increase/decrease of the inputs $Q_{\text{diss}}/Q_{\text{diss,box}}$ would affect the outside T_{out} and the box temperature T_{box}. The % difference in input refers to how much was added/removed to the input (100% means the input was doubled), while the % change is calculated as (y2-y1)/y1 ·100%, where y1 is the initial output and y2 is the output due to the changed input. This was performed for the initial values of the base station, during transmission in summer afternoon environmental conditions. The resulting graphs can be seen in Figure 7.43.

[49]URL: `http://lasp.colorado.edu/~bagenal/3720/CLASS6/6EquilibriumTemp.html` [Cited 19 June 2018]
[50]URL: `http://marsnews.com/the-planet-mars` [Cited 19 June 2018]

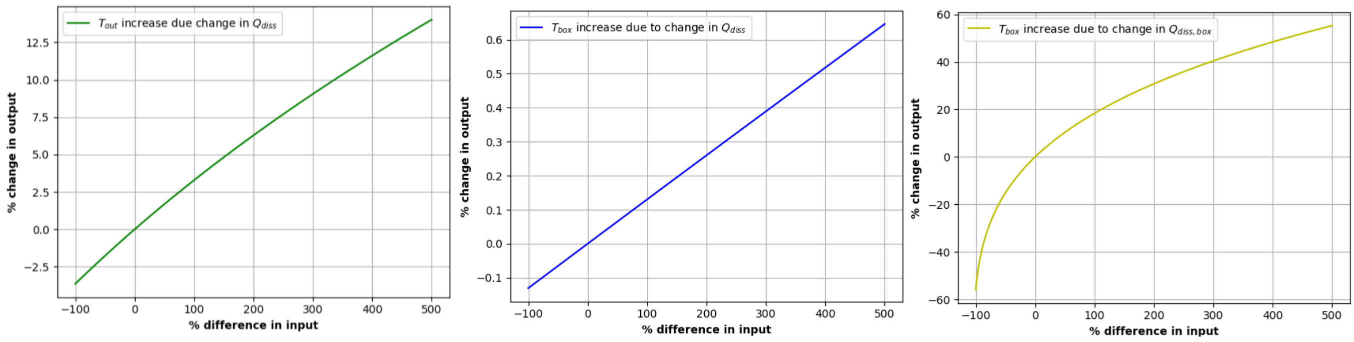

Figure 7.43: Change in T_{out} vs Q_{diss} (left), T_{box} vs Q_{diss} (middle) and T_{box} vs $Q_{\text{diss,box}}$ (right)

From the left graph, it can be seen that the outside surface temperature is not very sensitive to the power dissipated outside the thermal box, as having the input multiplied by 6 leads to slightly less than a 15% increase in the output temperature. This is due to the fact that steady state energy balance equations were used and the heat dissipated outside the box is summed with the incoming solar and planetary radiation. As a result, the overall heat input does not directly scale with the dissipated heat.

The middle graph shows that Q_{diss} has almost no effect on the box temperature T_{box}. It was chosen to model the box temperature to only be affected by the heat dissipated via the infrared radiation flux coming into the box from the surface structure with conduction and convection ignored. As a result, the box temperature is almost unaffected by a change of Q_{diss}, which, in reality, might have a significant effect, but a much more in-depth analysis would have to be performed to determine that.

Finally, the right graph shows that the heat dissipated inside the box $Q_{\text{diss,box}}$ has a very significant impact on the box temperature, where if it is doubled, the box temperature increases by 20% (from 311 K to 370 K), whereas if the input is decreased to 0, the box temperature decreases by 60% (from 311 K to 124.4 K). These are very extreme temperature fluctuations and result due to assuming that the only other heat incoming to the box is from the outside surface and the radiator, both of which are small compared to $Q_{\text{diss,box}}$. This shows that it is very important to have an accurate representation of the heat dissipated inside the thermal box, as it is by far the largest factor for the box temperature.

7.8. Navigation

In order for the UAV to perform the scientific mission autonomously, and to have the scientific payload meet its requirements in terms of resolution and accuracy, it requires precise positioning knowledge during flight. For that purpose, a navigation subsystem was designed, the requirements of which are presented in the following list:

- MARS-UAV-Navi-1: The subsystem shall have a accuracy of at least 0.1 m.
- MARS-UAV-Navi-2: The subsystem shall not have one point of failure.
- MARS-UAV-Navi-3: The subsystem shall have a safe mode.

On Earth, accurate location data to a fully autonomous UAV global positioning system (GPS) is used. However, no GPS exists on Mars. The Martian rovers use visual clues to track their position. This technique is successful, but only works on the rovers, due to their very low speed at 0.04 m/s [51]. Thus, in order for VITAS to perform its mission, a replacement for the GPS system must be developed. This system should then be further supported by secondary navigation systems.

7.8.1. Local Navigation Pseudolite System

Two main options were considered for the navigation subsystem. The first option was to demand or to wait for a Martian GPS to develop. The second option was to deploy new GPS beacons for MARS. The problem here is that the GPS beacons would lack knowledge of their whereabouts on Mars. A GPS transmitter transmits two things: its location and the exact time when sending the message. Locating it by means of visual inspection of Martian satellites is a possibility, but it would never give the exact location of the beacon as the best visual imaging satellite[52], the Mars Reconnaissance Orbiter does not provide sufficiently accurate images. This satellite has a resolution of 0.3 m which is not enough, as the error only grows and the requirement specifies that the accuracy should be at least 0.1 m.
In order for the navigation system to establish its own location, the GPS transmitters first would have to recieve GPS data. Second, one of the GPS beacons must be capable of moving. As a a result, the moving beacon could calibrate itself comparatively to the other beacons, after which it could transmit the updated locations to the stationary

[51]URL: https://mars.nasa.gov/mer/mission/spacecraft_rover_wheels.html [Cited 25 June 2018]
[52]URL: https://www.jpl.nasa.gov/news/news.php?release=2014-245 [Cited 25 June 2018]

beacons. When calibrated, this kind of system will offer a pointing accuracy lower than 0.1 m [LeMaster and Rock, 2003].

In order to have local navigation pseudolite system (LNPS) on a 2D plane, 3 beacons and one moving beacon are enough for the navigation to work. The beacons should not be placed in a range of 250 m from one another because at that point the system will start losing some of its accuracy due to the fact that the signals from the beacons would start to interfere with one another.

In MARS, VITAS would function the moving beacon, the base station itself would serve as a stationary beacon and additional small pseudolites were designed to act as the remaining stationary beacons. These beacons have to be self-sufficient as they are separated from the base station. To meet the requirements, the pseudolites require a transceiver, LNPS antenna and an atomic clock. In order to have full self-supporting beacons, a battery, solar panels, an electronic management system (EMS), and a thermal radiator were added. A hardware overview of the system is found in Figure 7.44. As the LNPS is less efficient if the beacons are all together, sufficient distance must be established between them. The decision was made to give the pseudolites small wings as its tripod, the end of the which would flick up as to provide with a positive moment so it generates lift. The entire deployment sequence can be seen in Figure 7.45, at ”1” the entry of the whole system in the Martian atmosphere is visualised, at ”2” the back shell is released and hereafter the beacons are deployed at an altitude of 2 km from the deck of the base station with 90°, separating the four pseudolites. These attachment points are spring loaded and pyrotechnic charged.

Furthermore, an altimeter is placed on the nose of the each beacon, so when the ground is at a range of 200 meter, the subsonic parachute deploys and slows it down to 5 m/s. Simultaneously, the wings fold forward via hinges on the leading edge and lock into place as seen at ”3”. At ”4” the touchdown is visualised where the parachute is released and simultaneously a small solid rocket booster is fired at the parachute, to prevent it from falling onto the pseudolite and obstructing it from the sun, allowing it to generate its power.

- MARS-Pseudo-Navi-1: The subsystem shall receive GPS data.
- MARS-Pseudo-Navi-2: The subsystem shall transmit GPS data.
- MARS-Pseudo-Navi-3: The subsystem shall operate self-sufficiently.
- MARS-Pseudo-Navi-4: The subsystem shall survive touchdown on Mars.
- MARS-Pseudo-Navi-5: The subsystem pseudo satellites shall be spaced at least 250 m away from each other.

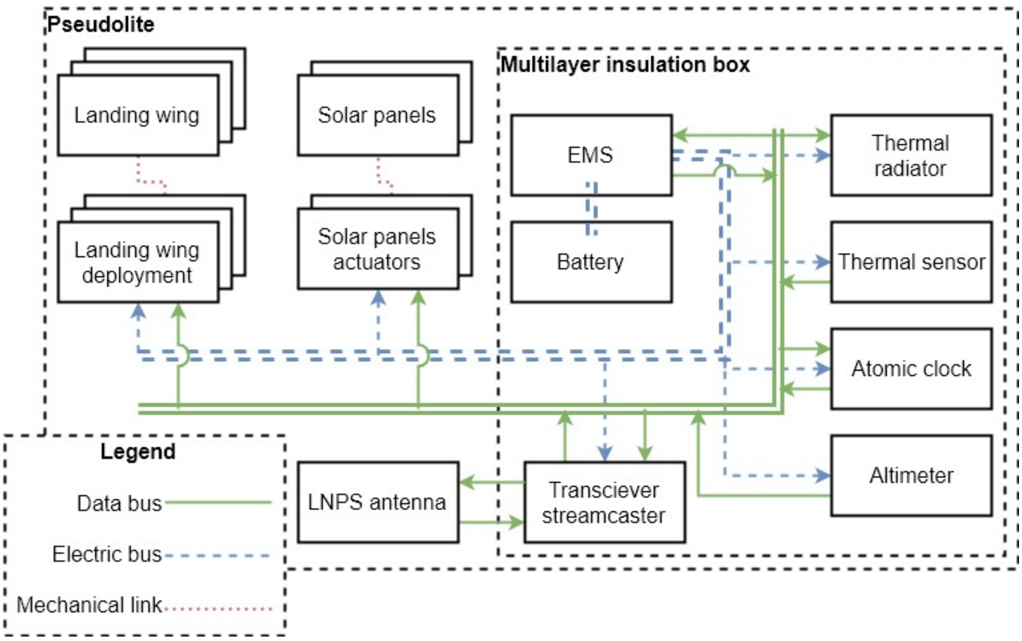

Figure 7.44: Hardware overview of the pseudolite

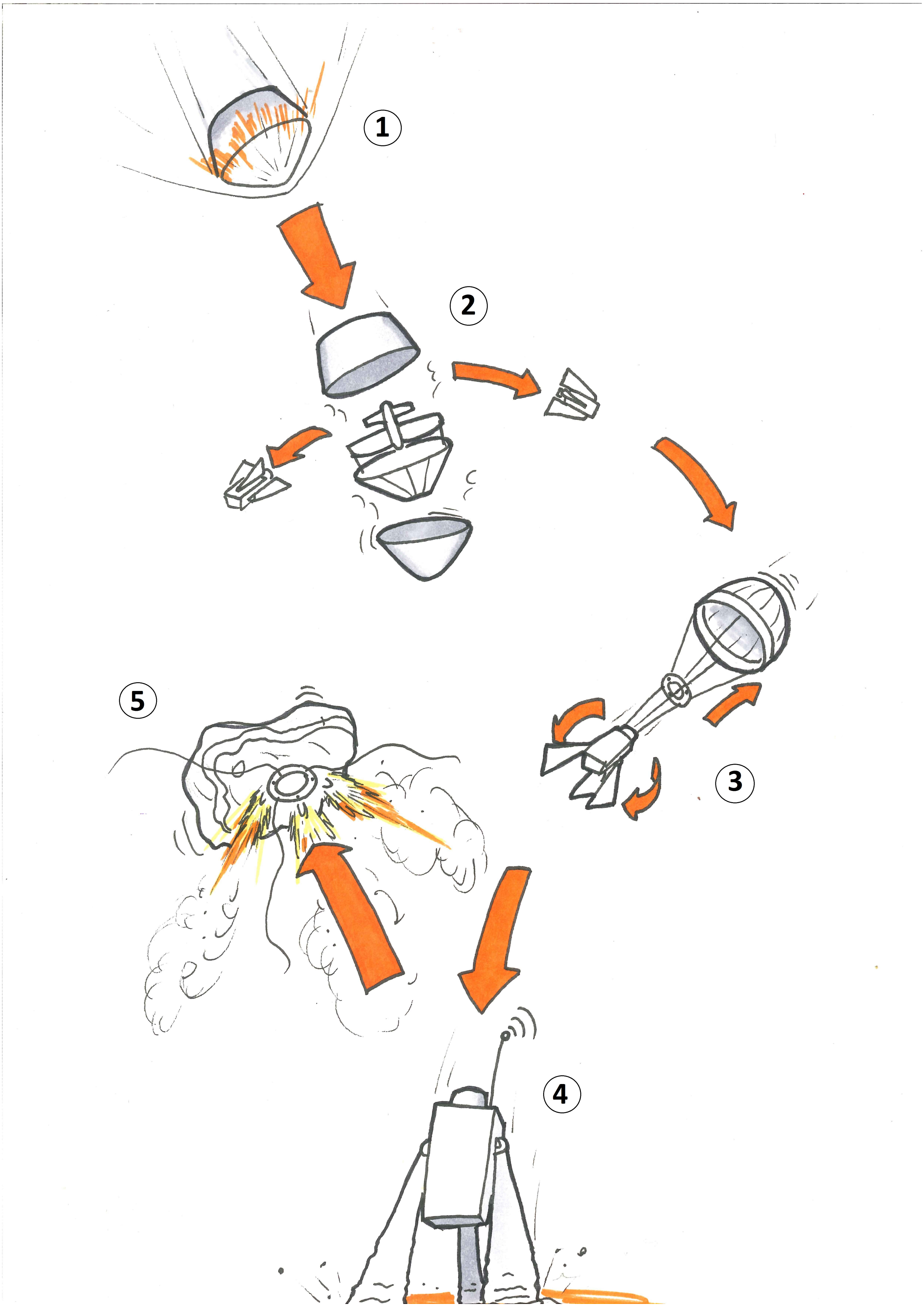

Figure 7.45: Deployment of the pseudolite.

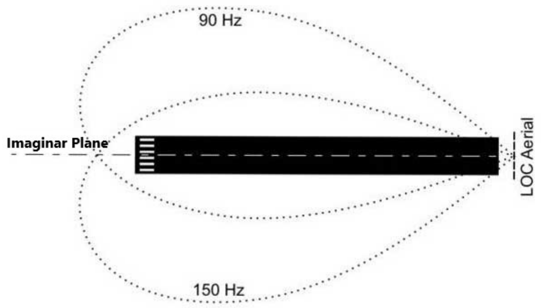

Figure 7.46: Horizontal radiation pattern

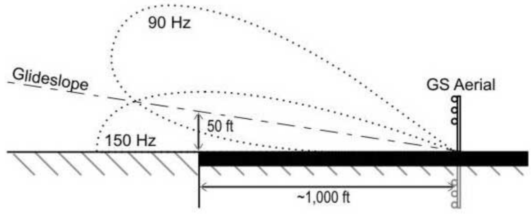

Figure 7.47: Vertical radiation pattern

7.8.2. Virtual Landing & Takeoff Strip

The most risky manoeuvre VITAS has to execute is the landing on the deck of the base station. In order to reduce the risk of the landing and take-off manoeuvre, an instrument landing system will be employed, which is normally used in the aviation industry to perform landing (in some cases totally autonomously).
This system uses a localizer, an antenna system, that only uses odd frequencies within the very high frequency range (30-300MHz). This antenna system sends two directional radiation patterns along the landing strip, each with an offset of a small angle, as can been seen at Figure 7.46. Each beam is a bearing amplitude-modulated wave with a harmonic signal. This harmonic is what sets the two beams apart, as one has an harmonic frequency of 90 Hz and the other has a frequency of 150 Hz. By measuring which of the beams is the "loudest", the system knows on which side of the imaginary vertical plane that these two beams create, it is located[53].

In aviation the same system is also used as a glide slope. That system is placed normal to the imaginary vertical plane but with an small angle with the ground to produce a horizontal plane that presents the glide slope as portrayed in Figure 7.47[54]. The glide slope beams have a different frequency in order to differentiate them from the other beam pattern. The intersection of these two planes presents a line which is the optimal landing path.
In MARS this system will be slightly modified. Firstly, the frequency is changed to the UHF, allowing to use the base station's and UAV's UHF antennae, thus reducing the overall weight of the design. The disadvantage of this change is the increased impact obstacles have on the beams and slightly reduced range, which is not a problem, as the original system has a range of 18 km. Secondly, in order to have a landing path for the UAV, the imaginary planes of both beams were placed normal to the deck of the base station. The imaginary planes of the beams are still normal to one another, as in the original configuration.

7.8.3. Navigation Overview

In order to make the navigation more precise and less prone to errors, an extra altimeter was added the payload of the UAV. The additional altimeter was angled forward at 60° in order for VITAS to measure upcoming changes in ground elevation. An altimeter was also added to the base station payload, which was pointed upwards to measure the distance between deck and UAV as it comes in for landing.

A second LNPS antenna was added to the UAV, the LNPS antenna should be placed on the end of the wing in for the UAV to have an unobstructed connection with all the beacons. As any UAV, VITAS will be equiped with a pitot tube for the system to measure its airspeed. In case there is a glitch in the LNPS system, an inertial measurement unit (IMU) was added. These units consist out of accelerometers and gyroscopes, and work together with the LNPS and airspeed data to further increase the position, altitude and attitude accuracy. An overview of the navigational hardware is presented in Table 7.32.

[53]URL: `http://www.landingsystem.com/` [Cited 25 June 2018]
[54]URL: `http://instrument.landingsystem.com/ils-ground-equipment/#localizer-transmitter` [Cited 25 June 2018]

Table 7.32: The equipment required on the UAV and base station for navigation. [55] [56] [57] [58] [59] [60] [61]

VITAS			
Instrument	**Mass [g]**	**Power [W]**	**Size [mm]**
2x LNPS Antenna	19	0	D31x50.4
Transceiver	119	4.8	92x55x18
Atomic clock	75	0.26	50.8x50.8x17.8
Altimeter	110	2	70x35.2x67.5
IMU + LNPS	115	3	85x74x36
Pitot tube	41	0	10Dx150
Total	**498**	**10.1**	**-**
Base Station			
Instrument	**Mass [g]**	**Power [W]**	**Size [mm]**
IMU + LNPS	115	3	85x74x36
Antenna LNPS	19	0	D31x50.4
4x Transceiver	119	1.6	92x55x18
4x UHF antenna	900	0	255x66.5x60
Atomic clock	75	0.26	50.8x50.8x17.8
4x Altimeter	110	2	70x35.2
Total	**5101**	**13.4**	**-**

7.9. Command & Data Handling

In this chapter the Command and Data Handling (CDH) subsystem is discussed and sized. First the requirements are set for the UAV and base station seperately, hereafter each CDH is sized and presented.

7.9.1. Data Volumes and Subsystem Requirements

Prior to setting up the requirements of the command and data handling (CDH), knowledge about the various data rates of the system was required. The scientific data rates are listed in Table 7.6.

Figure 7.48 shows that the total data rates of the scientific instruments on the VITAS. The data volumes are defined as follows:

- Per flight, VITAS will gather 28 Gb of scientific data. This is determined from the 41.5 Mbps data rate of the instruments, used for 606 s per flight.
- Scanning the entire Jezero crater would result in a total uncompressed data volume of 11.6 Tb. This is too large to fully send back to Earth and compression is required. It will be stored on the base station.
- Using lossless data compression via the Huffman compression [62] (meaning there is no loss in data or quality), a compression ratio equals to 1.5 is achieved which results in a total mission data of 7.7 Tb. This is still too large and cannot be fully sent back to Earth.
- Lossy compression is employed to allow to relay the entire data. A compression ratio of 10 [63] is used, resulting in a loss in quality. The scientific data volume is reduced to 1.16 Tb, which can fully be sent back to Earth.

[55] URL: `https://inertiallabs.com/ins.html` [Cited 25 June 2018]
[56] URL: `http://www.uavfactory.com/product/12` [Cited 25 June 2018]
[57] URL: `https://www.tersus-gnss.com/product/antenna-ax3705` [Cited 25 June 2018]
[58] URL: `http://www.mouser.com/ds/2/523/ds_ln_csac_e-952626.pdf` [Cited 25 June 2018]
[59] URL: `https://leddartech.com/app/uploads/dlm_uploads/2018/04/Spec-Sheets-LeddarOne-ENG-12avril2018-web.pdf` [Cited 25 June 2018]
[60] URL: `https://cdn.silvustechnologies.com/wp-content/uploads/2018/02/StreamCaster_4200_Datasheet.pdf` [Cited 25 June 2018]
[61] URL: `http://www.rfiwireless.com.au/media/downloads/pdfs/tla400.pdf` [Cited 25 June 2018]
[62] URL: `https://www2.cs.duke.edu/csed/poop/huff/info/` [Cited 25 June 2018]
[63] URL: `https://www.maximumcompression.com/` [Cited 25 June 2018]

In order to have a fully redundant and backed-up base station CDH, the storage requirement of the base station is doubled, as well as the amount of SBC's.

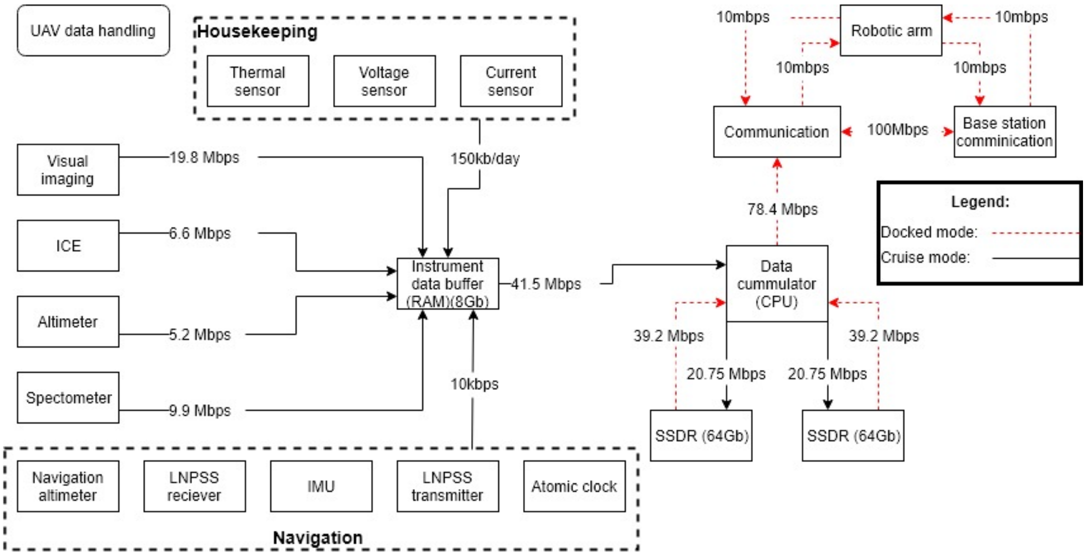

Figure 7.48: Data block diagram of the UAV.

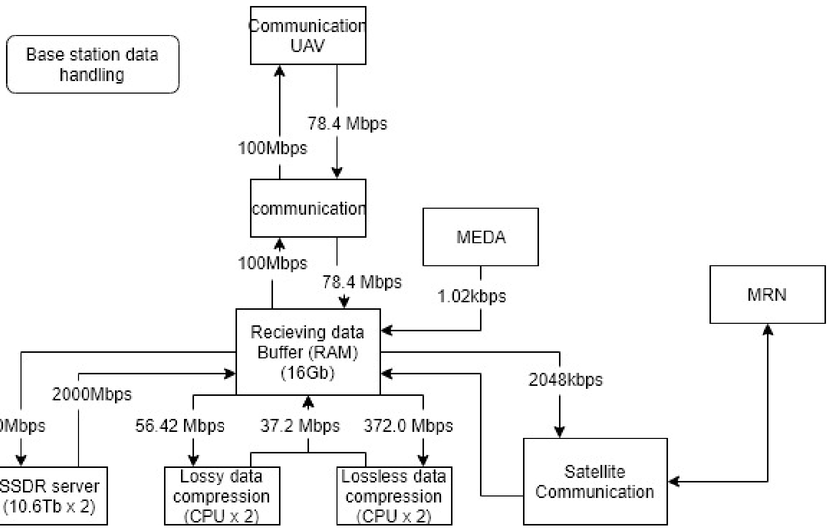

Figure 7.49: Data block diagram of the base station.

Figure 7.48 and Figure 7.49 present the data handling block diagrams of the UAV and the base station. These were established using the data speeds from the scientific payload, navigation and communication subsytems. The diagrams already show the implementation of the CDH subsystem.

From the data volume analysis and after looking into the needed data rates amongst the hardware components of both systems, the following requirement list for the CDH subsystem could be defined:

- MARS-UAV-CDH-1: The subsystem shall have a memory size of at least 28 Gb.
- MARS-UAV-CDH-2: The subsystem shall be capable of writing 41.5 Mbps continuously.
- MARS-UAV-CDH-3: The subsystem shall withstand Martian continuous radiation levels without failing in the expected lifetime.
- MARS-UAV-CDH-4: The subsystem shall have more than 1000 million instructions per second.
- MARS-Base-CDH-1: The subsystem shall have a memory size at least of 17.7 Tb.
- MARS-Base-CDH-2: The subsystem shall be capable of writing 100 Mbps continuously.
- MARS-Base-CDH-3: The subsystem shall be capable of losslessly compressing 28 Gb each sol with a compression ration of 1.5.
- MARS-Base-CDH-4: The subsystem shall be capable of compressing 28 Gb sol with a compression ration of 10.

- MARS-Base-CDH-5: The subsystem shall withstand continuous Martian radiation levels without failing in the expected lifetime.

7.9.2. UAV CDH Overview

The functions of the command and data handling on VITAS are the following:

- Flight computer operations
- Data handling operations
- Management of the other UAV subsystems

The central processing unit (CPU) should be capable of handling millions of instructions per second (IPS) for the autonomous functions to be performed on demand. In order to facilitate this, the decision was made not to compress any of the scientific data generated on the VITAS drone, in order to keep the communication line open for instruction from the navigation, as these have the utmost importance to be handled instantaneously. In Table 7.33 single board computers (SBC) are presented, and the most suitable one for the system is chosen. Only radiation hardened, off the shelf products were considered. This was done since the non-radiation hardened products have an increased probability of errors production, due to radiation releasing electrons in a transistor of a CPU, and giving a false positive. Moreover, some of these radiation hardened SBC's are equipped with error-correcting code, random-access memory (RAM), as these can detect errors if a bit has been incorrectly changed.

Table 7.33: Space hardened single board computers [64] [65] [66]

Model	Mass [g]	Power [W]	Form factor	MIPS	RAM [Gb]	Storage [Gb]
Alitech SPO-S	350	8.25	3U	3065	8	8
Bea	549	10.8	3U	2.1	1.024	0
Athena-2	998	16	6Ucompact	3065	8	32
Athena-3	998	16	6Ucompact	2450	8	32
Methusa	1.13	20	6U	2450	8	32
RCC 5	1.59	20	6U	2450	24	128

Based on the data in Table 7.33, Alitech SPO-S SBC was selected. This SBC was the lightest, used the least amount of power, had the smallest formfactor, and the highest MIPS of the selected SBC's. It has lower RAM and storage, only to the heaviest SBC. Only the two heaviest SBC's had enough storage equipped to hold the scientific data of one flight (28Gb).

The Alitech SPO-S SBC is capable of storing the operating system (OS) and the code to perform the mission. The selected SBC supports VxWorks 6.x, which is a very popular OS for space mission. It was used for all the Mars rovers [67] and in some aircrafts as the AgustaWestland Project Zero, a hybrid tiltrotor/lift fan aircraft [68].

To record and store the raw scientific data, the use of solid state drive recorders (SSDR) was required. Only radiation hardened SSDR's were considered, due to their embedded hardware error detection and correction. An overview of the options can be seen in Table 7.34.

Table 7.34: Space hardened solid state drive recorder. [69] [70] [71]

Model	Mass [g]	Power use [W]	Form factor	Storage size [Gb]	Write [Mbps]	Read [Mbps]
Alitech S992_8	200	2	3U	64	27.7	39.2
Alitech S992_16	217	2	3U	128	27.7	39.2
Alitech S992_32	234	2	3U	256	27.7	39.2
Alitech S992_64	250	2	3U	512	27.7	39.2
Seaker GEN3 FMC	635	2	6Ucompact	1536	615	580
TRRUST-Stor VPX RT	500	2	3U	3520	8000	8000

[64] URL:`http://www.rugged.com/sp0-s-3u-cpci-radiation-tolerant-powerpc-sbc` [Cited 25 June 2018]
[65] URL:`https://www.baesystems.com/en/our-company/our-businesses/electronic-systems/product-sites/space-products-and-processing/processors` [Cited 25 June 2018]
[66] URL:`https://www.seakr.com/catalog/#athena-2-sbc` [Cited 25 June 2018]
[67] URL: `https://www.extremetech.com/extreme/134041-inside-nasas-curiosity-its-an-apple-airport##-extreme-with-wheels` [Cited 25 June 2018]
[68] URL: `http://blogs.windriver.com/wind_river_blog/2014/04/agustawestland-project-zero-winner-of-2014-grover-bell-award.html` [Cited 25 June 2018]

To meet the writing requirements for the UAV in the most lightweight fashion requires 2 Alitech S992_8, weighing 400 grams. The other CDH UAV requirements were hereby met. An overview of the CDH in the UAV is presented in Table 7.35.

7.9.3. Base Station CDH Overview

The functions of the command and data handling on the base station are the following:

- Communication handling
- Data handling
- Manage the other subsystems
- Compressing scientific data

The same SBC's and SSDR's were considered for the base station, and are found in Table 7.33 and Table 7.34. To reduce the complexity of developing the system, the same SBC, Alitech SPO-S, was selected. This SBC was the better SBC out of the options, as described in Section 7.9.2. In order to find if the SBC has enough MIPS to comply with MARS-Base-CDH-3 and MARS-Base-CDH-4, it was found that an intel q6600 at 2.4GHz has 46 136MIPS and take 9.0 seconds to losslessly compress a 318 MB file with a compression ratio of 2.5[72][73]. Given that the base station CDH 2 SBC with each 3065 MIPS the expected lossless compression capabilities are

$$\frac{318\text{MB} \cdot 6130}{8\text{B/b} \cdot 9s \cdot 46136} = 37.52\text{Mbps},$$

The time it takes to complete on flight of data is

$$\frac{28\text{Gb}}{37.52\text{Mbps}} = 746s,$$

which is about 12 minutes and thus well under one sol. Requirement MARS-Base-CDH-3 is met, and since lossless compression requires the most computing power, requirement MARS-Base-CDH-4 is also met.
For the selection of SSDR, the preference was given to storage per mass and storage per size. From the selection in Table 7.34 TRRUST-Stor VPX RT SSDR was selected because it was superior in the categories previuosly mentioned. The requirement MARS-Base-CDH-7 requires 6 TRRUST-Stor VPX RT SSDR wired in a 2x3 setup so that it is fully backed up.
The base station CDH was placed in a rugged case that is designed to hold 8 3U formfactor cards. The rugged space grade case selected for the task was required to have a fully redundant power supply system. The case selected was the Alitech E900 3U Compact [74]. An overview of the CDH subsystem of the base station is presented in Table 7.35.

Table 7.35: An overview of the CDH subsystem of the UAV and base station.

VITAS				
Model	**Mass [g]**	**Power [W]**	**MIPS**	**Storage [Gb]**
Alitech SPO-S	350	8.25	3065	8
2x Alitech S992-8	200	2	0	64
Total	**750**	**12.25**	**3065**	**136**
Base Station				
Model	**Mass [g]**	**Power [W]**	**MIPS**	**Storage [Gb]**
2x Alitech SPO-S	350	8.25	3065	8
6x TRRUST-Stor VPX RT	500	2	0	3520
E900 3U Compact case	7937	5	0	0
Total	**11637**	**33.5**	**6130**	**21136**

[69]URL:http://rugged.com/s992-3u-cpci-radiation-tolerant-flash-memory [Cited 25 June 2018]
[70]URL:https://www.seakr.com/catalog/#athena-2-sbc [Cited 25 June 2018]
[71]URL:https://www.mrcy.com/siteassets/trrust-stor-radiation-tolerant-slc-nand-ssd.pdf [Cited 25 June 2018]
[72]URL: https://www.maximumcompression.com/data/summary_mf3.php [Cited 25 June 2018
[73]URL: https://en.wikipedia.org/wiki/Instructions_per_second [Cited 25 June 2018
[74]URL: http://rugged.com/e900-3u-compactpci-radiation-tolerant-enclosure [Cited 25 June 2018]

8 Future Development

At this point in time, mainly a feasibility analysis is presented. Many steps still have to be taken before the system can be launched to Mars. In Section 8.1 and Section 8.2, the work flow diagram and work breakdown structure for the post-feasibility study is given. In Section 8.3, the project Gantt chart for post-feasibility study can be found. Finally, the Verification and Validation techniques planned for the entire system can be found in Section 8.4.

8.1. Project Design & Development Logic

After the feasibility study, three major paths will have to be taken. These are the formulation of the project, carrying out public outreach and logistics & operations as seen in Figure 8.1. Formulation includes the preliminary design, which is followed up by the R&D and developing of the detailed design as presented in Figure 8.2. Carrying out public outreach includes meeting with investors and promoting the mission, as well as sharing the results of the mission. It runs parallel with the other steps. Every step would takes place until launching the mission except for sharing results, which runs up until the end of the mission. Finally, operations & logistics was divided into two big steps; pre-launch and post-launch. In the first step, collecting the material, transporting the system and preparing the launch occurs. During post-launch the operation centre would have to be managed to analyse the data.

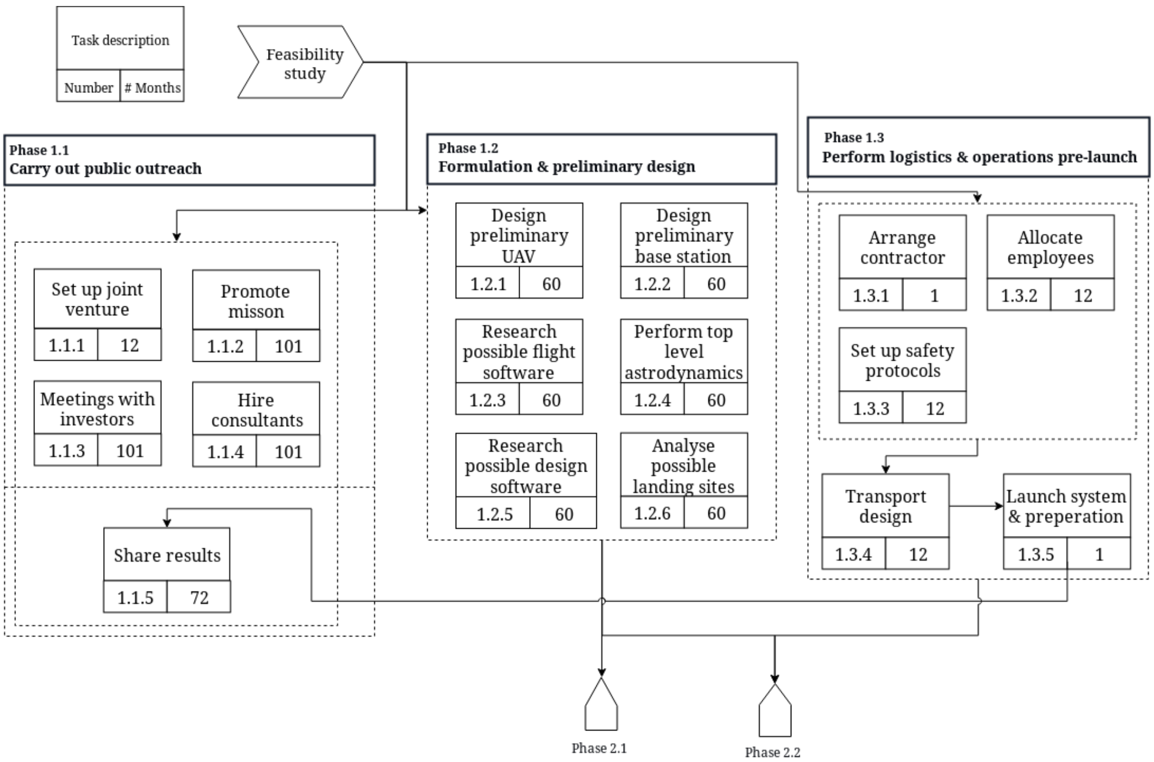

Figure 8.1: Phase 1 of the product development.

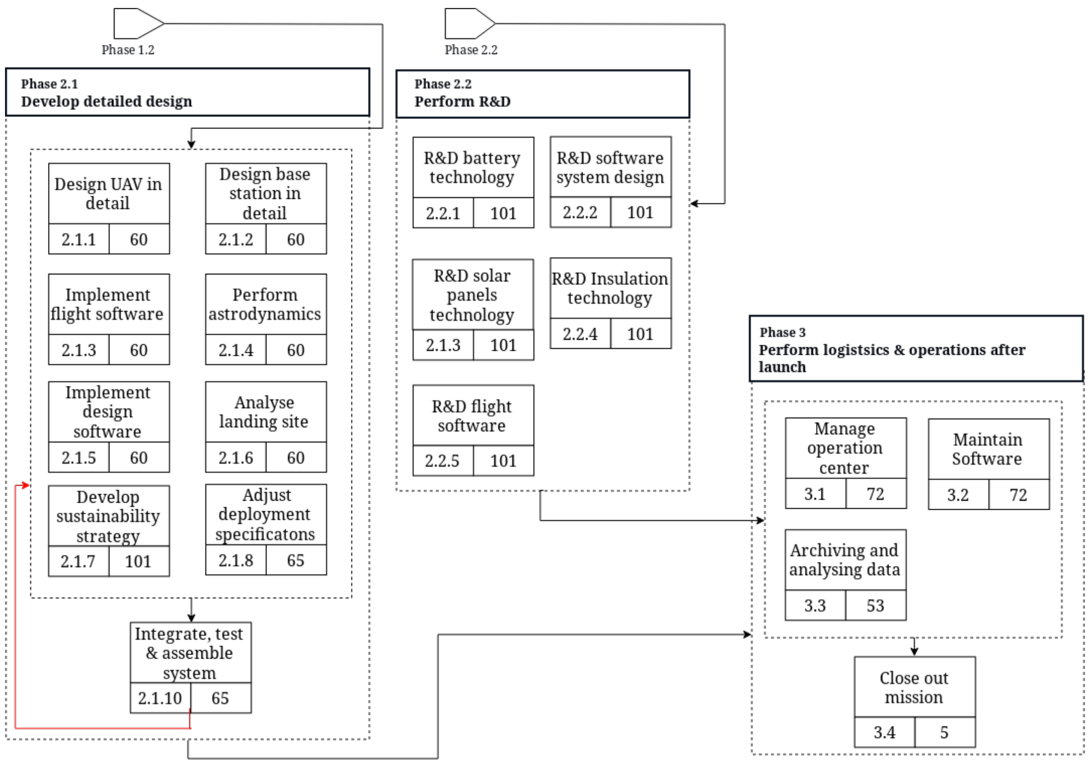

Figure 8.2: Phases 2 and 3 of the product development.

8.2. Work Breakdown Structure

To perform a cost analysis and to have a more detailed version of future processes, a top-level Work Breakdown Structure (WBS) was constructed, which is presented in Figure 8.3. All the time durations of the steps are included in the blocks, which were implemented in the Gantt chart in Section 8.3. All steps are under supervision of the project managers and system engineers during the process. Out of these, the main three steps were broken down into more detail. If a box is coloured in Figure 8.3 it means it consists out of more subdivisions and is either presented in Figure 8.4 or Figure 8.5.

Furthermore, in Section 6.3.3, the testing of the system is further explained and also depicts how the V&V process and the sensitivity analysis is included in the design of the system.

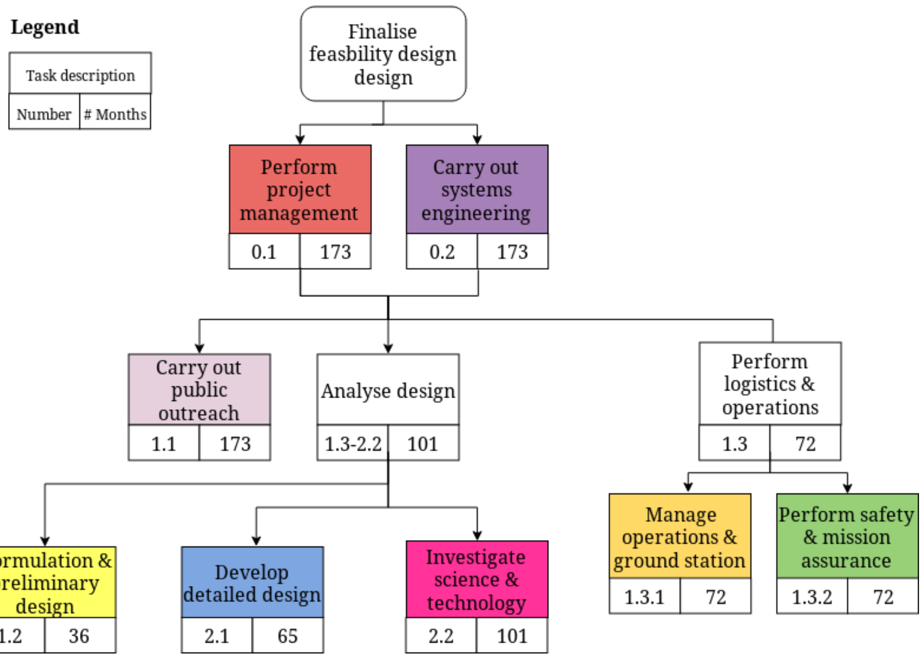

Figure 8.3: Top-level work breakdown structure of the mission.

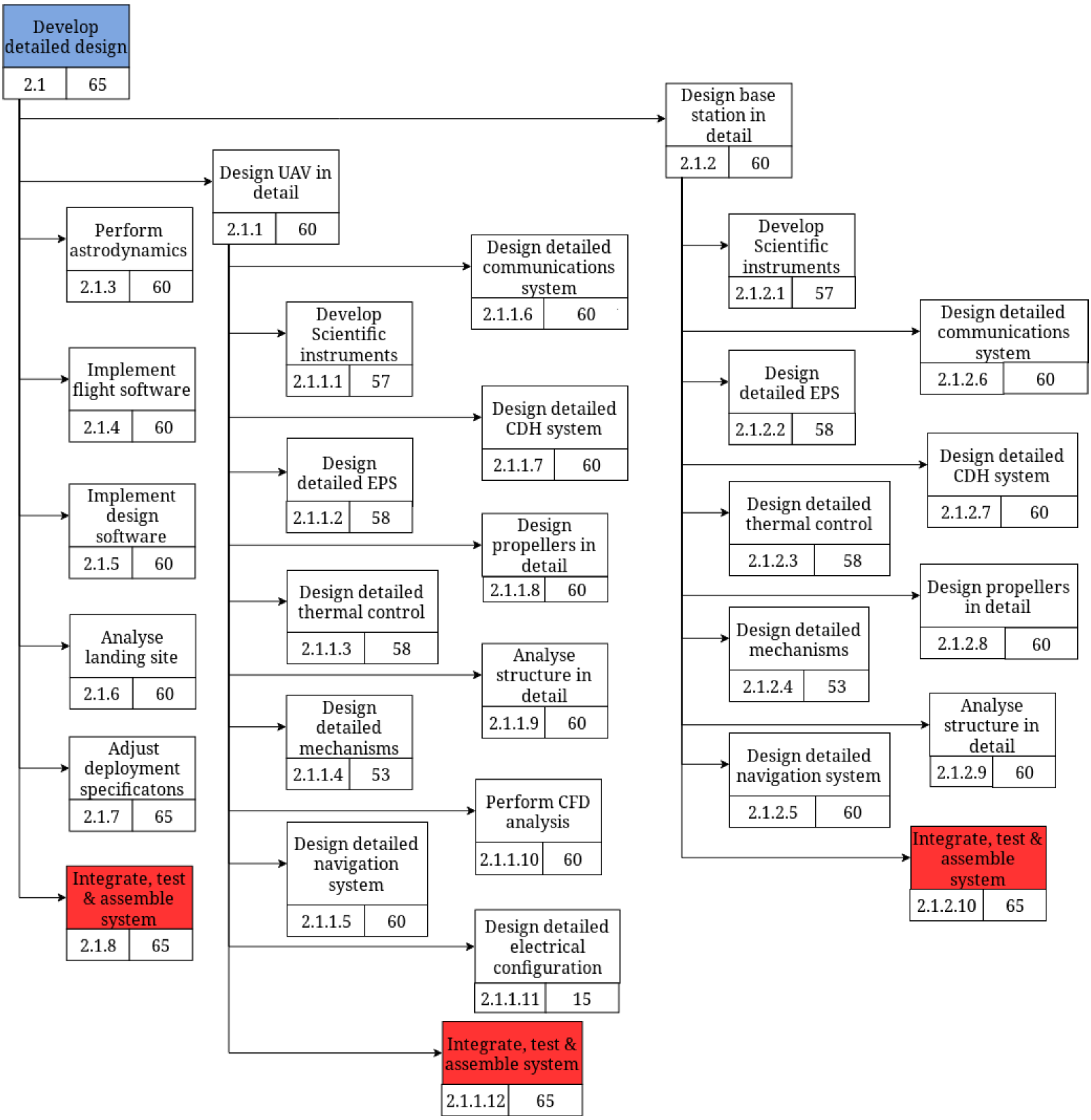

Figure 8.4: Work breakdown structure of the mission.

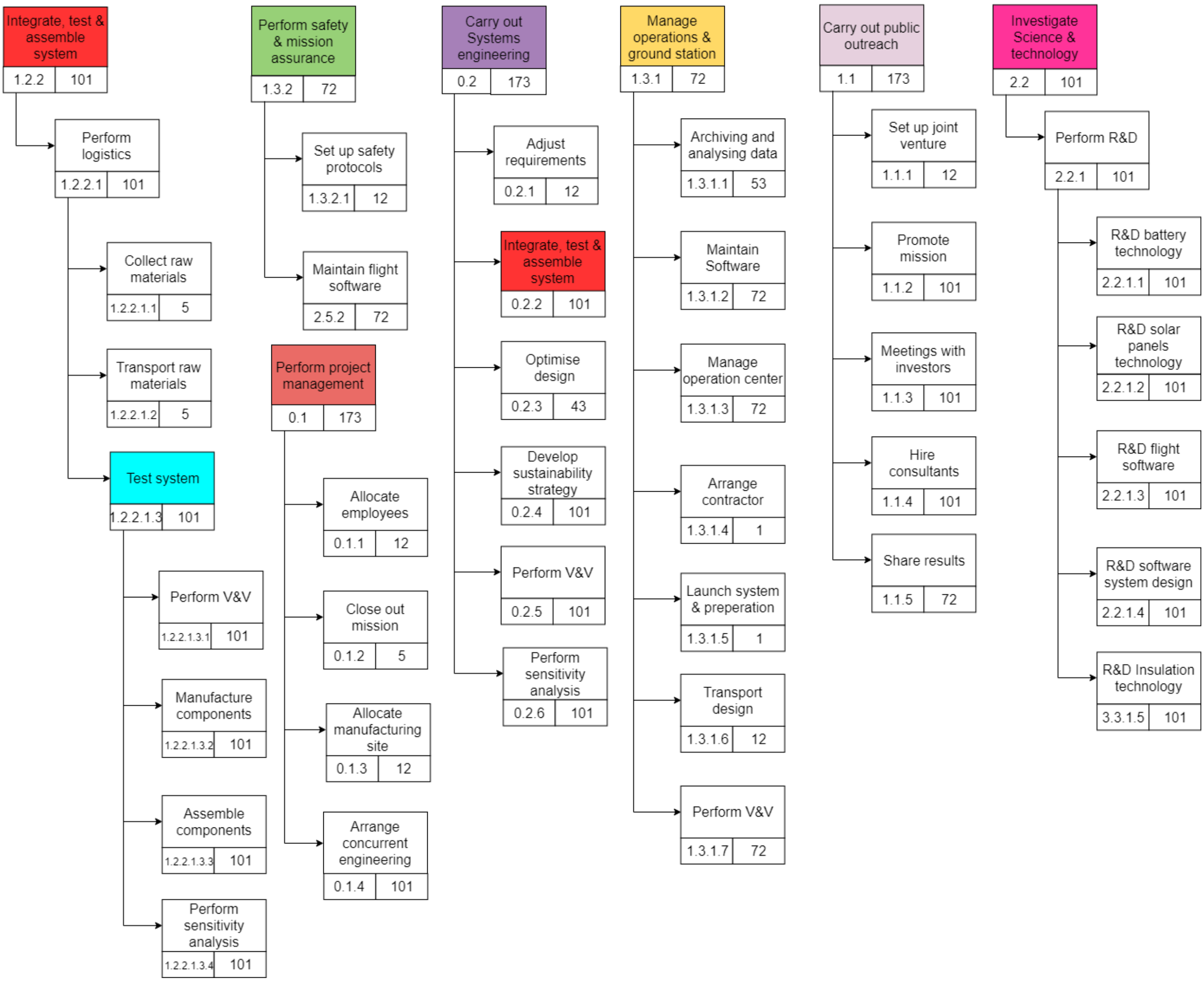

Figure 8.5: Work breakdown structure of the mission.

8.3. Project Gantt chart

In order to organise the WBS in time, a Gantt chart of the post-feasiblity study was made. Later on it was included in Chapter 9 to analyse the costs of the mission per year in current 2018 dollars. The feasibility study started on 20 April 2018 and finishes on 5 July 2018. Next, three years of formulation follow until July 2021. The development of the detailed design would be the next stage, which was expected to take until October 2026. The system is to be launched towards Mars in November 2026 and is expected to arrive on the surface in July 2027. The following 4.6 years, the mission will occur and data will be transmitted. About 75% of this data is compressed and 25% is uncompressed. Both would take about 2.3 years to transmit as defined in Chapter 4. At last, six months were allocated toward the closing out of the mission, which includes discussing results, documentation et cetera. Furthermore, logistics & operations and carrying out public outreach run in parallel with the design process.

	Name	Duration	Start	Finish
1	Analyse feasibility design	56 days	20/04/18 08:00	06/07/18 17:00
2	⊟ **Perform project management**	3,670 days	**09/07/18 08:00**	**30/07/32 17:00**
3	Allocate employees	262 days	09/07/18 08:00	09/07/19 17:00
4	Allocate manufacturing site	262 days	09/07/18 08:00	09/07/19 17:00
5	Arrange concurrent engineering	2,191 days	09/07/18 08:00	30/11/26 17:00
6	Close out mission	152 days	01/01/32 08:00	30/07/32 17:00
7	⊟ **Carry out systems engineering**	2,171 days	**09/07/18 08:00**	**02/11/26 17:00**
8	Adjust requirements	262 days	09/07/18 08:00	09/07/19 17:00
9	Optimise design	2,149 days	09/07/18 08:00	01/10/26 17:00
10	Develop sustainability strategy	2,149 days	09/07/18 08:00	01/10/26 17:00
11	Perform V&V	2,171 days	09/07/18 08:00	02/11/26 17:00
12	Perform Sensitivty analysis	2,171 days	09/07/18 08:00	02/11/26 17:00
13	Perform integration & testing	2,171 days	09/07/18 08:00	02/11/26 17:00
14	⊟ **Analyse design**	2,149 days	**09/07/18 08:00**	**01/10/26 17:00**
15	Formulation & preliminary design	785 days	09/07/18 08:00	09/07/21 17:00
16	⊟ **Finalise design**	2,149 days	**09/07/18 08:00**	**01/10/26 17:00**
17	⊟ **Develop detailed design**	1,364 days	**12/07/21 08:00**	**01/10/26 17:00**
18	Design UAV in detail	1,364 days	12/07/21 08:00	01/10/26 17:00
19	design base station in detail	1,364 days	12/07/21 08:00	01/10/26 17:00
20	Perform astrodynamics	1,364 days	12/07/21 08:00	01/10/26 17:00
21	Adjust deployment specifications	1,364 days	12/07/21 08:00	01/10/26 17:00
22	Implement flight software	1,364 days	12/07/21 08:00	01/10/26 17:00
23	Implement design software	1,364 days	12/07/21 08:00	01/10/26 17:00
24	Analyse landing site	1,364 days	12/07/21 08:00	01/10/26 17:00
25	Perform integration & testing & assemblin	1,364 days	12/07/21 08:00	01/10/26 17:00
26	⊟ **Investigate science & technology**	2,149 days	**09/07/18 08:00**	**01/10/26 17:00**
27	Perform R&D	2,149 days	09/07/18 08:00	01/10/26 17:00
28	⊟ **Perform logistics & operations**	3,518 days	**09/07/18 08:00**	**31/12/31 17:00**
29	⊟ **Manage operations & ground stations**	3,518 days	**09/07/18 08:00**	**31/12/31 17:00**
30	Archiving & analysing data	1,347 days	02/11/26 17:00	31/12/31 17:00
31	Maintain software	1,347 days	02/11/26 17:00	31/12/31 17:00
32	Manage operations center	1,347 days	02/11/26 17:00	31/12/31 17:00
33	Arrange contractor	785 days	09/07/18 08:00	09/07/21 17:00
34	Launch system & preperation	42 days	01/10/26 17:00	30/11/26 17:00
35	Transport system	289 days	01/10/25 17:00	10/11/26 17:00
36	⊟ **Perform safely & mission assurance**	2,733 days	**12/07/21 08:00**	**31/12/31 17:00**
37	Set up safety protocols	1,364 days	12/07/21 08:00	01/10/26 17:00
38	Maintain flight software	1,327 days	01/12/26 08:00	31/12/31 17:00
39	⊟ **Carry out public outreach**	3,518 days	**09/07/18 08:00**	**31/12/31 17:00**
40	Set up joint venture	260 days	09/07/18 08:00	05/07/19 17:00
41	Promote mission	2,149 days	09/07/18 08:00	01/10/26 17:00
42	Meeting with investors	2,149 days	09/07/18 08:00	01/10/26 17:00
43	Hire consultants	2,149 days	09/07/18 08:00	01/10/26 17:00
44	Share resulsts	1,327 days	01/12/26 08:00	31/12/31 17:00

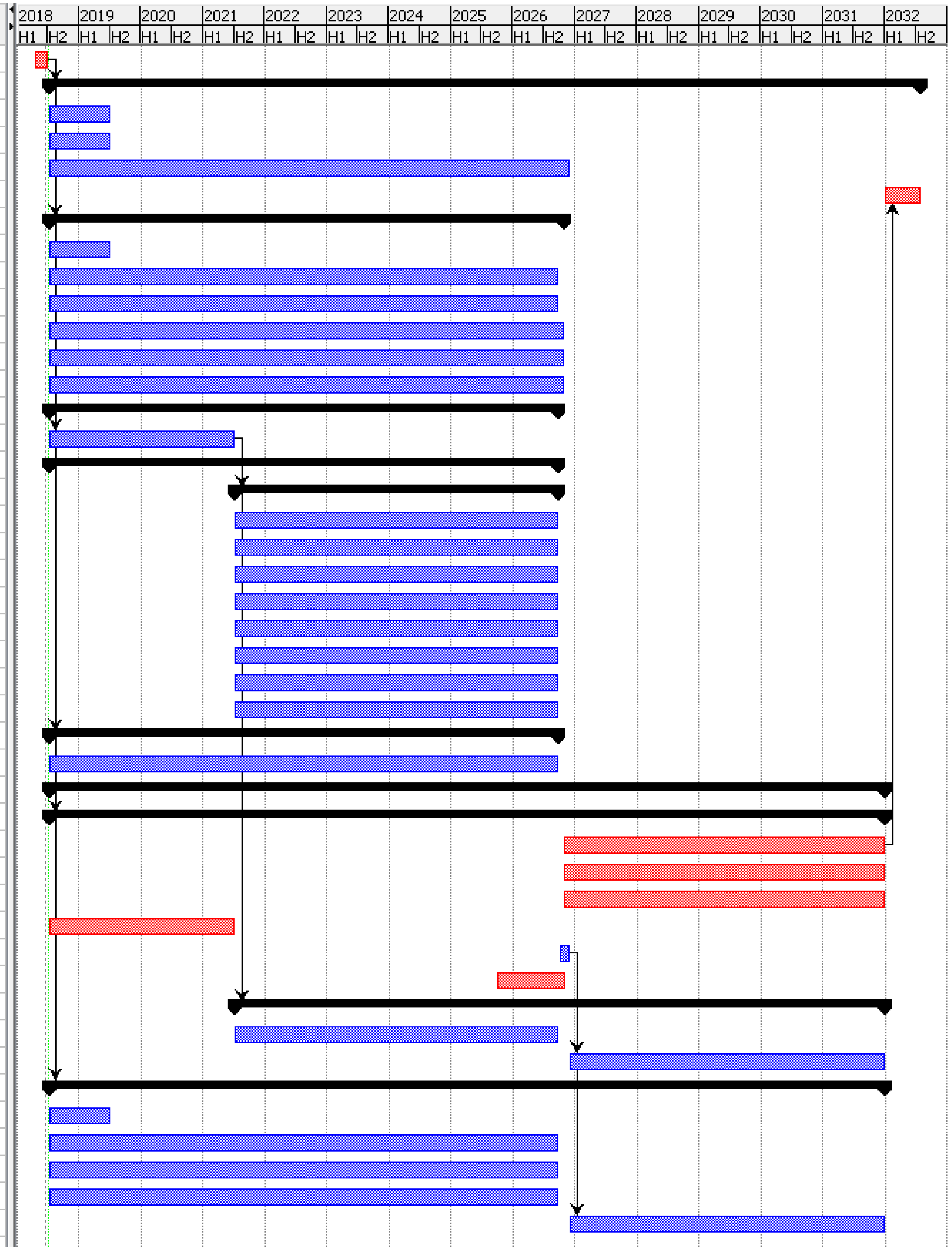

Figure 8.6: Gantt chart of future development.

8.4. Verification and Validation of MARS

To validate the entire design, various system tests will have to be performed. Once the subsystems are deemed to be verified to a sufficient extent, a prototype will have to be constructed for the entire UAV and base station to perform integration testing. First, a prototype will be constructed using cheaper, non-space grade off-the shelf components, which are still representative of their space-grade, radiation-hardened counterparts. Using the cheaper prototype will allow to determine whether any major integration errors were missed and need to be accounted for. Once the cheaper prototype has passed integration testing, the actual components will have to be used to construct a new one, for which the same tests will have to be performed. Once the subsystems of the new prototype do not have any unplanned interface issues, the integration tests will be considered passed.

The prototype will then be used for environmental testing. It will be exposed to conditions closely resembling the surface of Mars. First, the prototype will be exposed to very fine dust particles with a diameter of a few micrometers, consisting of maghemite or other ferric metals. This will simulate the impact of the Martian surface dust on the design and help determine whether the corresponding solar panel efficiency drop is as predicted. Additionally, the prototype will be placed in a vacuum chamber and exposed to temperature variations from -100 to 0 ^oC, simulating the pressure, atmospheric density and temperature conditions on Mars. Lastly, the prototype will be placed inside a shaker to simulate the vibration loads experienced during launch. The health of the system will be assessed after each test and if it copes with each environmental test, acceptance tests will follow.

The acceptance tests will be focused on determining whether the system complies with its scientific mission requirements. As the UAV prototype is designed to fly on Mars and not on Earth, it will be attached to an aircraft. The aircraft will be flown at the UAV's designed cruise altitude and velocity (150 m and 82.5 m/s, respectively). During flight, the UAV prototype will have its scientific payload active to test whether its gathered data complies with the mission requirements. Visual imaging and height mapping can be performed over any surface. For soil composition testing, the UAV prototype will be carried over a soil field, while to test its capabilities of detecting shallow ground ice deposits, slabs of ice will be burried at a depth of 10 m to determine whether they are detected. If the scientific data gathered complies with the requirements, the acceptance tests of the UAV prototype will be determined successful. The base station's MEDA instrument will not be exposed to such tests, as the Mars2020 rover's results will be available and the capabilities will be known.

Finally, qualification tests will be performed. For this, full-scale prototypes of the UAV and the base station will be required. Both prototypes will be exposed to 1500 cycles (representative of 4 years) of various conditions, such as temperature variations from 0 to -100 ^oC, draining and charging the batteries or UAV landing loads. Additionally, the components will be used 700 times (representative to number of flights), such as propellers operating at take-off power, science instruments being activated. Finally, a UAV prototype with the same size but weighing 2.7 times less (representative weight for higher gravitational acceleration on Earth) will be tested in a near vacuum chamber to take-off and land on a flat surface 500 times with exposures of wind gusts of up to 10 m/s in every direction. If the aforementioned tests are passed and each landing and take-off is successful, the qualification tests will be considered passed.

9
Cost Analysis

A detailed cost analysis has been performed for the MARS mission. In Section 9.1 the budget breakdown is performed, the masses and power are included as the used method for cost analyses of the subsystems and scientific instruments requires it. In Section 9.2 the cost over the different years of the project is analysed. Finally, in Section 9.3, means to fund the project are investigated.

9.1. Cost Breakdown

In Table 9.1 the budget breakdown of the mission is represented based on [Wertz and Larson, 1999, p.289-325] and [1] [2] [3] [4] [5] [6] [7] [8] [9] [10].

Several guidelines that should be taken into account when reading the table are:

- Development costs are included in all the subparts;
- Wages are included in all the subparts;
- Manufacturing costs are included in all subparts;
- Cost is estimated in 2018 dollars and 2026 dollars;
- Fiscal Year 2026 is included in the table as it is the year the launch is planned and most of the expenses should be covered by that time;
- To estimate future interest, an inflation model[11] is used;
- The total inflation from 2018 to 2026 is estimated to be 20.03%;
- The cost analysis performed is a level one estimation, and thus a preliminary analysis[10];
- A final contingency of 30% for the cost is added, while the power and mass have individual contingencies[10];
- All cost estimates reflect today's productivity levels and modern engineering processes[10];
- Statistical data of the Curiosity rover and MARS 2020 is used to estimate the cost of the project[2] [10];
- An IRR of 15% was chosen, as an economical stable project in the space industry should have at least this amount [Wertz and Larson, 1999, p.309];
- Salary per person is estimated to be $40,000 per year;
- Scientific instrument costs are based upon complexity, power required and mass;
- Other subparts estimations are based upon statistical data and an example is given in Table 9.2;
- CBE stands for Current Best Estimate, MEV for Maximum Expected Value and FY for Fiscal Year.

[1] URL: https://www.jpl.nasa.gov/news/news.php?feature=6603 [Cited 8 June 2018]
[2] URL: https://www.nasa.gov/press-release/nasa-awards-launch-services-contract-for-next-tracking-data-relay-satellite [Cited 8 June 2018]
[3] URL: https://www.ximea.com/en/products/hyperspectral-cameras-based-on-usb3-xispec/mq022hg-im-ls150-visnir [Cited 4 May 2018]
[4] URL: http://velodynelidar.com/vlp-16-lite.html [Cited 4 May 2018]
[5] URL: http://www.msss.com/brochures/xfov.pdf [Cited 4 May 2018]
[6] URL: https://pdfs.semanticscholar.org/bb28/558926c8584bcd54ccf9235c6af9a1119d42.pdf [Cited 4 May 2018]
[7] URL: http://www.msss.com/brochures/c50.pdf [Cited 4 May 2018]
[8] URL: https://www.nasa.gov/pdf/345955main_8_Exploration_%20FY_2010_UPDATED_final.pdf [Cited 8 June 2018]
[9] URL: http://www.iceaaonline.com/ready/wp-content/uploads/2017/09/EST01-Broder.pdf [Cited 8 June 2018]
[10] URL: https://www.nasa.gov/pdf/140643main_ESAS_12.pdf [Cited 9 June 2018]
[11] URL: https://www.statista.com/statistics/244983/projected-inflation-rate-in-the-united-states/ [Cited 8 June 2018]

Table 9.1: Budget breakdown MARS project

Budget breakdown MARS project										
Component	CBE (kg)	Contingency mass (%)	MEV (kg)	Nominal CBE (W)	Peak CBE (W)	Contingency power (%)	Nominal MEV (W)	Peak MEV (W)	FY2018	FY2026
Launch system									$ 262,000,000.00	$ 314,500,000.00
Launcher ATLAS									$ 132,000,000.00	$ 158,500,000.00
Safety operations									$ 20,000,000.00	$ 24,000,000.00
Transport of system									$ 10,000,000.00	$ 12,000,000.00
Other									$ 100,000,000.00	$ 120,000,000.00
UAV	12.38		13.94	1236.68	1951.21		1479.47	2336.12	$ 519,640,000.00	$ 623,720,000.00
Scientific instruments UAV	1.62		1.70	22.10	22.10		24.31	24.31	$ 12,830,000.00	$ 15,400,000.00
Spectrometer	0.21	5%	0.22	1.6	1.6	10%	1.76	1.76	$ 1,460,000.00	$ 1,750,000.00
Altimeter	0.59	5%	0.62	8	8	10%	8.8	8.8	$ 4,380,000.00	$ 5,260,000.00
Optical lens	0.20	5%	0.21	0	0	0%	0	0	$ 1,170,000.00	$ 1,400,000.00
ICE	0.40	5%	0.42	10	10	10%	11	11	$ 4,070,000.00	$ 4,890,000.00
Hyperspectral camera	0.21	5%	0.22	2.5	2.5	10%	2.75	2.75	$ 1,750,000.00	$ 2,100,000.00
Subsystems UAV	10.76		12.24	1214.58	1929.11		1455.16	2311.81	$ 506,810,000.00	$ 608,320,000.00
Thermal control	0.50	10.00%	0.50	11.1	25.1	20.00%	13.32	30.12	$ 14,210,000.00	$ 17,050,000.00
EPS	2.46	15.00%	2.84	1180	1869	20.00%	1416.10	2242.60	$ 140,270,000.00	$ 168,370,000.00
Propulsion	2.37	15.00%	2.72	0	0	0.00%	0.00	0	$ 185,680,000.00	$ 222,870,000.00
Structure	3.89	15.00%	4.46	0	0	0.00%	0.00	0	$ 32,410,000.00	$ 38,900,000.00
Communication	0.18	10.00%	0.20	12.55	12.875	10.00%	13.81	14.1625	$ 12,110,000.00	$ 14,530,000.00
Electrical equipment	0.17	30.00%	0.22	0	0	0.00%	0.00	0	$ 2,350,000.00	$ 2,820,000.00
Navigation	0.49	10.00%	0.54	1.6	4.8	10.00%	1.76	5.28	$ 29,600,000.00	$ 35,530,000.00
Mechanisms	0.12	20.00%	0.14	0	2	30.00%	0.00	2.6	$ 1,320,000.00	$ 1,590,000.00
CDH	0.79	5.00%	0.83	9.25	15.5	10.00%	10.18	17.05	$ 88,860,000.00	$ 106,660,000.00
Base Station	451.51		543.95	94.48	2670.20		108.05	3233.65	$ 981,270,000.00	$ 1,179,010,000.00
Scientific instruments base station	5.50	10.00%	6.05	1.7	17	10.00%	1.87	18.7	$ 15,800,000.00	$ 18,970,000.00
Subsystems base station	441.51		534.40	92.78	2653.20		106.18	3214.95	$ 965,470,000.00	$ 1,160,040,000.00

Table 9.1: Budget breakdown MARS project

Budget breakdown MARS project										
Thermal control	0.85	20.00%	1.02	0.10	30.10	20.00%	0.12	36.12	$ 26,830,000.00	$ 32,210,000.00
EPS	56.03	10.00%	61.64	0.00	1868.83	20.00%	0.00	2242.60	$ 50,920,000.00	$ 61,110,000.00
Structure	291.65	20.00%	349.89	0.00	0.00	0.00%	0.00	0.00	$ 179,670,000.00	$ 215,660,000.00
ADCS	4.25	10.00%	4.68	0.00	18.30	10.00%	0.00	20.13	$ 293,810,000.00	$ 352,660,000.00
Electrical equipment	58.70	30.00%	76.30	18.56	530.64	30.00%	24.12	689.83	$ 45,690,000.00	$ 54,850,000.00
Navigation	15.99	10.00%	17.59	33.60	122.80	10.00%	36.96	135.08	$ 191,350,000.00	$ 229,680,000.00
Mechanisms	2.00	20.00%	2.40	2.00	2.00	30.00%	2.60	2.60	$ 33,730,000.00	$ 40,490,000.00
CDH	11.64	10.00%	12.80	38.52	80.53	10.00%	42.38	88.58	$ 144,460,000.00	$ 173,380,000.00
Safety & assurance									$ 373,850,000.00	$ 448,740,000.00
Safety protocols									$ 46,730,000.00	$ 56,090,000.00
Mission assurance									$ 327,120,000.00	$ 392,650,000.00
Science									$ 510,560,000.00	$ 612,830,000.00
Flight software									$ 360,560,000.00	$ 432,790,000.00
Deployment & landing									$ 150,000,000.00	$ 180,040,000.00
Project Management									$ 233,660,000.00	$ 280,460,000.00
Rent manufacturing site									$ 233,660,000.00	$ 280,460,000.00
Systems engineering									$ 327,120,000.00	$ 392,650,000.00
Mission operations									$ 197,860,000.00	$ 237,270,000.00
Data transfer									$ 10,750,000.00	$ 12,900,000.00
Operation center									$ 186,930,000.00	$ 224,370,000.00
Integration, testing & assembling									$ 467,320,000.00	$ 560,930,000.00
Logistics									$ 46,730,000.00	$ 56,090,000.00
Public outreach									$ 110,000,000.00	$ 132,030,000.00
Consultants									$ 100,000,000.00	$ 120,030,000.00
Media content									$ 10,000,000.00	$ 12,000,000.00
Other									$ 217,810,000.00	$ 261,440,000.00
Contigency									30.00%	30.00%
Total									$ 5,522,170,000.00	$ 6,628,310,000.00
IRR									15.00%	15.00%
Sell price									$ 6,350,500,000.00	$ 7,622,560,000.00

In Table 9.2 an example is given of how the structures cost of the UAV is estimated. All the subsystems of the UAV and base station are estimated in a similar manner. The software, management, assurance, integration, testing & assemble and systems engineering are a percentage cost but are represented individually in Table 9.1 and thus were not included in the overall cost of the structure component.
First, the manufacturing cost[12]

$$\text{Cost manufacturing} = \text{Machining cost} \ \cdot \$30.99\text{Volume billet}, \tag{9.1}$$

with Volume billet being equal to $1.45\,\text{m}^3$. The machining cost is equal to

$$\text{Machining cost} = \$30.99\text{Volume billet} - \$2.12\text{Volume billet}. \tag{9.2}$$

The volume of the billet is estimated in Chapter 5. An extra contingency had to be taken on it as some material would go to waste.
Next, the management cost was estimated, which was assumed to be a percentage of the total cost excluded the software cost [Wertz and Larson, 1999, p.298]. This yields

$$\text{Management cost} = 7.124\% \cdot (\text{Total structure cost} - \text{Software cost}). \tag{9.3}$$

Furthermore, the cost of the wages equals

$$\text{Wages} = 15 \cdot 5 \cdot \$40,000, \tag{9.4}$$

with 15 people working for 5 full years fully dedicated to the structures department, which is based upon statistics from Wertz and Larson [1999, p.304]. The development cost equals[10],

$$\text{Development cost} \ = 61.53\% \cdot \text{Structure cost}. \tag{9.5}$$

The software costs were based upon how complex the system is, how reliable is has to be, if it has to be fully developed or just should be re-tested, and if it is made by experienced or by novice programmers or engineers. The factors involved were multiplied by 3.312, which was based on statistics. Based upon other programs developed in the industry, the following equations were obtained,

$$\text{Software cost} = 3.312 \cdot 1.15 \cdot (100,000)^{1.2} \cdot 1.15 \cdot 1.15 \cdot 1 \cdot 2 \tag{9.6}$$

It was assumed the program should exist out of 100,000 lines of source code [Wertz and Larson, 1999, p.319], should be completely made from scratch (factor 2), should be highly reliable (power 1.2), complex (factor 1.15) and be made by experienced engineers (factor 1.15). Another factor factor 1.15 was added to the equation as the statistic was based upon FY10. The interest from the FY10 to FY18 is 15%[11] and was therefore additionally implemented.
The assurance cost was estimated as follows,

$$\text{Assurance cost} = 14.27\% \cdot \text{Total structure cost}^{0.9422} \text{[Wertz and Larson, 1999, p.319]} \tag{9.7}$$

The integration, testing & assembling (IT&A) is estimated similarly [Wertz and Larson, 1999, p.319]

$$\text{IT\&A cost} = 14.57\% \cdot \text{Total structure cost}. \tag{9.8}$$

At last, the system engineering cost is also not included in the structure cost itself but is a percentage based on the total structure cost [Wertz and Larson, 1999, p.300], yielding

$$\text{Systems engineering cost} \ = 49.31\% \cdot (\text{Total structure cost} - \text{Management cost} - \text{Wages})^{0.8645}. \tag{9.9}$$

Table 9.2: Cost breakdown structures UAV

Budget breakdown structures UAV		
Component	FY18	FY26
Structure	$ 32,410,000.00	$ 38,890,000.00
Wages	$ 3,000,000.00	$ 3,600,000.00
Development	$29,410,000.00	$35,290,000.00
Software	$ 11,080,000.00	$ 13,300,000.00
Management	$ 2,640,000.00	$ 3,160,000.00
Assurance	$ 2,250,000.00	$ 2,700,000.00
Integration, testing & assembling	$ 6,340,000.00	$ 7,610,000.00
Systems engineering	$ 1,650,000.00	$ 1,990,000.00

[12]URL: `https://www.sciencedirect.com/science/article/pii/S1350630704000494` [Cited 7 June 2018]

9.2. Cost over the years

The cost over the different years was analysed and is presented in Figure 9.1. This was a vital aspect of the project as it has to be known how much money would have to be invested into the project by the investors and the MARS group each year. It can be noted that in the year 2023, most of the investors have to be gathered, otherwise the mission might be discontinued due to lack of budget.

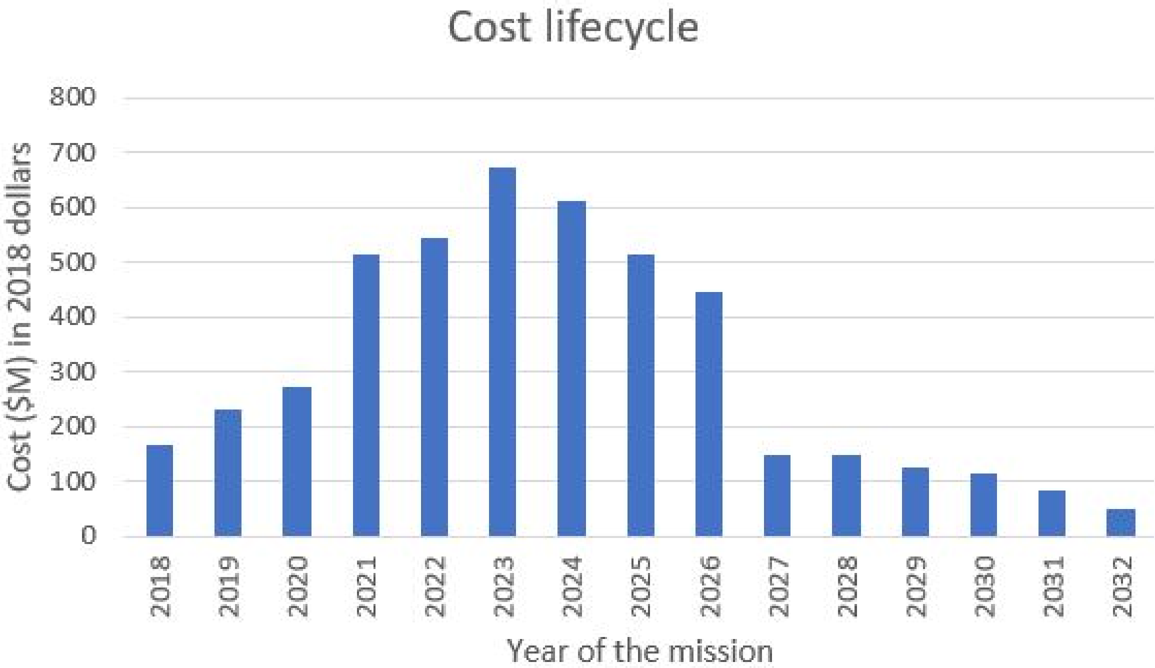

Figure 9.1: Cost over the different years based on Table 9.1 and Figure 8.6

9.3. Funding

As analysed in this chapter, the mission is quite expensive for any company. To attain such a high budget, capital should be raised through external means, which is analysed in this section.

As represented in Figure 9.1, each year a budget is required to continue the mission. The MARS group has to avoid as much risk as possible. Means of funding that require a high interest rate will not be accepted. This includes bonds with high interest rates. It was decided that the healthiest way to fund the project was through stock finance, which means the MARS group will sell a part of the company[13]. This will result in less profit for the MARS group, however the potential risk of losing money is lower. Furthermore, it will be focused on attracting angel investors, whom are investors that offer technical advice besides funding money. This is considered as a necessity as the engineers of the MARS group are inexperienced. Additionally, more ways of obtaining money are possible such as sponsoring. Awareness could be created through social media to attract stakeholders.

Next to that, Other companies might be interest in the R&D of e.g. battery development. Costs can be shared to investigate possible technological advancements. Companies might also be interested in adding scientific instruments to the base station, as there is still room left for extra payload. It can be added to the base station for a price or the profit gained through these extra instruments could be shared.

[13]URL: `https://www.tradefinanceglobal.com/finance-products/stock-finance/what-is-stock-finance/` [Cited 7 June 2018]

10
Sustainability

The sustainability strategy as set up in Chapter 3 has been implemented throughout the design of the system. An overview of the implementation in the design is shown in Section 10.1. How the design contributes to sustainability is presented in Section 10.2.

10.1. Implementation in Design

The way sustainability has been implemented in the design will be further elaborated upon in this section.

10.1.1. Subsystems

During the UAV concept trade-off, radio-isotope thermoelectric generators were not considered as means of power generation. Due to the low availability of the nuclear material and the risks imposed by having it launched to Mars, solar panels were chosen for power generation. Second, the chosen single tailsitter was the optimal design in terms of energy requirements and material usage. As a result of requiring less energy, less solar panel area was required on the base station which further reduces the total material usage for the mission.

For thermal control subsystem design, a requirement was set up not to use radio-isotope heating units. Instead, the design was aimed at using passive thermal control techniques which are both beneficial for sustainability in terms of limiting power usage and avoiding hazardous materials.

Additionally, toxic and hazardous materials were limited for the structure as much as possible. Only when it was critical for the design, toxic materials were considered. In the end, a beryllium-aluminium alloy was used as it performed best across the board. Beryllium is a toxic material for which no cure exists yet; however, since only one UAV has to be built, the probability of contamination would be low. In order to make deconstruction during future human missions safe, chips and fine particles could be prevented by implementing assembly features such as plastic screw guides and rubber fittings.

10.1.2. Environment

Contamination of Martian and terrestrial environment was also taken into account for the sustainability strategy. This was mainly done when selecting the launcher and the entry vehicle.

When selecting the launcher to carry the mission, lower propellant usage awarded additional points in the trade-off and additional points were awarded for launchers with reusable stages. In case the launch fails, not having a RTG on board will lower the contamination of Earth as well.

For the landing procedure, the skycrane mechanism was rejected in favour of the thruster as will be used on the ExoMars 2020 mission. This results in less waste being left on the surface of Mars, as the skycrane is designed to crash on the surface of Mars. This by definition contaminates the Martian surface, but it could also contaminate scientific data of the MARS system or other systems. In addition, less material is used to support the design if the skycrane is removed.

10.1.3. Existing Systems

It was attempted to make use of existing systems on Mars and integrating them into the mission. The Mars Relay Network was chosen to transmit the scientific data back to Earth. This not only adds to the value of the Martian orbiters, but also makes the base station communication design less demanding in terms of transmitter power requirements and component size.

10.1.4. Reusability

A particular focus is laid on having a reusable design for both systems: the UAV and the base station. The UAV is planned to be reused for future manned or unmanned missions by having it remain functional after its primary scientific tasks. The batteries were designed to still have a sufficient depth of discharge to provide for a flight range of over 50 km, making it usable for any additional mapping that might be required. Additionally, the batteries will be installed in such a way that they are easily replaceable for any future manned mission. The base station was designed such that it could be used by other missions and prove beneficial for other parties. The following points can be made:

- The base station can provide for data storage, processing and relay for other Mars surface missions. The CDH unit was designed such that it could have twice the amount of data generated by VITAS stored, leaving over 10 Tb that could still be used by other missions. The data will then be slowly relayed back to Earth using the MRN.
- The mass, power and volume budgets of the base station make it possible to include additional scientific instruments. This means that outside parties, on demand, can cooperate with MARS to include additional payload and gather more data.
- As the batteries are critical for the design of the UAV and base station, battery technology will be researched and possible advancements will be included in the design. Other companies in the space industry or other science branches could implement the advanced batteries into their system to e.g. save weight.

10.2. Contribution to Sustainability

Sustainability was not only considered during the design of the system. It was also aimed to design a system that contributes to sustainability. The product itself contributes to it due to its innovative aspects, a brief list of these aspects is as follows:

- Reuse of the mission
- Recycling of the mission
- Base station accessibility for future missions
- Demonstration of long-term solar power usability

The first way to contribute to sustainability is by reusing past Martian missions for the design. This is done by utilising existing Martian orbiters, namely NASA's Mars Odyssey, Mars Reconnaissance Orbiter and ESA's Mars Express. As long as they remain functional, they will be used to relay the data from the base station back to Earth. This eliminates the need to launch additional orbiters and demonstrates how past older missions can be still be used.

Secondly, MARS is organised in a way such that it can be used by future missions too. The UAV is designed such that it could be reused as a whole or for its parts. For example, modularity is implemented in the battery design. Any kind of future mission, manned or unmanned, could possibly replace the batteries. Additionally, the base station is also meant to be available for reuse. Other missions would be cheaper, lighter and thus less wasteful due to the available data storage and data relay on the base station. Also, the local navigational system will be made in such a way that it could also be used by Martian rovers, adding to their functionality and capabilities.

Finally, a goal of the product is to demonstrate that RTG's and RHU's are not a necessity for long-term planetary exploration missions. By using solar arrays for power generation, it is aimed to show that they are a viable option for Martian landers even with high power requirements. This will encourage future Martian missions to be designed around using solar energy. Also, the solar array stowing and deployment mechanisms can pave the way for missions which also require large amounts of power but are heavily constrained by the entry capsules.

11 Conclusion

The required launch vehicle, mission architecture and landing sites have been described. Due to its very high reliability, the Atlas V 541 launcher, along with the Mars Science Laboratory entry, descent and landing module were chosen to bring the system to Mars. It was decided to use a thruster system instead of the sky-crane concept to increase the accessible space inside the entry vehicle, as well as leading to less waste on Mars.

The launch is scheduled for November of 2026 and an arrival in July or August of 2027 is expected. A Hohmann transfer will be followed and the atmospheric entry will be performed using a heat shield, followed by parachute deployment and thruster activation until touch down. The Jezero Crater was chosen as the optimal landing site, due to its size, flat surface, low elevation and the availability of mineral deposits.

Various UAV concepts were investigated, but a single tail-sitter design was chosen for further development due to to its strong performance in terms of cruise speed, range and benefits regarding sustainability and mission complexity. An X-wing configuration was chosen due to the beneficial propeller clearance. A canard surface was also installed to provide pitch control, as no tail could be included behind the wing.

Stability and control aspects, as well as the aerodynamic performance of the UAV were major concerns. An SD7003 airfoil was chosen due to its high C_L/C_D, allowing for the highest range capabilities. The canard surface proved sufficient for longitudinal stability, with the cg location found to be 0.096 m behind the leading edge of the wing. The UAV's VTOL capabilities were evaluated with wind gusts present. It was found, that differential thrust was effective in providing gust resistance during take off and landing procedures. Lastly, the UAV's longitudinal and lateral dynamic stability was investigated. It showed that it is indeed stable, but responses to each mode showed that the modes damp out very slowly. However, this was deemed not to be a concern as active control is available at all times.

A significant amount of effort was put into looking into the material of choice for the flyer design and the structure's performance in surviving launch vibrations and loads. The optimal material was determined to be the AM-162 Beryllium-Aluminium alloy due to its high specific modulus and sheet metal properties. Although toxic, it was deemed that the negative effects can be negated using the correct assembly techniques and safety precautions. The lowest fundamental frequency was found to be that of the wing, at a value of 77 Hz, sufficiently higher than the required value. The overall design was sufficiently strong to withstand 7.5 g longitudinal and 2.5 g lateral loads.

The scientific data gathering capabilities of the VITAS drone were also assessed. The UAV will perform visual imaging using a C50 as well as the ECAM-NFOW cameras. The UAV was also tasked with height mapping, using the VLP-16 Lite altimeter. Ice deposits will also be studied using the WISDOM instrument. Lastly, soil analysis will be performed not by taking samples, but by using hyperspectral imaging with the XIMEA LS150-VISNR spectrometer.

The second key part of the MARS system studied was the base station design. It was deemed necessary for the design due to how many supporting functions it can provide for the flyer. It will provide power generation using solar panels and charge the UAV using a robotic arm. Additionally, the base station will act as a landing platform, provide guidance using a pseudo-satellite local positioning system, store and process the scientific data and relay it back to Earth. Lastly, the base station will perform scientific measurements: wind, precipitation and dust size/composition. It will have the MEDA instrument suite on board for that purpose.

An extensive market analysis and project cost estimation were also performed. It was concluded that with the current blooming state of the space industry, the markets to target for the mission are science, space flight and interplanetary human habitation. Also, with a 4.1% annual growth of the capital, with more and more attention being given to space exploration missions, it is a prime time to perform the MARS mission. To make the MARS mission more distinctive, reusability and recyclability of the system were made to be major focal points. After performing a cost analysis, the total project cost was estimated to be $4.6 billion and it will be sold for at least $5.1 billion for a return rate of 15%.

12
Recommendations

With the limited time available, only so much can be done with regard to designing a complex system such as the MARS. Therefore, more research and testing is required. In this chapter, further development techniques for each subsystem is presented..

Propulsion
No man-made machine has ever performed fixed wing flight on planet other than Earth. This made the development of a functional and efficient propeller capable of delivering sufficient thrust on Mars difficult and a lot of assumptions had to be made. In order to reduce the uncertainty regarding the propeller performance, full CFD analyses are required, which simulate the Martian atmosphere.

Also, since the propellers operate closely to compressible speeds, more research is required in supercritical propellers and their performance at higher turn rates.

During take-off and descent, the VITAS drone uses differential thrust for controllability. This implies the use of a swashplate system, as discussed in chapter 7, section 7.3. However, the exact parameters of this system and how much differential thrust could exactly be delivered is still unknown. More investigation in current swashplate technology would be required in order to have a better estimate of the differential thrust capabilities of the VITAS drone.

Thermal Control
A complex model of the entire system should be made in CATIA or ANSYS. A finite element thermal analysis should be performed to investigate the thermal behaviour of both boxes in depth to help better identify the required heat pipe layout, as well as the ideal component placement.

Additionally, at a later testing stage, the thermal box prototypes should be exposed to rigorous thermal testing. Thermal vacuum tests should be performed to test the number of thermal cycles the design can cope with in a near-vacuum environment. Balance tests should be performed by simulating the coldest and hottest environments, allowing to identify the critical heat transfer paths. These type of tests will allow for verification of the thermal control subsystem and also provide valuable experimental data for comparison and improvement of the used analytic models.

Structures
The design of the internal support structure of the VITAS drone had several setbacks, which caused the design process to lack coordination and structural optimisation techniques were therefore barely implemented. Due to the mission success being so dependent on the weight of the UAV, more investigation is required in structural optimisation and a detailed analysis about the joining methods being used in the assembly would result in a design with less contingency.

The main emphasis of the structural design was put on the UAV. In order to verify the structural integrity of the base station, its load cases have to be analysed better and suitable materials should be investigated.

The load cases analysed during the structural design were launch and flight loads. It was difficult to obtain qualitative data about the vibration loads acting on the Mars Science Laboratory during Martian entry, descent and landing, which resulted in these loads not being investigated. In order to ensure structural integrity during entry, the vibration loads have to be investigated more properly and the structure should be altered if required.

In order to validate the results from the structural analysis, a second stress analysis program should have been used. Unfortunately, due to schedule constraints, there were no resources available for adaptation to a new program. For a next project, sufficient time should be reserved for the adaptation of existing programs or developing analysis tools ourselves.

Scientific Instruments
The scientific instruments equipped on the UAV and base station have been chosen accordingly to existing missions. However, for these missions, the instruments were customised to the specific mission needs and environment. This optimisation was not performed during this project and could result in better power requirements and reduced mass.

The navigation system for the VITAS drone was limited to a preliminary design only, since proper resources were unavailable to the team. In order to have a better idea of the capabilities of the navigation system, the locator beacons have to be designed in more detail, especially their deployment system, since something similar has never been attempted before. Since the subsystem is crucial to the mission success, more research is required in order to ensure its functionality.

The WISDOM ice scanner was designed for low ground speeds, since it will be used on the Mars 2020 rover. It was decided to put the instrument on the UAV, expecting its results to be valid. However, whether the increased travel speed would influence the quality of the signal is unknown. The Doppler shift due to the increased scanning speed might compromise the data. In order to provide an estimate of how this would affect the data, more research is required into how the instrument exactly operates and whether it could be modified to work better during flight.

Aerodynamics

As discussed earlier, no other UAV has ever flown on Mars. Since the physical properties of the Martian atmosphere are radically different than those the Earth atmosphere, it's difficult to make estimations of how things fly on Mars. To have a good estimate of aerodynamic effects on Mars, wind tunnel tests on low Reynolds numbers have to be conducted, upon which computer models can be based which allow for detailed CFD analyses on the VITAS avionics.

During the sensitivity analysis on the airfoil, it became clear that the performance of the wing heavily depended on the airfoil performance. Therefore, more investigation about airfoil optimisation is required, maybe the development of a custom airfoil.

Stability and Control

Since VITAS has to fly in many different scenarios, the design of the control surfaces is a challenge on its own. In order to perform the required manoeuvres, more analysis is required regarding the control surface size and deflection, along with how the propeller flow influences the effectiveness of the control surfaces.

For the flight path and manoeuvres, more optimisation is required in order to find the optimal transition between vertical and horizontal flight, as well as the turning performance of VITAS.

Base Station

The main focus of the project was the development of VITAS, resulting in less emphasis on the detailed design of the base station. This resulted in the design of intricate systems such as the robotic arm to remain preliminary. For the robot arm to have a better design, further analysis concerning its requirements is necessary so it can be sized more properly.

The entry vehicle chosen for this mission was the same one used for the Curiosity rover and for the upcoming Mars 2020 mission. However, in order to allow for more freedom in the design of the base station and UAV, optimisation in the design of the entry vehicle is required. This can result in more available space for the stored systems, which could make the entire system more feasible.

Shortly before the finalisation of the system configuration, a radical change was implemented regarding the final descend onto the Martian surface. It was decided to discard the use of the sky crane and use thrusters on the base station instead. Since this change was implemented in such a late design stage, this system hasn't been sized properly. The thrust required to slow down the base station and required fuel amount wasn't investigated and therefore requires more research in order to be properly sized.

Power Storage and Generation

During the design, it became clear that battery power and storage capabilities would be critical parameters which define the feasibility of the entire system. In order to increase the feasibility of the UAV, more investigation in the use of future technology such as hybrid supercapacitor-battery systems is required, or designing the batteries custom to the mission needs, which would result in more efficiency and reduced mass.

Bibliography

[Arianespace 2012] Arianespace: *Soyuz User's Manual*. Boulevard d'Europe, Evry-Courcouronnes Cedex: , 2012

[Arianespace 2016] Arianespace: *Ariane 5 User's Manual*. Boulevard d'Europe, Evry-Courcouronnes Cedex: , 2016

[Balaram et al. 2018] Balaram, J. ; Canham, Timothy ; Duncan, Courtney ; Golombek, Matt ; Grip, Håvard Fjæ r ; Johnson, Wayne ; Maki, Justin ; Quon, Amelia ; Stern, Ryan ; Zhu, David: Mars Helicopter Technology Demonstrator. the American Institute of Aeronautics and Astronautics, Inc, January 2018. –

[Bershadsky et al. 2016] Bershadsky, Dmitry ; Haviland, Stephen ; Johnson, Eric N.: Electric Multirotor Propulsion System Sizing for Performance Prediction and Design Optimization / American Institute of Aeronautics and Astronautics. 2016. – . 57th AIAA/ASCE/AHS/ASC Structures, Structural Dynamics, and Materials Conference

[Boelhouwer et al. 2018] Boelhouwer, R.N.J ; Bunschoten, E.C. ; Debusscher, C.M.J ; Frijters, W. ; Goeverden, R.J. van ; Legrand, E.B. ; Matton, J. ; Paliusis, K. ; Verheyen, J.K.N.: Midterm Review: Martian Advanced Reconnaissance System / Delft University of Technology. June 2018. –

[Braun et al. 2006] Braun, Robert D. ; Wright, Henry S. ; Croom, Mark A. ; Levine, Joel S.: Design of the ARES Mars Airplane and Mission Architecture. In: *Journal of spacecraft and rockets* 43 (2006), 9, Nr. 5, p. 1031

[Ciarletti and Clifford 2017] Ciarletti, V. ; Clifford, S.: The WISDOM Radar: Unveiling the Subsurface Beneath the ExoMars Rover and Identifying the Best Locations for Drilling. In: *Astrobiology* ESA (2017)

[Coleman 1997] Coleman, Colin P.: A Survey of Theoretical and Experimental Coaxial Rotor Aerodynamic Research. Ames Research Center, 1997. –

[Colozza et al. 2001] Colozza, Anthony J. ; Miller, Christopher J. ; Reed, Brian D. ; Loyselle, Patricia L.: Overview of Propulsion Systems for a Mars Aircraft / NASA. 2001. –

[Cudahy et al. 2000] Cudahy, T.J. ; Hewson, R. ; Huntington, J.F. ; Quigley, M.A. ; Barry, P.S.: The performance of the satellite-borne Hyperion hyperspectral VNIR-SWIR imaging system for mineral mapping at Mount Fitton, South Australia. In: *Intspec* CSIRO Exploration & Min (2000)

[D.M.Kass and Y.L.Yung 1995] D.M.Kass ; Y.L.Yung: Loss of atmosphere from Mars due to solar wind-induced sputtering. In: *Science* 268 (1995), Nr. 5211, p. 97–99

[van Dosselaer 2014] Dosselaer, I. van: *Buoyant Aerobot Design and Simulation Study: BADS*, Delft University of Technology, Diplomarbeit, September 2014

[Drela 1989] Drela, Mark: XFOIL: An Analysis and Design System for Low Reynolds Number Airfoils. (1989)

[Drela 2001] Drela, Mark: Higher-Order Boundary Layer Formulation and Application to Low Reynolds Number Flows. (2001)

[Edwards et al. 2012] Edwards, C. D. ; Arnold, B. W. ; Bell, D. J. ; Bruvold, K. N. ; Gladden, R. E. ; Ilott, P. A. ; Lee, C. H.: Relay support for the Mars Science Laboratory and the coming decade of Mars relay network evolution. In: *2012 IEEE Aerospace Conference* (2012), March, p. 1–11. – ISSN 1095-323X

[Edwards et al. 2014] Edwards, C. D. ; Barela, P. R. ; Gladden, R. E. ; Lee, C. H. ; Paula, R. D.: *Replenishing the Mars relay network*. March 2014

[Edwards et al. 2003] Edwards, Charles D. ; Jedrey, Thomas C. ; Schwartzbaum, Eric ; Devereaux, Ann S.: *The Electra Proximity Link Payload for Mars Relay Telecommunications and Navigation*. 2003

[Fleishner 2013] Fleishner, Richard: InSight Instrument Deployment Arm. In: *15th European Space Mechanisms and Tribology Symposium* Vol. 718. Noordwijk, Netherlands, 2013

[Gilmore 2002] Gilmore, David G.: *Spacecraft Thermal Control Handbook, Volume 1- Fundamental Technologies*. 2nd. American Institute of Aeronautics and Astronautics/Aero Press, 2002. – 171–174 pp.

[Grewal and Levy 2008] Grewal, Dhruv ; Levy, Michael: *Marketing*. New York : McGraw-Hill, 2008. – 533 pp.

[Grip et al. 2018] Grip, Håvard F. ; Johnson, Wayne ; Malpica, Carlos ; Scharf, Daniel P. ; Mandić, Milan ; Young, Larry ; Allan, Brian ; Mettler, Bérénice ; Martin, Miguel S.: Flight Dynamics of a Mars Helicopter. JPL/Caltech, 2018. –

[Hamann and van Tooren 2006] Hamann, R.L. ; Tooren, M.J.L. van: *Systems Engineering & Technical Management Techniques, Part II*. 2006

[Harvard 2007] Harvard: *Harvard Business Review on Green Business Strategy*. Cambridge, Massachusetts 02138 : Harvard Business School Press, 2007. – 117 pp.

[Hepperle 2012] Hepperle, Martin: Electric Flight - Potential and Limitations, October 2012

[Ivanov 2000] Ivanov, Boris A.: Mars/moon cratering rate ratio estimates. In: *Space Science Reviews* 96 (2000), Nr. 1-4, p. 87–104

[John D. Anderson 2017] John D. Anderson, Jr: *Fundamentals of Aerodynamics, Sixth Edition*. New York : McGraw-Hill, 2017

[Koning et al. 2018a] Koning, W. J. F. ; Johnson, W. ; Allan, B. G.: Generation of Mars Helicopter Rotor Model for Comprehensive Analyses. (2018)

[Koning et al. 2018b] Koning, W. J. F. ; Romander, E. A. ; Johnson, W.: Low Reynolds Number Airfoil Evaluation for the Mars Helicopter Rotor. (2018)

[Kruse et al. 2003] Kruse, F.A. ; Boardman, J.W. ; Huntington, J.F.: Comparison of airborne hyperspectral data and EO-1 Hyperion for mineral mapping. In: *IEEE Transactions on Geoscience and Remote Sensing* (2003), August

[Kumar et al. 2001] Kumar, Bhavesh G. ; Singh, Raman P. ; Nakamura, Toshio: Degradation of Carbon Fiber-reinforced Epoxy Composites by Ultraviolet Radiation and Condensation. In: *Journal of Composite Materials* 36 (2001), Nr. 24, p. 2713–2733

[Laitone 1997] Laitone, E. V.: Wind tunnel tests of wings at Reynolds numbers below 70 000. In: *Experiments in Fluids* 23 (1997), November, Nr. 5, p. 405–409

[Lakdawalla 2018] Lakdawalla, Emily: *The Design and Engineering of Curiosity: How the Mars Rover Performs Its Job*. Cham, Switzerland and Chichester, UK : Springer International Publishing and Praxis Publishing, 2018

[LeMaster and Rock 2003] LeMaster, E. ; Rock, S.: A Local-Area GPS Pseudolite-Based Navigation System for Mars Rovers. (2003)

[Monteiro et al. 1995] Monteiro, J. ; Silvestre, M. ; Piggott, H. ; Andre, J. ; Morgado, J. ; Vizinho, R. ; Silvestre, M. ; al., M. S. et: Summary of Low-Speed Airfoil Data. In: *Journal of Physics: Conference Series* (1995)

[Olea et al. 2010] Olea, A. ; Montesano, A. ; Montesano, C. ; Arenas, S.: *Proceedings of the Fourth European Conference on Antennas and Propagation*. April 2010. – 1–5 pp.

[Olivero 2018] Olivero, Fabrizio: *AE3211-I - Systems Engineering and Aerospace Design - Lecture Notes*. Delft University of Technology, 2018

[Park et al. 2011] Park, Sang Y. ; Choin, Heug S. ; Choi, Won J. ; Kwon, Hyuk: Effect of vaccuum thermal cyclic exposures on carbon/epoxyUD composites. In: *Elsevier* 43 (2011), Nr. 2, p. 726–738

[Petrescu and Petrescu 2011] Petrescu, Florian I. ; Petrescu, Relly V.: *Near the flying time*. Lulu Publisher, 2011

[Raymer 2012] Raymer, Daniel P.: *Aircraft design : a conceptual approach*. Reston, VA : American Institute of Aeronautics and Astronautics, 2012

[Roskam 1985] Roskam, Jan: *Airplane design. Pt. 5. Component weight estimation*. Ottawa, Kansas : Roskam Aviation and Engineering, 1985

[Seddon and Newman 2011] Seddon, John ; Newman, Simon: *Basic Helicopter Aerodynamics*. Chichester : John Wiley & Sons, Ltd, 2011. – 287 pp.

[Selig et al. 2011] Selig, M. ; Deters, R. ; Williamson, G.: Wind Tunnel Testing Airfoils at Low Reynolds Numbers. In: *49th AIAA Aerospace Sciences Meeting* (2011)

[Selig and Guglielmo 1997] Selig, M. ; Guglielmo, J.: High-lift Low Reynolds Number Airfoil Design. (1997)

[SpaceX 2015] SpaceX: *Falcon 9 Launch Vehicle Payload User's guide*, 2015

[Stone and Clarke 2018] Stone, R.H. ; Clarke, G.: Optimization of Transition Manoeuvres for a Tail-Sitter Unmanned Air Vehicle (UAV). (2018), 06

[Taylor et al. 2006] Taylor, Jim ; Makovsky, Andre ; Barbieri, Andrea ; Tung, Ramona ; Estabrook, Polly ; Thomas, A. G.: *Mars Exploration Rover Telecommunications*. 2006

[Torenbeek 1996] Torenbeek, Egbert: *Synthesis of Subsonic Aircraft Design*. Dordrecht : Kluwer Academic, 1996. – ISBN 9789024727247

[ULA 2010] ULA: *Atlas V Launch Services User's Guide*, 2010

[U.S.GAO 2017] U.S.GAO, United States Government Accountability O.: *Sale Price Drives Potential Effects on DOD and Commercial Launch Providers*, 2017

[Vandaele et al. 2011] Vandaele, A.C. ; Daerden, F. ; E. Neefs, R. D. nad ; López-Moreno, J.-J. ; M.R. Patel, J. Rodriguez G. na d ; Bellucci, G. ; NOMAD team the: NOMAD, a Spectrometer Suite for NADIR and Solar Occultation Observations on the ExoMars Trace Gas Orbiter. Fourth International workshop on the Mars Atmosphere: modelling and Observations, 2011. –

[Wertz and Larson 1999] Wertz, James R. ; Larson, Wiley J.: *Space Mission Analysis and Design*. 3rd edition. Torrance, Calif. : Microcosm, 1999

[Witte 2015] Witte, Lars: *Touchdown Dynamics and the Probability of Terrain Related Failure of Planetary Landing Systems: A Contribution to the Landing Safety Assessment Process*, Universität Bremen, Dissertation, November 2015

[Yonezawa et al. 2016] Yonezawa, Koichi ; Abe, Kento ; Sunada, Shigeru: Propeller design and loss mechanisms in low-Reynolds-number flows. In: *Journal of Propulsion and Power* 32 (2016)

[Zandbergen 2018] Zandbergen, B.T.C.: *Aerospace Design & Systems Engineering Elements I, Spacecraft (bus) design & sizing*. 2018

A
Functional Flow Diagrams

In this appendix the FFD's are presented. The FFD's of the different project phases are established separately and displayed as follows: Phase 0 can be seen in Figure A.1. Phase 1 is shown in Figure A.2. Phase 2 is displayed in Figure A.3. Phase 3 is split up for VITAS and the base station and can be found in Figure A.4 and Figure A.5 respectively. Phase 4 is presented in Figure A.6. Finally, phase 5 can be seen in Figure A.7.

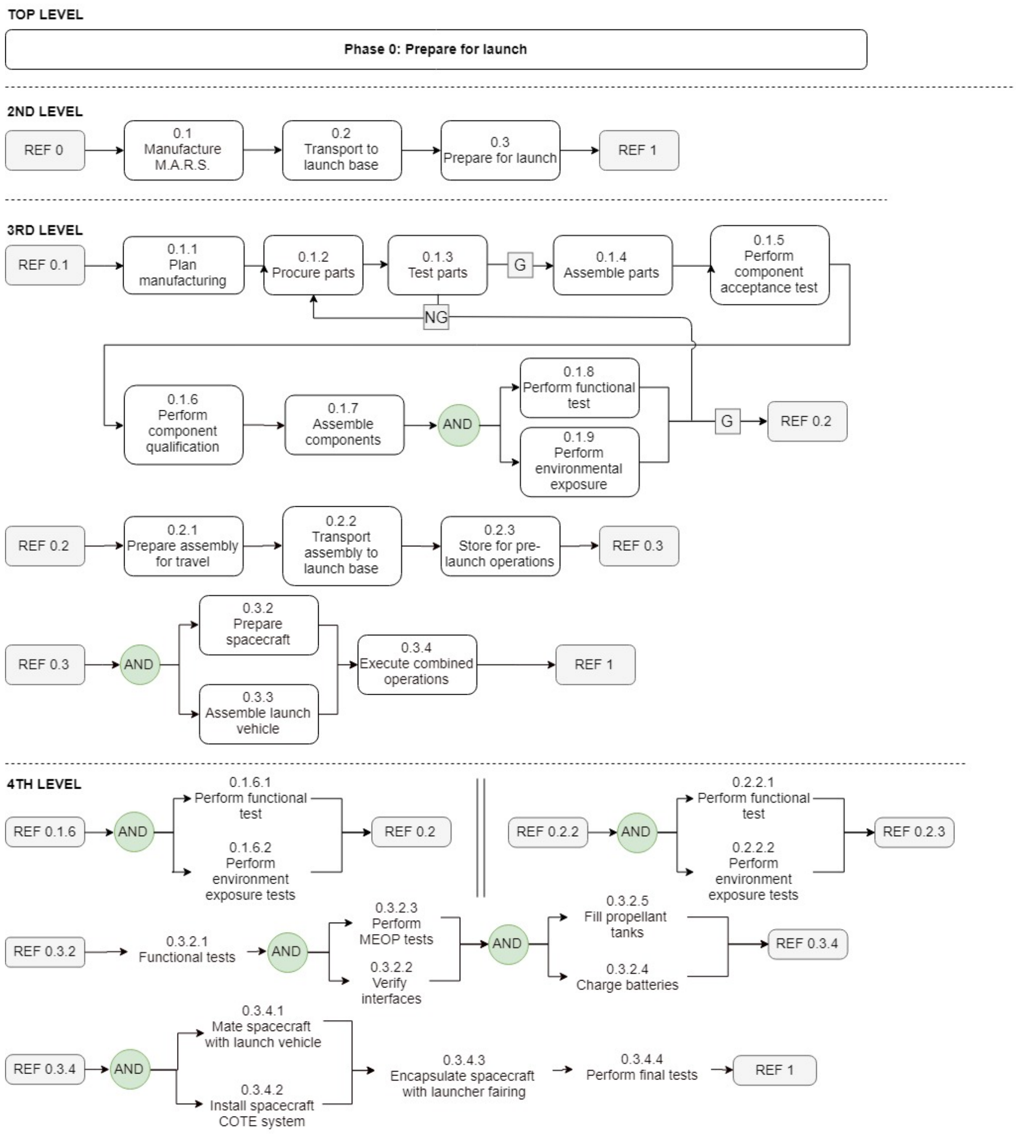

Figure A.1: The FFD for the pre-launch phase of the mission

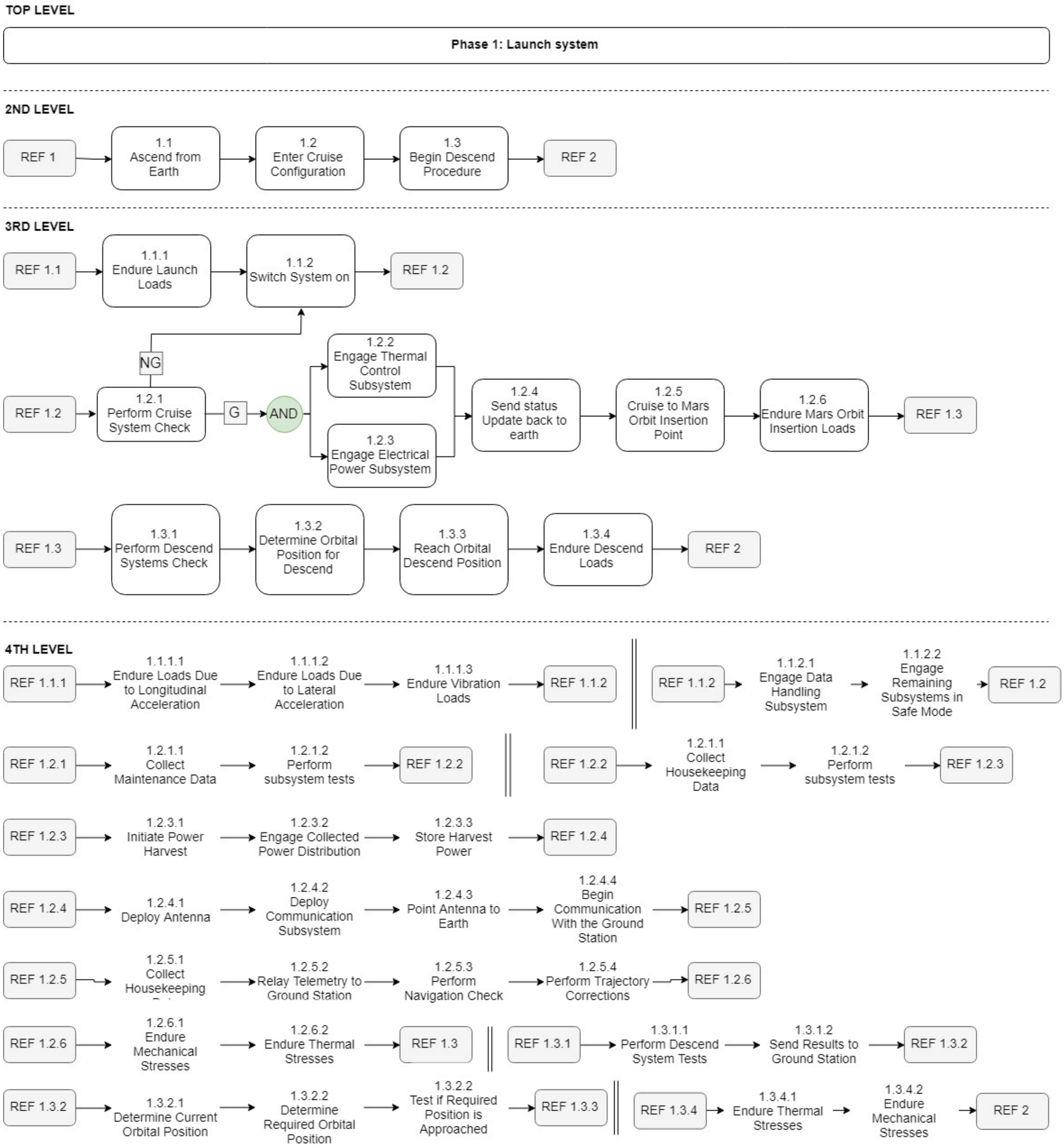

Figure A.2: The FFD for the launch phase of the mission

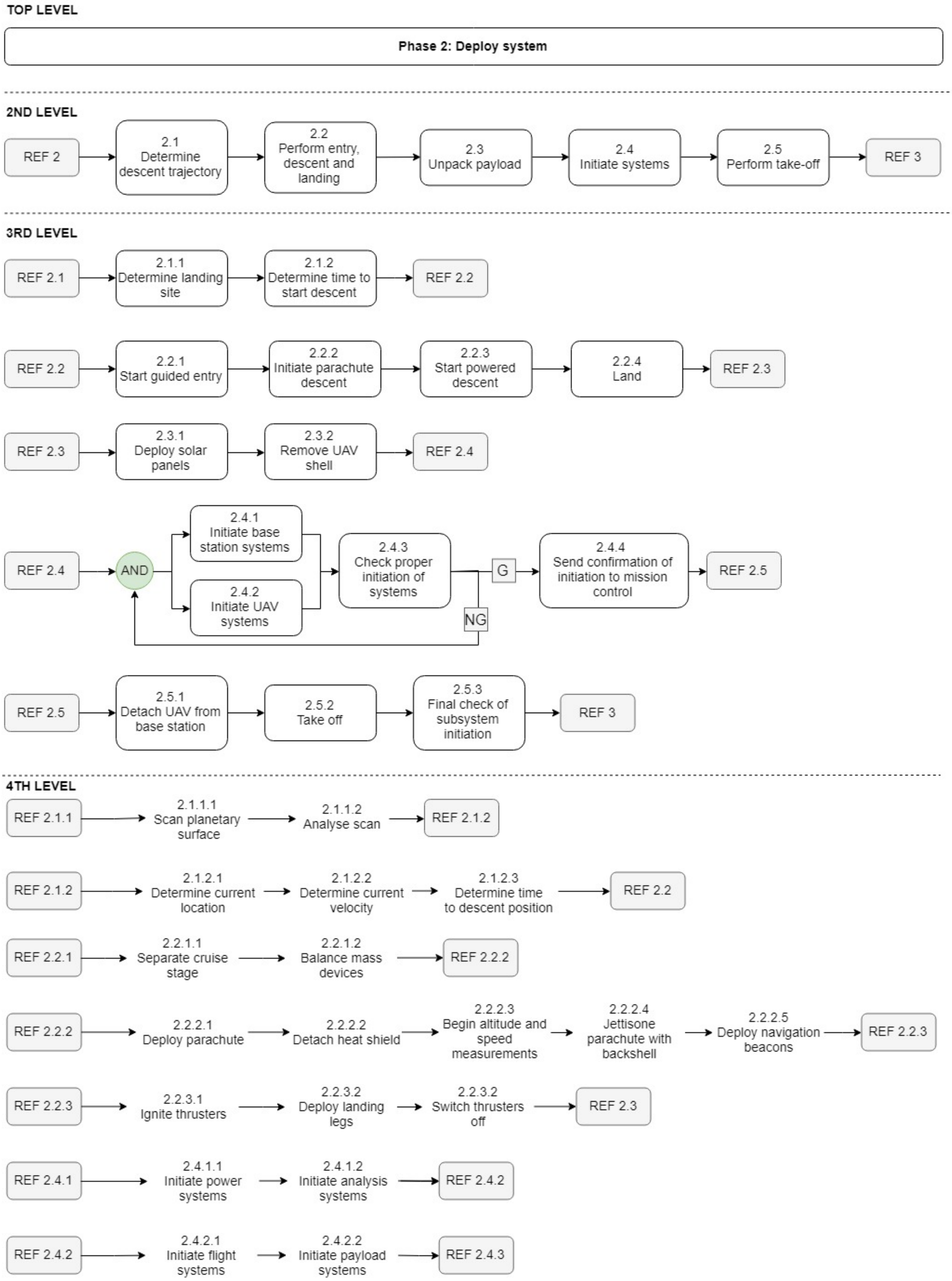

Figure A.3: The FFD for the deployment phase of the mission

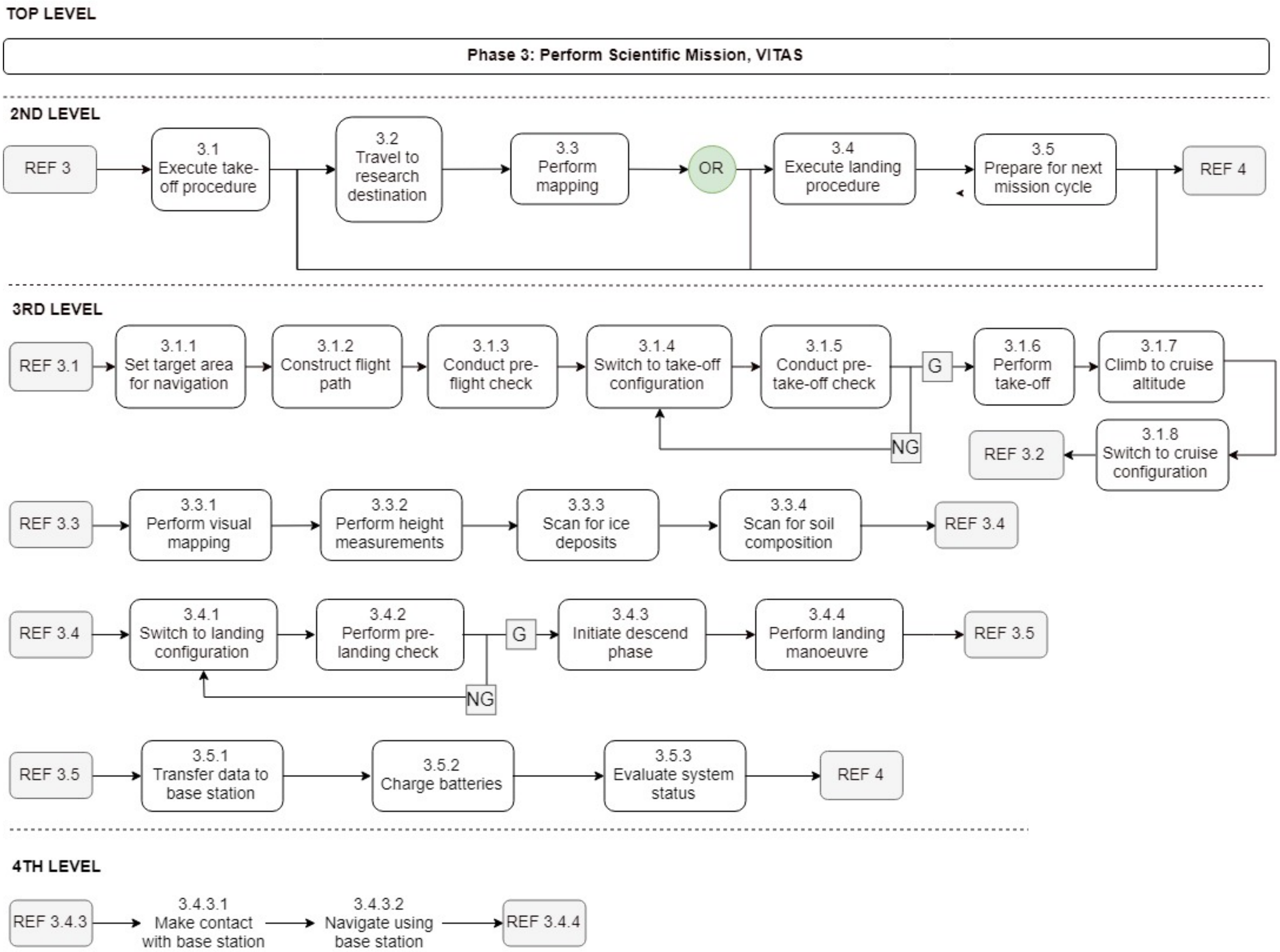

Figure A.4: The FFD for the scientific mission phase for VITAS

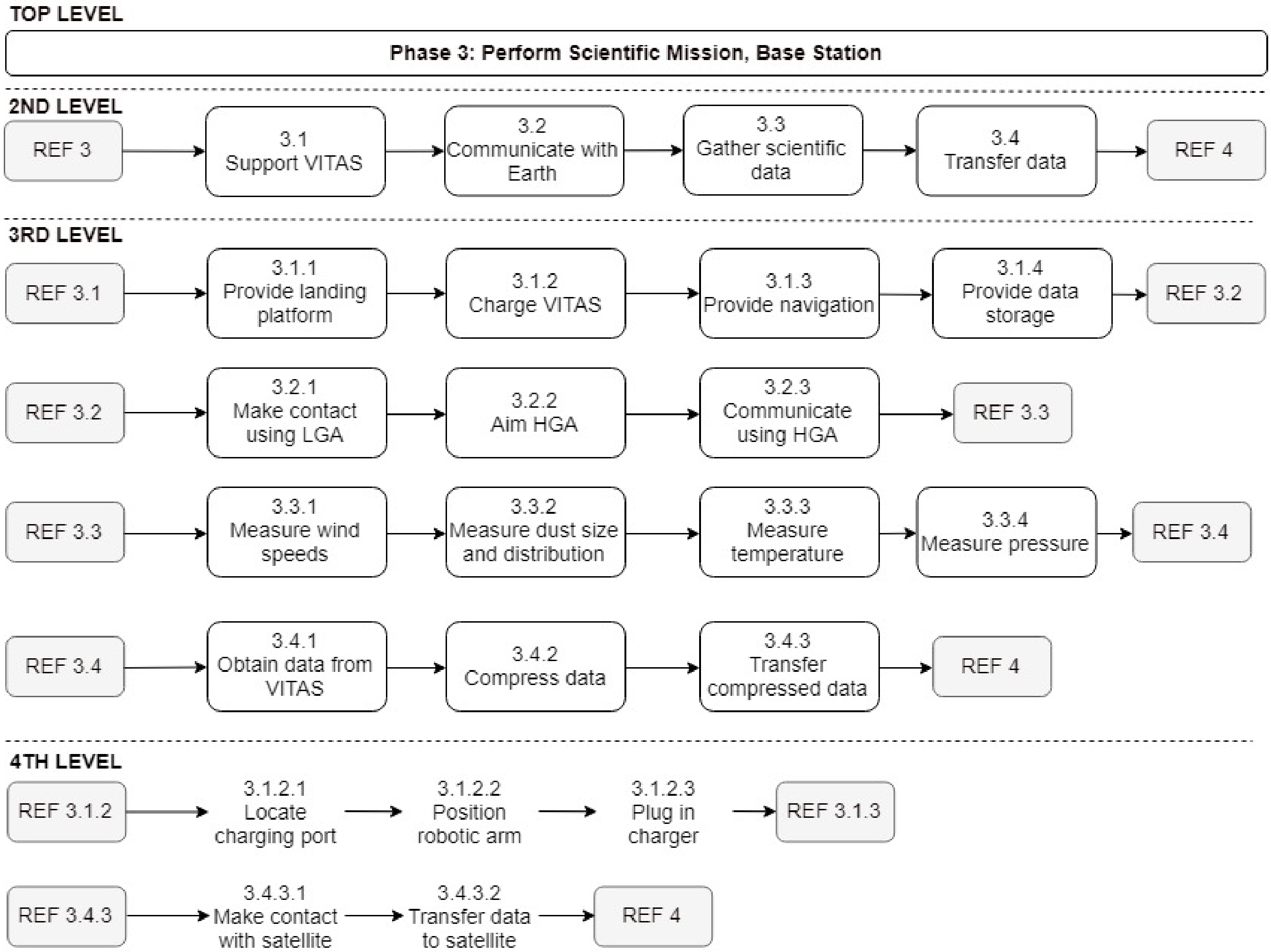

Figure A.5: The FFD for the scientific mission phase for the base station

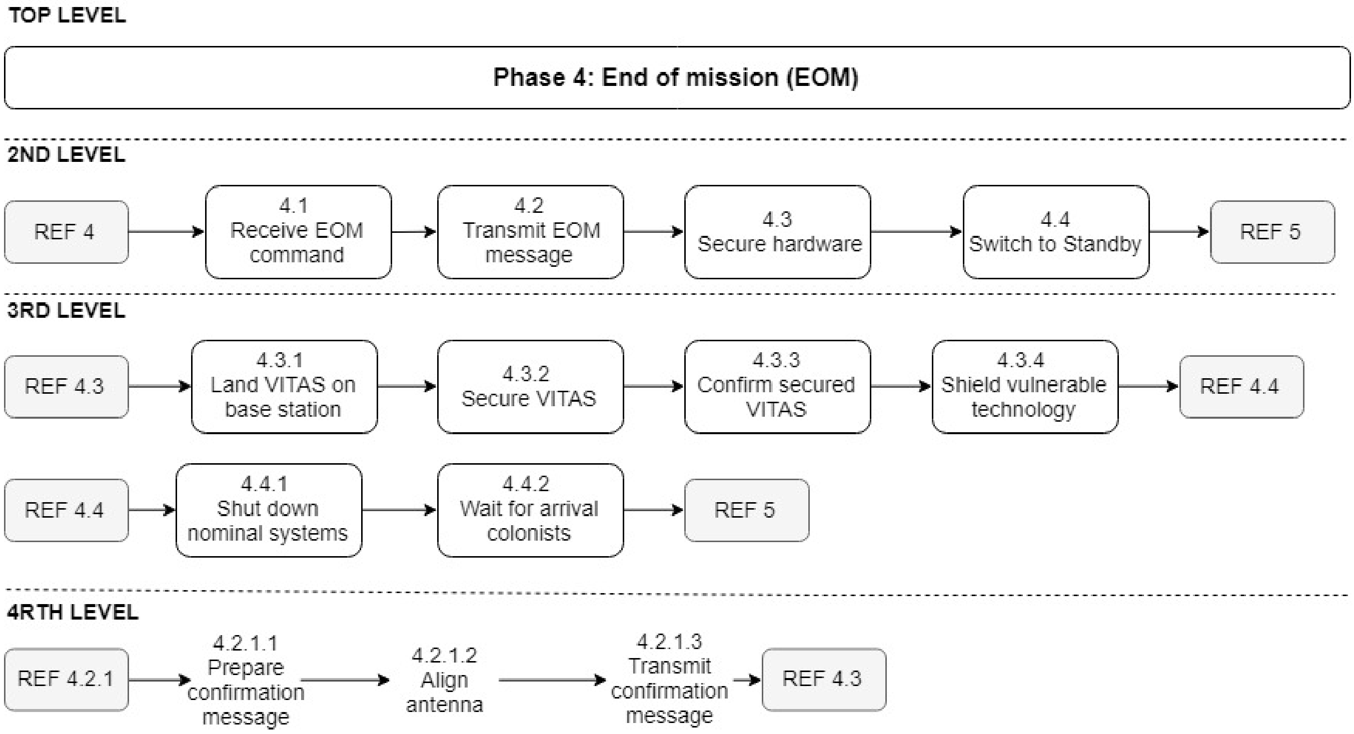

Figure A.6: The FFD for the end of mission phase

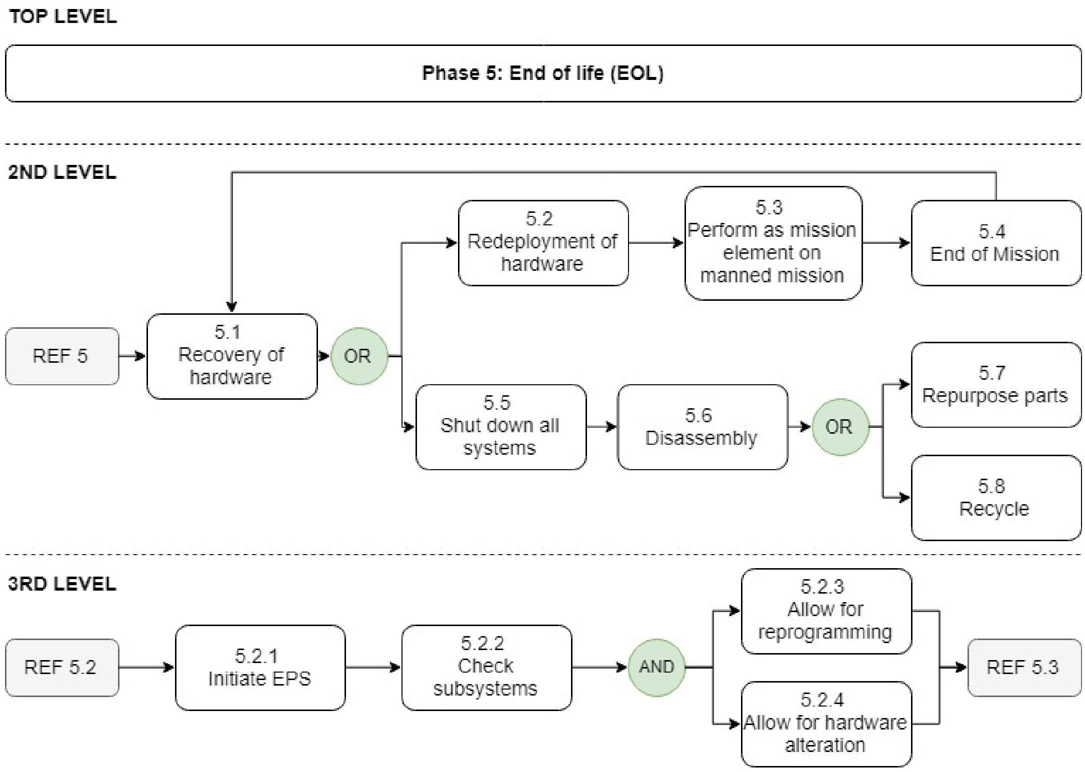

Figure A.7: The FFD for the end of life phase of the mission

B
Martian Environment

This appendix lists some relevant properties of the Martian atmosphere which have been used in the design calculations. Additionally, some external events characteristics for Mars that might influence the mission are identified as well.

B.1. Atmospheric Properties

Many approaches to a 'Martian standard atmosphere' have already been made [van Dosselaer, 2014]. However, there is no single data set that has a general preference. During the design process, the data from the Mars Global Surveyor was used.[1] This model defines two layers in the Martian atmosphere, above and below 7000 m altitude. The model is summarised in Table B.1. Furthermore, Table B.2 and Table B.3 provide some more gas properties and the atmospheric composition respectively.

Table B.1: Overview of the used model for the Martian atmosphere.

Layer	Temperature [°C]	Pressure [kPa]
< 7000 m	$T = -23.4 - 0.0222h$	$p = 0.699e^{-0.00009h}$
> 7000 m	$T = -31 - 0.000998h$	$p = 0.699e^{-0.00009h}$

Table B.2: Martian environmental parameters.[2] [3] [4]

Parameters	Mars	Earth	Unit
Average pressure	699	101400	Pa
Air density	0.015	1.217	kg/m^3
Average temperature	242	288	K
Gravitational acceleration	3.71	9.798	m/s^2
Ratio of specific heats	1.289	1.4	[-]
Speed of sound	219	343	m/s
Diurnal temperature range	184 - 242	283 - 293	K
Length day	24.6597	24.0	hours
Length year	686.977	365.25	days
Solar irradiance	586.2	1361.0	W/m^2
Rotation axis	25.0	23.44	degree

Table B.3: Mars atmosphere composition.[5] [6]

Mars		Earth	
Element	%	Element	%
CO_2	95.32	N_2	78.08
N_2	2.7	O_2	20.95
Ar	1.6	Ar	0.93
O_2	0.13	CO_2	0.04
CO	0.08		

B.2. External Events

The three most important external events on Mars to take in consideration are the effects of solar storms, Martian dust storms and meteor impacts. These are briefly discussed below.

Solar Storms

The weak magnetic field of Mars has caused the Martian atmosphere to degrade over the course of Mars' lifetime. In its early days, Mars might have housed liquid water and a thick atmosphere, but solar winds have gradually ionised

[1]URL: `https://www.grc.nasa.gov/www/k-12/airplane/atmosmre.html` [Cited 25 May 2018]
[2]URL: `http://www.braeunig.us/space/atmmars.htm` [Cited 3 May 2018]
[3]URL: `https://solarsystem.nasa.gov/planets/mars/in-depth/` [Cited 3 May 2018]
[4]URL: `https://nssdc.gsfc.nasa.gov/planetary/factsheet/earthfact.html` [Cited 23 May 2018]
[5]URL: `https://nssdc.gsfc.nasa.gov/planetary/factsheet/marsfact.html` [Cited 3 May 2018]
[6]URL: `https://nssdc.gsfc.nasa.gov/planetary/factsheet/earthfact.html` [Cited 23 May 2018]

the atmosphere and blew it into outer space. The degradation of the atmosphere is estimated to be about three bars of pressure over the course of 3.5×10^9 years (D.M.Kass and Y.L.Yung [1995]). This decrease in pressure is so slow, that it will have no effect on the mission.

Dust Storms

The main weather characteristic for Mars is the presence of dust storms. Dust storms happen every year. It can grow to the size of a continent and last for multiple weeks. Once every 3 Martian years (about 5.5 Earth years) there is a dust storm that covers the entire planet [7]. However, the wind speeds in these storms are lower than on Earth. In addition, the low atmospheric pressure and density cause the storms to be less intense than storms on Earth.

Meteor Impacts

The mission of M.A.R.S will take place over many years. It might be possible the exploration zone will be hit by a meteor, which can be of consequence for the mission. Since Mars is located near the asteroid belt and the Martian atmosphere is relatively thin, the surface is hit regularly by meteors. A probability estimate of meteors hitting an area on Mars in a certain time was found (Ivanov [2000]) to be $1.57 \times 10^{-15}\,\mathrm{yr}^{-1}\mathrm{km}^{-2}$. Multiplying this with the area of the exploration zone ($7854\,\mathrm{km}^2$) and the mission duration of five years, the probability of a meteor hitting the exploration zone during the mission is $6.16 \times 10^{-11}\,\%$. This probability is small, the risk of a meteor impact was deemed negligible.

To get an overview and comparison to Terrestial values of the basic Martian parameters they are presented in Table B.2. The chemical composition of the Martian atmosphere is shown in Table B.3.

[7]URL: https://www.nasa.gov/feature/goddard/the-fact-and-fiction-of-martian-dust-storms [Cited 03 May 2018]

C
Task Division

Preface .... Emiel
Executive Summary .... Rob

1 Introduction .... Robbert

2 Mission Objective
2.1 The Need for an Aerial Mars System .... Evert, Charles
2.2 Mission Concept .... Charles
2.3 Mission Task Requirements .... Charles

3 Market Analysis .... Wout, Jan

4 Mission Architecture
4.1 Mission Phases .... Rob
4.2 Mission Schedule .... Rob
4.3 Launcher Selection .... Kipras, Rob
4.4 Launch and Arrival Strategy .... Kipras
4.5 Landing Site .... Wout

5 Concept Analysis
5.1 Driving Requirements .... Jan
5.2 Concept Generation .... Kipras
5.3 Analysed Concepts .... Emiel
5.4 UAV Concept Trade-off .... Kipras
5.5 Sensitivity Analysis and Conclusions .... Kipras

6 Mars System Overview
6.1 General Overview .... Jan
6.2 VITAS .... Jan, Emiel, Charles
6.3 Base Station .... Robbert, Rob
6.4 Functional Breakdown Diagram .... Robbert
6.5 MARS System .... Robbert, Charles

7 Subsystem Design
7.1 Scientific Payload .... Jorne
7.2 Structures .... Evert
7.3 Propulsion .... Jan, Emiel
7.4 Stability and Control .... Charles, Emiel
7.5 Electrical Power System .... Wout
7.6 Communication .... Kipras
7.7 Thermal Control Subsystem .... Kipras
7.8 Navigation .... Jorne
7.9 Command & Data Handling .... Jorne

8 Future Development .... Wout

9 Cost Analysis .... Wout

10 Sustainability .... Wout, Kipras
11 Conclusion .... Kipras
12 Recommendations .... Evert